Toward the identification of a function of the "orphan" enzyme DHRS7

Inauguraldissertation

zur

Erlangung der Würde eines Doktors der Philosophie

vorgelegt der

Philosophisch-Naturwissenschaftlichen Fakultät

der Universität Basel

von

Selene Araya,
aus Lugano, Tessin

Basel, 2018

Genehmigt von der Philosophisch-Naturwissenschaftlichen Fakultät

auf Antrag von Prof. Dr. Alex Odermatt (Fakultätsverantwortlicher) und Prof. Dr. Michael Arand (Korreferent)

Basel, den 26.6.2018

_____

Dekan

Prof. Dr. Martin Spiess

I. List of Abbreviations

3α/βAdiol	3α/β-Androstanediol (5α-Androstane-3α/β,17β-diol)
3α/βHSD	3α/β-hydroxysteroid dehydrogenase
17β-HSD	17β-Hydroxysteroid Dehydrogenase
17αOHProg	17α-Hydroxyprogesterone
20α/βOHProg	20α/β-Hydroxyprogesterone
17α,20α/βdiOHProg	20α/βdihydroxyprogesterone
ADT	Androgen deprivation therapy
ANOVA	Analysis of variance
AR	Androgen Receptor
AKR	Aldo-Keto Reductase
ATCC	American Type Culture Collection
CAM	Cell Adhesion Molecule
CYP	Cytochrome P450
CBR1	Carbonyl reductase 1
CRPC	Castration resistant prostate cancer
Ct-value	Cycle threshold-value
DHRS7 (B/C)	Dehydrogenase/Reductase Short Chain Dehydrogenase Family Member 7 (B/C)
DHEA	Dehydroepiandrosterone
DHP	Dehydroprogesterone
DHT	5α-Dihydrotestosterone
DMEM	Dulbecco's Modified Eagle's Medium
DMSO	Dimethyl Sulfoxide
DTT	Dithiothreitol
E1	Estrone
E2	Estradiol
ECM	Extracellular Membrane
EDTA	Ethylenediaminetetraacetic acid
EMT	Epithelial-mesenchymal transition
ER	Endoplasmic Reticulum
ERα/β	Estrogen Receptor α/β
FBS	Fetal Bovine Serum

FDR	False discovery rate
FGF	Fibroblast growth factor
HEPES	4-(2-Hydroxyethyl)-1-Piperazineethanesulfonic Acid
HMDB	Human Metabolome Database
HPLC	High Performance Liquid Chromatography
HSD	Hydroxysteroid Dehydrogenase
IC50	Half-Maximal Inhibitory Concentration
LNCaP	Lymph node carcinoma of the prostate
mRNA	Messenger Ribonucleic Acid
n.d.	Not Detected
NADPH	Nicotinamide Adenine Dinucleotide Phosphate 6
NR	Nuclear Receptor
MAPK	Mitogen-activated protein kinase
MEM	Minimum Essential Medium
MW	Molecular Weight
PCa	Prostate cancer
PCR	Polymerase Chain Reaction
PPAR	Peroxisome Proliferator-Activated Receptor
PVDF	Polyvinylidene fluoride
RIPA	Radioimmunoprecipitation assay
RT	Room Temperature
SD	Standard Deviation
SDS	Sodium dodecyl sulfate
SDR	Short-Chain Dehydrogenase/Reductase
T	Testosterone
TBS-T	Tris-buffered saline with 0.1% (v/v) Tween 20
TEMED	Tetramethylethylenediamine
TLC	Thin-Layer Chromatography
Tris	Tris(hydroxymethyl)aminomethane
(UHP)LC-MS/MS	(Ultra High Performance) Liquid Chromatography/tandem Mass Spectrometry

Table of Contents

1 Summary

The short chain dehydrogenase DHRS7 has been previously described as a possible tumor suppressor, regulated during prostate cancer progression, with the potential of being a marker of prostate cancer. However, the function of DHRS7 and substrates with good affinity to be of potential physiological meaning remains unknown leaving it still classified as an "orphan" enzyme. These observations furthered the need to identify physiologically relevant substrates and understand the mechanisms affected by DHRS7 in endogenously expressing cell lines. In this thesis, *in vitro* assays were performed to help to characterize the activity of DHRS7. They showed DHRS7 has 3α and 20β reductase activities on the carbonyl of steroidal substrates, and interestingly revealed conversion of the main ligand of the androgen receptor dihydrotestosterone (DHT) toward the inactive 5α-androstane3α,17β-diol (3α-Adiol). This activity was further characterized through androgen receptor (AR) transactivation activity in an overexpressing system and biochemically through kinetic enzyme turnover assays. Moreover, this activity allowed to develop a novel screening lysate assay for substrates and inhibitors identification. However, no other promising physiologically relevant substrates were revealed.

In the second part, the phenotypic changes upon DHRS7 silencing were investigated in endogenous cell models by functional cancer assays, mass spectrometry and untargeted proteomics supported by cell cycle analysis, immunofluorescence, real time qPCR and western blot. These results disproved the modulation of the endogenous AR in the prostate cancer cell line LNCaP under DHRS7 depletion but supported the hypothesis of DHRS7 having a tumor suppressor role with protein changes observed for cell cycle, adhesion and migration relevant to the phenotype. Interestingly, protein changes involved in mechanisms relevant for tumor biogenesis were observed.

In conclusion, the results presented in this thesis extend the knowledge about DHRS7 *in vitro* activity, provide the characterization of an *in vitro* tool to test hypothesized substrates and inhibitors and suggest further investigation toward androgen receptor independent mechanisms.

2 Introduction

2.1 Prostate Cancer

Prostate cancer is the second most common cancer in men and is the leading cause of cancer related death among men globally (1.1 million cases, 307'000 deaths per year) [1]. Even though the prognosis is improving (the 5 years survival rate in Europe is currently about 93%) [2], some patients develop an aggressive form of the disease, despite primary treatment, leading to disease progression and death. The etiology of prostate cancer is complex but known to be associated with the non-modifiable risk factors age, ethnicity, and a family history of the disease [3, 4], and with environmental risk factors such as insulin-like growth factor-I (IGF-I) [5]. Inherent to this complexity seems to be the diversity of involved genetic and environmental factors.

The prostate is an exocrine gland in the male reproductive system located underneath the urinary bladder, in front of the rectum, and that surrounds the urethra. Usually, the cellular origin of prostate cancer is attributed to the epithelial cells of the peripheral zone (PZ) [6] (Figure 1A). The prostate zones consist of the prostatic epithelial acini, which are glandular structures arranged in a fibromuscular stromal network composed of columnar luminal and basal layer cells (Figure 1B). The basal layer is populated by stem cells, transit amplifying cells and committed basal cells. The prostatic epithelial acini are responsible for prostate secretions that drain into the urethra together with the spermatozoa and secretions from the seminal vesicles [7]. Prostatic acini, which progress into cancerous acini, are identified by specific micro environmental and molecular changes and with luminal hyperproliferation. The luminal epithelial cells, which in the healthy acini represent up to 60% of the total epithelial cell population increases to >99% in the cancerous acini, which coincides with the loss of the basal layer, disruption of the basement membrane, as well as immune infiltration and stroma reactivity [8].

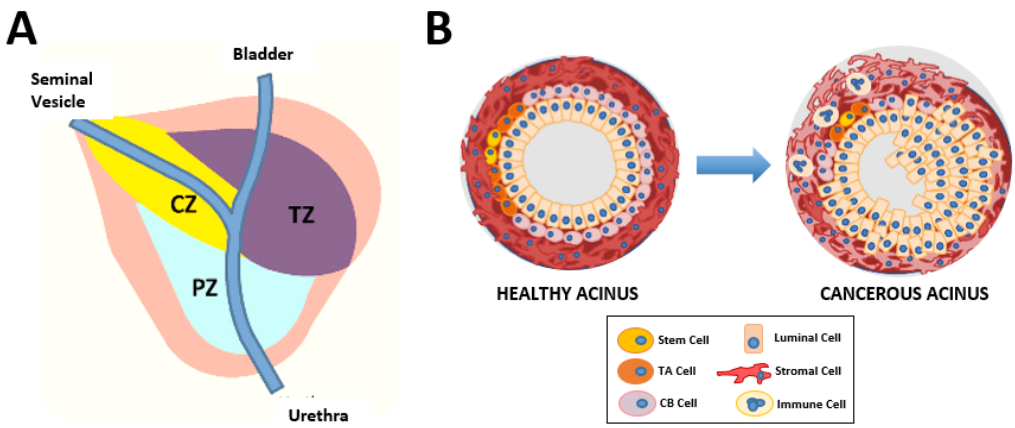

Figure 1: Adapted from [8]: Human prostate anatomy (A) and prostatic acinus architecture in health and cancer (B). CZ = central zone, TZ = transition zone, PZ = peripheral zone, TA = transit amplifying, CB = committed basal.

Luminal epithelial cells of the prostate are differentiated cells that synthesize and secrete the products of the seminal plasma, including prostatic-specific antigen (PSA, also called KLK3), prostate-specific acid phosphatase (PAP), polyamines and prostaglandins [7]. Luminal epithelial cells express the androgen receptor (AR) [9, 10], and they survive only in the presence of androgens [11]. Therefore, androgens, play a crucial role in the regulation of normal prostate physiology, but importantly, the dysregulation of androgen levels can aid cancer development and progression. In fact, in a healthy prostate and in androgen-dependent tumors, castration induces endothelial cell apoptosis, vascular regression and decreased blood flow [12, 13]. The production and secretion of androgens is regulated by the hypothalamus and the pituitary gland, as shown in Figure 2A.

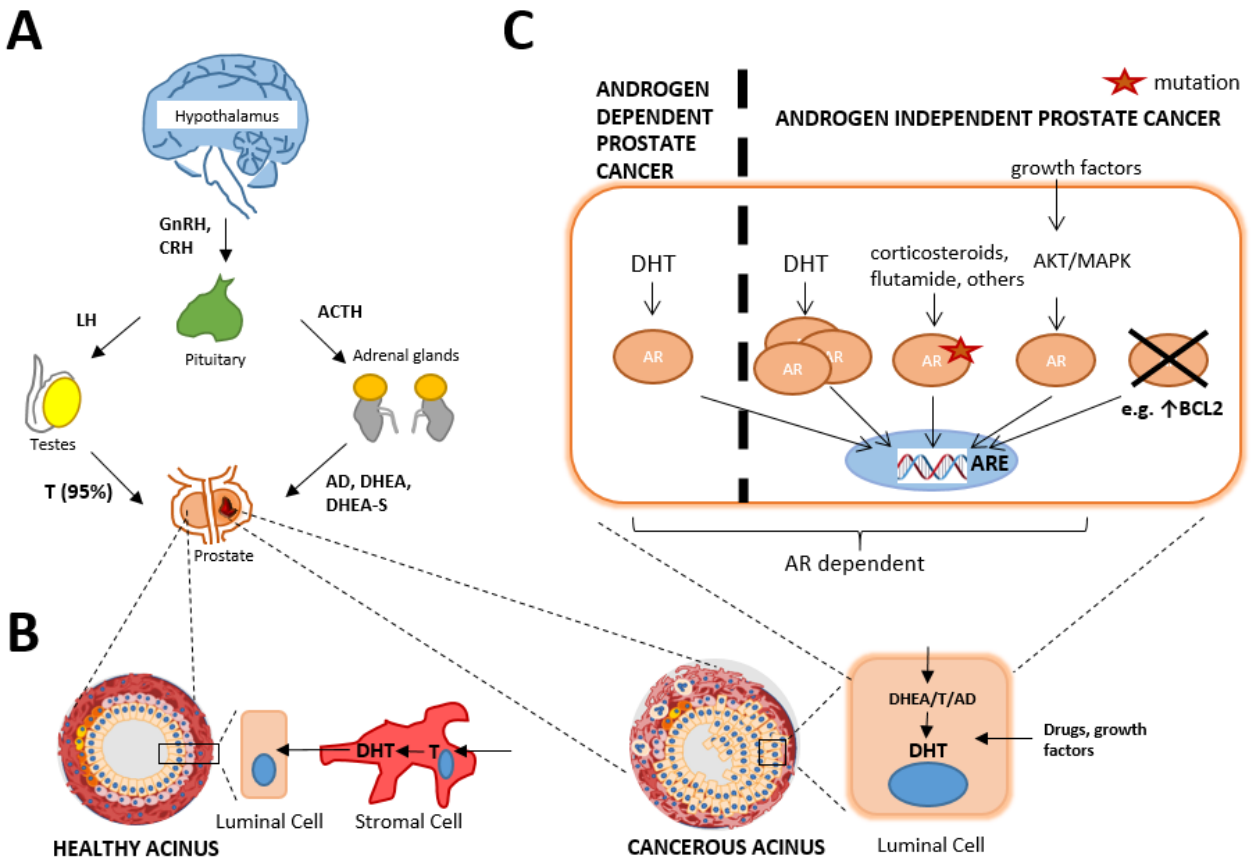

Figure 2: Regulation and production of androgens in the prostate and their use in the healthy prostate and in prostate cancer. A. Schematic representation of androgen production and secretion in the human body; B. Conversion of DHT into either healthy or cancerous acini (prostatic acini adapted from [8]); C. Schematic representation of the mechanisms of androgen dependent and independent prostate cancer adapted from [14]. GnRH = gonadotropin releasing hormone; T = testosterone, DHT = dihydrotestosterone, AD = androstenedione, CRH = corticotropin releasing hormone; LH = luteinizing hormone; ACTH = adrenocorticotropic hormone, DHEA = dehydroepiandrosterone, DHEAS = dehydroepiandrosterone sulfate, AR=androgen receptor, ARE = androgen response element.

The hypothalamus releases gonadotropin releasing hormone (GnRH) and corticotropin releasing hormone (CRH), stimulating the secretion of luteinizing hormone (LH) and adrenocorticotropic hormone (ACTH) from the pituitary. Circulating LH then stimulates the Leydig cells of the testes to produce and secrete testosterone (T) (ca. 95% of the total production) [15]. ACTH instead induces the adrenal production of weak androgens such as androstenedione (AD), dehydroepiandrosterone sulfate (DHEAS) and dehydroepiandrosterone (DHEA) that are subsequently converted to testosterone in peripheral tissues. The majority of circulating T is bound to plasma proteins (sex hormone binding globulin) and only a small portion remains free. As depicted in Figure 2B, it is commonly accepted that in a healthy prostatic acinus, free T diffuses into the stromal cells where it is converted into its active form DHT by the enzyme 5α-reductase [16]. DHT may signal within the stromal cell or participate in paracrine signaling with neighboring luminal cells that lack the internal machinery to produce its own DHT. Once in the cell, DHT

can exert its function by binding to the cytoplasmic AR with a dissociation constant of Kd = 10 pM [17], accounting as the most potent physiologically active androgen in humans [18]. The DHT/AR interaction results in a conformational change of the AR, leading to the dissociation of accessory proteins [19] and enabling its translocation into the nucleus, binding to androgen response elements (ARE) in the promoter region and initiating target gene transcription [20].

The molecular mechanisms initiating and driving prostate cancer are not fully understood, however, its development is a multistep process and androgen dependency initially plays a major role, which is reflected in the clinics since treatment options include androgen deprivation therapy (ADT). However, in some cases, patients can progress to develop androgen independent prostate cancer (or castration resistant prostate cancer); a clinical definition generally accepted for ADT refractory prostate cancer patients. Some of the currently hypothesized molecular mechanisms promoting prostate cancer are shown in Figure 2C [14].

In the setting of androgen dependent prostate cancer, the transformation into an aggressive phenotype is associated with a shift from paracrine towards an autocrine androgen stimulation [21], resulting in the activation of the AR in spite of low serum concentrations of testosterone [9, 10, 22, 23] (see Figure 2B). However, there are also AR independent mechanisms that drive prostate cancer [24], including increased protein expression levels or increased stability of the AR which condition the cancer cell to be hypersensitive to lower concentrations of ligands [25], as well as mutations within the ligand binding site of the AR that makes it responsive to non-natural AR ligands such as corticosteroids or antiandrogens such as flutamide [26-28]. A good example is the well-studied mutation T877A, also present in the prostate cancer cell line LNCaP [27]. The AR can also be activated by ligand independent processes such as growth factor pathways [29] (referred in this case as “outlaw” receptor [30]). Importantly, a common feature of the examples given above is that androgen dependent and independent mechanisms result in the dysregulated activation of the AR.

Alternatively, prostate cancer can be driven by truly AR-independent mechanisms [31], often present in AR negative tumors [32]. Specific proteins or pathways such as the anti-apoptotic B-cell CLL/lymphoma 2 (BCL2) [33], Wnt/β-catenin signaling [34], dysregulated or mutated oncogenes and tumor suppressor genes as ERG [35], RB1 and TP53 [36], phosphatase and tensin homolog (PTEN) and NKX3.1 [37], and many others have been suggested to play a role in prostate cancer development and progression [38].

Prostate cancer is asymptomatic; however, some men may suffer from urinary problems that persist over a long period of time [39]. In the clinic, prostate cancer is indicated by high serum PSA levels, a digital

rectal exam, and diagnosis is then confirmed with a transrectal biopsy [40]. The clinical stage is then assessed microscopically by Gleason score based on pathological scores ranging from 1 to 10. Lower scores represent tissue biopsies with small and more differentiated acinar glands, and higher scores represent tissue biopsies that are poorly differentiated with irregular and occasional gland formation [41]. The prostate cancer treatments used nowadays are mainly radiation therapy, chemotherapy, prostate surgery often by radical prostatectomy, but as gold standard ADT is used. ADT includes orchiectomy (the removal of the testis), administration of antiandrogens (e.g. flutamide, nilutamide, bicalutamide, enzalutamide, cyproterone acetate), androgen synthesis inhibitors (e.g. the CYP17A1 inhibitor abiraterone), and antigonadotropins [42]. Nevertheless, for metastatic castration-resistant prostate cancer, the effectiveness of current therapies is palliative, with an improvement in overall survival of 2-5 months compared to placebo [43, 44].

As prostate cancer lethality is still very high and clinical biomarkers such as PSA are limited by a lack of specificity [45], the molecular mechanisms leading to the formation and progression toward an aggressive prostate cancer phenotype as well as the identification of new informative biomarkers urgently need to be discovered.

2.2 Associations of Short Chain Dehydrogenases (SDRs) and Aldo Keto Reductases (AKRs) with Cancer

Several carbonyl reductase enzymes of the Short Chain Dehydrogenase (SDR) and the Aldo Keto Reductase (AKR) superfamilies have been shown to be associated with a number of different cancers, often hormone-related [46-48]. These enzymes may represent potential prognostic biomarkers or drug targets or anti-targets. However, for most of the enzymes identified, a direct mechanistic link with the cancer related endpoints highlighted in the studies remains to be elucidated. Table 1 summarizes main observations collected regarding the associations of AKRs and SDRs with human cancer in patients.

Table 1: Examples of SDR enzymes known to be associated with human cancer, their observed substrates, and intracellular localization. References are described throughout the text and complemented by [49]. ER=endoplasmic reticulum.

Enzyme	Type of human cancer	Known substrates	Intracellular localization
CBR1	lung, breast, intestine, colon, uterine endometrial	xenobiotics, prostaglandin F2α	cytoplasm
3βHSD1	breast, prostate	pregnenolone, 17α-hydroxypregnenolone, DHEA	ER, mitochondria
17βHSD1	breast, prostate	E1, DHT	-
17βHSD2	breast, prostate	E2, T, androstenediol	ER
17βHSD4	breast, prostate	DHT, fatty acids	peroxisome
17βHSD12	ovarian, breast	E2, very long fatty acids	ER
RDH10	non-small-cell lung cancer, glioma	all-trans retinol	ER, mitochondria, lipid droplets
RDH11	non-small-cell lung cancer	all-trans-retinal, 9-cis, all-trans-retinol	ER
DHRS9	colorectal	retinoic acid, progesterone, allopregnanolone, 3αAdiol	peroxisome
AKR1C1	breast, prostate	DHT, progesterone, 5α-androstanedione	cytoplasm
AKR1C2	breast, prostate	DHT, progesterone, dihydroprogesterone, 5α-androstanedione	cytoplasm
AKR1C3	breast, prostate, adenocarcinoma and squamous cell carcinoma in the lung, skin squamous cell carcinoma, gastrointestinal tumors	DHT, 5α-androstanedione, androsterone, prostaglandin E2	cytoplasm
17βHSD6	prostate	retinoic acid, DHT	ER

For example, carbonyl reductase 1 (CBR1) has been found to play a role in tumor metastasis and growth [50], possibly by inducing epithelial to mesenchymal transition [51]. This enzyme was decreased with

progressive uterine endometrial cancer development [51]. Moreover, decreased expression of CBR1 promoted ovarian cancer cell proliferation and invasion, and its overexpression decreased cell proliferation [52]. Among different metabolites, CBR1 can convert the prostaglandin E2 (PGE2) to prostaglandin F2α (PGF2α) [53-55]. PGE2, in the setting of endometrial cancer has been shown to increase proliferation through activation of the PGE2 receptor subtype 4 (EP4) [56]. However, CBR1 can convert many xenobiotics with higher affinity, and therefore its endogenous role in prostaglandin metabolism is questionable [57, 58]. To add to the complexity of the associations between CBR1 and different cancer types, CBR1 was shown to be elevated in cancer tissues of lung, breast, intestine, and colon [59]. Clearly further research needs to be conducted to understand the link between the expression of CBR1 in different cancer types and identify the physiological substrate(s) responsible for the association with cancer.

Another SDR, 3βHSD1, was shown to be a prognostic factor in hormone-dependent estrogen receptor (ER) positive breast cancer, indicating a decreased risk of recurrence [60]. Additionally, it has been recently shown to be a prognostic biomarker in advanced prostate cancer [61]. Interestingly, a gain of function single nucleotide polymorphism (SNP) (1245C; N367T, population frequency 22%) has been associated with hereditary and sporadic prostate cancer susceptibility and castration-resistant recurrence [62-64]. 3βHSD1 seems to be important in the pathophysiology of steroid hormone-related disease because of its crucial role in the synthesis of steroids. In fact, 3βHSD1 has been characterized for the following reactions: the oxidation and isomerization of progesterone from pregnenolone, 17OHProg from 17α-hydroxypregnenolone, and androstenedione from DHEA [65, 66]. The products of these reactions may enhance cancer cell proliferation, in particular progesterone by activating the progesterone receptor.

Other SDRs implicated in hormone-related cancers belong to the 17β-hydroxysteroid dehydrogenase (17βHSD) family, which includes enzymes that catalyze the oxidation or reduction of sex steroids on their 17β-hydroxy or -keto groups. For example, the expression of 17βHSD1 has been positively associated with breast cancer. In fact, 17βHSD1 was reported in up to 60% of breast cancer cases [67, 68] and it associates with adverse clinical outcome for the patients [67]. *In vitro*, its expression positively correlates with the increased proliferation of breast cancer cell line T47D, estradiol (E2) to estrone (E1) activation, and concomitant DHT inactivation [69]. Furthermore, stable overexpression of 17βHSD1 in the breast cancer cell line MCF-7 increased migration and altered estrogen receptor α (ERα), ERβ and AR pathways [70]. SiRNA 17βHSD1 mediated knock-down in MCF-7 cells further impeded S phase entry from G0-G1,

suggesting cell cycle arrest [71]. This body of work offers a convincing mechanism to bridge the association observed between 17βHSD1 and breast cancer development.

Another important 17βHSD, 17βHSD2, has been oppositely shown to be involved in the inactivation of estrogens and androgens (catalyzing the conversion of E1 to E2, testosterone to androstenedione, and androstenediol to DHEA) [72, 73], The immunoreactive detection of 17βHSD2 is lost in the vast majority of breast cancer patients [67], and has polymorphisms associated with breast and prostate cancer progression (rs1364287, rs2955162, rs1119933, rs9934209) [74]. However, the 17βHSD2 knock-out mouse model suggests a phenotype that was not due to a reduced estrogen or androgen action, but instead to an impairment of retinoic acid signaling [75, 76]. To address 17βHSD2's specific role in different types of hormone dependent and independent cancers, molecular mechanisms needs to be further investigated.

17βHSD4, also known as peroxisomal multifunctional enzyme type 2 (MFP-2) because of its peroxisomal localization [77, 78], is important in the context of prostate cancer. Specifically, 17βHSD4 mRNA and protein overexpression have been associated with prostate cancer mortality [79], and positively correlates with the Gleason grading system [80]. Additionally, the presence of a single SNP in 17βHSD4 has been associated with the efficacy of androgen-deprivation therapy [63]. Moreover, a recent publication shows that 17βHSD4 isoform 2 is the unique isoform able to inactivate testosterone and DHT to AD and 5α-Androstanedione, respectively, and has been shown to be lost in castration-resistant prostate cancer [81]. This enzyme is also known to inactivate estrogens and plays an important in the bile acid metabolism, and peroxisomal β-oxidation [78]. However, the expression of 17βHSD4 tissue specific isoforms and its peroxisomal localization adds to the complexity of its different physiological role in different organs. For example, supporting 17βHSD4's ability to take on multiple roles in different tissues, in the liver of 17βHSD4 knock-out mice show a phenotype characterized by the accumulation of very long chain fatty acids and branched fatty acids, as well as altered bile acid metabolism [82, 83]. The testis of the same animal showed an accumulation of very long chain fatty acids and branched fatty acids which was accompanied by fertility problems which may be due to altered androgen metabolism [83].

17βHSD7 has not been shown to correlate to cancer severity in clinical samples; however, inhibition of 17βHSD7 using specific small molecules, resulted in the significant shrinking of breast cancer tumors in xenograft models [84]. Interestingly, in *in vitro* models 17βHSD7 seems to activate E1 and inactivate DHT into the weak estrogen 5α-Androstane-3β,17β-diol (3β-Adiol) [85]. Inhibition of 17βHSD7 in the ER positive breast cancer cell lines MCF-7 and T47D resulted in reduced levels of E2, higher levels of DHT and

decreased proliferation accompanied by G0/G1 cell cycle arrest [71, 84]. This body of work offers a convincing mechanism to bridge the association observed between 17βHSD7 and breast cancer development in xenograft models.

17βHSD12 overexpression has been associated with poor survival in patients with ovarian cancer [86, 87], however its role in breast cancer is contradictory [88, 89]. Silencing 17βHSD12 in ovarian tumor cells resulted in growth inhibition and increased apoptosis [86, 87], however its enzymatic activity, converting E1 to E2 [90], was not altered in T47D breast cancer cells with 17β-HSD12 knock-down [91]. Supporting other substrates to be explanatory for the role of 17β-HSD12 in this breast cancer cell line, it has been shown that 17β-HSD12 performs reactions resulting in the elongation of very long chain fatty acids [90, 92]. Its role in long chain fatty acid metabolism in the setting of breast cancer is further supported by the observation that in clinical samples the presence of 17β-HSD12 correlates with COX2 expression as opposed to ER expression [87].

Another SDR, 17βHSD6, has a misleading nomenclature, since it shows the ability to catalyze oxidation reactions at the 3-hydroxy position and not on the 17β-hydroxy group. It has been found to be decreased in human prostate cancer biopsies of greater severity according to the Gleason grade [93], and to be upregulated in patients undergoing androgen deprivation therapy [94]. This enzyme has been shown to activate 3α-Androstanediol (3α-Adiol) in DHT [94], providing a possible mechanism by which it is linked to prostate cancer.

Recently, also the SDRs retinol dehydrogenases RDH10 and RDH11 have been associated with cancer. RDH10, an enzyme localized in endoplasmic reticulum, mitochondria and lipid droplets [95], has been linked to glioma progression and non-small cell lung cancer [96, 97]. In the glioma cell lines U87 and U251, upregulation of RDH10 is associated with a more aggressive phenotype and silencing using specific siRNA reduced the survival, proliferation and invasiveness as well as tumor growth in nude mice through the regulation of the TWEAK-NF-κB axis [96]. RDH10 has been shown to oxidize all-trans retinol to all-trans retinal in overexpressing cells [98], but this observation has not been linked to its role in glioma. In fact, the retinoic acid all-trans retinal is a precursor of all-trans retinoic acid that functions as a ligand towards the nuclear receptors RARs, RXRs, or PPARβ/-δ. Binding of all-trans retinoic acid to these receptors results in the inhibition of cell-cycle progression in a variety of human cancer cells though direct or indirect modulation of cyclins, CDKs, and cell-cycle inhibitors [99]. Further, RDH11 was significantly decreased in non-small-cell lung cancer [100], and similar to RDH10, it has been reported to metabolize retinoic acids [101], but this reaction has not been linked to its role in cancer. Low protein expression of another SDR,

DHRS9, correlates with colorectal cancer progression and poor survival, suggesting it also as potential prognostic biomarker [102]. Like RDH10 and RDH11, DHRS9 has a role in retinoid metabolism by conversion of all-trans retinal to retinoic acid, however with low activity. DHRS9 can also metabolize the conversion of allopregnanolone to dihydroprogesterone (DHP) and 3α-Adiol to DHT [103, 104], but it is not clear if its ability to metabolize these substrates explains DHRS9's associations to colorectal cancer.

AKRs have also been associated with the pathogenesis and progression of several types of cancer. Overexpression of AKR1C1 and AKR1C2 have been observed in invasive bladder cancer [105, 106], breast cancer [107], and prostate cancer [108, 109]. AKR1C1 and AKR1C2 appear to have a major role in androgen metabolism, where they function as 3α-hydroxysteroid dehydrogenases inactivating the AR ligand DHT. in prostate cancer cells. If these mechanisms would be physiologically relevant in these prostate cancer samples because of their overexpression, you would expect these enzymes to act as tumor suppressors but in respect this association these mechanisms do not correlate [110]. However, in breast cancer cell lines AKR1C1 and AKR1C2 mainly affect progesterone signaling by deactivating progesterone, as suggested by overexpression and siRNA mediated silencing studies in T47D and MCF-7 cells [107].

On the other side, AKR1C3 overexpression has been associated with many cancer types: prostate cancer [17, 47, 111], breast cancer [17], adenocarcinoma and squamous cell carcinoma in the lung [112], skin squamous cell carcinoma [113], cervical cancer [114], and gastrointestinal tumors [115]. Specifically, AKR1C3 overexpression seems to be a promising biomarker for prostate cancer progression [116, 117]. Stable expression of AKR1C3 in the androgen-independent prostate cancer cell line, DU145, increased its proliferation [118]. Alternatively, siRNA depletion of AKR1C3 decreased DHT-dependent MCF-7 breast cancer cell growth [119]. These results do not clearly define whether AKR1C3 exerts its cancer promoting effects by hormone dependent or independent mechanisms and this could be partly explained by its ability to react with multiple substrates in different tissues. For example, AKR1C3 catalyzes the conversion of prostaglandins H2 and D2 into PGF2α and 9α,11β-PGF2α, respectively [120], however, can also metabolize the androgens testosterone to Δ4-androstene-3,17-dione [121] and deactivates DHT, and as well estrogen and progesterone [48]. Positive promoter regulation of the oncogene lipocalin 2 following AKR1C3 downregulation, decreased migration and invasiveness and changed cytoskeleton dynamics in cervical cancer cells SiHa and 293T, but this has not been linked with the enzymatic activity of AKR1C3 [114]. Many potent and selective inhibitors of AKR1C3 have been developed and described; most still require preclinical optimization [122], but one is currently prepared in phase I [personal communication].

Taken together, the mechanisms underpinning the numerous SDR and AKR associations with cancers are complex and further research is required to enable to understand the usefulness of these enzymes as potential novel clinical targets, anti-targets, or biomarkers. The reasons why a number of the enzymes belonging to the two super-families, SDR and AKR, are so selective for specific substrates and yet others can be rather promiscuous, can partially be explained by their biochemical characteristics, which will be discussed in detail in the following subchapter.

2.3 Carbonyl Reductases of the SDR and AKR Families

The short-chain dehydrogenase reductase (SDR) superfamily [Figure 3] is one the largest protein classes of oligomeric oxidoreductases. There are currently a total of 163,120 identified members as in Uniprot, and they are present in all forms of life [123]. They are subdivided in the following subfamilies; the classical SDR folds, subdivided into three clusters C1 (yellow), C2 (green) and C3 (blue), the extended SDR fold (violet), and the atypical members (dark pink).

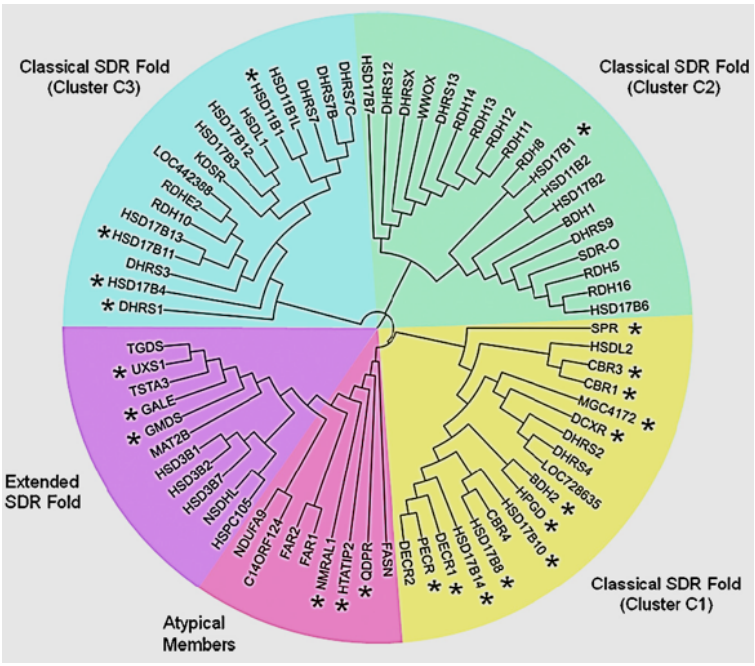

Figure 3: Adapted from [124]: SDR superfamily divided in "classical folds" clustered in C1, C2 and C3, "extended fold", and "atypical members". Short branch lengths represent proteins that are phylogenetically close, while longer branch lengths indicate broader evolutionary relationship.

SDRs can be cytosolic, microsomal or mitochondrial, and show catalytic activities toward a wide range of substrates (e.g. retinoids, steroids, polyols, fatty acids derivatives, prostaglandins, and xenobiotics), with enzymes showing also multifunctionality [123, 125]. More than 70 SDR members have been identified in the human genome [46, 126]. They are implicated in a wide range of physiological functions, with several

exerting an essential role in the synthesis and inactivation of steroid hormones. The active steroids in their target tissues can activate their respective nuclear receptors leading to target gene expression [127]. Additionally, SDRs have an important toxicological role in phase I or functionalization metabolism, by inactivating potentially toxic xenobiotics or by activating relatively harmless xenobiotics into reactive metabolites that may be conjugated and excreted from the body [128]. Moreover, an increasing number of single-nucleotide poly-morphisms have been identified in SDR genes, and a variety of inherited metabolic diseases are linked to genetic defects in SDR genes [129]. However, currently the physiological roles of most of the SDRs are unknown or inadequately characterized with structural information available for only approximately 20 members [127]. This knowledge gap has driven the search to uncover their physiological substrates and characterize their molecular mechanisms. The SDRs currently characterized target a broad substrate spectrum, which can be explained by the relatively low sequence identity between different SDR enzymes (15–30%). SDRs only inherit a few conserved sequence regions (e.g. glycine-rich motif (TGxxxGxG amino acid sequence) or a catalytic triade/tetrade that form the active site (S-Y-K/N-S-Y-K amino acid sequence)) [123, 124, 130]. In contrast, the tertiary structure is similar [131], with the highly conserved Rossman-fold responsible for the NAD(P)(H) cofactor binding site that participates in the catalysis in the ligand binding region.

Besides the SDRs, the AKR superfamily contains many carbonyl reductases. The AKRs share a common catalytic reaction mechanism and consist of approximately 40 multi-functional enzymes [132]. Similar to the SDRs, several AKRs are known to play a role in steroid metabolism but they have a broad range of substrates. The human members of the AKR1C subfamily comprise four monomeric cytosolic NADP(H)-dependent enzymes: AKR1C1, AKR1C2, AKR1C3 and AKR1C4 [48, 133]. In contrast to the SDRs, they share an increased sequence identity of ca. 86% and consist of a basic structure containing α-helices and β-strands repeated 8 times to form a barrel like tertiary structure [134]. Interestingly, AKR1C4 is liver-specific, AKR1C3 is mostly prominent in the prostate and mammary glands, and AKR1C1 and AKR1C2 are the major isoforms in the testis, brain, and are also highly expressed in the lung and liver [48].

Members of the SDR and AKR superfamilies often exert their action toward a specific ketone or aldehyde moiety of a carbon of the common basic sterane structure of the steroids (Figure 4, carbon positions numbered). In some cases, the enzymes name refers to the reaction toward a moiety on a specific carbon position (e.g. 11βHSDs act on carbon 11 leading toward a hydroxyl substituent on a beta plane of the steroid). However, names can be misleading as there may be activity toward multiple carbon positions to which the name does not reflect the preferred reaction.

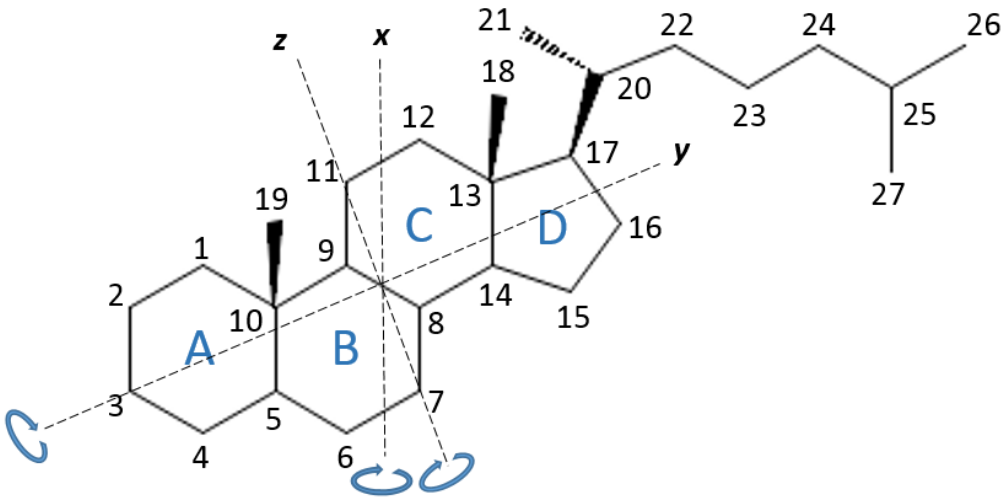

Figure 4: Common steroid structure with numbered carbons and ring letters used for nomenclature and three rotational plans x, y, z of the steroid molecule.

The steroidal core structure consists of three cyclohexane rings (A,B,C) and one cyclopentane ring (D) fused together [135]. Because of the molecular symmetry of this structure, SDR and AKR enzymes often show ligand promiscuity by binding carbonyl or hydroxyl groups on carbons opposite on specific symmetry plans (*x, y or z*) of the structure [136]. Usually, AKRs work at the 3-, 17-, and 20-ketosteroid positions [137], instead SDRs work either similarly on the same positions, or on the 11- or 7- positions. A good example is 11βHSDs that acts preferentially toward the carbon in 11-position, but also toward 7-position for 7-ketocholesterol and 7-ketolitocholic acid [138]. The similar catalytic mechanism for both SDRs and AKRs is a bi-bi kinetic in which the cofactor binds first and leaves last in two sequential isomerization steps [110], as depicted in Figure 5.

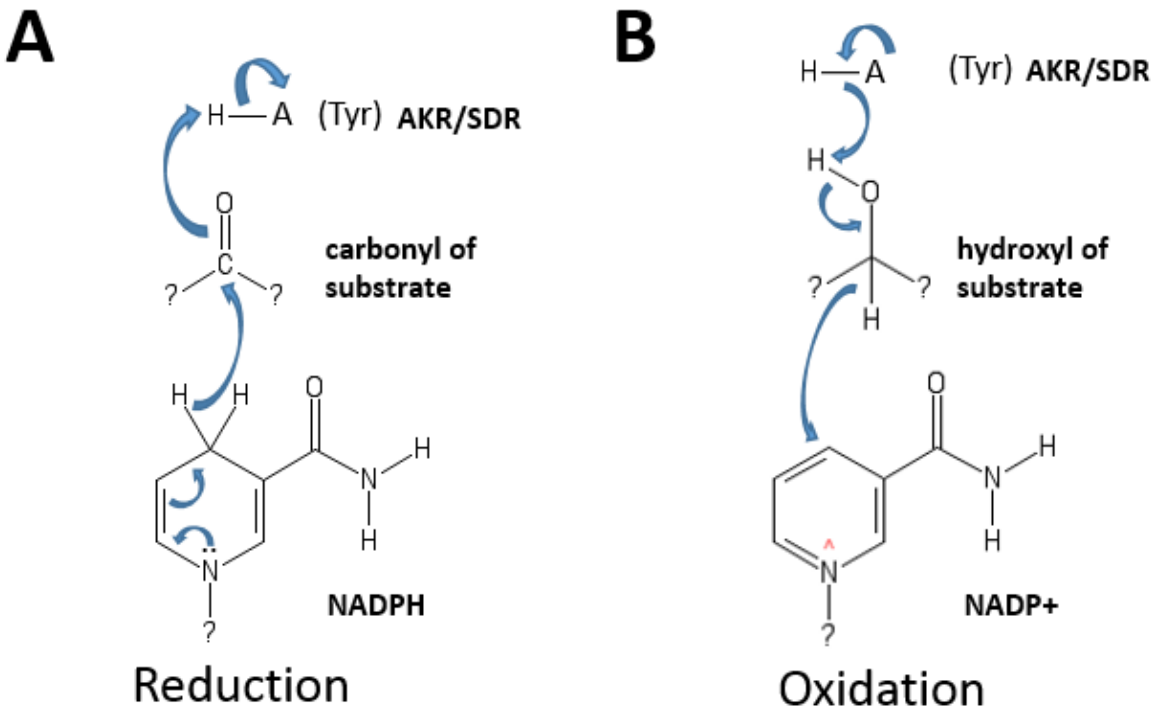

Figure 5: The reaction mechanism catalyzed by carbonyl reduction by SDR and AKR enzymes. A. Under reduction, the cofactor NAD(P)H binds and donates a proton to the carbonyl residue of the substrate, that binds to the tyrosine (Tyr) of the active site of the enzyme AKR or SDR accepting another proton. B. Under oxidation, the cofactor NAD(P)+ accepts a proton from the hydroxy group of the substrate, and tyrosine (Tyr) of the active site of the enzyme donates electrons to create a carbonyl group.

It is generally believed that the enzymatic preference toward dehydrogenation or reduction *in vivo* is determined by the cellular localization, pH conditions (reduction is more likely to happen in acidic conditions, instead oxidation is more likely to happen in alkaline conditions), cellular compartment concentration ratio of cofactor NA(P)D+/NAD(P)H [139], as well as substrate and product availability. Usually, because of the prevalence of oxidised NAD(H), NAD(H)-dependent enzymes with cytosolic localization will likely oxidize their substrates; on the other side and due to abundance NADPH in the cytosol, NADP(H)-dependent enzymes localized to cytoplasm will likely act as reductases [49].

A schematic overview of the synthesis and inactivation of steroid hormones with the key reactions performed by HSDs (in orange) and AKRs (in green) is depicted in Figure 6. These enzymes work concomitantly with cytochrome P450 (CYP) and 5α reductases (SDR5) enzymes [140].

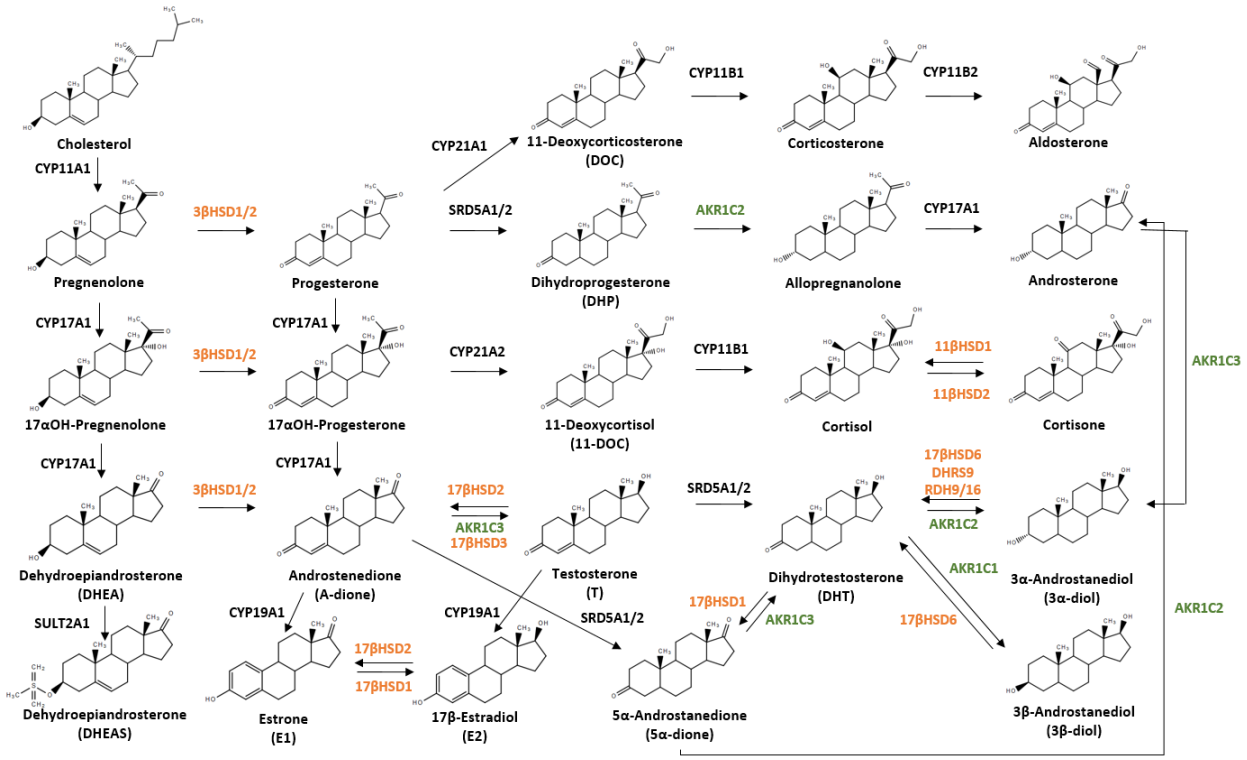

Figure 6: Schematic overview of steroidogenesis and androgen synthesis according to [17, 137, 140, 141].

2.4 The "Orphan" Enzyme DHRS7

The SDR family member 7 (DHRS7), also named retSDR4, and according to the systematic nomenclature SDR34C1, is a poorly characterized microsomal enzyme, which is a member of the cluster C3 (Figure 3). The *DHRS7* gene is located on human chromosome 14q23.1 and encodes two isoforms produced by alternative splicing: the isoform 1 consists of 339-amino acid enzyme (ca. 38 kDa) and the isoform 2 consists of 289-amino acids and misses the amino acids 1-50 of isoform 1 at the N-term (ca. 32 kDa). Isoform 1 with its sequence, predicted Rossman fold, active site, and intermembrane domain regions is shown in Figure 7.

A

MNWELLLWLLVLCALLLLLVQLLRFLRADGDLTLLWAEWQGRRPEW
ELTDMVVWVTGASSGIGEELAYQLSKLGVSLVLSARRVHELERVKRRC
LENGNLKEKDILVLPLDLTDTGSHEAATKAVLQEFGRIDILVNNGGMS
QRSLCMDTSLDVYRKLIELNYLGTVSLTKCVLPHMIERKQGKIVTVNSIL
GIISVPLSIGYCASKHALRGFFNGLRTELATYPGIIVSNICPGPVQSNIVE
NSLAGEVTKTIGNNGDQSHKMTTSRCVRLMLISMANDLKEVWISEQ
PFLLVTYLWQYMPTWAWWITNKMGKKRIENFKSGVDADSSYFKIFKT
KHD

B

Sequence identity	Motif	Predicted amino acid sequence
Active site (AS)	YxxxK	203-207
Rossman Fold (RF)	TGxxxxGxG	56-69
Intermembrane domain		5-23

C

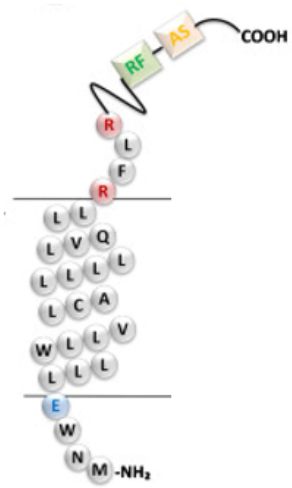

Figure 7: Predicted 2D structure of DHRS7. Amino acid sequence of DHRS7 from N- to C- term (A), with predicted intermembrane domain (Rossman Fold (RF) in green and active site (AS) in yellow adapted from [125], and intermembrane domain in violet based on TMHMM prediction [142], and relative 2D structure (the positively charged amino acids close the membrane spanning domain are labelled in red, the negative amino acids are labelled in blue) (C).

DHRS7 was first cloned from the retina [143], and its mRNA is present in various tissues including the retina, liver, kidney, adrenal gland, digestive tract, thyroid, being particularly high in prostate and salivary gland [144]. At the protein level, DHRS7 is particularly high in thyroid, liver, intestine, adrenal gland and prostate (but not measured in the salivary gland) [145]. Interestingly, DHRS7 is localized to the membrane of the endoplasmic reticulum, as shown in endoplasmic reticulum preparation [146], in human prostate cell lines [147], as well as in heart muscle and the spleen of the rat [148, 149]. However, nuclear rim staining in rat liver has also been observed [148, 149].

Reduced expression of DHRS7 was observed in the epithelial cells of prostate cancer [150], and later confirmed in biopsies of greater severity as measured by Gleason score [147]. SiRNA depletion of DHRS7 resulted in enhanced proliferation, migration and decreased adherence in a prostate cancer cell line [147]. Moreover, an upregulation in DHRS7 protein was shown in prostate cancer LNCaP cells treated with miR-663, which induced proliferation with an increased number of cells in S-phase cell cycle [151]. They investigated DHRS7 as it was suggested to have a sequence that would be mutually complementary to miR-663, a potential player in the transition to a castration resistant prostate cancer phenotype.

Additionally, an abstract indicated that the androgen receptor positive breast cancer cell line MCF-7 [152] transfected with DHRS7 was shown to have an increased number of cells in the S-phase and *DHRS7* depletion using shRNA transfected into the MCF-7 cell line increased the number of cells in the G2/M

phase of the cell cycle [153], suggesting cell cycle arrest and cell cycle downregulation, respectively. They also observed downregulation of DHRS7 in breast infiltrating carcinoma compared to breast cancer *in situ.* However, detailed information reporting these results are not accessible.

Taken together, the role of DHRS7 in cancer through androgen receptor dependent or independent mechanisms is still unclear. Based on the mechanisms of metabolism of other SDRs and the proliferation effects observed upon its silencing, DHRS7 may play a role in androgen receptor dependent prostate cancer by decreasing the levels of active androgens, eventually leading to diminished nuclear translocation and activation of the androgen receptor (AR); on the other hand, it might contribute to the metabolism in castration resistant prostate cancer (CRPC), promoting cancer progression, even in the absence of testicular or adrenal androgens. This could happen through the production of a ligand that would inhibit prostate cancer progression. Its role as possible tumor suppressor needs to be further elucidated.

In addition to prostate cancer, altered expression of DHRS7 has been observed in other human diseases, animal and cellular models. However, the following observations were not the primary focus of the publications. An increase in DHRS7 mRNA was observed in the muscle of patients with diabetes mellitus type 2 [154]. Additionally, DHRS7 was upregulated following fatty acid treatments in MIN6 insulinoma cells [155]. Moreover, altered expression of DHRS7 has been observed in the liver of rat and mouse models of the following conditions/diseases: DHRS7 mRNA was upregulated during liver regeneration following hepatectomy [156], and DHRS7 mRNA was downregulated in streptozotocin induced diabetic rats following resveratrol treatment [157]. Furthermore, DHRS7 protein expression was increased in the liver of protein kinase C (PKC) knock-out mice when fed with high-fat diet [158]. Instead, DHRS7 mRNA upregulation was observed also under free fatty acids treatment in goose hepatocytes *in vitro* [159].These observations could be due to a cellular adaptation in response to altered fatty acid metabolism or inflammation changes.

Interestingly, DHRS7 mRNA was determined to be ca. 180 times higher in male compared with female obese ZSF1 rats (a model of type 2 diabetes) [160], suggesting sex related effects. As well, DHRS7 mRNA increased ca. 30 fold and 20 fold in mouse liver treated with the murine constitutive androstane receptor (CAR) agonist TCPOBOP (1,4-Bis-[2-(3,5-dichloropyridyloxy)]benzene, 3,3’,5,5’-Tetrachloro-1,4-bis(pyridyloxy)) and the pregnane X receptor (PXR) ligand PCN (pregnane-16α-carbonitrile), respectively [161]. CAR and PXR are nuclear receptor which play an important role for the elimination of cholesterol and xenobiotic metabolism [162].

As shown in Figure 3, the phylogenetically closest SDR genes to DHRS7 are the poorly characterized *DHRS7b* (SDR32C1) and *DHRS7c* (SDR32C2), the well characterized *11β-HSD1* (SDR26C1), the sparsely characterized *17β-HSD12* (SDR12C1) and well characterized *17β-HSD3* (SDR12C2) [163]. DHRS7B loss of function studies in mice showed this protein to be important for adipogenesis and consequent PPARγ activation [164], whereas DHRS7C, whose expression is enriched in adipose tissue and muscles, seems to have a role in maintaining intracellular Ca^{2+} homeostasis, its overexpression in muscle activates mTORC2 enhancing glucose metabolism and muscle performance, and works as an all-trans-retinol dehydrogenase [165-167]. Further, 11β-HSD1 is well known to metabolize the inactive cortisone to the active steroid cortisol and to have a role in the regulation of local tissue glucocorticoid concentrations [168-172]. 17β-HSD12 seems to be important for the fatty acid elongation cycle by regulating arachidonic acid synthesis by the reduction of 3-ketoacyl-CoAs [173, 174]. Finally, 17β-HSD3 metabolizes androstenedione into the active androgen testosterone [175, 176].

In vitro assays reported that DHRS7 metabolizes endogenous substrates bearing a carbonyl group; on a steroid structure (estrone, cortisone, Δ 4-androstene-3,17-dione), toward the retinoid all-trans-retinal, and on exogenous substances (1,2-naphtoquinone, 9,10-phenantrenequinone, benzoquinone, nicotine-derived nitrosamine ketone (NKK), isatin, nitrosamine 4-(methyl-nitrosamino)-1-(3-pyridyl)-1-butanone), 3,4-hexanedione, and diphynylethandione), with preference toward the cofactor NADP(H) [145, 146]. However, these activities were shown with supraphysiologic concentrations of candidate substrates toward the purified DHRS7, and they were calculated mainly with indirect cofactor measurements methods. Michaelis–Menten kinetic parameters were calculated only for all-trans-retinal leading to low affinity (Km = 24.3 mM, Vmax = 270.3 nmol/ (min x mg)) [145]. However, DHRS7 is still considered an “orphan" enzyme, i.e., an enzyme whose endogenous substrates are not known, as these *in vitro* observations do not provide as yet convincing evidence for a physiological function of the enzyme.

2.5 Deorphanization

To “deorphanize” proteins is a crucial step to understand their physiological roles in health and disease and to evaluate and understand adverse and/or beneficial unintentional “off-target” drug effects. Unfortunately, the exciting opportunity to characterize the function of these “orphan” proteins remains a major challenge, and especially for membrane proteins, such as many of the SDRs, which are embedded in the organelle bilayers or the cell surface [177].

Approaches to deorphanize SDRs vary from targeted methods such as sequence comparison, structural insight with the help of crystallization and *in silico* modelling, as well as assays were by targeted substrates are used. On the other hand, with the absence of *a priori* knowledge of substrates, untargeted high throughput biology methods (DNA and RNA microarrays, proteomics, lipidomics and metabolomics) are often chosen [177-179]. A summary of the current techniques is depicted in Table 2.

Table 2: Adapted from [179]: Strategies for identification of new enzyme functions and metabolic pathways of orphan enzymes.

Techniques available	Enzyme/ genetic requirements	Purposes	Advantages	Inconveniences	Key technologies
In vitro activity-based profiling	Purified, homogeneous enzyme	Track enzyme-induced changes in a complex metabolite extract	High throughput. No *a priori* knowledge of substrates and products, and type of chemistry catalyzed.	Purification of enzyme to homogeneity. Culture of host species. Recombinant expression might lead to loss of native partner or post-translational modifications required for activity. Substrates might not be present at quantifiable levels in molecular extract.	Protein purification, LC/GC/CE-MS, NMR, libraries of spectral data
Ex vivo metabolomics profiling – genetically modified/chemicall y treated organism	None or verified genetic knock-out/over-expression strain of organism of interest	Identify one enzymatic reaction or pathway that is disturbed upon deletion/alteration of levels of a particular enzyme	High throughput. No *a priori* knowledge of substrates and products, and type of chemistry catalyzed. No enzyme purification required. Preservation of native enzyme partners and post-translational modifications.	Culture of host species. Candidate substrates and products might constitute secondary effect changes. Levels of substrates/products might be tightly controlled and not change. Chemical with a clear phenotype must be available.	Genetic manipulation LC/GC/CE-MS, NMR, libraries of spectral data
Activity-based protein profiling	None	Track of a specific class of enzymes towards a probe	High throughput. Identify active enzymes. Highly specific for chemistry and enzyme class. No enzyme purification required. Preservation of native enzyme partners and post-translational modifications.	Culture of host species. Highly selective and specific probe need. Subsequent identification of physiological substrates.	Chemical probe, gel electrophoresis, imaging, protein identification
Computational enzymology	High-resolution structure	Identification of putative substrates, products and intermediates based on structural determinants.	High throughput *in silico* approach. No *a priori* knowledge of substrates, and type of chemistry catalyzed.	Relies on strength of ligand docking software and accuracy of crystal structure. Identified compounds might not exist in the host organism.	Docking virtual libraries, computation
X-ray crystallography	Purified, homogenous enzyme High resolution structure	Identity trough co-purified small molecules	Tightly bound ligands can directly lead to the identity of substrates/products/intermediates	Co-purification with tightly bound metabolite. Enzymes must be crystallized, and structure solved at high resolution.	Protein purification, crystallization, structure, determination

3 Aims of the Thesis

Mechanisms leading to prostate cancer development and progression are heterogeneous and not clearly understood; therefore, it remains a major challenge to fill the knowledge gaps to help improve the therapy of patients. Reduced expression of DHRS7, a member of the SDR family, is associated with prostate cancer progression and severity. Loss of DHRS7 through siRNA depletion caused prostate cancer cell lines to exhibit a more aggressive phenotype. However, as with many other SDRs associated with cancer, the specific mechanisms underlying the observational phenotype have not been characterized. Particularly, it remains unclear if DHRS7 plays a role through androgen -dependent or -independent mechanisms. Experiments conducted using purified DHRS7 identified several potential low affinity endogenous and exogenous substrates. However, the candidate substrates were not tested in biological systems, the activity assays were mainly performed using supraphysiological concentrations, and they were measured via indirect cofactor consumption measurements. Additionally, the known endogenous physiological actions of these candidates provide no explanation for the functional effects observed in the prostate cancer cell lines.

The work undertaken in this thesis was designed to provide further insights into the function of DHRS7. In a first part, data will be presented showing the *in vitro* activity of the "orphan" enzyme DHRS7 toward selected substrates. In addition, further characterization of the observed association between the expression of DHRS7 and cancer progression will be explored using molecular and cell biology techniques in cancer cell lines endogenously expressing DHRS7. The following experimental aims have been addressed:

(1) **To identify potential DHRS7 substrates.** Recombinant and stable human DHRS7 expression in intact HEK-293 cells was used to test DHRS7 activity towards selected substrates. Candidate substrates were chosen based on literature search, phylogenetic similarity of DHRS7 to other SDR enzymes, and the potential of the candidates to stimulate cellular proliferation. Analytical methods used to identify and quantify the analytes comprised mass spectrometry and radioactivity assays. Functional relevance of promising relevant activity for proliferative effect in prostate cancer was further explored with androgen receptor transactivation assays in overexpressing cells. Furthermore, an activity assay using cell lysates and microsomal endoplasmic reticulum preparation of stably transfected DHRS7 cells was used to validate previous results and screen for new potential substrates and inhibitors.

(2) **To understand potential physiological roles of DHRS7.** Human cell lines endogenously expressing DHRS7 derived from breast and prostate cancers were used to characterize functional and phenotypic effects of DHRS7 following siRNA depletion. Techniques used range from cancer cell phenotypic assays, disruption of adrenal steroidogenesis assay, and an improved time-dependent untargeted proteomics method based on LC-MS/MS analysis. Some of the altered proteins detected through proteomics analysis were validated by cell cycle analysis, as well as western blot and immunofluorescence analyses. Some of these altered proteins following siRNA mediated DHRS7 knock-down raised new hypotheses on phenotypical changes denoting increased cancer aggressivity.

4 Chapter 1: Toward the Identification of Substrates of DHRS7

As it is the case for other SDRs and AKRs enzymes, a clear explanation for the mechanism of action that underpins the association of DHRS7 with cancer remains to be uncovered. DHRS7 is an "orphan" enzyme and may exert metabolic activity toward substrates present in the tissue of interest, which may, in part, be responsible for the observed aggressive cancer phenotype. The manipulation of DHRS7 may contribute to clinical adverse health effects, since DHRS7 showed the potential to be a tumor suppressor gene in prostate cancer. Therefore, it is important to identify and characterize the substrates and potential non-selective inhibitors of DHRS7. In this first chapter, the aim was to characterize the *in vitro* activity of potential physiologically relevant substrates of DHRS7.

As highlighted in chapter 2.5 of the introduction, "deorphanization" remains a major challenge and the strategy selected to undertake this difficult task must be planned carefully according to the knowledge available on the enzyme of interest. Regarding DHRS7, the following strategies were taken into consideration and led to the selection of a targeted "deorphanization" method:

- **DHRS7 is an endoplasmic reticulum membrane bound enzyme.** This makes a x-ray crystallization approach with further structural studies very difficult as with other membrane bound proteins [177]. However, with this approach, an important challenge with respect to the protein is to obtain high quantity and purity following overexpression and isolation from the endoplasmic reticulum, as well as solubilization and reconstitution of the protein while preserving the macromolecular organization [180]. The latter aspect is specifically tedious regarding membrane proteins as it must be performed in a physiological buffer and this leads to complications in the x-ray analysis. Because of these complexities a crystallization approach was not considered in the present project.

- **DHRS7 is a member of the SDRs superfamily**. SDRs enzymes have a broad substrate spectrum, share low sequence similarity, and are in most cases also able to convert multiple substrates [129]. Thus, phylogenetically related and well characterized members, such as 11βHSD1 (sequence identity (38%) and similarity of alignment (57%)), may not necessarily be structurally similar enough to set up a *in silico* tool for DHRS7 substrate prediction and substrate docking studies. Moreover, substrate docking based on publicly available databases, such as the human metabolome database (HMDB, www.hmdb.ca), is only successful if the predictable active site shows clear spatial hints for the docking of substances. This approach was previously used by our group but showed to be too speculative to generate valuable hypotheses for selection of substrates to screen [unpublished data].

Nevertheless, functional redundancy regarding 3D structure could translate in activity towards similar substrates between 11βHSD1 and DHRS7 and represents a valuable point of departure for selecting compounds to test. Consequently, the known substrate of the well-characterized and phylogenetically related 11βHSD1 and 17βHSD3, the glucocorticoid cortisone and the androgen androstenedione, respectively, represent interesting candidates to test.

- **DHRS7 shows reductive activity towards carbonyl compounds in the presence of a cofactor and behaves as tumor suppressor in prostate cancer cell lines.** Specifically, a recent study based purely on activity assays with purified DHRS7 to test potential substrates revealed that DHRS7 catalyzed the reduction of cortisone to cortisol, androstenedione to testosterone, and all-trans-retinal to all-trans-retinol [145, 146]. However, the affinities calculated in these studies were at supraphysiological concentrations. Nevertheless, it is important to note that measurements of activities of purified membrane enzymes such as DHRS7 have their disadvantages; one being the potential for inaccurate folding during expression and purification steps, which may result in potential loss of activity (according to [145, 146] DHRS7 was purified from microsomes of DHRS7 overexpressed Sf9 insect cells), another disadvantage being suboptimal conditions of the activity measurements. Taking these limitations into account, studies carried out in the DHRS7 endogenously expressing prostate cancer LNCaP cell line do not support or do not clearly demonstrate activity towards the previously mentioned reductive reactions. In fact, DHRS7 has been shown to be a potential tumor suppressor in prostate cancer by increasing proliferation and migration and decreasing adhesion in LNCaP under siRNA mediated downregulation [147]. Current evidence does not indicate the potential for one of the afore mentioned substrates to be linked with DHRS7 in LNCaP, since:
    - cortisone and cortisol addition showed no proliferation effects in LNCaP [181];
    - testosterone, the potential product of the reaction by reduction to androstenedione, causes an increase rather than a decrease in the proliferation of LNCaP cells [182];
    - all-trans retinal and the reductive product all-trans retinol are not known for their proliferation effects in LNCaP. However, all-trans retinoic acid (a product of all-trans retinal) and its analogues, showed divergent proliferation effects in LNCaP [182, 183] with a biphasic profile [182] that seems to be dependent on the passage of the cells [184].

For these reasons, and in addition to the glucocorticoid cortisone and the androgen androstenedione, the retinoid all-trans retinal was also validated in activity assay with DHRS7 in low concentrations ranges.

- **DHRS7 is expressed in many organs of the human body with increased protein expression in tissues involved in exocrine and/or endocrine metabolism**. The protein expression patterns of DHRS7 suggest that potential substrates may be hormones, chemicals involved in or a part of exocrine secretion, or chemicals important for epithelial phenotype and/or differentiation. Thus, as for other SDRs, glucocorticoids, steroidal hormones, prostaglandins, and retinoic acids could all represent potential candidates to investigate. Regarding these classes of substrates, in addition to cortisone, androstenedione, and all-trans retinal, the androgen DHT and progesterone – both important metabolites in the context of prostate cancer, will be tested. Interestingly, both DHT and progesterone have been shown to increase proliferation in LNCaP cells by activation of their respective nuclear receptors [185-190]. Additionally, other substrates which share steroidal biochemistry symmetry will be further explored (see Figure 4 of the introduction).

- **Immortalized human cell lines are biological models expressing functional transport systems and they are metabolically active**. Human cell models allow us to study the metabolism of substrates in the presence of cofactor at physiological concentrations in a cellular environment. However, it is important to understand their limitations with respect to the substrates tested. For example, for an activity assay to work the substrate must be transported across the plasma membrane and be able to directly access the intracellular compartment in which the tested enzyme resides by avoiding binding to intracellular proteins (e.g. DHRS7 is expressed at the endoplasmic reticulum membrane). Metabolites unable to pass through cell membranes must be tested using protein preparations. Moreover, the candidate substrates should not be metabolized by other enzymes in the chosen cell model. For these reasons, different biological systems are used and validated to study enzyme activity.

These aspects set the basis for the following planned strategy summarized as a workflow in Figure 8.

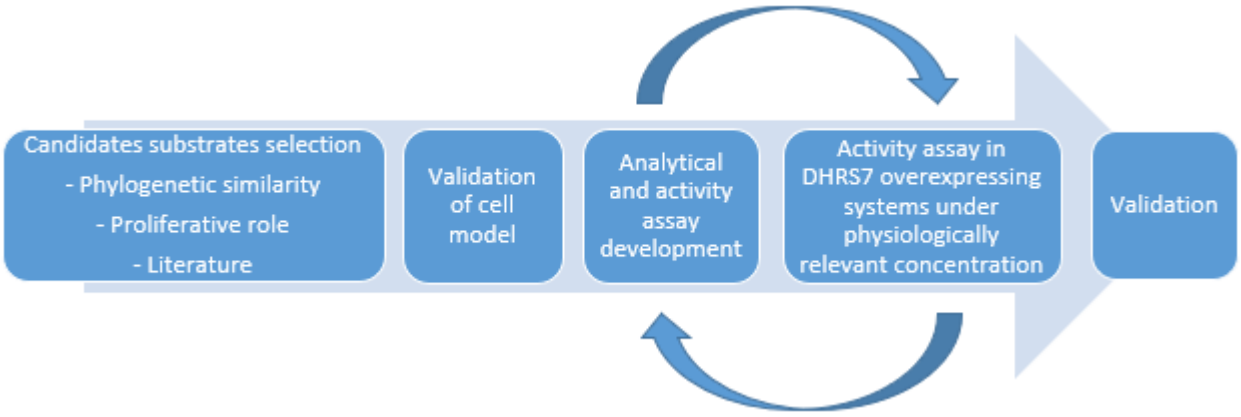

Figure 8: Workflow of strategy attempted to characterize in vitro DHRS7 activity.

The first section of this chapter presents a published article showing activity assays in intact HEK 293 cells ectopically expressing human DHRS7 (validated in the result section 4.2.2.1) for the candidate substrates cortisone, androstenedione and the main AR ligand DHT. All experiments where performed at a physiological concentration and LC-MS/MS and radioactivity following TLC separation (further referred only as radioactivity) methods were used to analyze the activity of DHRS7. DHT showed the most promising potential to be a relevant substrate and was investigated further using an AR transactivation reporter assay. Results suggest that DHRS7 may potentially play a protective role by reducing the AR activity in the presence of DHT. Moreover, the orientation of microsomal DHRS7 was tested and confirmed that the active site faces the cytoplasm and not the lumen of the endoplasmic reticulum.

With the previous publication, *in vitro* overexpression assays showed that DHRS7 possess characteristics of a 3α/20β reductase toward steroidal structures showing similarity to AKR1C enzymes, especially AKR1C2, and that DHRS7 metabolized the active androgen dihydrotestosterone (DHT) to the inactive 3αAdiol. In the second section of this chapter, to further characterize DHRS7's metabolism toward steroids in the 3α/20β positions, the DHRS7 HEK 293 cell line was used for *in vitro* screenings. Results are presented for four compounds with the potential for metabolism in the 3α/20β positions using intact cells and LC-MS/MS analysis.

Next, the model compound DHT was used to develop an optimized DHRS7 lysate activity assay to validate previous observations and to be used as a screening tool for the discovery of new substrates and inhibitors of DHRS7. The lysate activity assay avoids *a priori* development of an analytical LC-MS/MS method for quantification of the each of the studied metabolites, which is low throughput, time consuming, and expensive. Using the screening tool, results are presented from 24 candidate substrates selected based on

the publication and results presented in this chapter, the compounds potential biochemistry activity according to literature, and xenobiotics having a possible role in cancer.

Finally, data will be presented showing our attempts to calculate an apparent Km for DHT using lysate and microsomes isolated from the DHRS7 HEK 293 cells and analyzed by radioactivity.

4.1 Published article: DHRS7 (SDR34C1) - a New Player in the Regulation of Androgen Receptor Function by Inactivation of 5α-Dihydrotestosterone?

Journal of Steroid Biochemistry and Molecular Biology 171 (2017) 288–295

Contents lists available at ScienceDirect

Journal of Steroid Biochemistry and Molecular Biology

journal homepage: www.elsevier.com/locate/jsbmb

DHRS7 (SDR34C1) – A new player in the regulation of androgen receptor function by inactivation of 5α-dihydrotestosterone?

Selene Araya, Denise V. Kratschmar, Maria Tsachaki, Simon Stücheli, Katharina R. Beck, Alex Odermatt*

Division of Molecular and Systems Toxicology, Department of Pharmaceutical Sciences, University of Basel, Klingelbergstrasse 50, 4056 Basel, Switzerland

ARTICLE INFO

Keywords:
DHRS7
SDR34C1
Androgen
Metabolism
Steroid
Dehydrogenase
Dihydrotestosterone

ABSTRACT

DHRS7 (SDR34C1) has been associated with potential tumor suppressor effects in prostate cancer; however, its function remains largely unknown. Recent experiments using purified recombinant human DHRS7 suggested several potential substrates, including the steroids cortisone and Δ4-androstene-3,17-dione (androstenedione). However, the substrate and cofactor concentrations used in these experiments were very high and the physiological relevance of these observations needed to be further investigated. In the present study, recombinant human DHRS7 was expressed in intact HEK-293 cells in order to investigate whether glucocorticoids and androgens serve as substrates at sub-micromolar concentrations and at physiological cofactor concentrations. Furthermore, the membrane topology of DHRS7 was revisited using redox-sensitive green-fluorescent protein fusions in living cells. The results revealed that (1) cortisone is a substrate of DHRS7; however, it is not reduced to cortisol but to 20β-dihydrocortisone, (2) androstenedione is not a relevant substrate of DHRS7, (3) DHRS7 catalyzes the oxoreduction of 5α-dihydrotestosterone (5αDHT) to 3α-androstanediol (3αAdiol), with a suppressive effect on androgen receptor (AR) transcriptional activity, and (4) DHRS7 is anchored in the endoplasmic reticulum membrane with a cytoplasmic orientation. Together, the results show that DHRS7 is a cytoplasmic oriented enzyme exhibiting 3α/20β-hydroxysteroid dehydrogenase activity, with a possible role in the modulation of AR function. Further research needs to address the physiological relevance of DHRS7 in the inactivation of 5αDHT and AR regulation.

1. Introduction

DHRS7 belongs to the large family of short-chain dehydrogenase/reductase (SDR) enzymes, with at least 75 members in the human genome that are involved in various essential physiological functions [1,2]. SDRs share a conserved NAD(P)(H) cofactor binding region, the so-called Rossmann-fold, a catalytic tetrad Asn-Ser-Tyr-Lys motif in the majority of the members, and a dimerization region [3]. They are involved in the metabolism of a wide array of substrates including steroids, bile acids, oxysterols, fatty acids, retinoids, carbohydrates and xenobiotics, and they typically share low sequence identity between 20 and 30%. To date, the functions of about half of all SDR enzymes is still unknown and uncovering their functions remains a challenge.

The physiological function of DHRS7 still remains to be elucidated. Nevertheless, reduced DHRS7 expression has been found in prostate cancer [4,5], and knock-down of DHRS7 in human LNCaP prostate cancer cells enhanced cell proliferation and migration but reduced cell adhesion [5], suggesting a role as tumor suppressor. DHRS7 was shown to be an endoplasmic reticulum (ER) membrane protein, and its catalytic moiety proposed to face the ER-luminal compartment [6]. Previous studies reported the expression in Sf9 cells and purification of recombinant human DHRS7 [7] and proposed several endogenous (cortisone, estrone, Δ4-androstene-3,17-dione (androstenedione), all-trans-retinal) and exogenous substrates (diphenylethanedione, 3,4-hexanedione, metyrapone, isatin, the tobacco constituent NNK, oxcarbazepine, 1,2-naphthoquinone) [6,8]. However, so far, the relevance of DHRS7 in the metabolism of these substrates was not further studied.

The present work aimed to further characterize possible physiologically relevant steroidal substrates of DHRS7 that might play a role in the observed inhibitory effects on prostate cancer cell proliferation and tumor aggressiveness. A possible role of DHRS7 in the interconversion of cortisone/cortisol was studied due to the anti-proliferative, pro-apoptotic effects of cortisol, whereas a possible role in the interconversion of androstenedione/testosterone and 5α-dihydrotestosterone (5αDHT)/3α-androstanediol (3αAdiol) was assessed due to the modulation of androgen receptor (AR) activity and prostate cancer cell

* Corresponding author.
E-mail address: Alex.Odermatt@unibas.ch (A. Odermatt).

http://dx.doi.org/10.1016/j.jsbmb.2017.04.013
Received 7 March 2017; Received in revised form 10 April 2017; Accepted 26 April 2017
Available online 27 April 2017
0960-0760/

proliferation/aggressiveness. As the reaction direction of SDR enzymes depends on the intracellular cofactor availability, an intact cell system was used for the activity experiments. Finally, regarding its potential AR modulatory function, the membrane topology of DHRS7 was revisited.

2. Experimental procedures

2.1. Molecular cloning and expression constructs

The full-length untagged (DHRS7), C-terminally (DHRS7-FLAG) and N-terminally (FLAG-DHRS7) FLAG-tagged DHRS7 constructs were produced by PCR amplification of the coding sequence from a donor vector and subcloned into pcDNA3 vector (Life Technologies, Zug, Switzerland). PCR amplified untagged (AKR1C2) and C-terminally FLAG-tagged AKR1C2 (AKR1C2-FLAG) were also cloned into pcDNA3 vector. All constructs were verified by sequencing. Untagged hexose-6-phopshate dehydrogenase (H6PDH) and C-terminally Myc-tagged H6PDH (H6PDH-Myc), untagged and C-terminally FLAG-tagged 11β-HSD1, 11β-HSD2 and 17β-HSD3 expression plasmids were described earlier [9–12]. The N-terminally FLAG-tagged AR (FLAG-AR) construct was kindly provided by Dr. J. J. Palvimo (Institute of Biomedicine, Helsinki, Finland) [13].

The plasmids for the expression of roGFP2 fusion proteins with full-length DHRS7 (DHRS7-roGFP2) or with the N-terminal DHRS7 membrane anchor region (aa 1–56) (DHRS7(1–56)-roGFP2) were generated using a pcDNA3 plasmid containing the roGFP2 nucleotide sequence between the endonuclease restriction sites *Eco*RV and *Xba*I. A linker sequence (TCAGGAGGA) was added upstream of the roGFP2 sequence. The sequences corresponding to nucleotides 1–168 of DHRS7 or full-length DHRS7 were PCR amplified from a donor vector and subcloned upstream of roGFP2 between the restriction sites *Hind*III/*Eco*RV. The resulting DHRS7 proteins contain at the C-terminus a three amino acid linker (Ser-Gly-Gly) followed by roGFP2.

2.2. Cell culture

Human Embryonic Kidney-293 cells (HEK-293, ATCC, Manassas, VA, USA) were cultured at 37 °C and 5% CO_2 in Dulbecco's Modified Eagle Medium (DMEM, Sigma-Aldrich, St. Louis, MO, USA) supplemented with 10% fetal bovine serum (FBS, Connectorate, Dietikon, Switzerland), 100 U/mL penicillin, 100 µg/mL streptomycin, 10 mM HEPES buffer, pH 7.4, and 1% MEM non-essential amino acid solution.

2.3. Western blot

HEK-293 and LNCaP cells in 6-wells plates were lyzed using 100 µL RIPA buffer (Sigma-Aldrich) and centrifuged at 14,000 × *g* for 10 min at 4 °C. Supernatants were collected and protein concentrations quantified using the Pierce bicinchoninic acid protein assay kit (Thermo Scientific, Rockford, IL, USA). Samples were prepared in Laemmli solubilization buffer containing 5% β-mercaptoethanol and incubated at 95 °C for 5 min. Total protein (20 or 30 µg) was separated by SDS-PAGE on a 12% acrylamide gel and transferred to Immun-Blot polyvinylidene difluoride (PVDF) membranes (Bio-Rad Laboratories, Hercules, CA, USA). For detection of the FLAG epitope, the membrane was blocked using 10% defatted milk in 20 mM Tris buffer, pH 7.4, containing 140 mM NaCl and 0.1% Tween-20 (TBS-T) for 1 h and incubated with the mouse monoclonal FLAG M2 antibody (Sigma-Aldrich) at a dilution of 1:2000 in 5% defatted milk in TBS-T overnight at 4 °C. After washing with TBS-T, the membrane was incubated with horseradish peroxidase (HRP)-conjugated goat anti-mouse secondary antibody (Sigma-Aldrich) for 1 h at room temperature. The protein bands were visualized using a Fujifilm ImageQuant™ LAS-4000 (GE Healthcare, Glattbrugg, Switzerland) using the Immobilon Western Chemiluminescent HRP substrate kit (Merck, Kenilworth, NJ, USA). Thereafter, membranes were stripped for 10 min at room temperature in 200 mM glycine, pH 2.2, containing 1% Tween-20 and 0.1% SDS, washed twice with PBS and twice with TBS-T, followed by reincubation using rabbit anti-Myc polyclonal antibody (ab9106, Abcam, Camdridge, UK) at a dilution 1:2000 in 5% defatted milk in TBS-T for 1 h, followed by visualization of H6PDH-Myc using a HRP-conjugated goat anti-rabbit secondary antibody (1:2000) in 5% defatted milk in TBS-T. Endogenous DHRS7 was detected as described earlier [5]. The housekeeping control cyclophilin A (PPIA) was detected using a rabbit anti-human PPIA polyclonal antibody (1:2000) (Abcam, Camdridge, UK) in blocking solution for 1 h, followed by incubation with HRP-conjugated goat anti-rabbit secondary antibody (1:2000) in 5% defatted milk in TBS-T.

2.4. Enzyme activity measurements

HEK-293 cells (1.5×10^6) seeded into 10 cm dishes were transiently transfected by the calcium phosphate precipitation method with 8 µg of either construct DHRS7-FLAG, 11β-HSD1-FLAG or 17β-HSD3-FLAG and 8 µg of pcDNA3 vector without insert. For cotransfection with H6PDH-Myc, cells were transfected with 8 µg of the corresponding SDR plasmid and 8 µg of H6PDH-Myc. Cells transfected with 16 µg of pcDNA3 served as negative control. Transfected cells (30,000) were seeded in 100 µL medium in 96-well plates pre-coated with poly-lysine (Sigma-Aldrich), followed by incubation for 24 h at 37 °C. The medium was replaced by 50 µL charcoal-treated DMEM (2 g charcoal/500 mL medium, stirring for 1 h at room temperature, followed by centrifugation at 3200 × *g* for 10 min and sterile filtration using 0.2 µm nitrocellulose membranes) supplemented with 100 U/mL penicillin, 100 µg/mL streptomycin, 10 mM HEPES buffer, pH 7.4, with or without the 11β-HSD1 inhibitor BNW16 [14], and enzyme activity measurements were performed by adding cortisone or androstenedione (Sigma-Aldrich) at a final concentration of 200 nM, containing 50 nCi ^{3}H-cortisone or 50 nCi ^{3}H-androstenedione (American Radiolabeled Chemicals, St. Louis, MO, USA). At different time points reactions were stopped by adding 20 µL of methanol containing 2 mM unlabeled cortisone and cortisol (Sigma-Aldrich) or androstenedione and testosterone (Steraloids, Newport, RI, USA). An amount of 20 µL of supernatant was loaded onto TLC plates (Macherey-Nagel, Oensingen, Switzerland). Steroids were separated using chloroform/methanol at a 9:1 ratio for cortisone/cortisol, and chloroform/ethyl acetate at a 4:1 ratio for androstenedione/testosterone. Corresponding substrate and product amounts were determined by scintillation counting.

To determine possible formation of cortisol from cortisone by DHRS7 expressing HEK-293 cells, samples were separated by TLC as described above. Cortisol and 20β-dihydrocortisone (20βDHE) migrated with comparable Rf values. Spots were excised, followed by steroid extraction from the silica matrix and LC–MS/MS analysis of the extracts.

To measure the oxoreduction of 5αDHT to 3αAdiol, 100,000 cells transfected with 0.5 µg of either plasmid for DHRS7-FLAG or AKR1C2-FLAG or with pcDNA3 vector without insert (negative control) in 24-well plates were incubated in 500 µL charcoal-treated DMEM supplemented with 100 U/mL penicillin, 100 µg/mL streptomycin, 10 mM HEPES buffer, pH 7.4, and 5αDHT as indicated. After incubation at 37 °C, supernatants were collected and stored at −20 °C prior to quantification of steroids by LC/MS.

2.5. Quantification of steroids by LC/MS/MS

Steroid concentrations were determined as described in the Supplementary information. Briefly, to each sample (400 µL) internal standard (cortisol-D4, 100 µL, 125 nM) was added and proteins were precipitated with ice cold acetonitrile (1 mL). Samples were incubated for 20 min at 4 °C by thoroughly shaking and centrifuged (10 min, 16,000 × *g*, 4 °C). Supernatants were evaporated to dryness and

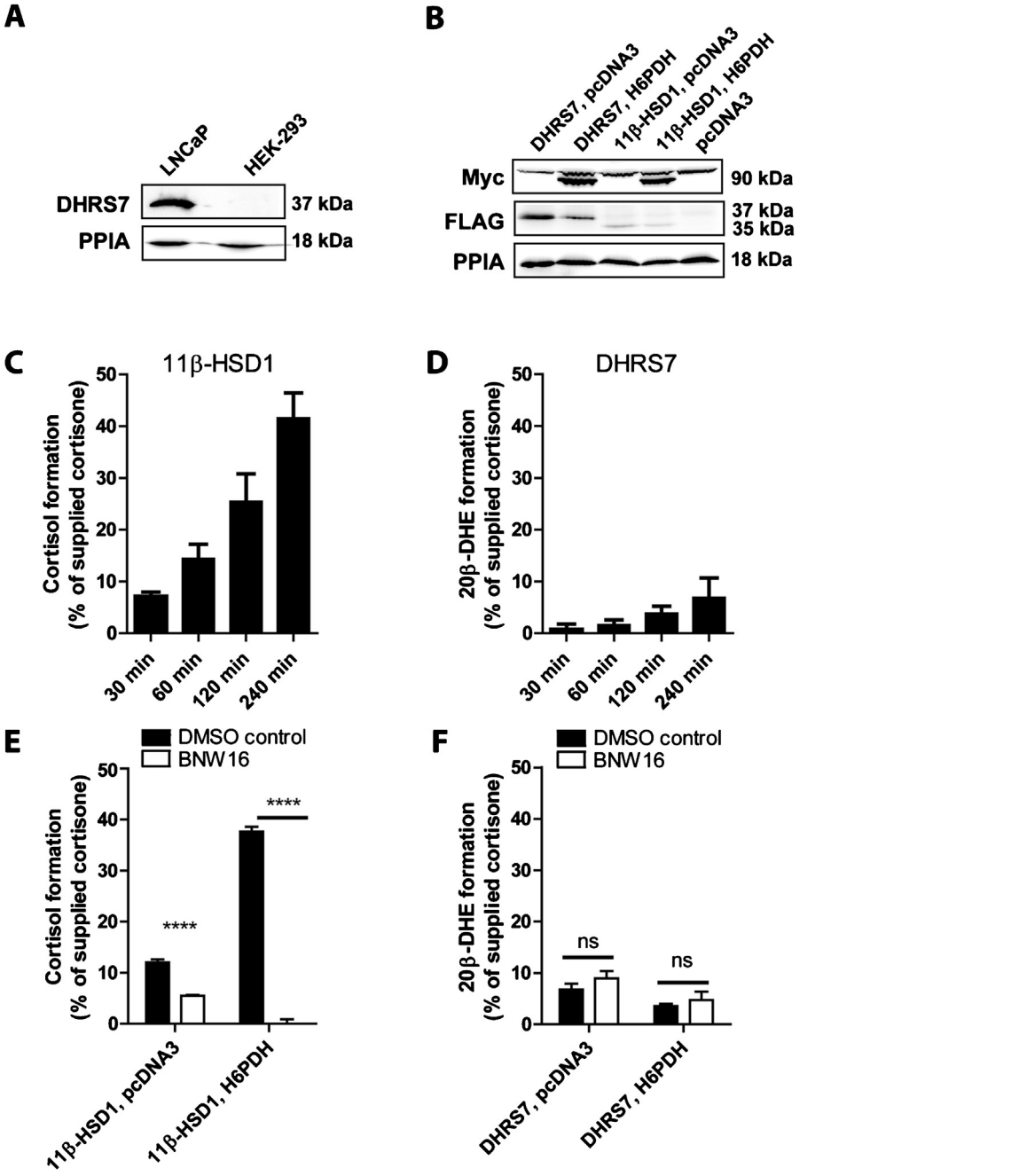

Fig. 1. Oxoreduction of cortisone by 11β-HSD1 and DHRS7. (A) The absence of endogenous expression of DHRS7 in HEK-293 cells was verified by western blotting (20 μg total protein), with PPIA serving as loading control. (B) The expression of DHRS7-FLAG and 11β-HSD1-FLAG, and H6PDH-Myc with PPIA serving as loading control were detected by western blotting (30 μg total protein). The time-dependent oxoreduction of (C) cortisone to cortisol, and (D) cortisone to 20β-DHE was determined in HEK-293 cells transiently expressing either 11β-HSD1-FLAG or DHRS7-FLAG (mean ± S.D. from three independent experiments performed in triplicates). The effects of 11β-HSD1 inhibitor and coexpression with H6PDH were analyzed on the oxoreduction of cortisone to (E) cortisol or (F) 20β-DHE. Steroids were separated by TLC and quantitated following scintillation counting (C,E) or analyzed by LC–MS/MS (D,F). ns (not significant); ****$p < 0.0001$.

reconstituted in 50 μL methanol. Steroids were separated and quantified by ultra-pressure LC–MS/MS (UPLC–MS/MS) using an Agilent 1290 UPLC coupled to a 6490 triple quadrupole mass spectrometer equipped with a jet-stream electrospray ionization interface (Agilent Technologies, Santa Clara, CA, USA). Analytes were separated using a reverse-phase column (1.7 μm, 2.1 × 150 mm; Acquity UPLC BEH C18; Waters). Masshunter software (Agilent Technologies) was used for data acquisition and analysis.

2.6. Androgen receptor transactivation assay

AR transactivation was assessed as described previously [15], with minor modifications. Briefly, HEK-293 cells (100,000 cell/well) were transiently transfected with Fugene HD (Promega, Fitchburg, WI, USA) at a reagent to DNA ratio of 3 to 1 with plasmids for FLAG-AR (0.135 μg/well), and either DHRS7-FLAG, AKR1C2-FLAG or pcDNA3 without insert (0.225 μg/well), pCMV-lacZ β-galactosidase control (0.012 μg/well) and TAT3-TATA luciferase reporter (0.133 μg/well). After 24 h cells were transferred to charcoal-treated DMEM and cultivated for 1 h at 37 °C. The medium was replaced with fresh

charcoal-treated DMEM containing various concentrations of 5αDHT (diluted from stock solutions in DMSO, final concentration of 0.1% DMSO) or vehicle control (0.1% DMSO), followed by incubation for 24 h. Cells were lyzed in 60 µL of Tropix lysis solution (Applied Biosystems, Foster City, CA) supplemented with 0.5 mM dithiothreitol (DTT) and frozen at −80 °C prior to determination of luciferase and β-galactosidase activities on a SpectraMax-L luminometer (Molecular Devices, Devon, UK) as described earlier [15].

2.7. Immunofluorescence and imaging analysis

HEK-293 cells seeded on glass coverslips were transiently transfected with either construct 11β-HSD1-FLAG, 11β-HSD2-FLAG, DHRS7-FLAG or FLAG-DHRS7, and washed twice 48 h later with PBS, fixed with 4% formaldehyde for 12 min and washed three times with PBS. For permeabilization of all cellular membranes cells were treated with 0.3% Triton X-100 for 5 min while for selective permeabilization of the plasma membrane the cells were incubated with 14 µM digitonin for 3 min at room temperature. Cells were washed twice with PBS and incubated for 30 min with blocking solution containing 2% defatted milk. Cells were then incubated for 1 h at room temperature with mouse monoclonal anti-FLAG M2 antibody (Sigma-Aldrich), and washed four times with PBS, followed by incubation for 40 min with Alexa Fluor 488 goat anti-mouse IgG and Hoechst-33342 nucleic acid stain (Molecular Probes, Eugene, OR). After four washes with PBS, cells were mounted in Mowiol 4–88. The samples were analyzed using an Olympus Fluoview 1000 laser scanning confocal microscope (Olympus, Center Valley, PA). To determine the number of cells staining positive in the presence of Triton X-100 or digitonin, approximately 1000 cells were counted per sample in three independent experiments.

The live cell microscopy experiments to determine the oxidation status of the roGFP2-fusion proteins were performed essentially as described earlier [9]. Briefly, following 48 h of expression of the roGFP2-fusions in HEK-293 cells, fluorescence emission intensities were measured after excitation at 405 nm and 488 nm at steady state, after complete oxidation of roGFP2 with 5 mM diamide, and after complete reduction with 20 mM DTT. The degree of oxidation (OxD) of roGFP2 was calculated, based on the following equation:

$$OxD\text{roGFP2} = \frac{R - R_{red}}{\frac{I_{min}}{I_{max}}(R_{ox} - R) + (R - R_{red})}$$

where R, R_{red} and R_{ox} are the 405/488 nm emission ratios at steady state, after complete reduction and oxidation, respectively, and I_{min} and I_{max} the fluorescence intensities of fully oxidized and reduced roGFP2 after excitation at 488 nm.

2.8. Statistical analysis

Activity assay data were analyzed using two-way ANOVA with Bonferroni post-test for multiple comparisons with GraphPad Prism 5 software. Values represent mean ± S.D.

3. Results

3.1. DHRS7 shows low activity in converting cortisone to 20β-DHE

Based on recent reports on the ability of DHRS7 to convert cortisone to cortisol [6,8], the present study aimed to assess the relevance of DHRS7 in the oxoreduction of cortisone by comparing its activity with that of 11β-HSD1, the well-known SDR responsible for this reaction [16]. Since the function of DHRS7 remains largely unknown and the membrane-bound enzyme might lose its activity upon removal from the ER, an intact cell system, HEK-293, was chosen to investigate potential substrates of DHRS7. Using an antibody that yields a strong signal for DHRS7 in LNCaP prostate cancer cells (Fig. 1A) and in the human prostate, as reported earlier [5], no signal could be detected in HEK-293 cells, thus indicating the absence of endogenous DHRS7 expression in this cell line. HEK-293 cells also do not express endogenous 11β-HSD1 [11]. For facilitated detection, C-terminally FLAG-tagged DHRS7 (DHRS7-FLAG) and 11β-HSD1 (11β-HSD1-FLAG) were expressed in HEK-293 cells in the presence or absence of H6PDH-Myc (Fig. 1B), yielding bands in western blots at the expected sizes. Cells were subsequently incubated with 200 nM cortisone, followed by the determination of cortisol formation. Time-dependent cortisol formation was observed for 11β-HSD1 (Fig. 1C). A 6–8 times lower activity for the formation of a product migrating on TLC with a Rf comparable to that of cortisol was observed for DHRS7 (Fig. 1D); however, LC–MS/MS analysis revealed that this product corresponds to 20β-DHE. Interestingly, while coexpression with H6PDH significantly increased 11β-HSD1 activity as reported earlier [12] (Fig. 1E), it had no or even a slight inhibitory effect on the DHRS7-mediated 20-oxoreduction activity (Fig. 1F), indicating that DHRS7 functions independently of ER-luminal H6PDH-generated NADPH. Furthermore, the selective 11β-HSD1 inhibitor BNW16 [14] abolished 11β-HSD1 activity (Fig. 1E) but did not affect DHRS7-mediated 20-oxoreduction of cortisone (Fig. 1F).

3.2. DHRS7 does not play a relevant role in the conversion of androstenedione to testosterone

Since androstenedione was recently proposed as a substrate of DHRS7 [6,8], its metabolism was analysed in intact HEK-293 cells expressing either 17β-HSD3-FLAG or DHRS7-FLAG. 17β-HSD3 time-dependently converted the supplied 200 nM androstenedione to testosterone (Fig. 2A). In contrast, no activity could be detected for DHRS7, even after prolonged incubation time (Fig. 2B). Knock-down of DHRS7 was earlier found to enhance prostate cancer cell proliferation and aggressiveness [5]. Thus, a role for DHRS7 in androgen inactivation rather than activation would be in line with these earlier observations. Therefore, the reverse reaction was also tested but no activity could be detected upon incubation of DHRS7 expressing HEK-293 cells for 4 h with 200 nM testosterone (not shown).

3.3. DHRS7 catalyzes the inactivation of the AR ligand 5αDHT to 3αAdiol

Next, a possible role of DHRS7 in the inactivation of 5αDHT was investigated. The metabolism of 5αDHT to 3αAdiol was analyzed by LC–MS/MS in culture supernatants of intact HEK-293 cells expressing either human DHRS7-FLAG or AKR1C2-FLAG as positive control, or in supernatants of cells transfected with pcDNA3 as negative control. A time-dependent (Fig. 3A) and concentration-dependent (Fig. 3B) formation of 3αAdiol was detected for both DHRS7 and the positive

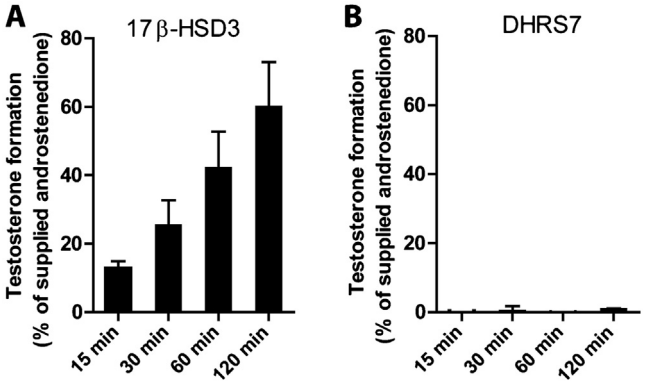

Fig. 2. Lack of substantial oxoreduction of androstenedione to testosterone by DHRS7. HEK-293 cells transiently expressing 17β-HSD3-FLAG or DHRS7-FLAG were incubated with 200 nM radiolabeled androstenedione for 15 to 120 min, followed by determination of testosterone formation. Data represent mean ± S.D. from three independent experiments.

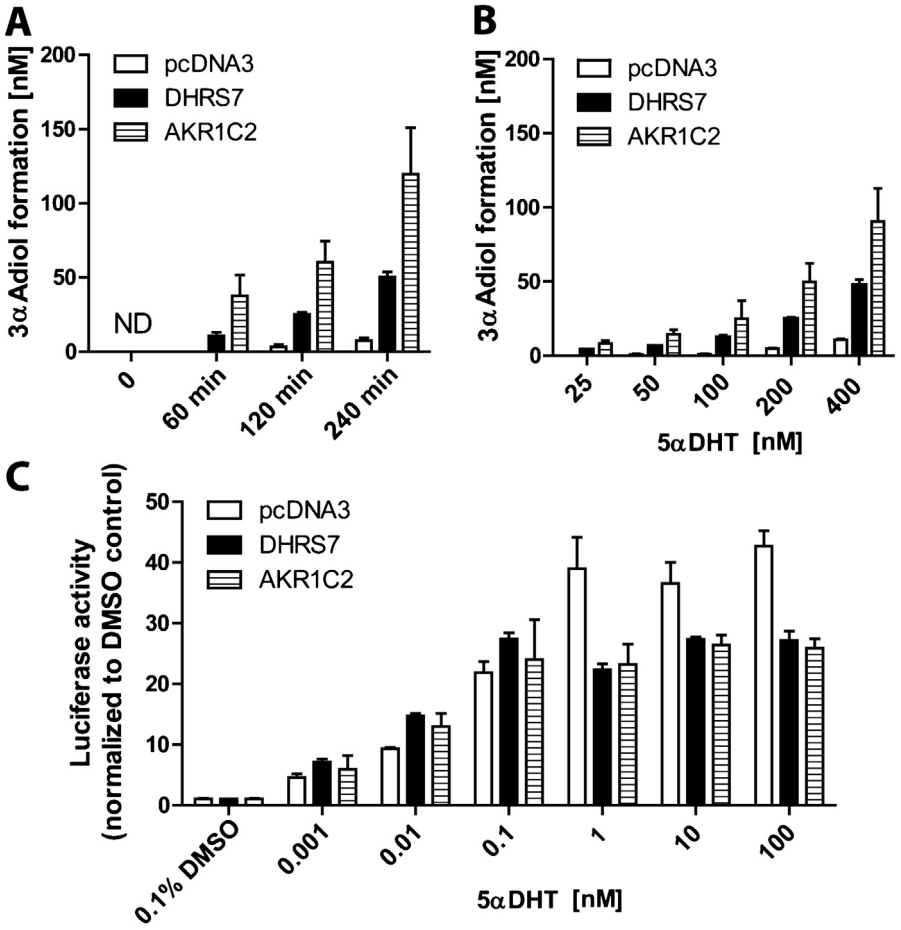

Fig. 3. Oxoreduction of 5αDHT to 3αAdiol by DHRS7. (A) The time-dependent oxoreduction of 200 nM 5αDHT to 3αAdiol and (B) the concentration-dependent oxoreduction of 5αDHT upon incubation for 240 min was determined in HEK-293 cells transfected with pcDNA3 vector without insert (negative control), pcDNA3 constructs containing AKR1C2-FLAG (positive control) or DHRS7-FLAG. Data represent mean ± S.D. from three independent experiments performed in triplicates. (C) Impact of DHRS7 and AKR1C2 on AR transactivation by 5αDHT. HEK-293 cells were transfected with plasmids for FLAG-AR, and DHRS7-FLAG, AKR1C2-FLAG or empty pcDNA3 vector, the androgen-sensitive TAT3-TATA-luciferase reporter gene and a galactosidase transfection control. Cells were incubated for 24 h with various concentrations of 5αDHT (DMSO concentration was 0.1% in all samples and 0.1% DMSO served as vehicle control), followed by determination of luciferase activity normalized to the internal galactosidase control. Data were normalized to vehicle control (0.1% DMSO) and represent mean ± S.D. from three experiments. ND, not determined.

control AKR1C2, whereby approximately two times higher activity was observed for the latter. The reaction of DHRS7 was stereo-specific and no 3βAdiol was formed. The oxidation of 3αAdiol to 5αDHT was also not catalyzed in intact HEK-293 cells expressing DHRS7 (not shown).

3.4. DHRS7 suppresses the 5αDHT-mediated AR transactivation

A concentration-dependent increase of 5αDHT-driven AR transactivation was observed in the absence of androgen metabolizing enzymes, reaching a plateau at a concentration of 1 nM (Fig. 3C). Upon coexpression with DHRS7 or the positive control AKR1C2 a similar concentration-dependent stimulation of AR activity was observed at lower concentrations of up to 0.1 nM 5αDHT; however, at concentrations of 1 nM and higher both DHRS7 and AKR1C2 were able to suppress AR transactivation.

3.5. The catalytic moiety of the microsomal enzyme DHRS7 is facing the cytoplasm

The present study showed that DHRS7 activity is not stimulated by ER-luminal H6PDH-mediated NADPH generation, unlike 11β-HSD1 activity. This suggested either the dependence of DHRS7 on an alternative ER-luminal source of NADPH or that DHRS7 may not face the ER-lumen as proposed by a recent report [8]. Therefore, the membrane topology of DHRS7 was revisited.

First, HEK-293 cells expressing DHRS7-FLAG, 11β-HSD1-FLAG, 11β-HSD2-FLAG or FLAG-DHRS7 were subjected to either selective permeabilization of plasma membranes using digitonin or complete permeabilization with Triton X-100. Following immunofluorescence staining using a primary anti-FLAG antibody and a secondary fluorescent anti-mouse antibody, the percentage of cells stained positive after treatment with digitonin was compared with that of the positive control Triton X-100 (set as 100%). Fig. 4A shows representative confocal images and Table 1 summarizes the quantification of three independent experiments. The percentage of positively stained cells following treatment with Triton X-100 or digitonin were comparable for the positive control 11β-HSD2-FLAG and for full-length DHRS7-FLAG, indicating a cytoplasmic orientation of the catalytic moiety of these two enzymes. In contrast, the FLAG epitope at the C-terminus of 11β-HSD1 or at the N-terminus of DHRS7 was protected against antibody staining by the ER membrane in case of selective plasma membrane permeabilization with digitonin, indicating ER-luminal orientation of the catalytic moiety of 11β-HSD1 and of the very short N-terminal part upstream of the membrane-spanning region of DHRS7 (Fig. 4C).

Second, fusion proteins DHRS7-roGFP2 and DHRS7(1–56)-roGFP2 were analyzed by live imaging using laser-scanning confocal microscopy after excitation with 405 nm and 488 nm and calculation of the percentage of roGFP2 oxidation at steady state (Fig. 4B). Both DHRS7-roGFP2 constructs showed a relatively low percentage of oxidation at

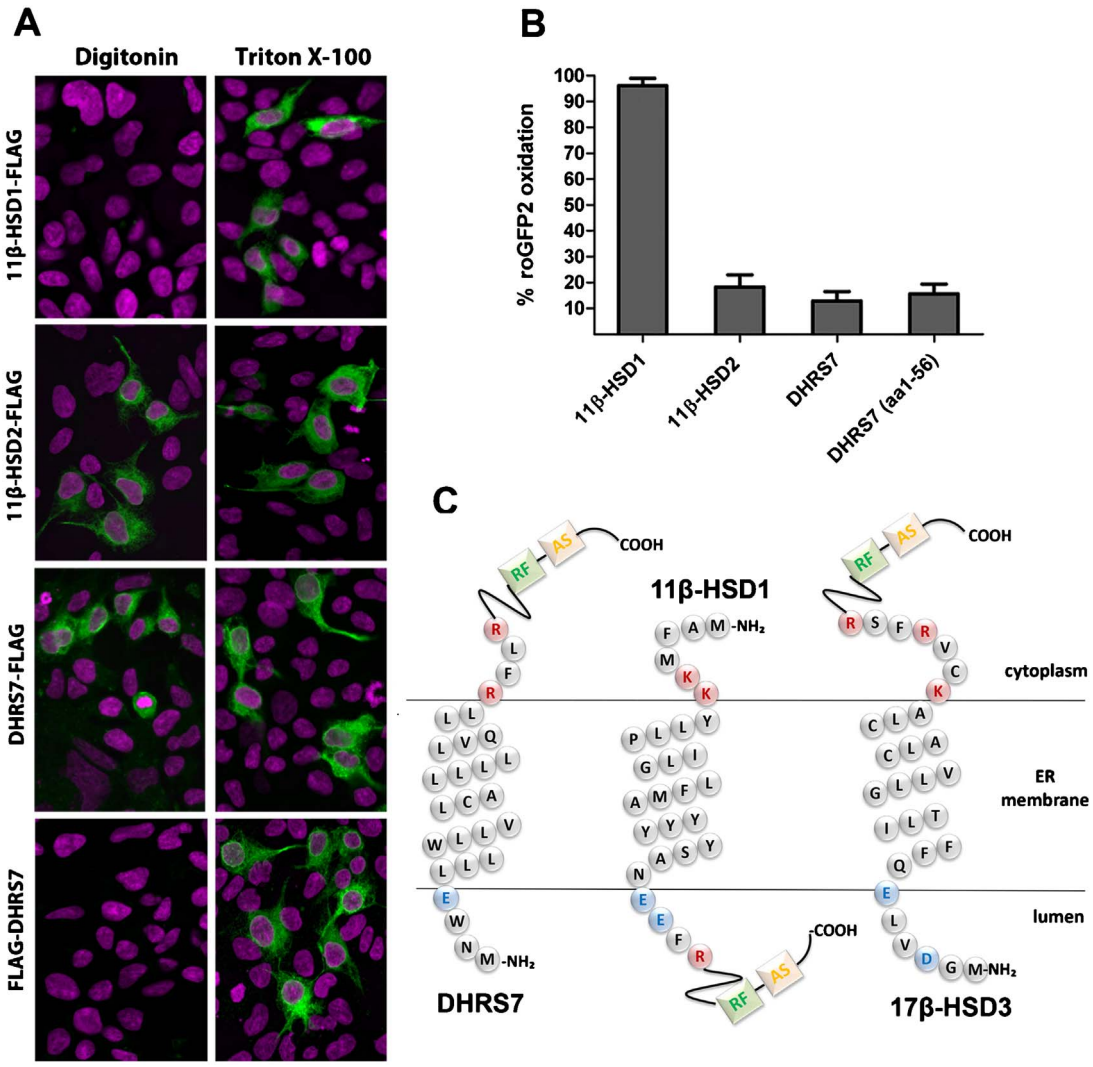

Fig. 4. Determination of the membrane topology of DHRS7. (A) Selective permeabilization experiments for determination of the topology of DHRS7. DHRS7-FLAG or FLAG-DHRS7 were expressed in HEK-293 cells. 11β-HSD1-FLAG and 11β-HSD2-FLAG served as controls for ER-luminal and cytosolic orientation, respectively. Cells were fully permeabilized with Triton X-100 or plasma membranes were selectively permeabilized with digitonin, followed by incubation with anti-FLAG M2 and Alexa Fluor 488 and Hoechst-33342 (FLAG in green, Hoechst in magenta). (B) Determination of the percentage of roGFP2 oxidation. DHRS7-roGFP2 or DHRS7(1–56)-roGFP2 fusion proteins were transiently expressed in HEK-293 cells, and 48 h post-transfection live imaging experiments were performed for determination of the percentage of oxidation of roGFP2 (mean ± S.D. from three independent experiments). The values for 11β-HSD1-roGFP2 and 11β-HSD2-roGFP2 fusions are shown for comparison of a known ER-luminal and cytosolic protein, respectively, and have been calculated from previous experiments [9]. (C) Topology of DHRS7, 11β-HSD1 and 17β-HSD3 in the ER-membrane with amino acids represented by one letter code notation (positively charged in red, negatively charged in blue). RF, Rossmann fold; AS, active site.

Table 1
Quantification of selective permeabilization experiments for determination of the topology of DHRS7. Around 1000 cells were counted per experiment. Data represent the percentage of Hoechst-33342 positive cells that also showed positive staining with anti-FLAG antibody. To assess selectively plasma membrane permeablized cells, the percentage of Triton X-100 positive cells was set as 100% and the relative percentage of positive cells after digitonin treatment is shown. All values represent mean ± S.D of at least three independent experiments.

Expressed protein	Triton X-100	Digitonin	Relative rate of digitonin positive cells [%]
11β-HSD1-FLAG	23.4 ± 1.6	1.3 ± 0.4	5.5 ± 1.5
11β-HSD2-FLAG	26.3 ± 0.8	25.3 ± 0.9	96.2 ± 0.6
DHRS7-FLAG	23.9 ± 1.6	23.0 ± 1.8	96.1 ± 1.6
FLAG-DHRS7	22.9 ± 1.3	1.0 ± 0.4	4.3 ± 2.0

steady state (OxD value expressed as a percentage), similar to that of 11β-HSD2-roGFP2, typical for a cytoplasmic orientation of the sensor. In contrast, 11β-HSD1-roGFP2 showed a high percentage of oxidation, typical of a ER-luminal orientation of the sensor. The measurements of oxidation for 11β-HSD1-roGFP2 and 11β-HSD2-roGFP2 have been performed in previous work [9].

Third, an inspection of the distribution of charged amino acids in the primary sequence of DHRS7 is in favour of a cytoplasmic orientation of the catalytic moiety of DHRS7 (Fig. 4C). In fact, the fourth residue at the N-terminus of the protein is a glutamate, immediately upstream of the single membrane spanning helix that is followed by an arginine residue at position 24 and another arginine at position 27. Positively charged residues at the cytoplasmic and negatively charged residues at the ER-luminal side are important determinants for the orientation of a membrane spanning helix and are also present in the related SDRs 11β-HSD1 and 17β-HSD3 (Fig. 4C) [10,11,17]. The charge distribution supports a membrane topology of DHRS7 with its N-terminus in the ER lumen and the main part of the protein with the cofactor binding site and catalytic center in the cytoplasm.

4. Discussion

The closest relatives of DHRS7 within the SDR family are DHRS7b

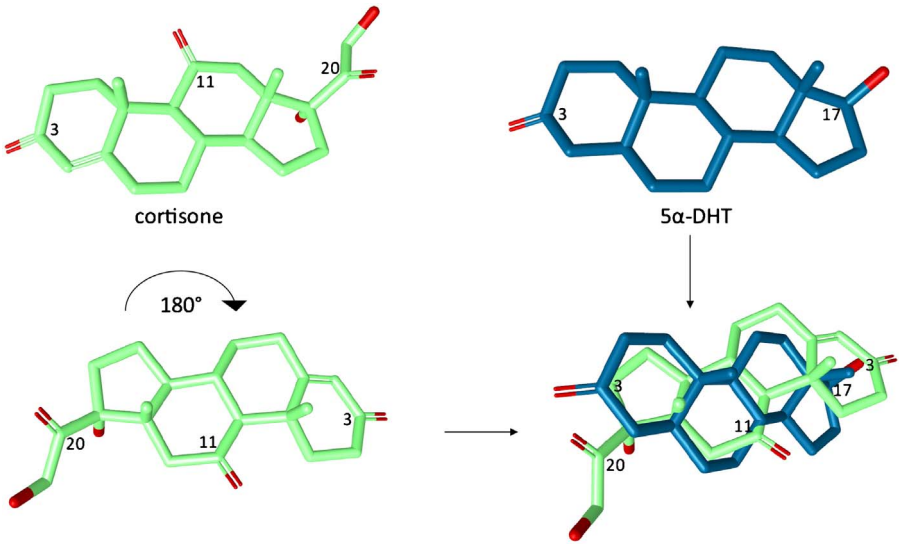

Fig. 5. Rotational symmetry of the two DHRS7 steroid substrates cortisone and 5α-DHT. 3D structures of cortisone (in green) and 5α-DHT (in blue) are shown in the upper panel. Cortisone rotated 180° (East-West rotation) is shown in the lower panel on the left, and overlay of 5α-DHT and the East-West rotated cortisone, revealing the close proximity of the 3-oxo group on 5α-DHT and the 20-oxo group on cortisone, is shown on the lower panel on the right. (For interpretation of the references to colour in this figure legend, the reader is referred to the web version of this article.)

(SDR32C1), DHRS7c (SDR32C2), 11β-HSD1 (SDR26C1), 17β-HSD12 (SDR12C1) and 17β-HSD3 (SDR12C2) [18]. The evolutionary relationship of these enzymes represents a starting point for a substrate search. In this respect, Wsol and co-workers proposed for the first time several potential substrates, including 1,2-naphtoquinone, all-trans-retinal, the tobacco compound NNK, but also the steroids cortisone and androstenedione; some of these substrates are shared with the closely related enzymes 11β-HSD1 and 17β-HSD3 [6,8,19]. Although DHRS7 can accept androstenedione as a substrate at very high concentrations (activity observed at 25 μM or higher) [6,8], the present study showed that this enzyme is not able to convert androstenedione to testosterone at a physiologically relevant concentration of 200 nM in intact cells. Under the same conditions 17β-HSD3 efficiently catalyzed this reaction. Thus, DHRS7 is unlikely to have a physiological role in generating testosterone from androstenedione. Such a role would anyhow be against the evidence that loss of DHRS7 enhances cancer cell proliferation and aggressiveness [5]. Also, the reverse reaction, which would be in line with a tumor-suppressive effect of DHRS7, could not be detected.

However, the data of this study suggest a role of DHRS7 in the inactivation of 5αDHT to 3αAdiol. Compared to the well-described AKR1C2, the activity of DHRS7 was approximately two times lower. However, for both DHRS7 and AKR1C2 comparable suppressive effects on AR transactivation could be observed at 5αDHT concentrations of 1 nM and greater, supporting a role of these enzymes in inactivating 5αDHT. DHRS7 expression has been found in tissues including prostate, adrenals, thyroid, intestine, kidney and liver [8], where inactivation of 5αDHT is important to control appropriate AR signaling. Although the present study revealed 5αDHT as a substrate of DHRS7 and suggests a protective effect towards AR activation, the physiological relevance remains to be further investigated. The identified oxoreduction of 5αDHT should help optimizing enzyme purification conditions, allowing to determine enrichment factors for specific activity, and measuring kinetic parameters of DHRS7. Follow-on studies also need to address the impact of DHRS7 on AR-mediated signaling in cell models expressing endogenous levels of this enzyme. Furthermore, studies using clinical samples and addressing whether DHRS7 has a role in androgen-dependent prostate cancer should be performed.

The present study also revealed that DHRS7 can catalyze the 20-oxoreduction of cortisone, although the observed activity was very low and its physiological relevance is questionable. Nevertheless, DHRS7 possesses 3α/20β-HSD activity, stimulating further research in this direction. Steroid molecules can adopt different binding orientations in metabolizing enzymes, due to their rotational symmetry as illustrated in Fig. 5 [20], and as shown by structural analyses of the yeast *Streptomyces hydrogenans* 3α/20β-HSD [21]. Previous reports, using HPLC for steroid separation, suggested conversion of cortisone to cortisol by DHRS7 [6,8]. In the present study, cortisol formation could not be detected. It needs to be noted that 20β-DHE could not be separated from cortisol using TLC and a 9:1 methanol:chloroform solvent, emphasizing that more powerful separation methods and, ideally, compound fragmentation and mass-spectrometry should be used. Thus, the use of authentic standards and LC–MS/MS (or GC–MS/MS) in order to identify substrates and products is advantageous for the characterization of "orphan" enzymes.

The DHRS7-mediated 20-oxoreduction of cortisone was not stimulated upon coexpression with H6PDH, in line with the cytoplasmic orientation of the ER membrane-anchored DHRS7 as determined by using roGFP fusions and selective plasma membrane permeabilization experiments. These findings are in conflict with an earlier report [6], who proposed an ER-luminal orientation of DHRS7. These investigators applied the proteinase K protection assay using microsomes of DHRS7 expressing Sf9 cells. Upon incubation with proteinase K a band for DHRS7 was still detected, although at a considerably weaker intensity than that of the positive control. In the presence of Triton X-100 the band for DHRS7 was no longer detectable and an ER-luminal orientation was proposed. However, proteinase K is still active in the presence of detergent; in fact, its activity can be stimulated by detergents because of an increased accessibility on the protein substrates. Therefore, suitable positive and negative controls, i.e. similar proteins but with opposite membrane topology, should ideally be included in proteinase K protection assays. The roGFP fusions used in the present study offer the advantage that they provide information on the membrane topology in living cells. The cytoplasmic orientation of DHRS7 is further supported by the presence of the negatively charged Glu-4 and the positively charged residues Arg-24 and Arg-27, flanking the membrane helix at the ER-luminal and cytoplasmic side, respectively (Fig. 4C).

In conclusion, the present study revealed that the ER-membrane anchored enzyme DHRS7 is oriented towards the cytoplasm and Exhibits 3α/20β-HSD activity. The ability of DHRS7 to convert 5αDHT to 3αAdiol suggests a role in the modulation of AR transcriptional activity. Further research is needed to address the potential tumor suppressor role of DHRS7.

Conflict of interest

The authors declare that they have no conflict of interest.

Acknowledgements

This work was supported by the Swiss National Science Foundation project grant 31003A-159454. AO was supported by the Novartis Foundation as Chair for Molecular and Systems Toxicology.

Appendix A. Supplementary data

Supplementary data associated with this article can be found, in the online version, at http://dx.doi.org/10.1016/j.jsbmb.2017.04.013.

References

[1] B. Persson, Y. Kallberg, J.E. Bray, E. Bruford, S.L. Dellaporta, A.D. Favia, R.G. Duarte, H. Jornvall, K.L. Kavanagh, N. Kedishvili, M. Kisiela, E. Maser, R. Mindnich, S. Orchard, T.M. Penning, J.M. Thornton, J. Adamski, U. Oppermann, S.D.R. The, The SDR (short-chain dehydrogenase/reductase and related enzymes) nomenclature initiative, Chem. Biol. Interact. 178 (1–3) (2009) 94–98.

[2] Y. Kallberg, U. Oppermann, B. Persson, Classification of the short-chain dehydrogenase/reductase superfamily using hidden Markov models, FEBS J. 277 (10) (2010) 2375–2386.

[3] C. Filling, K.D. Berndt, J. Benach, S. Knapp, T. Prozorovski, E. Nordling, R. Ladenstein, H. Jornvall, U. Oppermann, Critical residues for structure and catalysis in short-chain dehydrogenases/reductases, J. Biol. Chem. 277 (28) (2002) 25677–25684.

[4] T.L. Romanuik, G. Wang, O. Morozova, A. Delaney, M.A. Marra, M.D. Sadar, LNCaP Atlas: gene expression associated with in vivo progression to castration-recurrent prostate cancer, BMC Med. Genomics 3 (2010) 43.

[5] J.K. Seibert, L. Quagliata, C. Quintavalle, T.G. Hammond, L. Terracciano, A. Odermatt, A role for the dehydrogenase DHRS7 (SDR34C1) in prostate cancer, Cancer Med. 4 (2015) 1717–1729.

[6] H. Stambergova, L. Skarydova, J.E. Dunford, V. Wsol, Biochemical properties of human dehydrogenase/reductase (SDR family) member 7, Chem. Biol. Interact. 207 (2014) 52–57.

[7] A. Skarka, L. Skarydova, H. Stambergova, V. Wsol, Purification and reconstitution of human membrane-bound DHRS7 (SDR34C1) from Sf9 cells, Protein Expr. Purif. 95 (2014) 44–49.

[8] H. Stambergova, L. Zemanova, T. Lundova, B. Malcekova, A. Skarka, M. Safr, V. Wsol, Human DHRS7, promising enzyme in metabolism of steroids and retinoids? J. Steroid Biochem. Mol. Biol. 155 (Pt. A) (2016) 112–119.

[9] M. Tsachaki, J. Birk, A. Egert, A. Odermatt, Determination of the topology of endoplasmic reticulum membrane proteins using redox-sensitive green-fluorescence protein fusions, Biochim. Biophys. Acta 1853 (7) (2015) 1672–1682.

[10] B. Legeza, Z. Balazs, L.G. Nashev, A. Odermatt, The microsomal enzyme 17β-hydroxysteroid dehydrogenase 3 faces the cytoplasm and uses NADPH generated by glucose-6-phosphate dehydrogenase, Endocrinology 154 (1) (2013) 205–213.

[11] A. Odermatt, P. Arnold, A. Stauffer, B.M. Frey, F.J. Frey, The N-terminal anchor sequences of 11β-hydroxysteroid dehydrogenases determine their orientation in the endoplasmic reticulum membrane, J. Biol. Chem. 274 (40) (1999) 28762–28770.

[12] A.G. Atanasov, L.G. Nashev, R.A. Schweizer, C. Frick, A. Odermatt, Hexose-6-phosphate dehydrogenase determines the reaction direction of 11β-hydroxysteroid dehydrogenase type 1 as an oxoreductase, FEBS Lett. 571 (1–3) (2004) 129–133.

[13] H. Poukka, U. Karvonen, O.A. Janne, J.J. Palvimo, Covalent modification of the androgen receptor by small ubiquitin-like modifier 1 (SUMO-1), Proc. Natl. Acad. Sci. U. S. A. 97 (26) (2000) 14145–14150.

[14] D. Schuster, E.M. Maurer, C. Laggner, L.G. Nashev, T. Wilckens, T. Langer, A. Odermatt, The discovery of new 11β-hydroxysteroid dehydrogenase type 1 inhibitors by common feature pharmacophore modeling and virtual screening, J. Med. Chem. 49 (12) (2006) 3454–3466.

[15] K.R. Beck, T.J. Sommer, D. Schuster, A. Odermatt, Evaluation of tetrabromobisphenol A effects on human glucocorticoid and androgen receptors: a comparison of results from human- with yeast-based in vitro assays, Toxicology 370 (2016) 70–77.

[16] J.W. Tomlinson, E.A. Walker, I.J. Bujalska, N. Draper, G.G. Lavery, M.S. Cooper, M. Hewison, P.M. Stewart, 11β-hydroxysteroid dehydrogenase type 1: a tissue-specific regulator of glucocorticoid response, Endocr. Rev. 25 (5) (2004) 831–866.

[17] C. Frick, A.G. Atanasov, P. Arnold, J. Ozols, A. Odermatt, Appropriate function of 11β-hydroxysteroid dehydrogenase type 1 in the endoplasmic reticulum lumen is dependent on its N-terminal region sharing similar topological determinants with 50-kDa esterase, J. Biol. Chem. 279 (30) (2004) 31131–31138.

[18] J.E. Bray, B.D. Marsden, U. Oppermann, The human short-chain dehydrogenase/reductase (SDR) superfamily: a bioinformatics summary, Chem. Biol. Interact. 178 (1–3) (2009) 99–109.

[19] E. Maser, E. Richter, J. Friebertshauser, The identification of 11β-hydroxysteroid dehydrogenase as carbonyl reductase of the tobacco-specific nitrosamine 4-(methylnitrosamino)-1-(3-pyridyl)-1-butanone, Eur. J. Biochem. 238 (2) (1996) 484–489.

[20] R. Lathe, Y. Kotelevtsev, Steroid signaling: ligand-binding promiscuity, molecular symmetry, and the need for gating, Steroids 82 (2014) 14–22.

[21] D. Ghosh, C.M. Weeks, P. Grochulski, W.L. Duax, M. Erman, R.L. Rimsay, J.C. Orr, Three-dimensional structure of holo 3α, 20β-hydroxysteroid dehydrogenase: a member of a short-chain dehydrogenase family, Proc. Natl. Acad. Sci. U. S. A. 88 (22) (1991) 10064–10068.

4.2 Further Characterization of DHRS7 Activity

4.2.1 Methods

4.2.1.1 Cell Culturing

The human embryonic kidney cell line HEK 293 (ATCC, Manassas, VA, USA) was cultivated in Dulbecco's modified Eagle's medium (DMEM, Sigma-Aldrich, St. Louis, MO, USA) supplemented with 10% fetal bovine serum (FBS, Connectorate, Dietikon, Switzerland), 100 U/mL penicillin, 100 µg/mL streptomycin (Life Technologies, Grand Island, NY, USA), 10 mM 4 (2 hydroxyethyl)-1-piperazineethanesulfonic acid (HEPES) buffer at pH 7.4 (Gibco life technologies, Carlsbad, CA, USA), and 1% minimum essential medium (MEM) non-essential amino acids solution (Sigma Aldrich, St. Louis, MO, USA). The African green monkey *Cercopithecus aethiops* kidney cell line CV1 cells (ATCC, Manassas, VA, USA) was cultivated in Eagle's Minimum Essential Medium with Earle's Balanced Salts (Sigma-Aldrich, St. Louis, MO, USA) supplemented with 10% fetal bovine serum (FBS, Connectorate, Dietikon, Switzerland), 100 U/mL penicillin, 100 µg/mL streptomycin (Life Technologies, Grand Island, NY, USA), 2 mM L-glutamine, 1 mM sodium pyruvate. The human prostate cancer cell line LNCaP was purchased from ATCC (LGC Standards GmbH, Wesel, Germany), cultivated in RMPI 1649 media (R8758; Sigma) supplemented with 10% fetal bovine serum (FBS) and penicillin (100 U/mL) /streptomycin (100 µg/mL).

4.2.1.2 Transient and Stable Transfection

For transient transfection, 40'000 CV1 cells/well into 24-well plates were transfected with Fugene© 3 to 1 plasmid concentration (C-term flagged DHRS7 or empty vector pcDNA3) after 24 h. Instead, for production of lysate for western blotting, $1x10^6$ HEK 293 were transfected with the calcium phosphate method as described elsewhere [191] with 8 µg of plasmid (C-term FLAG tagged 17βHSD6 [192], or empty vector pcDNA3).

For stable transfection, HEK 293 at a dilution of 200.000 cells/ml were transfected with 8 µg of C-term flagged DHRS7 plasmid in a 10 cm^3 dish, with the calcium phosphate method as described elsewhere [191]. For stable transfection selection, after 24h cells were grown into selection medium for other 24h (800 µg/ml G418, (Sigma-Aldrich)), diluted to get single cells in 96well plates, and the following days grown into conditioned medium (cell culture media used to cultivate HEK 293 cells). Single colonies of clones were passaged until selected based on amount of mRNA and protein of DHRS7 quantified through qPCR and western blotting, respectively. Seven clones were selected, based on mRNA amount and clone number 3 was selected for further experiments based on highest DHRS7 expression per protein amount.

4.2.1.3 Determination of RNA Expression

Cell material was collected, and RNA isolated with the RNeasy Mini Kit and QIAcube (Qiagen, Venlo, Netherlands) according to the manufacturer's instructions. The samples were stored at -80 °C. Quality and quantity of RNA was assessed using a NanoDrop ND-1000 (V3.8.1; Witec AG, Lucerne, Switzerland). Reverse transcription was performed using the M-MLV Reverse Transcriptase Kit (M368B; Promega, Wallisellen, Switzerland) according to the manufacturer's instructions. Briefly, the tubes were incubated at 65 °C for 5 min at low shaking intensity with 500 ng of oligo-dT primers (Ref. AB1247; Thermo Fisher Scientific, Waltham, MA, USA) and 2000 ng of total RNA in DNase/RNase free water (Bioconcept).Afterwards, to each tube were added 20 U of M-MLV reverse transcriptase (Ref. M368C; Promega, Fitchburg, WI, USA), 10 U of RNase inhibitor (Ref. 03 335 402 001; Roche, Basel, Switzerland), and 0.5 mM dNTP mix (Ref. U151B; Promega) in a final reaction volume of 20 µL with M-MLT reverse transcription buffer (Ref. M531A; Promega) and 10% (v/v) DNase/RNase free water. The tubes were incubated in a thermomixer for 1 h at 42 °C at low shaking intensity, chilled on ice, diluted to 5 ng/µL, and stored at -20 °C. QPCR was performed with the SYBR Green detection method using the Kapa SYBR FAST qPCR Master Mix (Ref. KK4602; Kapa Biosystems, Roche). 10 ng of complementary DNA were mixed with SYBR Green Master Mix and 4 pmol of the forward and reverse primer sequences (Microsynth AG, Balgach, Switzerland) are shown in the supplementary data).

qPCR was performed in a Corbett Rotor-Gene 6000 (Qiagen) with an initial hold at 95 °C for 10 min, followed by 40 cycles of melting at 95 °C for 10 s, annealing at 60 °C for 15 s, and elongation at 72 °C for 20 s. Relative quantification of gene expression was done using the 2-ΔΔCt method [193] by normalizing genes of interest to cyclophilin A (PPIA).

4.2.1.4 Western blotting

60% confluent cells were lysed RIPA buffer and centrifuged at 12,000g for 10 min at 4°C. The supernatant was collected and protein concentration quantified using the Bradford method. Samples were heated at 95°C for 5 min in Laemmli buffer (5 mmol/L Tris HCl, pH 6.8, 10% glycerol [v/v], 0.2% sodium dodecyl sulfate [SDS] [w/v], 1% bromophenol blue [w/v]) and stored at −20°C until used. 30 µg of lysates were separated by a 12.5% Tris-glycine SDS-polyacrylamide gel and transferred to Immun-Blot® PVDF polyvinylidene difluoride membranes (162- 0177; Bio-Rad Laboratories, Hercules, CA) at constant 230 mA for 1 h. For detection of DHRS7, the membrane was blocked using 2% milk (v/v) for 1 h at room temperature, followed by incubation with the mouse anti-human DHRS7 polyclonal antibody (ab69348; Abcam, Cambridge, UK) at a dilution of 1:500 (v/v) in 2% milk (v/v), overnight at 4°C. After washing with

Tris- buffered saline (20 mmol/L Tris- base, 140 mmol/L NaCl) containing 0.1% Tween20 (v/v) (TBS- T), the membrane was subsequently incubated with horseradish peroxidase-conjugated goat anti-mouse secondary antibody (Jackson Immuno Research, Suffolk, UK) for 1 h at room temperature. For PPIA detection, the membrane was blocked using 10% milk (v/v) overnight at 4°C, followed by incubation with the rabbit anti-human PPIA polyclonal antibody (ab41684; Abcam) at a dilution of 1:2000 (v/v) in 2% milk for 1 h at room temperature. After washing with TBS-T, the membrane was subsequently incubated with horseradish peroxidase- conjugated goat anti- rabbit secondary antibody (Santa Cruz Biotechnology, Santa Cruz, CA) at a dilution of 1:1000 (v/v) in 2% milk (v/v). After washing the membranes in TBS- T, images were visualized using the Immobilon Western Chemiluminescent HRP substrate kit (Millipore, Schaffhausen, Switzerland), and a FujiFilm ImageQuant™ LAS-4000 detector (GE Healthcare, Glattbrugg, Switzerland) using the chemiluminescence detection setting. Membranes were exposed 1 second. For microsomes, 6 µg of protein of cytoplasmic fraction were loaded, for the other samples from microsomal preparation, 15 µg of protein were used. The antibody for mouse anti-human 17βHSD6 polyclonal antibody (ab88892; Abcam, Cambridge, UK) was diluted 1:1000 and for mouse anti-human 17βHSD10/ERAB monoclonal antibody (ab10260; clone number 5F3, Abcam, Cambridge, UK) was diluted 1:1000 and 20 µg of lysates were used.

4.2.1.5 Activity Assay in Intact Cells

For steroidal background activity measurements with LC/MS, HEK 293 were seeded 120’000 cells/well in 24-well poly lysine coated wells and activity was performed after 24 h. For CV1, activity performed after supplemental 24 h. For the activity, cells were washed with PBS, and incubated at 37°C in charcoal treated/serum free medium, containing 200 nM of either progesterone, 17HOProg, cortisol, or DHP (Steraloid, Newport, RI, USA). 400 µL of supernatant was collected and stored at -20°C.

4.2.1.6 Cell Lysates

Human embryonic kidney cells (HEK 293) stably expressing DHRS7 clone 3 were washed with ice cold phosphate-buffered saline and collected in Falcon tubes in 200 µL aliquots. After centrifugation at 1200xg for 4 min, supernatant was removed, and the cell pellets were snap frozen and stored at -80°C. Protein concentration were determined with the Pierce BCA Protein Assay Kit (Thermo Fisher Scientific, MA, United States).

4.2.1.7 Microsomes Isolation

Microsomes preparation was based on [194], with minor modification. Briefly, DHRS7 stably transfected HEK 293 10x 10cm dish, washed with PBS, cells were scraped and transferred to falcon tube, washed with

ice cold PBS, centrifuged twice at 4°C 4 min 150g. Cell pellet was resuspended in 1.5ml homogenization buffer homogenized with a 2 mL glass pestle (15 strokes – 3 min on ice – 15 strokes). The solution was centrifuged 4°C 20min at 12'000g. The supernatant was centrifuged at 4°C for 1 h at 106'000g. The supernatant was discarded, the pellet was washed once, and further resuspended in 30ul TS2 buffer. Samples were snap frozen and stored in -80°C. Protein concentration were determined with Pierce BCA Protein Assay Kit.

4.2.1.8 Radioactivity Assay

4.2.1.8.1 Intact Cells

For activity measurements with MS/MS, stable or non-transfected HEK 293 were seeded 120'000 cells/well poly lysine coated 24-well plates, instead, activity assay in CV1 was performed after 24 h of transient transfection into 24-well plates. For the radioactivity assay, HEK 293 non-transfected and DHRS7 stably transfected cells were seeded (100'000 cells/well) into 96-well plates poly lysine coated, CV1 were seeded into (60'000 cells/well) into 96-well plates. After 24 h, cells were washed with PBS, and incubated for 0 h - 1 h - 2 h - 4 h - 8 h at 37°C in charcoal treated/serum free medium, containing 200 nM DHT (10 nM of radioactive). Reactions were stopped by adding 20 µL of excessive amounts of unlabeled substrate and product (1:1, 1 mM in methanol) and 20 µL of mixture was collected and applied to the TLC plate (TLC, pre-coated TCL-plates SIL G 25 UV254, Macherey-Nagel, Düren, Germany). Unlabeled steroids were purchased from Steraloids (Newport, RI, USA) and radiolabeled steroids from Perkin-Elmer (Boston, MA, USA). A 1:4 mixture of ethyl acetate and chloroform was used as solvent to separate steroid using thin-layer chromatography (TLC, pre-coated TCL-plates SIL G-25 UV254, Macherey-Nagel, Düren, Germany). Steroids were separated though a solution of ethyl acetate to chloroform (1:4) and incubated for 1 h. For the visualization, the TLC plate was dried for 10 min and sprayed with a 3% v/v sulfuric acid in water, incubated 5 min in the oven at 60°C, and 10 min with increasing temperature toward 160°C. Scratch silica into vials to be measured for radioactivity and add scintillation cocktail (IRGASAFE Plus, Zinsser Analytic, Frankfurt am Main, Germany) was added and liquid scintillation counting (TRI CARB 2100TR, PerkinElmer Inc., Wellesley, MA, USA) was performed to quantify the remaining substrate concentration and the product formation.

4.2.1.8.2 Lysate

To determine enzyme activity, cell pellets of DHRS7 stably transfected in HEK 293 were thawed, diluted to 2 µg/µL in TS2 buffer (100 mM NaCl, 1 mM EGTA, 1 mM EDTA, 1 mM MgCl2, 250 mM sucrose, 20 mM Tris-HCl, pH 7.4, with or without 1mM DTT or 250mM glycerol) or MOPS buffer (100mM NaCl, 1mM EGTA,

1 mM EDTA, 1 mM MgCl2, 20mM MOPS, with or without 250 mM sucrose), lysed either by freeze-thaw or sonicated (0.3 cycles, 20% amplitude, UP50H, Hielscher Ultrasonics, Teltow, DE) and incubated in a 96-well polymerase chain reaction (PCR) plate on a thermoshaker (ThermoStat plus, Eppendorf, Hamburg, Germany) at 37°C for 1 h with final dilution 1µg/µL. The DHRS7 activity assay was performed in the presence of 200 nM DHT, containing 5 nM of [1,2,4,5,6,7-3H(N)]-dihydrotestosterone and either NADPH 0.5mM or regeneration system (250 µM of the cofactor $NADP^+$, 1 mM glucose-6-phophate, and 1 U of glucose 6 phosphate dehydrogenase from baker's yeast *S. cerevisiae* (all from Sigma-Aldrich, St. Louis, MO, USA)). Reactions were stopped by adding 10 µL of excessive amounts of unlabeled substrate and product (1:1, 1 mM in methanol) and 10 µL of mixture was collected and applied to the TLC plate. Further steps were performed as described previously for intact cells (method section 4.2.1.8.1)

4.2.1.8.3 Microsomes

Microsomes of DHRS7 stably transfected in HEK 293 were thawed, diluted to 2 µg/µL in TS2 buffer, and incubated in a 96-well polymerase chain reaction (PCR) plate on a thermoshaker (ThermoStat plus, Eppendorf, Hamburg, Germany) at 37°C for 1-2-4 h at final dilution 1 µg/µL. Following steps were performed as described for lysate. Reactions were stopped by adding 10 µL MeOH of 1 mM DHT and 3αAdiol and 10 µL of lysate was collected and applied to the TLC plate.

4.2.1.9 Quantification of Analytes for Activity Assay by LC/MS

Analysis of analytes from culture supernatants was performed according to [191], with modifications depending on the metabolite. Briefly, the activity assay samples and calibrators stored in -20°C were thawed and internal standard was added if available (the analytes DHT and 3αAdiol were evaluated based on the internal standards DHT-D3, and 3αAdiol-D3, respectively). For 3βAdiol, 5βDHT, and progesterone, the amount was estimated based on the calibration curve; and DHP, cortisol, 20β-dihydrocortisol were evaluated only qualitatively. Calibration curve was prepared with the analytes to quantify and serial dilution of 50% concentration performed in the same matrix used for biological material subjected to activity in the cell culture. Protein precipitation was performed by adding 1 mL ice-cold acetonitrile, shaking vigorously 30 min at 4°C and 1350 rpm (Thermomixer comfort, Eppendorf), centrifuged at 4°C 10 min and 16100 rcf, and transferring to fresh tubes. Samples were then evaporated into Genevac with settings 35 °C HPLC fraction and reconstituted in 50 µL methanol by shaking vigorously 10 min at 4°C, centrifuged (4°C, 10 min; 16100 rcf), and the supernatant transferred in LCMS vial (with inserts V=200 µL). Metabolytes were identified and quantified according to standards or calibration curves, performed by Dr. Denise Kratschmar. Analytes with S/N≥5 are described as not quantified (NQ), S/N≥3 as not detected (ND).

4.2.1.10 Chemicals

For activity assay analyzed with LC/MS the steroids DHT (CAS Nr. 521-18-6), DHT-D3 (CAS Nr. 79037-34-6), 3αAdiol (CAS Nr. 1852-53-3), 3αAdiol-D3 (CAS Nr. 7037-33-5), 3βAdiol (CAS Nr. 571-20-0), 5βDHT (CAS Nr. 571-22-2), DHP (CAS Nr. 566-65-4), cortisol (CAS Nr. 50-23-7), 20β-dihydrocortisol (CAS Nr. 116-58-5), and progesterone (CAS Nr. 57-83-0), 20αOHProg (CAS Nr. 145-14-2), 20βOHProg (CAS Nr. 145-15-3), 17OHProg (CAS Nr. 68-96-2), 17α,20αdiOHProg (CAS Nr. 652-69-7), and 17α,20β-diOHProg (CAS Nr. 1662-06-2), were all purchased from Steraloids (Newport, RI, USA).

For inhibitors screening, abiraterone acetate (CAS Nr. 154229-18-2), sertaconazole (CAS Nr. 99592-39-9), tioconazole (CAS Nr. 65899-73-2), butoconazole (CAS Nr. 64872-76-0), daunorubicin (CAS Nr. 23541-50-6), all-trans retinal (CAS Nr. 116-31-4), glycyrrhizic acid (CAS Nr. 1405-86-3), 9,10-Phenanthrenequinone (CAS Nr. 84-11-7), and 1.2-Naphthoquinone (CAS Nr. 524-42-5) were purchased by Sigma were obtained from Sigma–Aldrich (Buchs, CH). As quinones showed low solubility, 9,10-phenanthrenequinone was first diluted in a stock solution of 10 mM DMSO, instead 1,2-napthoquinone was diluted in a stock solution of 1 mM in DMSO. Instead tamoxifen (CAS Nr. 10540-29-1) was obtained by Invivogen (San Diego, CA, USA). Drostanolone (CAS Nr. 58-19-5), methasterone (CAS Nr. 3381-88-2), oxandrolone (CAS Nr. 53-39-4), oxyndrolone (CAS Nr. 53-39-4), oxystanolon (synthesized by Dr. Daniela Schuster), and mesterolone (CAS Nr. 1424-00-6) were obtained from Lipomed (Cambridge, MA, USA). 7,27-dihydroxycholesterol (7oxo, 27OHC acid) (CAS Nr. 240129-43-5), and 7-keto-25-hydroxycholesterol (7keto-25-OHC) (CAS Nr. 64907-23-9) were obtained by Avanti Polar Lipids. 5α-dihydro-DOC (CAS Nr. 298-36-2) and cortisone (CAS Nr. 53-06-5) were diluted in methanol and purchased from Steraloids (Newport, RI, USA), T0504 (Roche, BS, CH). Prostaglandin E2 (CAS Nr. 362-24-6) and prostaglandin F2α (CAS Nr. 38562-01-5) were diluted in ethanol and purchased from Adipogen (San Diego, CA, USA), and Sigma, respectively. Stock solutions were prepared in dimethyl sulfoxide (DMSO) and stored at -20°C. BNW16 was used as a specific 11βHSD1 inhibitor according to [195].

4.2.1.11 Statistics

Two-way ANOVA with Bonferroni post-test for multiple comparison was used for the activity assay. Student t-test was used for comparison of DHT DHRS7 stable lysate activity to assess substrates and inhibitors.

4.2.2 Results

4.2.2.1 Selection for Cell Model

The green monkey CV1 cell line is often used as a model cell line in steroid and oxidoreductase studies [134]. In order to confirm if it was possible to study the effects of DHRS7 on DHT metabolism in CV1 cells, first, we quantified the endogenous (background) level of DHT conversion. Supernatants from CV1 cells transfected with plasmid pcDNA3 or DHRS7 and treated with 100 nM DHT where collected. Supernatant spiked with 100 nM DHT that was in quick contact with an empty well (named as "contact well") was used as a control. DHT and 3αAdiol were quantified using ultra-high-pressure LC-MS/MS (Figure 9).

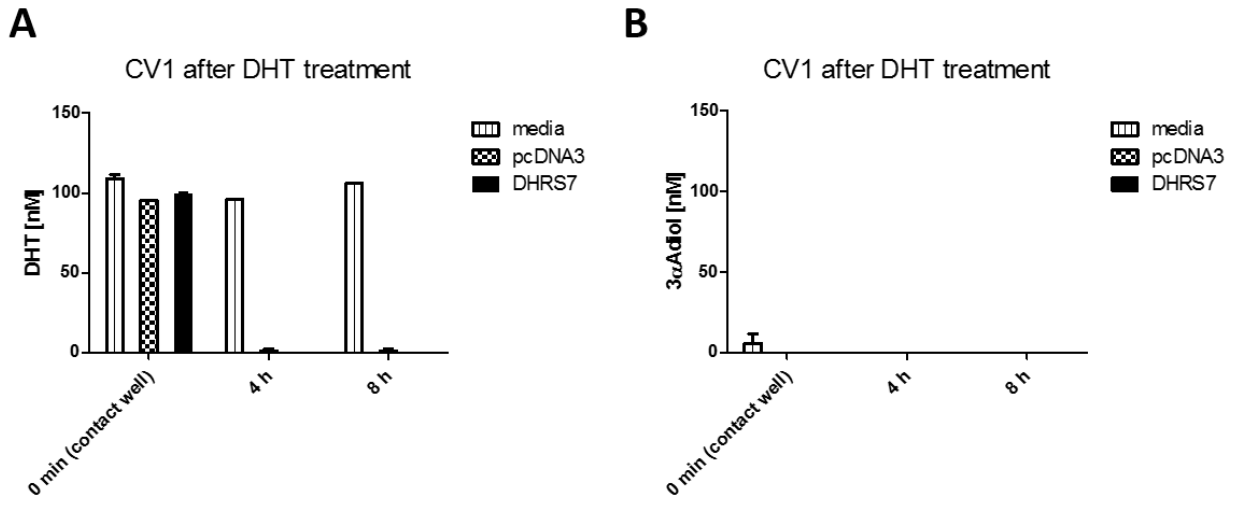

Figure 9: Quantification of DHT (A) and 3αAdiol (B) in supernatant of CV1 transfected with pcDNA3 and DHRS7 compared to incubated media after DHT treatment. The experiment was performed in duplicates and expressed as mean ± SD.

DHT exposed to CV1 cells (Figure 9A) was fully metabolized at both the 4 h and 8 h time points both in the pcDNA and DHRS7 transfected cells, indicating strong background conversion. Surprisingly, 3αAdiol (Figure 9B), the expected product of DHRS7 metabolism, was not detected. This might indicate further metabolism of 3αAdiol in CV1 cells. For these reasons, CV1 cells were not selected as model cell line for DHRS7 metabolism studies. In order to validate the use of HEK 293 cells (shown to have a minimal background conversion of DHT [191]), as an alternative to CV1 cells for measuring DHT conversion following DHRS7 overexpression, the levels of DHT and 3αAdiol were quantified. In addition, the reverse reaction of 3αAdiol to DHT was also investigated in this model (Figure 10).

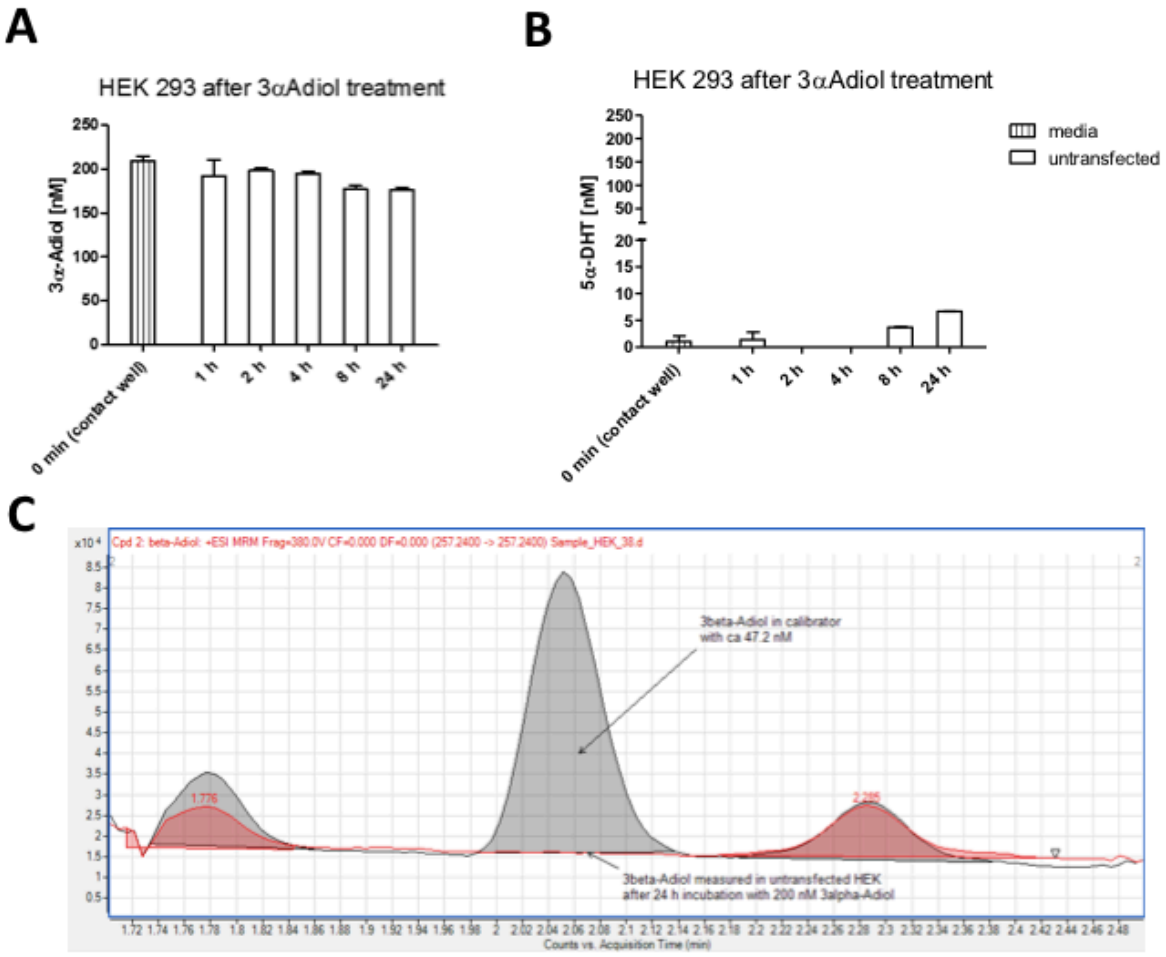

Figure 10: Quantification of 3αAdiol (A) and DHT (B) in supernatant of HEK 293 compared to incubated media after 3αAdiol treatment, and the absence of 3βAdiol in HEK 293 after 24 h incubation with 200 nM 3αAdiol (C) (in red, compared to 3βAdiol in calibrator with concentration of 47.2 nM). The experiment was performed in duplicates and expressed as mean ± SD.

The oxidative conversion of 3αAdiol to DHT in HEK 293 cells was very weak with only ca. 6 nM of DHT detected following 24 h treatment with 200nM 3αAdiol (Figure 10A and B). No 3βAdiol was detected (Figure 10C). The oxidation of 3αAdiol to DHT has been reported to be catalyzed by the enzymes 17βHSD6, 17βHSD10, RDH16, RDH5, and DHRS9 [23, 196-200]. To further support the observation that the HEK 293 cells lack the sufficient machinery to strongly support the oxidative reaction and would thus be a favorable model to study DHRS7 driven DHT reduction metabolism and kinetics in comparison to CV1, the protein expression levels of the microsomal 17βHSD6, and the mitochondrial 17βHSD10 protein [201] were measured by immunoblotting (Figure 11).

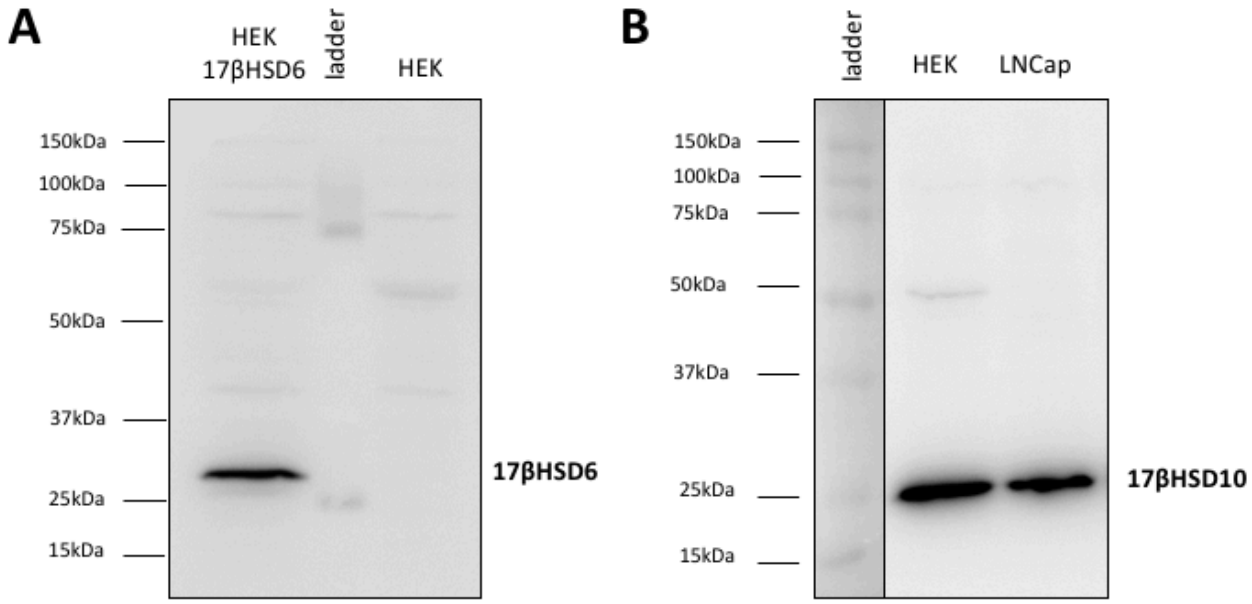

Figure 11: Expression of 17βHSD6 and 17βHSD10 in HEK 293. A. Protein expression of 17βHSD6 (30 kDa) in HEK 293. HEK 293 cells transfected with C-terminal FLAG tagged 17βHSD6 and the prostate cancer cell line LNCaP were used as positive control according to [23]. B. Protein expression of 17βHSD10 (27 kDa) in HEK 293. LNCaP cell lysate was used as positive control according to Baumann et al. [198].

HEK 293 cells do not express endogenous 17βHSD6 protein (Figure 11A). HEK 293 cells express high endogenous 17βHSD10 protein (Figure 11B). The low affinity of 17βHSD10 (ca. 34 µM [202]) to 3αAdiol may help explain the observed low 3αAdiol metabolism at the later time points, however the expression of other 3α-HSDs should be assessed.

For the purpose to test the reductive capacity of DHRS7 in HEK cells, a stable HEK 293 cell line expressing DHRS7 was established. Seven clones of HEK 293 stably expressing DHRS7 were selected with the G418 antibiotic and were assessed based on protein expression, compared to non-transfected cells and the positive LNCaP cell lysate control (Figure 12). Clone 3 was selected for further experiments according to its high DHRS7 expression in the immunoblot (figure 12).

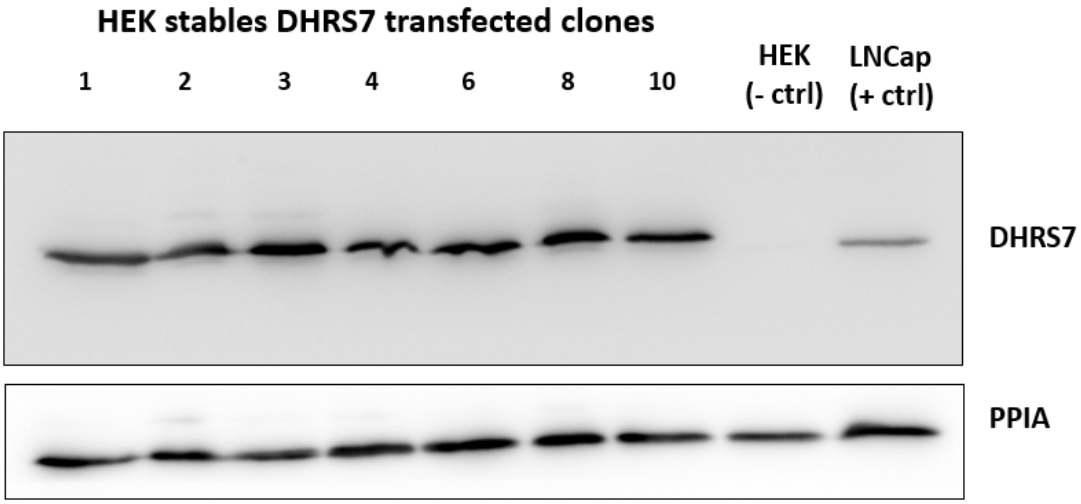

Figure 12: Expression of DHRS7 in seven selected DHRS7 HEK 293 stable clones (1,2,3,4,6,8). DHRS7 is highly expressed in all the cloned cell lines. Whole LNCaP cell lysates were used as a positive control.

Clone 3 was selected for further experiments according to its increased DHRS7 expression in the western blot (figure 12).

4.2.2.2 Activity Assay toward Selected Steroids on Position 3α and 20β

The HEK 293 stably expressing DHRS7 clone 3 cells were incubated with hypothesized potential substrates of DHRS7 and compared to the background conversion of non-transfected HEK 293 cells. Based on the observations of reductive behavior of DHRS7 toward the carbonyl moiety of cortisone in position 20 leading to a 20β hydroxy, and DHT in position 3 leading to a 3α hydroxy of the steroidal structure [191], and the assumptions made in the introduction of chapter 1 (section 4) , the four candidates' substrates steroids present in Figure 13 were tested.

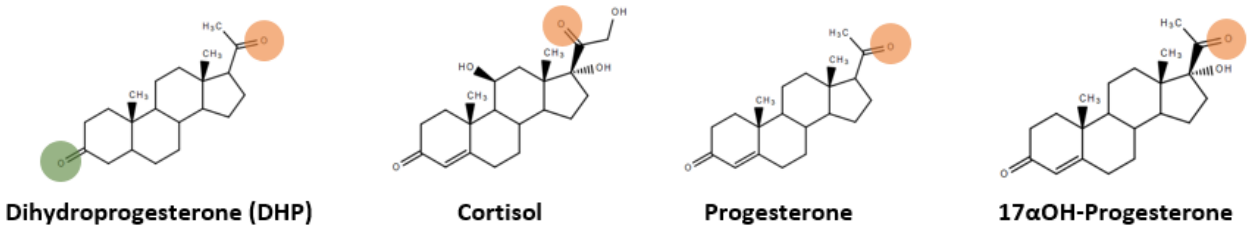

Figure 13: Tested candidates' substrates steroids (in light green reaction expected in position 3 leading to a 3α product, light red reaction expected in position 20 leading to a 20β product).

A preliminary qualitative analysis was performed for the analytes DHP (Figure 14A), cortisol (Figure 14B) and its expected 20β-reduction product 20β-dihydrocortisol (Figure 14C).

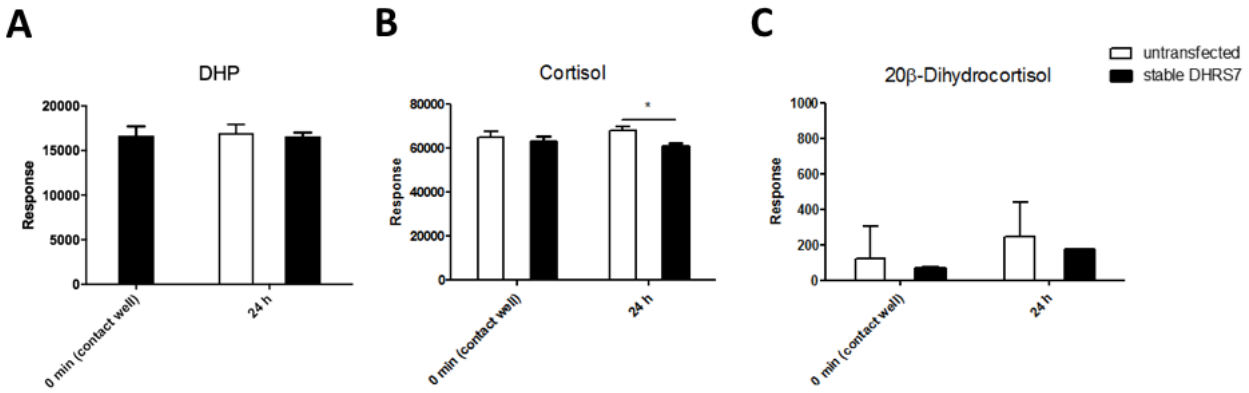

*Figure 14: Qualitative assessment for activity of DHRS7 in intact cells before and after 24 h incubation with 200nM tested substrates DHP (A), cortisol (B) and relative hypothesized product 20β-dihydrocortisol (C). The experiment was performed in triplicates and expressed as mean ± SD. *p<0.05.*

The activity assays revealed no qualitative differences between the supernatant of the stable DHRS7 HEK 293 cells vs. untransfected control cells after 24h DHP incubation (Figure 14A). A small, significant decrease was detected for cortisol after incubation for 24 h (Figure 14B) however, the predicted metabolite 20β-dihydrocortisol was not changed (Figure 14C). These metabolites were not studied further.

Instead, progesterone was quantified at different incubation times (Figure 15) and the following products were also measured: the expected product 20βOHProg, the unexpected reduction product on position 20 to a 20α carbonyl, 20αOHProg, and finally a potential product 17αOHProg, as highlighted in Figure 6 in the introduction.

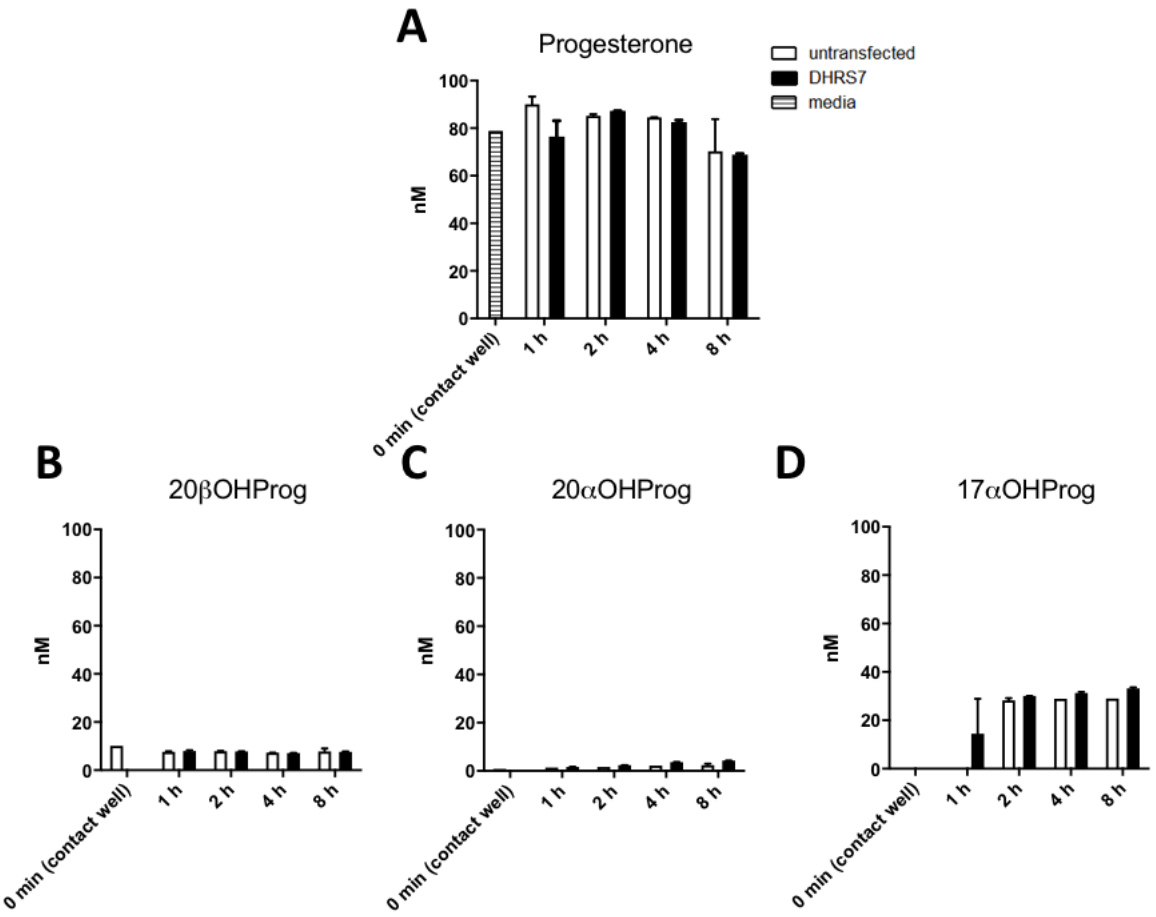

Figure 15: Quantification of products formation after incubation with progesterone (A) and the hypothesized products 20αOHProg (B), 20βOHProg (C), and 17αOHProg (D). The experiment was performed in triplicates and expressed as mean ± SD.

Quantification by LC-MS/MS revealed no change in the levels of progesterone at any time point in the DHRS7 HEK cells, the untransfected HEK 293 control cells, and media control (Figure 15A).

The expected product 20βOHProg was detected in equal amounts of ca. 10 nM in the DHRS7 HEK cells, the untransfected HEK 293 control cells, but was not detected in the media control. (Figure 15B). Instead, a minimal time-dependent increase in the levels of 20αOHProg was detected in stably transfected DHRS7 and untransfected HEK 293 cells (Figure 15C), as well as for 17αOHProg (Figure 15D). The latter metabolite was detected at a concentration of ca. 15-35 nM with values close to the limit of detection after 1 h. Taken together, no promising differences were observed for the evaluated products from the hypothesized substrate progesterone. To support the findings of this experiment, a progesterone receptor transactivation experiment was performed by Simon Stücheli, a master student that I supervised. The progesterone receptor was activated using 10 nM progesterone in the presence of DHRS7 plasmid

transfected into HEK 293 cells as in the published work [191]. No differences in progesterone receptor transactivation were observed between DHRS7 and pcDNA3 transfected HEK293 cells (unpublished data).

To test for DHRS7 activity towards 17OHProg, the potential metabolites 17α,20βdiOHProg and 17α,20αdiOHProg were quantified. A significant time-dependent increase of 17α,20βdiOHProg and 17α,20αdiOHProg was observed following incubation of 200 nM of 17OHProg in both DHRS7 HEK 293 and untransfected controls (Figure 16A and B). However, comparison of DHRS7 HEK 293 vs untransfected HEK controls showed the levels of 17α,20βdiOHProg were higher in the DHRS7 HEK cells, and conversely the levels of 17α,20αdiOHProg were lower in DHRS7 HEK cells compared to the untransfected HEK controls. This was most pronounced after 4 h were a two-fold difference was observed for both metabolites (Figure 16A and B).

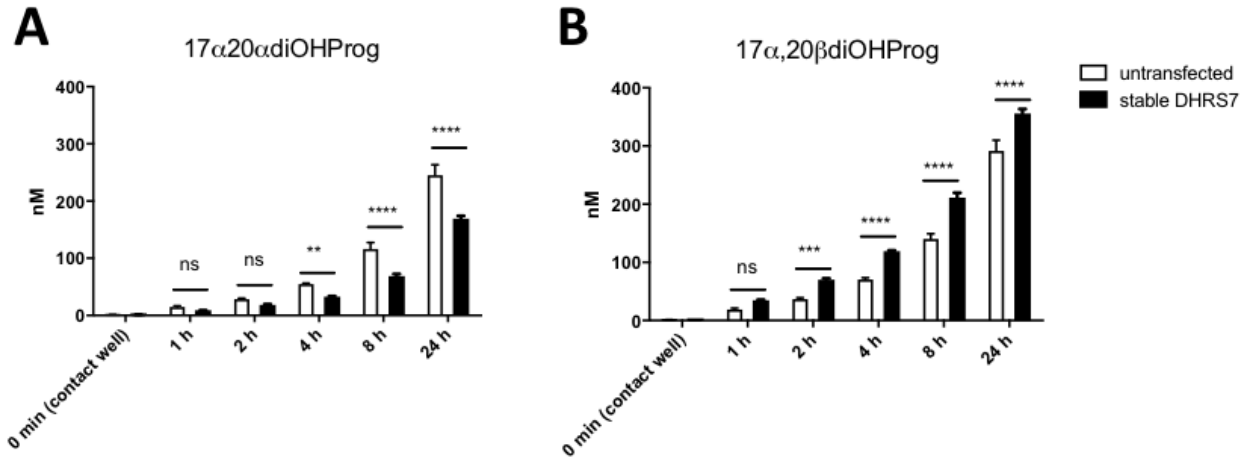

*Figure 16: Quantification of products formation of 17α,20αdiOHProg (A) and 17α,20βdiOHProg (B) after incubation with 200nM 17αOHProg. The experiment is one representative of two independent experiments and was performed in triplicates and expressed as mean ± SD. ns=not significant, *p<0.05, **p<0.001, ****p<0.005.*

4.2.2.3 An in vitro Method to assess Substrates and Inhibitors of DHRS7

4.2.2.3.1 Visualization and Identification of DHT and 3αAdiol

A method to evaluate potential competitive substrates and inhibitors of DHRS7 is needed. Based on the observed reduction of DHT to 3αAdiol in HEK 293 cells transfected with DHRS7, I used radioactive DHT as a model substrate to develop a cell free system to measure conversion using TLC separation and scintillation cocktail.

Before quantifying the levels of radioactive analytes DHT and 3αAdiol, the visualization and identification of the two metabolites was established. 10 µL of 1 mM of non-radioactive mixed analytes and pure compounds were applied to a TLC plate and separated in a 1:4 mixture of ethyl acetate and chloroform.

Following separation, compounds were dried, sprayed with 3% v/v sulfuric acid in water, and heated. The visualized analytes on a TLC plate are present in Figure 17, from where the "Rf" was calculated as cm analyte front/cm solvent front.

A

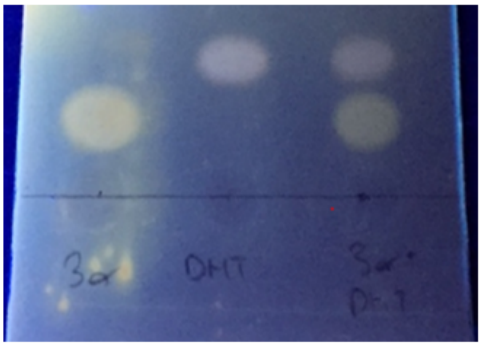

B

	Rf (cm solute front/cm solvent front)
DHT	0.333 (2/3)
3αAdiol	0.166 (1/6)

Figure 17: Characteristics of the analytes 3αAdiol and DHT on the TLC plate under UV light after separation. A. Visualization of DHT and 3αAdiol. B. Rf values of DHT and 3αAdiol.

Spraying with 3% v/v sulfuric acid in water allowed to visualize the analytes otherwise not seen under UV light (data not shown). The 3αAdiol is visualized as a yellow spot and the DHT as a violet spot (Figure 17A). Rf values corresponded to 0.333 for DHT, and 0.166 for 3αAdiol (Figure 17B).

4.2.2.3.2 Radioactivity Assay in Intact Cells with DHT

To validate the radioactivity assay, DHRS7 HEK 293 stably expressing cells were seeded in 96 well plates, and radioactivity counts of DHT and 3αAdiol were compared to results generated from the mass spectrometry method (Figure 18). The radioactivity assay had to be performed in a 96wells for safety and costs issues. The LC-MS/MS analysis had to be performed in 24-well plate format to avoid decreased sensitivity for the detection of physiological concentrations of the analytes in nM ranges.

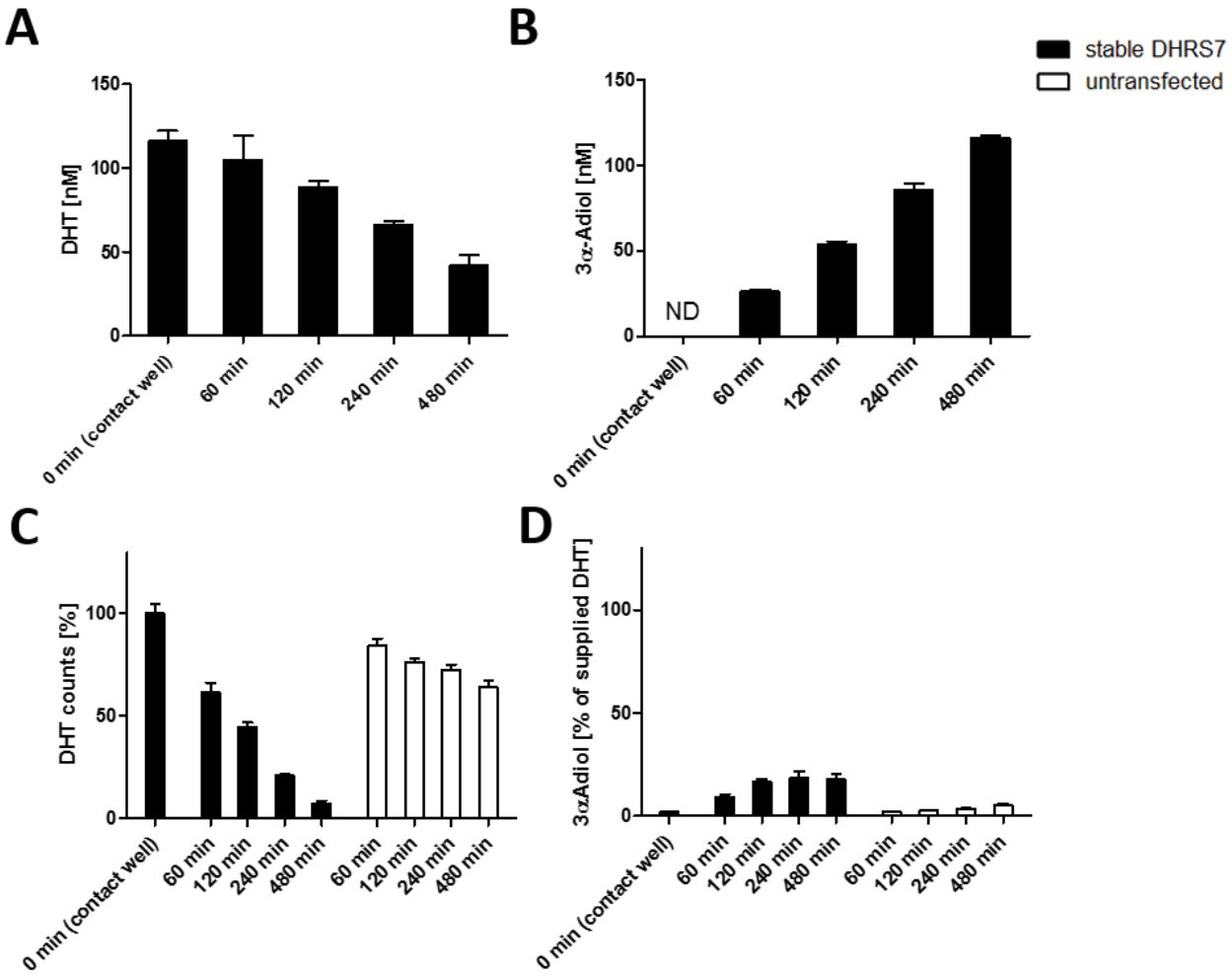

Figure 18: Comparison of DHT and 3αAdiol analytes in HEK 293 quantified with MS/MS in 24-well plates format (A, B) with radioactivity assay in 96-wells format (C, D) after DHT treatment. The experiments were performed in triplicates and expressed as mean ± SD. ND=not detected as S/N<3.

The activity assay performed in intact cells using the 24-well format and analyzed by mass spectrometry showed that 3αAdiol formation was increased in a time-dependent manner reaching ca. 30 nM/h (Figure 18B), whilst DHT was conversely decreased in a time-dependent manner at ca. 20 nM/h (Figure 18B). The formation of 3βAdiol was not detected (supplementary data in section 9.1.1.3), which was also observed in transiently transfected HEK 293 cells in the published work [191]. The radioactivity assay performed in 96 well plates showed a time-dependent decrease of DHT in DHRS7 HEK 293 cells (ca. 40% after 1 h, 55% after 2 h, 80% after 4 h, and 95% after 8 h) (Figure 18C) compared to the untransfected HEK 293 control cells (ca. 20% after 1 h, 25% after 2 h, 30% after 4 h, and 35% after 8 h). However, the 3αAdiol radioactive counts in the DHRS7 HEK 293 cells showed similar values after 2 h, 4 h and 8 h, with very low background values measured in untransfected HEK 293 control cells (Figure 18D).

4.2.2.3.3 Radioactivity Assay in Lysate

In order to optimize a radioactivity cell lysate assay for further screening of potential substrates or inhibitors of DHRS7 according to DHT reduction, the following conditions were compared: cofactor supplementation, buffer, lysate solubilization, protein concentration and time dependency from frozen pellet.

First, conversion of DHT to 3αAdiol was measured in 1 µg/µL of untransfected HEK 293 cells or DHRS7 HEK 293 stable lysates for 1 h in phosphate-free buffers prepared according to manufacturer instructions, different to the phosphate buffer previously used [145, 146].

The buffers utilized in the following experiments where MOPS pH6.8 or TS2 pH7.4. Both buffers were supplemented with either 500 µM NADPH or a regeneration system (described as "RS" in Figure x. Briefly, 250 µM of the cofactor NADP+, 1 mM glucose-6-phophate, and 0.5 U of glucose 6 phosphate dehydrogenase) (Figure 19A). Afterwards, the regeneration system was also modified by the substituting NADP+ for NADPH (described in Figure as "NADPH-RS"). TS2 buffer was also supplemented with the addition of DTT or glycerol. Finally, the cell lysates were solubilized by sonication or freeze-thawing of the frozen cell pellet (see Figure 19B).

After the reaction with 3% sulfuric acid, the TLC plate appear to display additional unspecific spots when tested in the TS2 buffer plus the regeneration system without the lysate incubated for 1 h (Lane 1 in Figure 19C), plus lysate incubated for 1 h (Lane 2 in Figure 19B), and plus lysate incubated for 0 h (Lane 3 in Figure 19C).

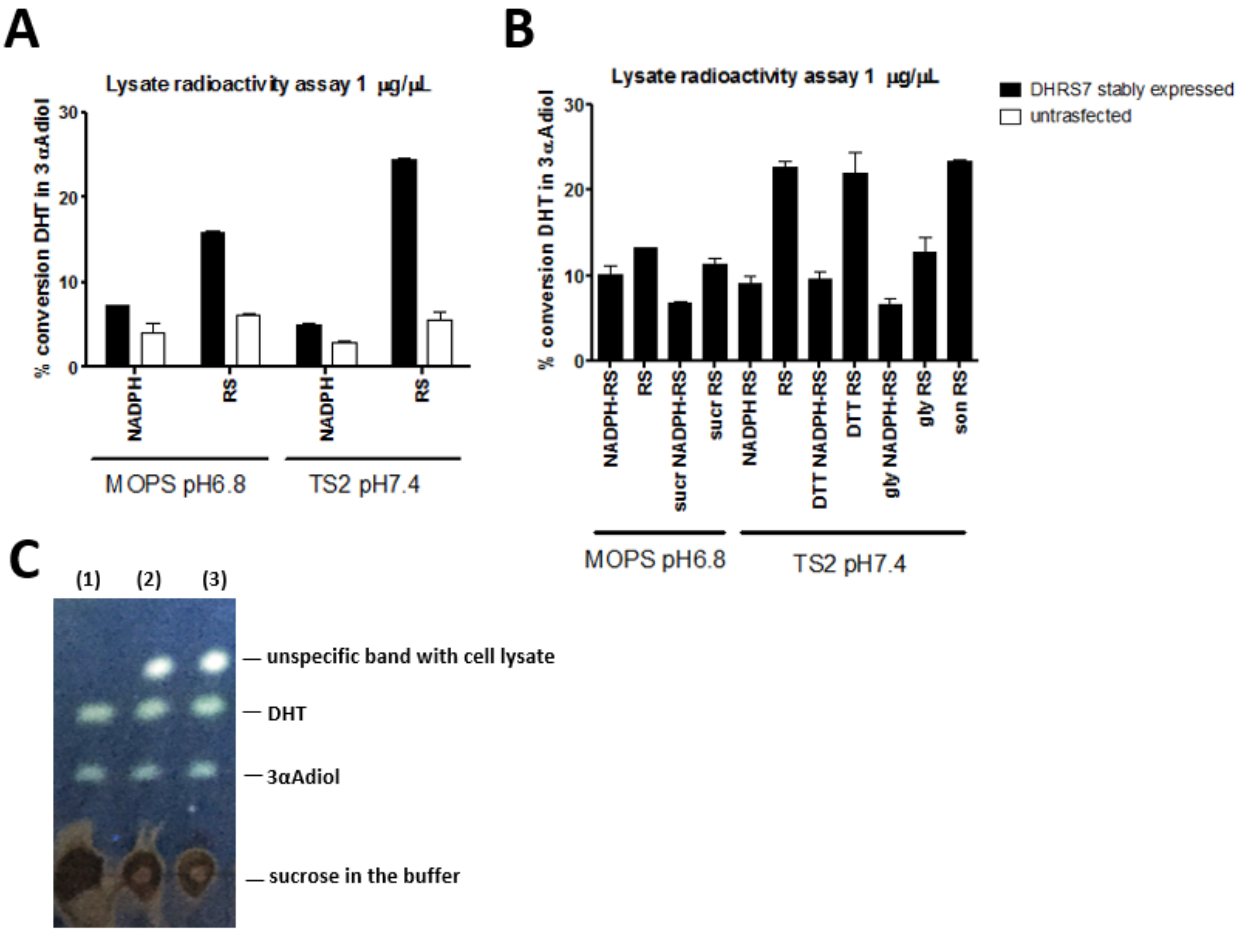

Figure 19: Radioactivity assay optimization with 1 µg/µL for 2 h. A. Regeneration system versus cofactor NADPH in MOPS pH6.8 or TS2 pH7.4 buffers. B. Regeneration system (RS) versus regeneration system with NADPH instead of NADP+ (NADPH-RS), in different MOPS pH6.8 and TS2 pH7.4 buffer preparations (Sucr=sucrose, DTT= dithiothreitol, gly=glycerol instead of sucrose), C. Visualization of spots under UV light on TLC plate following radioactivity assay in lysate with TS2 pH7.4 buffer, addition of stop mix, separation, and reaction with 3% sulfuric acid (1) without lysate incubated for 1 h, (2) with lysate incubated for 1 h, and (3) with lysate incubated for 0 h. The experiments were performed in duplicates and expressed as mean ± SD

The best conversion rates (ca. 25%) were achieved after one hour with the TS2 buffer with a NADPH regeneration system under the physiological pH of 7.4 (Figure 19A). These conditions can facilitate the oxidation step of NADP+ by the enzyme G6PDH (present in the regeneration system) that facilitates the constant NADPH production needed to sustain the reduction of DHT by DHRS7. In fact, with the use of NADPH alone without the NADPH regeneration system, the activity assay at pH 6.8 seemed to perform better. Importantly, the background DHT activity in the lysate of non-transfected HEK 293 is much lower, reflecting what previously observed in intact cells (Figure 18).

The use of different combinations of MOPS pH6.8 buffer, reducing agent DTT, glycerol instead of sucrose, and sonication to solubilize of the lysate, did not increase the conversion rate (Figure 19B). Interestingly, the visualization of the selected reaction plus lysate compared to without lysate allowed for the

identification of an unspecific band (Figure 19C) that showed no radioactivity counts (data not shown), and a black spot that did not migrate, which was identified as sucrose (present only in the sucrose buffer conditions previously measured). For this reason, an additional control using no lysate was added to ensure the correct spots are scratched from the TCL plate for DHT and 3αAdiol.

The optimized buffer TS2 pH7.4 was used for evaluating DHRS7 HEK 293 stable lysate for time (Figure 20A and B) and lysate protein concentration dependency (Figure 20C and D). The results are shown as for Figure 18, with the percentage of DHT (Figure 20A and 20C) and corresponding 3αAdiol counts (Figure 20B and 20D) compared to control.

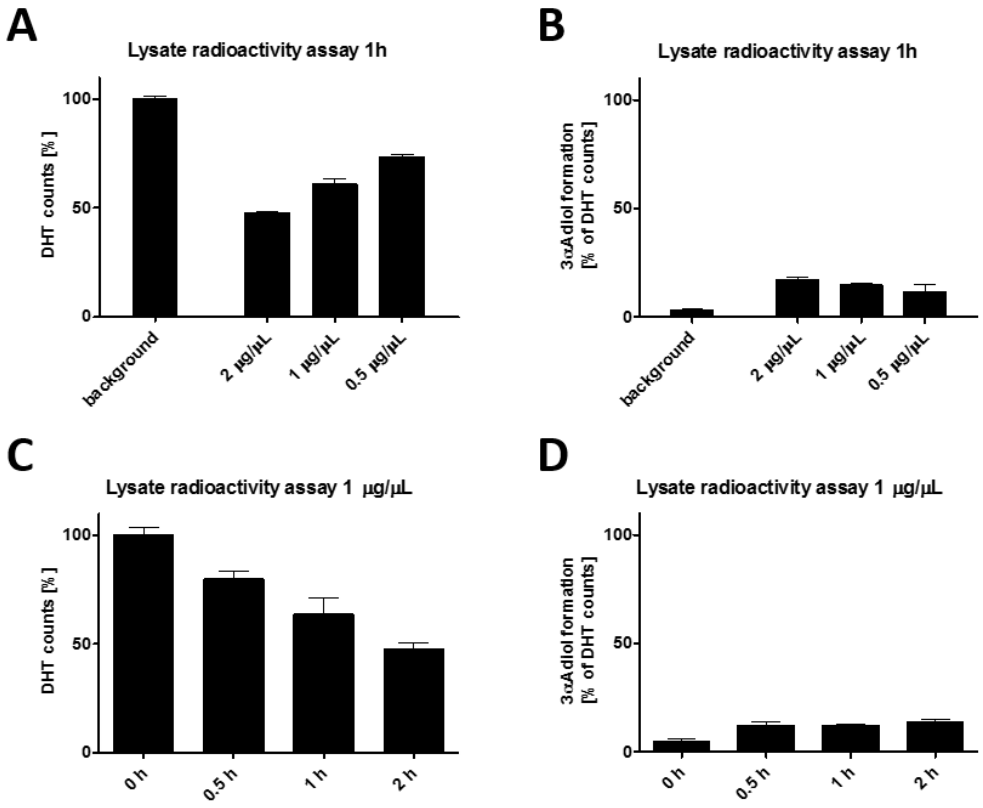

Figure 20: Protein concentration (A, B) and time dependence of DHT (C, D) and 3αAdiol (B) in lysate of HEK 293 stably expressing DHRS7. The two experiments were performed in duplicates and expressed as mean ± SD.

An increasing lysate protein concentration and time dependent DHT metabolism was observed in both experiments (Figure 20A-B and Figure 20C-D). However, 3αAdiol counts did not proportionally increase as already observed with the intact cells in both cases.

To understand whether the loss of 3αAdiol counts in the radioactivity assay is due to further metabolism in HEK 293 cells in the radioactivity assay, the assay was performed in the presence of CYP7B1 inhibitors,

an enzyme hypothesized to metabolize 3αAdiol [203, 204]. However, no changes in DHT and 3αAdiol counts were observed (data not shown). For the study of potential novel substrates or inhibitors of DHRS7 with the potential to inhibit competitively the reduction of DHT, the conditions of 1 h incubation time and 1 µg/µL of DHRS7 protein lysate concentration for the lysate radioactivity assay was chosen as being in a good trade-off between the linear range of DHT consumption (ca. 40±5% decrease) whilst maintaining low 3αAdiol counts loss.

4.2.2.3.4 Test of Substrates and Inhibitors with a Lysate Radioactivity Assay

The screening of possible substrates and inhibitors based on the newly optimized conditions (previous subchapter) is shown in Figure 21 and was performed with 24 candidate substrates at a concentration of 5 µM. Both the substrates and inhibitors were selected for the following reasons:

- Expected steroidal compounds reacting with DHRS7 based on the results of the intact cells assays: 17OHProg (Figure 16) and cortisone [191];
- The compound all-trans-retinal based on observation by Stambergova et al. [145];
- The xenobiotic compounds 9,10-phenanthrenequinone and 1,2-naphtoquinone based on [146, 205];
- The AKR1C2 substrate prostaglandin PGE_2 with its respective product PGF2α according to Nishizawa et al. [206], because of its similar 3αHSD reductive behavior in the literature [191];
- Predicted inhibitors and substrates of the related and well characterized enzyme 11βHSD1 through an in house *in silico* model (unpublished data) according to the activity observed for cortisone [191];
- Anabolic steroids with a carbonyl in position 3 alpha, hypothesized to produce a 3 alpha reduced product;
- Cancer drugs used in the context of prostate and breast cancer;

In order to maintain the integrity of the assay, a quality control threshold for the conversion of the model substrate DHT was assessed for every individual experiment. Based on the results in Figure 19 the conversion threshold of “buffer (- ctrl)” vs. “vehicle 0.5% (+ ctrl)” was set at 23±5%. Experiments failing to reach this threshold were repeated.

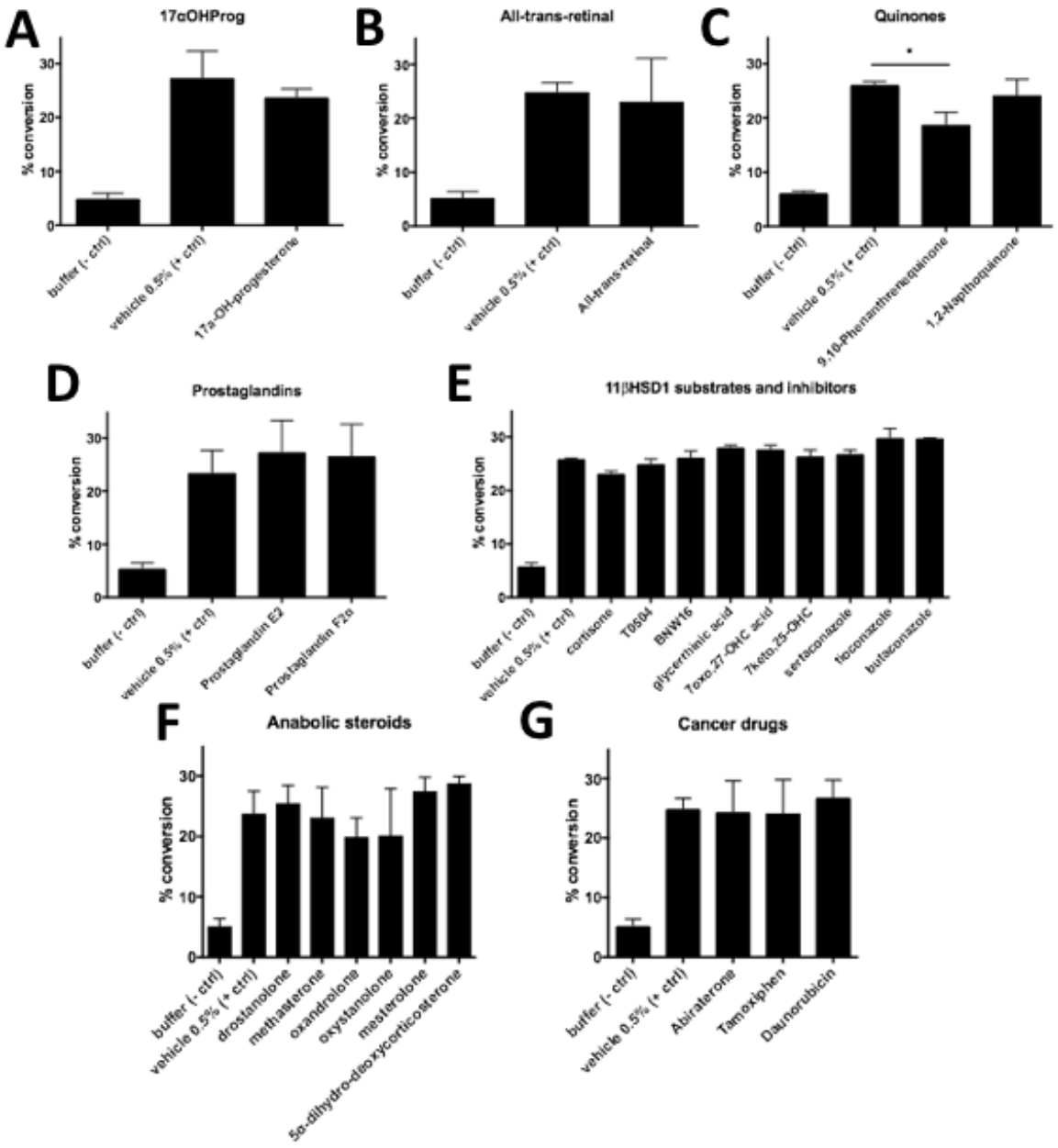

*Figure 21: Substrates and inhibitors screening with a concentration of 5 µM through radioactivity assay with 200nM DHT in lysate of HEK 293 stably expressing DHRS7: 17αOHProg (A), all-trans-retinal (B), the quinones 1,2-napthoquinone and 9,10-phenanthrenequinone (C), the prostaglandins PGE2 and PGF2α (D), possible 11ßHSD1 substrates and inhibitors (E), the anabolic steroids hypothesized to be reduced in position 3alpha (F), and the cancer drugs flutamide, abiraterone, tamoxiphen and daunorubicin (G). Lysate with 200 nM DHT, a NADPH regeneration system in buffer TS2 pH 7.4 incubated 1 h with 1 µg/µL of DHRS7 HEK 293 protein lysate concentration and 0.5% DMSO served as positive control (labelled as "vehicle 0.5% (+ ctrl)"), and buffer with 200 nM DHT, a NADPH regeneration system in buffer TS2 pH 7.4 incubated 1 h and 0.5% DMSO served as negative control (labelled as "Buffer (- ctrl)"). Data between two until four independent experiments, each performed in duplicates, was normalized to 100% vehicle control and expressed as mean ± SD. *p<0.05.*

All but one of the potential inhibitors or substrates screened in the DHRS7 HEK 293 cell lysates assay were negative. 9,10-phenanthrenequinone showed a small but significant inhibition of DHT conversion (see

Figure 21C). An IC_{50} value for 9,10-phenanthrenequinone was determined by qualitatively evaluated by LC-MS/MS after incubation with untransfected HEK and DHRS7 HEK 293 cells for 1 µM. However, the preliminary IC_{50} calculation suggested a super-physiological value of 17.45 ± 1.9 µM (data not shown). Additionally, 9,10-phenanthrenequinone was undetectable after 24 h incubation in either the untransfected or DHRS7 HEK 293 cells. This may be due to further endogenous metabolism by a yet to be identified enzyme present in HEK cells or degradation of the compound (data not shown). Studies for this metabolite were not continued.

4.2.2.4 Approximation of an Apparent Km

The optimized radioactivity assay showed that the conversion of the substrate DHT to the metabolite 3αAdiol was significantly enhanced in the DHRS7 HEK 293 stable cells compared untransfected HEK cells. However, an important limitation of this experiment was that the total counts disappeared with longer incubation times in the radioactivity assay, both in intact cells and lysate protein preparations. Further metabolism of 3αAdiol cannot thus be excluded and may affect the kinetics of the DHT reaction. Nevertheless, knowing the limitations of the assay, an attempt to calculate an apparent Km in lysate and microsomes based on DHT consumption was performed. According to the principles of Michealis-Menten kinetic [207], a linear product formation range was chosen. For lysate according to Figure 20, 1 µg/µL protein after 1 h was chosen, and an apparent Km value and Vmax were calculated through Bets Fit values model and are present in Figure 22A-B. For the microsomal preparations a time-dependent radioactivity assay was first performed after control of the preparation with increased DHRS7 concentration per protein amount in order to choose the condition for best linear product formation range (see Figure XC-E). Again a 1 µg/µL protein after 1 h was chosen. Nevertheless, due to technical limitations using frozen preparations of microsomes, resulting in high variability between independent experiments, Km value could not be calculated (data not shown).

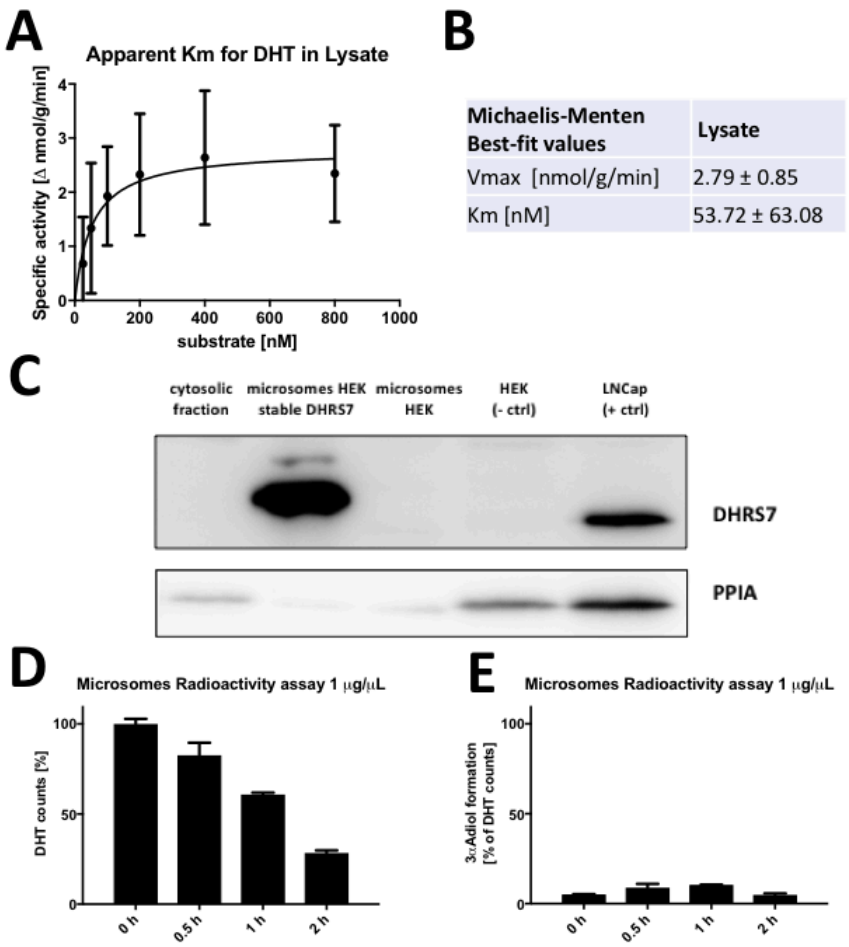

Figure 22: Calculation of apparent Km and Vmax in lysate and microsomes. A-B. Apparent Km in lysate (The experiment was performed in three independent experiments, two performed in triplicates, one performed in duplicates), C. Microsomal preparation shows increased DHRS7 expression in the microsomes of HEK stably expressing DHRS7. D-E. Time dependent radioactivity assay with 200 nM DHT, 1 µg/µL in microsomes. The experiment was performed in duplicates.

A Vmax of 2.8 ± 0.8 nmol/g/min and a Km of 53.7 ±63.1 nM were shown in whole cell lysates (Figures 22A-B). To increase the concentration of DHRS7 per total protein compared to whole cell lysate, microsomal preparations were used and showed increased DHRS7 amount in the microsomal preparationderived from DHRS7 stably expressing HEK 293 cells (Figure 22 C). Microsomal preparations showed a time dependent decrease in DHT (Figure 22 D). A concomitant, non-proportional increase in 3αAdiol was observed (figure 22E). An attempt to calculate a Km in microsomes was also attempted by using the experimental conditions; 1 µg/µL protein lysate and 1 h incubation according to the linear activity observed in Figures 22D-E. However, variability between experiments was consistently observed which prevent the calculation of the Km. Because of this technical issue and the high amount of cells needed for the isolation of microsomes (1 µg/µL microsomal protein needed for each measurement to be perform in triplicate), this experiment was not continued.

4.2.3 Discussion

The investigations presented in this chapter revealed that DHRS7 is oriented towards the cytoplasm of the endoplasmic reticulum membrane and shows 3α/20β-HSD reductive activity towards some steroidal compounds, similar to AKR1C enzymes, particularly AKR1C2. This reductive activity was observed for the 20-oxoreduction of cortisone to 20β-dihydrocortisone as well as for the reduction of 17αOHProg to 17α,20βdiOHProg (low activity of questionable physiological relevance), and for the 3-oxoreduction of DHT to 3αAdiol (potential of suppressing AR activity in the presence of DHT), as shown by activity assays in DHRS7 overexpressing HEK 293 cells. The information gained with this targeted "deorphanization" approach helped to characterize the *in vitro* activity of DHRS7; however, the physiological relevance of these reactions, in particular for the reduction of the potent AR ligand DHT, needs to be further addressed.

Regarding the activity of DHRS7 towards DHT, Zemanová et al. recently showed DHT to be a substrate by use of a combination of *in silico* structural homology modelling based on the structure of 11βHSD1, structure-based docking calculations by screening of an in-house database and a Human Metabolome Database publicly available database (HMDB, www.hmdb.ca), as well as experimental evaluations with purified DHRS7 where a Km of 48.4 ± 8.2 µM and a Vmax of 34.4 ± 4.2 nmol/mg/min were calculated [208]. However, the HPLC technique used was not able to differentiate between the alpha and beta reduced forms of the product(s). In the published work presented in this chapter, I addressed this knowledge gap by taking advantage of an improved LC-MS/MS method [191]. The Michealis-Menten kinetic values obtained are different from those of preliminary observations by Zemanová et al. In fact, the study of the reduction of DHT in whole cell lysate radioactivity assays suggests a much lower apparent Km of 53.7 ± 63.1 nM and a Vmax of 2.8 ± 0.8 nmol/g/min. Zemanová et al. used a phosphate buffer with cofactor supplementation using a glucose-6-phosphate dehydrogenase regeneration system for the calculation of kinetic values. This buffer/system can interfere with the assay by decreasing the calculated affinity values, according to the manufacturer's instructions and Domagh et al. [209]. Nevertheless, observations made in whole cell lysate radioactivity assays should be confirmed using purified DHRS7 protein and the optimized conditions for the lysate assay (see Figure 19), possibly with a parallel measurement using LC-MS/MS, which would need to be improved in order to quantify low nanomolar concentrations of DHT and 3αAdiol in a high protein content matrix.

The investigations described in the result section 4.2.2 on DHRS7 expressing HEK 293 cells revealed that only 17αOHProg was reduced on the 20β position, as it was the case for cortisone [191], out of the four tested metabolites that were reduced on the 3α and/or 20β position (20β dihydroprogesterone, cortisol,

progesterone, and 17αOHProg). Interestingly, both 17αOHProg and cortisone have a hydroxyl moiety in position 17 (see chemical structures in Figure 6 of the introduction). This chemical feature could contribute to facilitate the reaction. However, this aspect needs to be further addressed. Nevertheless, 17α-OH-progesterone was not confirmed as a competitive inhibitor of DHT reduction in the lysate radioactivity assay (see results section 4.2.2.3.4) and it is highly likely that it has no functional effects in the context of prostate cancer. Indeed, Grigoryev et al. [210] observed an increased proliferation of LNCaP prostate cancer cells following treatment with 50 nM of 17αOHProg, which corresponds to concentrations about 10-fold higher than found in the plasma under physiological conditions. Moreover, the reaction of 17α-OH-progesterone to 17α,20βdiOHProg should be confirmed in transiently DHRS7 overexpressed HEK 293 cells to exclude adaptive effects encountered following the integration of the transgene in stably transfected HEK 293 clones [211], and possibly further explored on a more physiological level by studying DHRS7 in endogenously expressing systems.

The radioactivity assay performed with lysate based on DHT reduction was unable to identify novel substrates or confirm all-trans-retinal as substrate by (competitive) inhibition of DHT reduction. Regarding this novel screening assay for candidate substrates and inhibitors of DHRS7, a positive inhibitor of DHT activity has not been identified yet and future discovery would help to optimize the assay. In this respect, 4,4-dimethylbenzil and benzyl were predicted as novel exogenous substrates of DHRS7 by docking their carbonyl group to the same catalytic amino acid Y203 of the active site of DHRS7 as DHT (see Figure 7 of the introduction) allowing the transfer of protons for reduction [208]. Regarding the negative result observed for the all-trans-retinal activity, it needs to be considered that this compound is extremely sensitive to light, oxidation, air and it is insoluble in water. Therefore, it may be the case that a higher degree of enzyme purity with decreased membrane contaminants is required to optimize this specific reaction. Similar observations apply for the negative result obtained for prostaglandin E2 (figure 21D). However, this potential candidate substrate was confirmed to be a negative substrate with the purified DHRS7 preparation, possibly only docking in the active side of DHRS7 observed by fluorescence titration of the holoenzyme but not metabolized towards the carbonyl moiety to the potential product prostaglandin F2α [208]. Additionally, in order to avoid precipitation issues in aqueous buffer preparation for lipophilic compounds as both all-tans-retinal and prostaglandins, conjugation with BSA should be tested.

5 Chapter 2: Functional and Phenotypical Characterization Following DHRS7 Depletion

In the first chapter, it was shown that DHRS7 can catalyse the reduction of the carbonyl in position 3 and 20 (3α/20β) of the steroidal backbone of the androgen DHT, the glucocorticoid cortisone, and possibly also the progestin 17αOHProg. This evidence suggested that DHRS7 may play a role in steroidal hormone dependent cancers and/or for adrenal steroidogenesis. For this reason, cell lines expressing endogenous DHRS7 from breast, prostate, and adrenal gland origin, were investigated in order to functionally and phenotypically characterize changes following DHRS7 depletion using siRNA targeted molecules. The following experimental approaches were used:

1. **Cancer and steroidogenesis assays performed in breast and adrenal cancer cell lines**. This approach tested whether the increase in proliferation, migration, and the decreased adhesion previously observed in the prostate cancer cell line LNCaP following DHRS7 depletion, are also observed in other cancer models involved in steroid hormone metabolism. In the context of breast cancer for example, Zhang Wei-Hong et al. [153] observed that immunohistochemical staining in human breast cancer *in situ* expressed higher DHRS7 protein compared to breast infiltrating carcinoma tissues, suggesting a role of DHRS7 in the context of breast cancer progression. To test this hypothesis, in this chapter steroid hormone dependent and independent breast cancer and adrenal cancer cell models were selected to investigate proliferation, adhesion and migration following DHRS7 depletion.

   Additionally, the adrenal cell line H295R was used to assess adrenal steroidogenesis following DHRS7 down-regulation. This approach aimed to support the hypothesis that DHRS7 plays a role in steroid metabolism in the adrenals, since DHRS7 is highly expressed in adrenal tissue [191] and metabolizes steroidal compounds as shown in chapter 1 (section 4);

2. **Untargeted proteomics approach following DHRS7 downregulation.** The prostate cancer cell line LNCaP was investigated using an untargeted proteomics approach at multiple time points following DHRS7 siRNA mediated depletion. This strategy allowed to:
   - Characterize the LNCaP phenotype with regard to the protein expression of SDRs and nuclear receptors;

- Test if DHT is the relevant substrate responsible for the phenotypic changes observed in LNCaP cells, which endogenously express DHRS7 and AR, by quantifying changes of androgen receptor downstream proteins;
- Quantify proteins related to proliferation, migration, and adhesion following DHRS7 knock-down;
- Generate new hypotheses underlying the observed aggressive cancer phenotype following DHRS7 knock-down;

The untargeted proteomics method was first improved with the aim to reliably identify and quantify a high number of proteins. A number of proteins identified following analysis were further validated through immunofluorescence, western blotting, cell cycle analysis, and AR transactivation.

5.1 Assessing the Phenotype of Breast and Adrenal Cancer Cell Lines under siRNA mediated DHRS7 Silencing

5.1.1 Methods

5.1.1.1 Cell Culturing

MCF-7, HCC1954, and T47D cells were a kind gift from prof. Bentires-Alj, from FMI institute, MDA-MB-453 were instead purchased by ATCC (Manassas, USA). MCF-7 cells were cultivated in Dulbecco's modified Eagle's medium (DMEM) containing 2mM L-glutamine and 4.5 g/L glucose, T47D in RPMI-1640, MDA-MB-453 in RPMI, HCC1569 in RPMI-1640, all supplemented with 10% FBS and 1% (v/v) penicillin–streptomycin (Sigma–Aldrich) at 37°C in a humidified 5% CO2 atmosphere. All the cell lines were tested monthly for mycoplasma contamination.

The human adrenocortical carcinoma cell line H295R (ATCC, Manassas, USA) was cultivated in Dulbecco's modified Eagle's medium (DMEM)/Ham's nutrient mixture F-12 (1:1, v/v) (Life Technologies, Zug, Switzerland), supplemented with 1% (v/v) IST + Premix (BD Bioscience, Bedford, MA, USA), 2.5% (v/v) Nu-serum (Lot: 2342913, BD Bioscience, Bedford, MA, USA), 15 mM HEPES buffer and 1% (v/v) penicillin–streptomycin (Sigma–Aldrich) at 37 C with a humidified 5% CO2 atmosphere. The Nu-serum consists of 25% newborn calf serum and 75% of a proprietary formulation containing epidermal growth factor, endothelial cell growth supplement, insulin, transferrin, triiodothyronine, progesterone, estradiol, testosterone, cortisol, selenous acid, ophosphorylethanolamine, glucose, amino acids, vitamins and other trace elements and nutrients in its Ham's F12 medium base. The concentrations of the supplements are not declared by the supplier. For the functional experiments, passages between 10 and 13 were used.

5.1.1.2 Determination of RNA Expression

Performed as described in method section 4.2.1.3 with primers sequences depicted in supplementaries section 9.1.1.2. For RARα, the primers were the same as used by Kalitin et al. [212].

5.1.1.3 Western Blotting

See method section 4.2.1.4. Protein loaded corresponded to 30 µg.

5.1.1.4 SiRNA mediated Silencing of DHRS7

For proliferation, adhesion and migration assays, 3 x 10^5 cells were reverse transfected in a 6 cm dish with 7.5 µL RNAiMax reagent and final concentration of 25 nM of siRNA targeting DHRS7 (D-009573-02; Thermo Scientific, Waltham, MA) or a nontargeting siRNA negative control (D-001810-03-20; Thermo Scientific) diluted in 2 mL OptiMEM. For the steroidogenesis assay in H295R, the procedure was adapted for 24 wells format (1.25 µL RNAiMax and 25 nM siRNA final concentration diluted in 66.6 µL OptiMEM).

5.1.1.5 Cell Proliferation Measurement by xCELLigence

Seeding in xCELLigence (ACEA Biosciences, San Diego, CA) 96-well format was after 24 h of siRNA mediated silencing as following: 10000 cells/well for T47D, MDA-MB-453, and HCC1569, 15000 cells/well for H295R, and 5000 for MCF-7. Proliferation was determined kinetically using the xCELLigence system according to the manufacturer's protocol. Cell proliferation measurements were performed in triplicates with programmed signal detection every 15 min after seeding and background of media was subtracted. Data acquisition and analyses were performed using the RTCA software (version 1.2; ACEA).

5.1.1.6 Cell Adhesion

96-well plates were coated with 50 μg/mL fibronectin, collagen type IV (Sigma Chemical Co., St. Louis, MO), or nothing, and blocked with 0.5% bovine serum albumin (BSA) in cell medium for 45 min at room temperature. MCF7 cells were seeded at 1×10^5 cells per well and allowed to adhere for 60 min, as previously described [213]. Wells were then washed twice with PBS, fixed with 100 µL of crystal violet solution (0.1% crystal violet in 25% MeOH in water) and left for 5 min at room temperature. The number of adherent cells in each well was quantified through staining with 0.1% crystal violet (w/v) in 25% methanol (v/v), followed by optical density (OD) absorption measurement at wavelength of 565 with a photometer (Molecular Devices, Sunnyvale, California). Cell adhesion experiments were performed in triplicates.

5.1.1.7 Transwell Cell Migration

The migration assay for MCF-7 was performed as previously described with minor modifications [147], and slightly adapted for H295R according to [214]. Briefly, 24 h post transfection, 5×10^4 for MCF-7 and 2×10^5 for H295R scrambled siRNA and DHRS7 siRNA cells were resuspended in 100 µL serum-free media and placed into the upper compartment of a Transwell chamber with 8.0-µm pore polycarbonate of a 24-well plate (Corning, New York, United States). Instead, the bottom chamber contained 600 µL of 10% FBS for MCF-7 and 2.5% and 5% Nu-serum for H295R supplemented cell culture media as chemo-attractant. After 24 h incubation, cells were stained with 0.1% crystal violet (w/v) (C3886; Sigma) in 25% methanol (v/v). No migrated cells in the upper chamber were removed using a cotton swab. Images of migrated cells which adhered to the bottom of the filter were captured with 10 photos at 20× magnification using a light microscope (Zeiss Axiovert 100; Carl Zeiss Microscopy GmbH, Feldbach, Switzerland) and cells counted using the threshold setting on Image J.

5.1.1.8 Steroidogenesis Assay

The H295R steroidogenesis assay was performed according to the OECD test guideline [215]. Briefly, H295R cells were reverse transfected with 15uL RNAiMax reagent and 25 nM of siRNA targeting DHRS7 (D-009573-02; Thermo Scientific, Waltham, MA) or a nontargeting siRNA negative control (D-001810-03-20; Thermo Scientific) diluted in 2mL OptiMEM and seeded in 12-well plates at a density of 400,000 cells/well in complete medium. The medium was replaced 48 h later with fresh phenol free medium supplemented with 10 µM Forskolin (CAS Nr. 66575-29-9, Sigma–Aldrich (Buchs, Switzerland)), DMSO (0.1% (v/v)) served as vehicle control. Cells were incubated for 24 h and 950 µL culture supernatants were collected and stored at -20°C until further analysis.

5.1.1.9 Extraction and Targeted Steroids Quantification by UPLC-MS/MS

Targeted analysis of steroid hormone levels in H295R culture supernatants was performed as previously described [216] with the help of a selective solid-phase extraction (SPE) and a highly sensitive UPLC-MS/MS. Extraction and steroidal measurements were performed by Dr. P. Strajhard. Briefly, for solid-phase extraction, 1 ml of each H295R cell supernatant was mixed with 0.1 ml of protein precipitation solution (0.8 M zinc sulfate in water/methanol 50/50, v/v) that contained deuterium-labeled aldosterone, corticosterone, androstenedione and testosterone as internal standards. After incubating the samples in a shaker for 10 min at 4°C with thorough shaking (1300 rotations/min), they were centrifuged for 10 min at 16000 g at 4°C. The supernatants (950 ml) were transferred to Oasis HLB SPE cartridges, preconditioned with methanol and water. Steroids were eluted with 1 ml of methanol after washing once with 1 ml of water and twice with 1 ml of methanol/water (10/90, v/v). The samples were evaporated to dryness and then reconstituted in 25 ml of methanol. The separation and quantification of the steroids was performed by ultra-high pressure LC–MS/MS (UHPLC–MS/MS) using an Agilent 1290 UPLC coupled to an Agilent 6490 triple quadrupole mass spectrometer equipped with a jet-stream electrospray ionization interface. The steroids were separated using a reverse-phase column (Waters Acquity UPLC BEH C18, 1.7 mm, 2.1 mm, 150 mm) and a mobile phase A and B, consisting of water–acetonitrile–formic acid (95/5/0.1; v/v/v) and (5/95/0.1; v/v/v), respectively. For data acquisition and analysis, Mass Hunter software (Agilent Technologies) was used. Stock solutions (10 mM and/or 1 mM) of above mentioned steroids were prepared in ethanol or methanol.

5.1.1.10 Statistic

For the statistical analysis of proliferation, migration and adhesion assays, the Student's t-test for parametric variables was used, with probabilities reported as two-tailed. Quantification of steroids was

analyzed through one-way ANOVA with Bonferroni post-test for multiple comparisons. The steroid levels measured in the supernatants of incubated H295R cells labelled with ND expressed a signal to noise (S/N) <3.

5.1.2 Results

5.1.2.1 Cancer assays in DHRS7 depleted breast cancer cell lines

The role for DHRS7 in different breast cancer cell lines was investigated following a promising observation in a pilot study in our laboratory performed by Dr. Julia Seibert in the breast cancer cell line ZR-75-1 [217]. The following cell lines were selected for further functional experiments based on their DHRS7 expression levels: T47D, MDA-MB-453, HCC1569, and MCF-7. DHRS7 was depleted using siRNA targeted molecules and cell proliferation was measured after 24 h by xCELLigence (Figure 23).

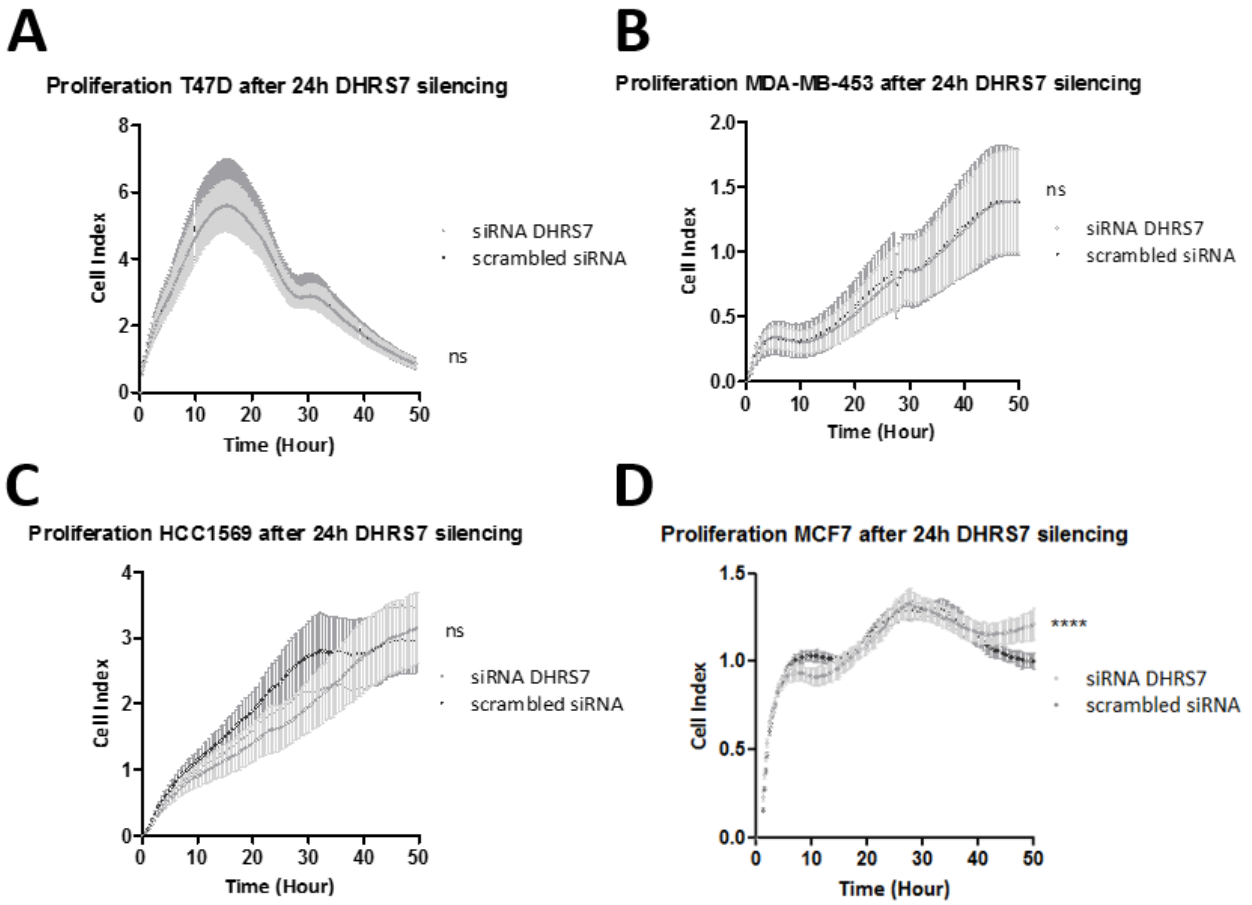

Figure 23: Proliferation after siRNA mediated silencing in breast cancer cell lines for T47D (A), MDA-MB-453 (B), HCC1569 (C), and MCF-7 (D). Experiments performed in triplicates and data expressed as mean ± SD.

No significant differences were observed in the T47D, MDA-MB-453, and HCC1569 cell lines. A small but significant increase in proliferation was observed in the MCF-7 cell line after 40 h. This cell line was then selected for adhesion and migration assays (Figure 24).

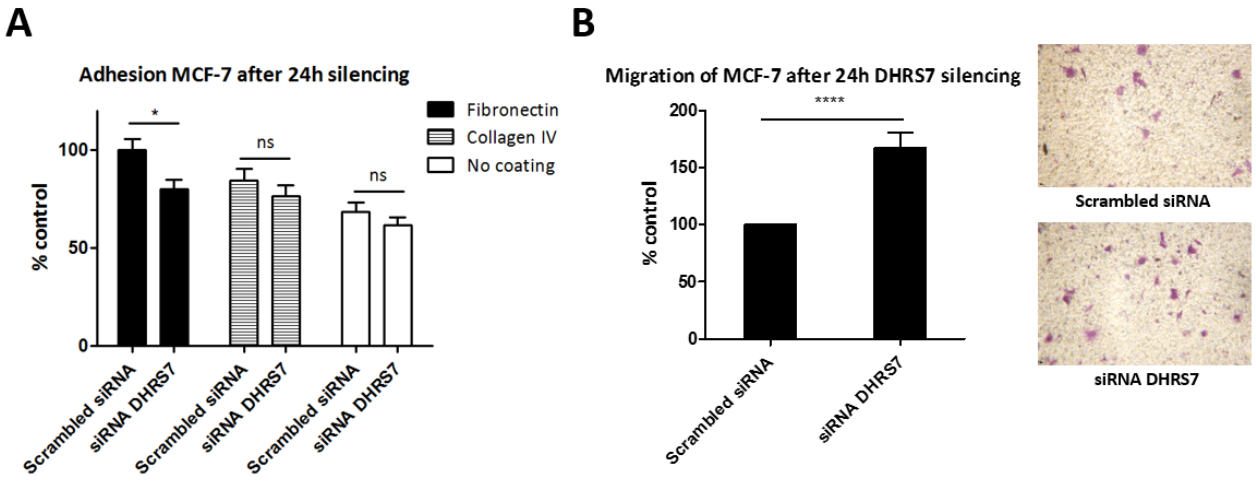

*Figure 24: Cell adhesion with fibronectin and collagen IV (A) and cell migration (B) assays for MCF7 cells. The cell adhesion was performed in three independent experiments, each performed in triplicates and, and migration in three independent experiments based on stained cells in 10 fields scanned at 20x magnification setting and analyzed using ImageJ with two representative pictures shown. Data are expressed as mean ± SD. Statistical analysis was performed using the Student's t-test. ns=not significant, *p<0.05, ****p<0.001.*

Adhesion of MCF-7 following 24 h DHRS7 siRNA mediated depletion showed a 20% decrease in adhesion on plates coated in fibronectin, a glycoprotein of the extracellular matrix that binds to membrane-spanning receptor proteins called integrins (Figure 24A). No changes in migration where observed for non-coated and collagen IV coated plates (Figure 24B).

5.1.2.2 Phenotype of the adrenal H295R under siRNA mediated DHRS7 silencing

First, the expression of DHRS7 was investigated in the adrenal cell line H295R, hypothesized to have high DHRS7 expression levels, similar to the one observed in human adrenal tissue [55] (Figure 25A-B). Additionally, DHRS7 expression was also quantified through different passages (Figure 25C), to control for possible changes in the expression, as H295R are known to loose differentiation at higher passages in culture that could affect steroidogenesis [215].

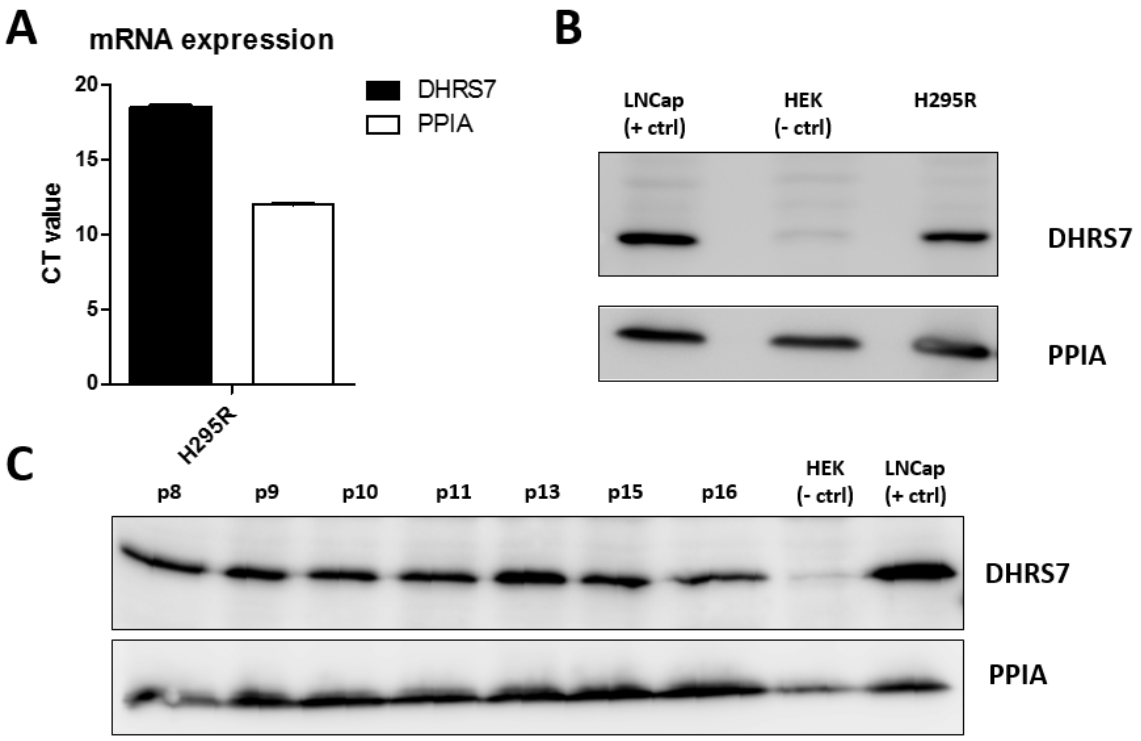

Figure 25: Expression of DHRS7 in the human adrenal steroidogenesis cell line H295R. mRNA expression (A) and protein expression in passage 5 (B) and protein expression between passages 8 and 16 (C) of DHRS7 and the housekeeping gene PPIA.

As shown in Figure 25A-B, H295R express high levels of DHRS7 mRNA and protein, and is not influenced by higher cell passage number (Figure 25C).

The functional effect of DHRS7 depletion was investigated using proliferation and migration assays. As shown in Figure 26, DHRS7 protein depletion is observed after 48 h and 72 h.

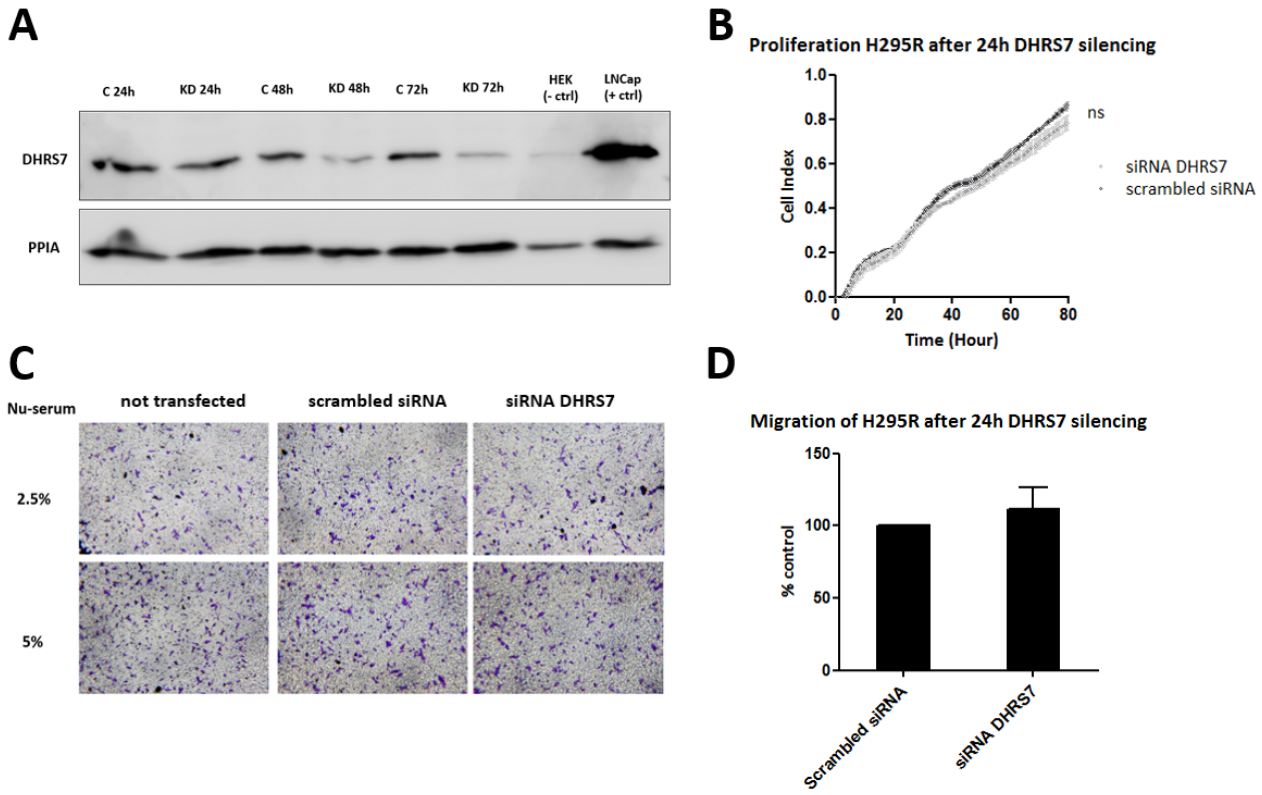

Figure 26: No significant effect on proliferation and migration on H295R cells after 24h siRNA mediated DHRS7 silencing. A. Expression of DHRS7 after siRNA mediated DHRS7 silencing after 24 h, 48 h, and 72 h (C: scrambled siRNA, KD: siRNA DHRS7). B. Proliferation of H295R cells after 24h. Experiments performed in two independent experiments in triplicates and data expressed as mean ± SD. C. Representative images of H295R in transwell after migration with 2.5% and 5% Nu-serum concentration. D. Percentage of H295R migrated cells after 24 h transfection siRNA DHRS7 versus scrambled siRNA with 5% Nu-serum.

No significant effects were observed in proliferation and migration (Figure 26).

To address the possible role of DHRS7 towards hormones involved in adrenal steroidogenesis, steroidogenesis profiling following DHRS7 depletion was performed. Briefly, following 24 h DHRS7 siRNA mediated depletion, H295R cells were exposed to either a medium control or Forskolin (to induce steroidogenesis through the cAMP pathways [218]). According to [216], Forskolin stimulation is important as it must be considered that the basal steroidogenesis rate in H295R cells is not under the control of a circadian rhythm as in the human body. The following endogenous steroid hormones were measured and quantified by LC-MS after a further 48 h incubation: progesterone, 17αOHProg, cortisol, cortisone, corticosterone, 11-deoxycorticosterone (DOC), aldosterone, 11-deoxycortisol (11-DOC), dehydroepiandrosterone (DHEA), dehydroepiandrosterone sulfate (DHEAS), androstenedione, testosterone, DHT, and 3αAdiol (see Figure 27). For steroidal structure and enzymes related reactions, please refer to Figure 6 of the introduction.

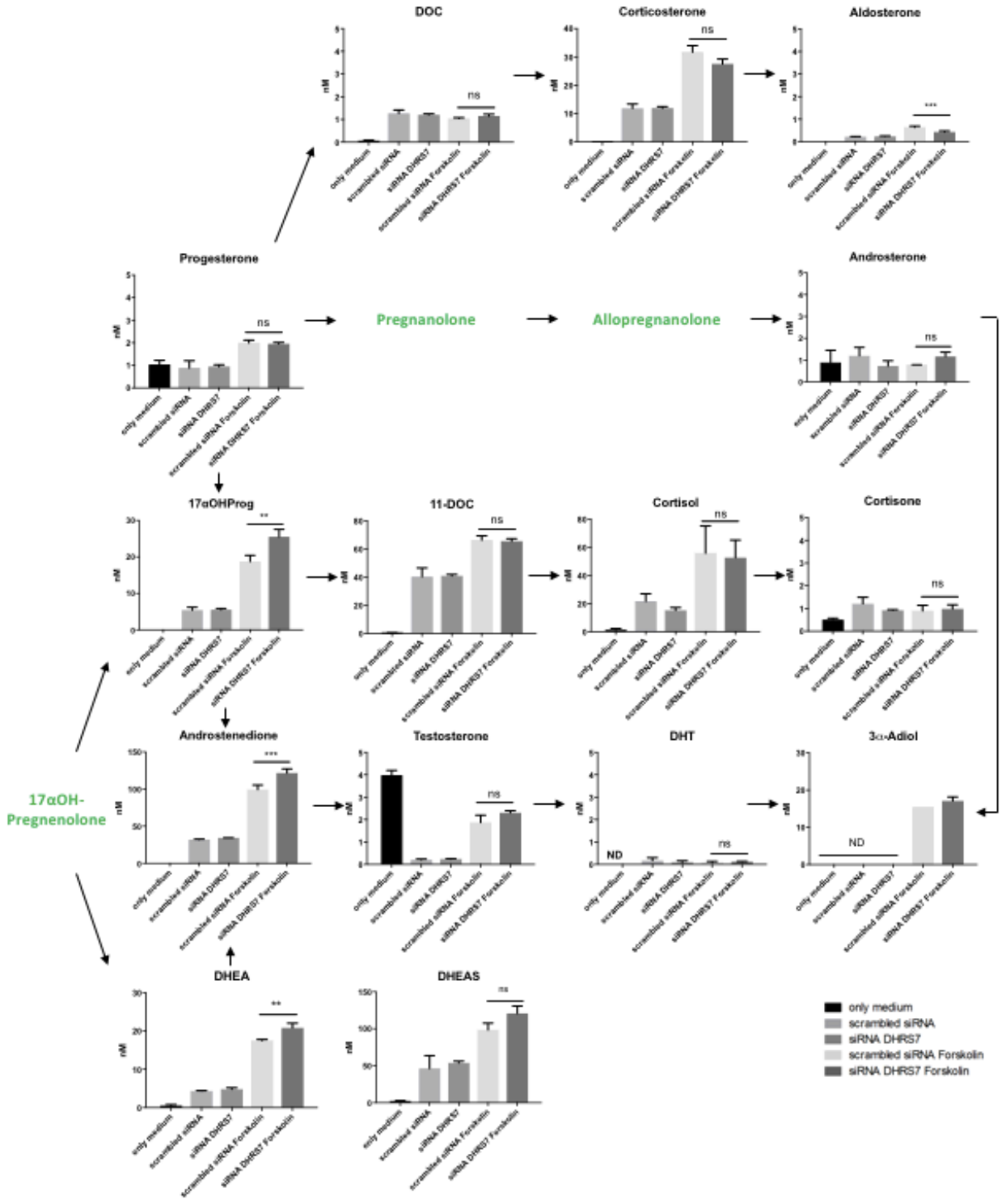

*Figure 27: Quantification of steroids in the human adrenal cell line H295R upon DHRS7 silencing and steroidogenesis induction. 17αOHProg, androstenedione, DHEA are significantly increased and androsterone is significantly decreased in DHRS7 depleted and forskolin treated cells. The experiment was performed in triplicates. In green, 17αOH-pregnenolone, progesterone and allopregnenolone were not measured, 3αAdiol was detected only once in scrambled siRNA Forskolin condition. ***p≤0.0001, **p≤0.001, ns=not significant, ND=not detected as signal to noise ratio<3.*

The quantified steroids were not changed following DHRS7 depletion under non-stimulated conditions (without Forskolin) (Figure 27). However, DHRS7 depletion under stimulated conditions (with Forskolin) showed a statistically significant upregulation in the steroids 17αOHProg, androstenedione, and DHEA. Additionally, under these experimental conditions, androsterone was detected to be slightly downregulated (Figure 27). DHT was close to the limit of detection and showed no significant changes in any of the conditions tested (Figure 27). 3αAdiol was detected only in the forskolin treated samples but was also close to the limit of detection. These two androgens are mainly produced in the prostate, as highlighted in Figure 2 in the introduction.

5.1.3 Discussion

Amongst the breast and adrenal cancer cell lines tested, only the breast cancer cell line MCF-7 exhibited a small but significant difference in proliferation as measured by xCELLigence. This observation is supported by a report in the literature which showed an increased number of cells in the S-phase of the cell cycle in DHRS7 overexpressing MCF-7 cells and conversely, an increased number of cells in the G2 phase in DHRS7 depleted MCF-7 cells, which both suggest modulation of DHRS7 affects proliferation [153]. Additionally, data presented in this chapter showed that MCF-7 cells exhibited a small decrease in adhesion (ca. 20%) using extracellular matrix protein fibronectin coated plates, yet there was an 170% increase in the number of migrating cells following DHRS7 depletion.

These two functional effects often correlate with each other as they imply mechanistic changes to the cytoskeleton arrangement by decreasing cell contacts with neighbouring cells. However, these assays do not always correlate to functional differences in proliferation, as observed by Dr. Julia Seibert [147] in DU-145 and PC3 cell lines where adhesion and migration correlated but not proliferation. Interestingly, in the thesis of Dr. Julia Seibert, another breast cancer cell line, ZR-75-1, showed promising differences in proliferation and migration following DHRS7 depletion [217].

Functional effects observed on proliferation, adhesion and migration in breast, prostate and adrenal cancer cell lines studied until now, following DHRS7 depletion, may be explained by different characteristics of the cell lines. Among many influencing factors intrinsic to the cell lines, differential expression levels of endogenous DHRS7, nuclear receptor expression and doubling time kinetics may play an important role. For example, both the breast cancer cell lines ZR-75-1 and MCF-7, as well as the prostate cancer cell LNCaP have their similarities in that they are all metastatic, originate from the luminal epithelia of their respective organ, and are positive for the androgen receptor [185, 187, 189, 190, 219, 220]. However, LNCaP and ZR-75-1 cells, showed more pronounced proliferation differences following DHRS7 depletion than MCF-7 cells. Both LNCaP and ZR-75-1 cells have a long doubling times of ca. 60 h and 54 h [221], respectively, whereas MCF-7 cells have a doubling time of ca. 38 h. Furthermore, LNCaP cells also expressed the highest DHRS7 protein levels compared to all the cell lines studied in this thesis. Whether the aforementioned intrinsic cell characteristics influence the behavior of the cell lines following DHRS7 depletion remains to be confirmed and further investigations are needed to tackle this knowledge gap.

The adrenal epithelial cancer cell line H295R, did not show any relevant effects in the functional cancer assays for proliferation and migration. They have a doubling time of ca. 36 h [222]. H295R cells were subjective to changes in proliferation, invasion or migration following downregulation of KIAA0101 [223]

or beta catenin [214]. However, under the tested conditions, the role of DHRS7 in this cell line might be related to functions independent of cancer phenotypical changes. Alternatively, the cellular machinery needed to enable DHRS7 cancer related effects seen in other cell models might not be expressed in this cell line. H295R cells derive from steroidogenic tissue (adrenals) and not androgenic tissue (prostate or testis) or estrogenic tissue (breast), therefore, it could be hypothesized that H295R cells are not responsive to DHRS7 silencing because the substrates responsible for the effects are not present. Alternatively, another explanation could be that the amount of DHRS7 downregulated was insufficient to exert an important functional difference.

On the other side, the steroidogenesis profile in H295R cells with depleted DHRS7 showed some small differences in the levels of 17αOHProg, androstenedione, DHEA, and androsterone only after Forskolin stimulation. These small changes might be related to the modulation of CYP17A1 as all these metabolites are targets of this enzyme (see Figure 6 of the introduction). However, this should be addressed by quantitative analyses.

5.2 Assessing the Phenotype of LNCaP Prostate Cancer Cells under siRNA mediated DHRS7 Silencing by Untargeted Proteomics

5.2.1 Methods

5.2.1.1 Cell culturing

The human prostate cancer cell line LNCaP was purchased from ATCC (LGC Standards GmbH, Wesel, Germany), cultivated in RMPI 1649 media (R8758; Sigma) supplemented with 10% fetal bovine serum (FBS) and penicillin (100 U/mL) /streptomycin (100 µg/mL). For the experiments, passages between 18 and 25 were used.

5.2.1.2 SiRNA mediated silencing of DHRS7

$3x10^6$ LNCaP cells were reverse transfected in 10 cm dishes with 15 µL RNAiMax reagent and 25 nM of siRNA targeting DHRS7 (D-009573-02; Thermo Scientific, Waltham, MA) or a nontargeting siRNA negative control (D-001810-03-20; Thermo Scientific) diluted in 2mL OptiMEM.

5.2.1.3 Western blotting

Samples were heated at 95°C for 5 min in Laemmli buffer (5 mmol/L Tris HCl, pH 6.8, 10% glycerol [v/v], 0.2% sodium dodecyl sulfate [SDS] [w/v], 1% bromophenol blue [w/v]) and stored at −20°C until used. 20µg of lysates were separated by a 12.5% Tris- glycine SDS-polyacrylamide gel and transferred to ImmunBlot polyvinylidene difluoride membranes (162- 0177; Bio-Rad Laboratories, Hercules, CA) at constant 230 mA for 1 h. For detection of DHRS7, the membrane was blocked using 2% milk (v/v) for 1 h at room temperature, followed by incubation with the mouse anti-human DHRS7 poly-clonal antibody (ab69348; Abcam, Cambridge, UK) at a dilution of 1:1000 (v/v) in 2% milk (v/v), overnight at 4°C. After washing with Tris- buffered saline (20 mmol/L Tris- base, 140 mmol/L NaCl) containing 0.1% Tween20 (v/v) (TBS- T), the membrane was subsequently incubated with horseradish peroxidase-conjugated goat anti-mouse secondary antibody (Jackson Immuno Research, Suffolk, UK) for 1 h at room temperature. For PPIA detection, the membrane was blocked using 10% milk (v/v) overnight at 4°C, followed by incubation with the rabbit anti- human PPIA polyclonal antibody (ab41684; Abcam) at a dilution of 1:2000 (v/v) in 2% milk for 1 h at room temperature. After washing with TBS-T, the membrane was subsequently incubated with horseradish peroxidase- conjugated goat anti- rabbit secondary antibody (Santa Cruz Biotechnology, Santa Cruz, CA) at a dilution of 1:1000 (v/v) in 2% milk (v/v). After washing the membranes in TBS- T, images were visualized using the Immobilon Western Chemiluminescent HRP substrate kit (Millipore, Schaffhausen, Switzerland), and a FujiFilm ImageQuant™ LAS-4000 detector (GE Healthcare, Glattbrugg, Switzerland) using the chemiluminescence detection setting. For quantification of AR, cOmplete™ Mini protease inhibitor cocktail [Roche] was added in the RIPA buffer for lysis, and a monoclonal anti-AR (Ref.

sc-7305; Santa Criz Biotechnology) in dilution 1:200, and a polyclonal goat anti-mouse (Ref. A0168; Sigma-Aldrich) diluted 1:2000 were used.

5.2.1.4 Cell Proliferation Measurement by xCELLigence

The xCELLigence DP device (ACEA Biosciences, San Diego, CA) was used to validate functional cell proliferation in real- time with adapted DHRS7 siRNA mediated silencing, according to [147]. The cells were seeded 24 h after siRNA mediated silencing. For test of proliferation following DHT treatment, cells seeded after 24 h siRNA mediated silencing were treated with DHT or DMSO vehicle concentrations after 24 h. Measurements were recorded from this time point every 5 minutes and results are presented with a normalized Cell Index (CI).

5.2.1.5 Androgen Receptor-dependent transactivation assay

LNCaP cells (50,000 cells/well for AR transfection) were seeded in poly-l-lysine coated 24-well plates, incubated for 24 h. For the AR transactivation assay cells were transfected with or without human AR (190 ng/well), pCMV-lacZ β-galactosidase control (10 ng/well) and TAT3-TATA luciferase reporter (300 ng/well). For AR transactivation with endogenous AR under siRNA mediated DHRS7 reverse transfection, pCMV-lacZ β-galactosidase control (10 ng/well), TAT3-TATA luciferase reporter (300 ng/well), 1.25 µL/well siRNA (DHRS7 and scrambled control, see methods section 5.2.1.2) solution and 166 ng/well of lipofectamine. The cells were then washed with steroid-free RPMI (cRPMI) and cultivated for 2 h at 37 °C. Efficiency of transfection was also checked with a green-fluorescence plasmid after 24 h. This culture medium was then replaced with fresh cRPMI containing DHT or DMSO as vehicle control followed by incubation for 24 h. Cells were lysed in 60 µl of tropix lysis solution (Applied Biosystems, Foster City, CA) supplemented with 0.5 µM dithiothreitol and frozen at −80 °C for at least 30 min. Luciferase activity was determined in 20 µl lysate adding 100 µl of D-luciferin-firefly substrate solution at a final concentration of 0.47 mM D-luciferin, 53 mM ATP, 0.27 mM coenzyme A, 0.13 mM EDTA, 33.3 mM dithiothreitol, 8 mM MgSO4, 20 mM tricine, pH 7.8. β-galactosidase activity was measured in 20 µl lysate using the Tropix kit. Samples were measured using a SpectraMax-L luminometer (Molecular Devices, Devon, UK).

5.2.1.6 Cell cycle Analysis

After 48 h siRNA mediated silencing of LNCaP in 10 cm^2 dish, cells were resuspended, washed with 5mL PBS, fixed in 3 mL 70% ice-cold ethanol in PBS, and stored in -20°C in 15 mL Falcon tubes until staining. Cells were then washed with PBS by centrifugation in swing rotor centrifuge (5 min, 200 g), resuspended in PBS fixed in 70% ice-cold ethanol, and stored in −20 °C until staining. Cells were stained for at least 30 min in the dark with a solution containing 25 µg/ml propidium iodide (Sigma), 50 µg/ml RNAse (Sigma).

The DNA content in the treated and mock-treated groups was measured by flow cytometry analysis using a FACSCanto II flow cytometer (Becton–Dickinson, San Jose, CA); 50'000 events were analyzed for each sample. FlowJo® (Becton, Dickinson & Company, NJ, USA) was used to analyze cell cycle distribution. The analysis were performed in the FACS Core Facility of the Biozentrum of Basel.

5.2.1.7 Mass Spectroscopy

After siRNA mediated silencing of LNCaP in 10 cm^2 dish, samples were washed three times with 5mL ice-cold PBS and homogenized in 1 mL ice-cold 50 mM Tris-HCl, pH 8.0, 75 mM NaCl, 8 M urea lysis buffer with protease inhibitors (complete mini, Roche) and 1 mM PMSF for 10 minutes. Scraped cells were sonicated three times 60 sec at 4°C with 20% output with 2 min rest between cycles, centrifuged 12000 rpm for 10 minutes at 4°C, and the supernatant collected and stored at -80°C. Bradford was performed to detect protein concentration.

For further samples preparation for the preliminary analysis of DHRS7 knock-down for 48 h, proteins were prepared according to [224, 225], without TIO_2 phosphopeptide enrichment. Breifly, the lysate was reduced with 2.5 mM DTT at 37°C for 1 h and alkylated with 7.5 mM iodo acetamide for 15 min in the dark at room temperature. The lysate was applied onto a PD10 desalting column and the proteins were eluted with 4 M urea buffer with 50 mM Tris-HCl, pH 8.0, and 75 mM NaCl. The protein-containing fractions (as measured by 280 nm absorbance) were pooled. The protein concentration was determined with the Bradford assay (BioRad, Medical Laboratories, CA, USA) according to the manufacturer's recommendations. The protein pools were stored at -20°C. The PD10 desalted protein pools were digested twice with the endoproteinase LysC (Wako Chemicals, Neuss, Germany) at 1:100 enzyme to substrate ratio (w/w) for two hours at 37°C. The urea concentration was lowered to 2 M with 50 mM Tris-HCl, pH 8.0 before digestion with trypsin (1:100 w/w) for two hours at 37°C. A second overnight digestion with trypsin (1:100 w/w) was done at 37°C. Trypsin digestion was stopped by adding trifluoro-acetic acid to 1% final concentration and pH<2 was checked. Peptides were desalted on C18 SepPak cartridges (50 mg packing material, Waters, Dättwil, Switzerland). The cartridges were primed with 250 µl methanol and 250 µl 80% acetonitrile/0.1% TFA and equilibrated with 750 µl 0.1% TFA. The digest was applied onto the C18 SepPak cartridge and the flow through was collected. The flow through was re-applied and the cartridge was washed with 1250 µl 0.1% TFA. Bound peptides were eluted with 350 µl 80% acetonitrile/0.1% TFA and collected into an Eppendorf tube. The absorbance of the eluate was measured at 280 nm and peptide concentration was estimated according to Wisniewski et al. [226]. For cation exchange, peptides were separated in six different fractions with HiTrapTM SP cartridge (GE Healthcare) with 1 ml of a saturation

buffer containing 7 mM KH2PO4, pH 2.65, 30% AcCN (vol/vol), 500mM KCl. Later petides were resuspended in a buffer containing 7 mM KH2PO4, pH 2.65, 30% AcCN (vol/vol), also used for collection of unbound peptides ("flow through"). The other peptides were collected by desorb the bound peptides with 7 mM KH2PO4, pH 2.65, 30% AcCN (vol/vol), and increasing concentrations of KCl: 50 mM, 100 mM, 150 mM, 250 mM, 350 mM. The six fractions were dried in a Speed Vac and stored at -20°C. The desalted digests were aliquoted and dried in a SpeedVac, resuspended in 30 µL 0.1% AcOH/2% AcCN/0.005% TFA and 2 µL injected onto the micro column.

For samples preparation for the analysis of DHRS7 knock-down for the three time-points of 24 h, 36 h, and 48 h, proteins were prepared with an imporved method as described for the preliminary analysis of 48 h knock-down. Briefly, the lysate was reduced with 10 mM DTT at 55°C for 30 min and alkylated with 50 mM iodo acetamide for 15 min in the dark at room temperature. To stop the reaction, 2-mercaptoethanol 0.33% (v/v) was applied. The lysate was applied onto a PD10 desalting column and the proteins were eluted with 4 M urea buffer with 50 mM Tris-HCl, pH 8.0, and 75 mM NaCl. The protein-containing fractions (as measured by 280 nm absorbance) were pooled. The protein concentration was determined with the Bradford assay (BioRad, Medical Laboratories, CA, USA) according to the manufacturer's recommendations. The protein pools were stored at -20°C. The PD10 desalted protein pools were digested twice with the endoproteinase LysC (Wako Chemicals, Neuss, Germany) at 1:100 enzyme to substrate ratio (w/w) for two hours at 37°C. The urea concentration was lowered to 2 M with 50 mM Tris-HCl, pH 8.0 before digestion with trypsin (1:100 w/w) for two hours at 37°C. A second overnight digestion with trypsin (1:100 w/w) was done at 37°C. Trypsin digestion was stopped by adding trifluoro-acetic acid to 1% final concentration and pH<2 was checked. Peptides were desalted on C18 SepPak cartridges (50 mg packing material, Waters, Dättwil, Switzerland). The cartridges were primed with 250 µl methanol and 250 µl 80% acetonitrile/0.1% TFA and equilibrated with 750 µl 0.1% TFA. The digest was applied onto the C18 SepPak cartridge and the flow through was collected. The flow through was re-applied and the cartridge was washed with 1250 µl 0.1% TFA. Bound peptides were eluted with 350 µl 80% acetonitrile/0.1% TFA and collected into an Eppendorf tube. The absorbance of the eluate was measured at 280 nm and peptide concentration was estimated according to Wisniewski et al. [226]. The digests were aliquoted into 150 µg portions, dried in a Speed Vac and stored at -20°C. The desalted digests were aliquoted and dried in a SpeedVac. The digested samples were dissolved in 20 mM ammonium formate, pH 4.5 (solvent A) and injected at 30 µL/min onto a 250 x 1 mm Vydac 218TPN C18, 300 Å, packed with 5 µm particles. Bound peptides were eluted at 30 µL/min with a linear gradient from 2% solvent B (20 mM ammonium formate, pH 4.5 containing 80% acetonitrile) to 50% B in 100 min. The eluent was collected into a microtiter plate

and the fractions were concatenated into six pools (pools of every sixth fraction). The pools were dried individually and subjected to LC-MS analysis by Prof. Paul Jenö and Suzanne Moes. A separating column (0.075 mm x 30 cm) packed with Reprosil C18 reverse-phase material (2.4 µm particle size, Dr. Maisch, Ammerbuch-Entringen, Germany) was used. The column was connected on line to an Orbitrap Lumos instrument (Thermo Scientific, Reinach, Switzerland). The solvents used for peptide separation were 0.1% formic acid in water (solvent A) and 0.1% formic acid and 80% acetonitrile in water (solvent B). 1.3 µg of peptide digest was injected with an Easy-nLC capillary pump (Thermo Scientific) set to 0.25 µl/min. A linear gradient from 0 to 35% solvent B in solvent A in 150 min was delivered with the nano pump at a flow rate of 0.25 µl/min. The eluting peptides were ionized at 2.5 kV. The mass spectrometer was operated in data-dependent mode. The precursor scan was done in the Orbitrap set to 120,000 resolution. Fragmentation of peptides was done by HCD (higher collisional dissociation) while the fragment ions were mass analyzed in the ion trap part of the instrument. A top twenty method was run so that the twenty most intense precursors were selected for fragmentation. The MS/MS spectra were then searched against a SwissProt human databank updated monthly.

The MS/MS data were searched with Proteome Discoverer 2.2 (Thermo Scientific) set to Mascot and SEQUEST search engines with 10 ppm precursor ion tolerance, while the fragment ions were set to 0.6 Da tolerance. The following modifications were used during the search: carbamidomethyl-cysteine was set as a fixed, and oxidized methionine and protein N-terminal acetylation were set to variable modification. The peptide search matches were set to 'high confidence', which corresponds to 1% false discovery rate (FDR). Relative protein quantification was done with the Minora module of Proteome Discoverer 2.2. and version Scaffold_4.8.4 (Proteome Software Inc., Portland, OR) was used to validate MS/MS based peptide and protein identifications. Quantification results are presented for results obtained with Scaffold_4.8.4. Peptide identifications were accepted if they could be established at greater than 8.0% probability to achieve an false discovery rate less than 1.0% by the Scaffold Local FDR algorithm. Protein identifications were accepted if they could be established at greater than 98.0% probability and contained at least 3 identified peptides. Protein probabilities were assigned by the Protein Prophet algorithm (*Nesvizhskii, Al et al, Anal. Chem. 2003;75(17):4646-58*). Proteins that contained similar peptides and could not be differentiated based on MS/MS analysis alone were grouped to satisfy the principles of parsimony.

5.2.1.8 Statistic

To define statistical relevant changed proteins, the software Perseus v.1.5.8.5, was used. Statistically changed proteins between siRNA scrambled control and siRNA DHRS7 samples were detected by

transforming normalize ion intensities to log2 and performing t-test with FDR of 5.0% and default settings for each individual time-point. For clustering analysis, data were normalized to Z-score and represented based on Euclidean model.

To detect unique expressed proteins, siRNA scrambled control (labelled as “C”) and siRNA DHRS7 samples (labelled as “KD”) where filtered for reciprocal absence or detection of normalized ion intensities. To exclude false positive or false negative data, the data were compared to normalized ion intensities of LNCaP lysate not treated in the following ways: uniquely detected proteins in “KD” a selection of proteins that were never detected for “NT” and “C”, and with no opposite regulations in previous time points or contrasting between “NT” and “C”. On the other side, for selection of proteins uniquely detected in “C”, the proteins should have been always present in “C” and in “NT” but never in “KD”, and “C” and “NT” must correlate in previous time points.

For cell cycle analysis, a t-test was applied.

5.2.1.9 Indirect immunofluorescence

LNCaP cells were seeded on glass coverslips for 24 h. Cells were than washed twice with PBS, fixed with 4% paraformaldehyde solution for 15 min and washed three times with PBS. Complete permeabilization of all cell membranes was achieved by incubation of cells with 0.1% Triton X-100 for 10 min. After washing, blocking solution containing 1% BSA was added for 15 min, followed by incubation with primary antibody for 1 h. The antibodies used were mouse polyclonal anti-DHRS7 diluted 1:100 (ab69348, Abcam), and a monoclonal rabbit anti-E-cadherin diluted 1:50 (Ref. #3195; Cell Signaling Technology, Danvers, MA, USA). Cells were then washed four times and incubated for 30 min with Alexa Fluor® 488 goat anti-mouse IgG. Hoechst-33342 was included in the secondary antibody solution (Molecular Probes®, Eugene, OR) in a final concentration of 0.1 µg/µL. After three washes with PBS, the cells were mounted in Mowiol 488 and the slides were left to settle for several hours at room temperature. Stainings were analyzed on an Olympus Fluoview 1000 laser scanning confocal microscope (Olympus, Center Valley, PA).

5.2.2 Results

5.2.2.1 Method development for measuring an optimized LNCaP proteome under DHRS7 silencing

Method development was performed to increase the protein identification until at least 3000 proteins identified based on at least 1 peptide filtered for "high confidence" (corresponding to 1% FDR) using LC-MS/MS detection, performed with the Thermo Finnigan TSQ Quantum Classic Mass Spectrometer System. To help achieve such a high coverage of proteins, $3x10^6$ LNCaP cells were processed with two additional steps to a standard internal protocol used by prof. Paul Jenö: gel filtration and cation exchange (in yellow in the protocol flow chart in Figure 28A). This procedure allowed to increase the coverage as illustrated in Figure 28B.

A

B

	Identified proteins
before	917
gel filtration and cation exchange	3039

Figure 28: Overview of the approach used to increase capturing the LNCaP proteome by addition of gel filtration and cation exchange in the protocol. A. Sample preparation workflow (in yellow the added steps). B. Number of identified proteins before and after protocol improvement based on one peptide.

By adding these additional steps, the total number of proteins identified based on single peptide detection was improved from 917 to 3039 (Figure 28B). The protocol was implemented for the analysis in Figure 30.

The siRNA mediated knock-down conditions were optimized to perform DHRS7 depletion with $3x10^6$ LNCaP cells, as used for the increased achieved sensitivity (Figure 28). Three criteria were tested; morphology of the cells (microscopic evaluation), DHRS7 protein depletion (immunoblotting) and for condition 2 functional proliferation (performed using xCELLigence®) (figure 29A-D).

A

	Condition 1	Condition 2	Condition 3
OptiMEM [µL]	2000	2000	2000
siRNA [nM]	25	25	15
RNAiMAX [µL]	30	15	30
Total volume [µL]	12000	12000	12000

B

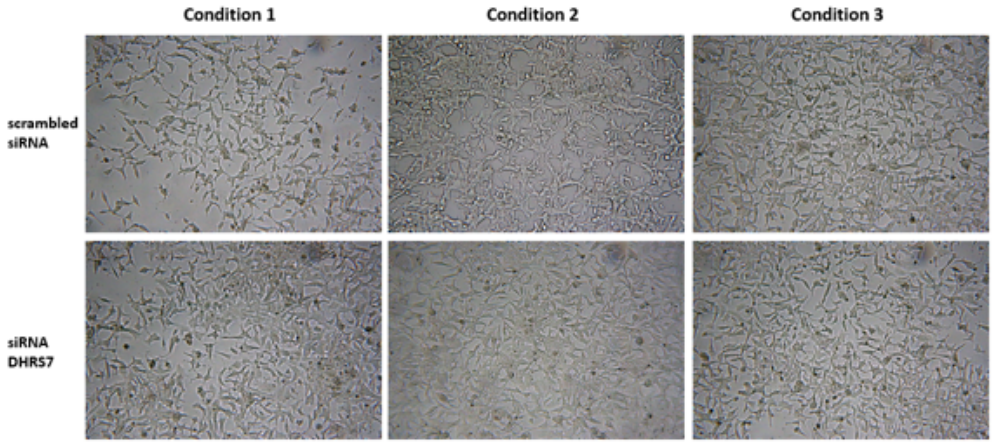

C

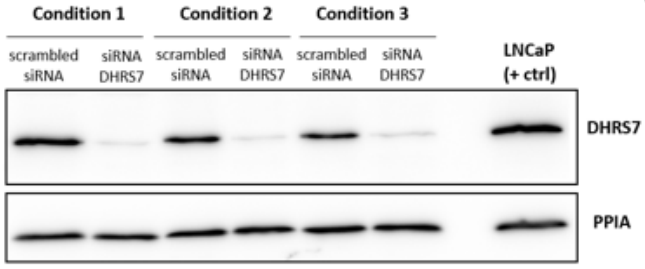

D

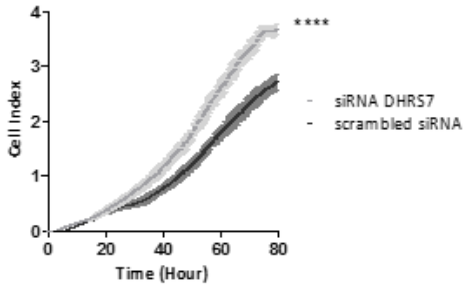

*Figure 29: A. Validation of DHRS7 knock-down protocol for 3 millions cells. A. Conditions used for effective silencing; B. representative pictures with 10x magnification before lysis after 48h siRNA mediated silencing; and C. Western blotting of 20 µg LNCaP lysates for the three conditions used; D. Cell proliferation of LNCaP cells after 24 h siRNA mediated DHRS7 silencing with the selected "condition 2" in xCELLigence. The experiment was performed in duplicates and expressed as mean ± SD. ****=p<0.0001.*

Condition 2 was selected based on appreciable DHRS7 protein downregulation whilst maintaining morphological integrity as observe in the representative images in Figure 29B and C. This condition also showed a significant increase in proliferation in the following DHRS7 depletion (Figure 29D).

In order to help understand the mechanisms which caused the LNCaP cells to proliferate at an increased rate following DHRS7 siRNA depletion, a global proteomic analysis of the LNCaP cells at the 48 h timepoint vs. scrambled control was performed. For each condition, three biological replicates were tested. The

Orbitrap ELITE MS Hybrid Ion trap mass spectrometer was selected to analyze the samples. Protein identification was performed with 1% FDR and on at least one single peptide identification. The relative quantification was performed by Scaffold and the statistical analysis by Perseus.

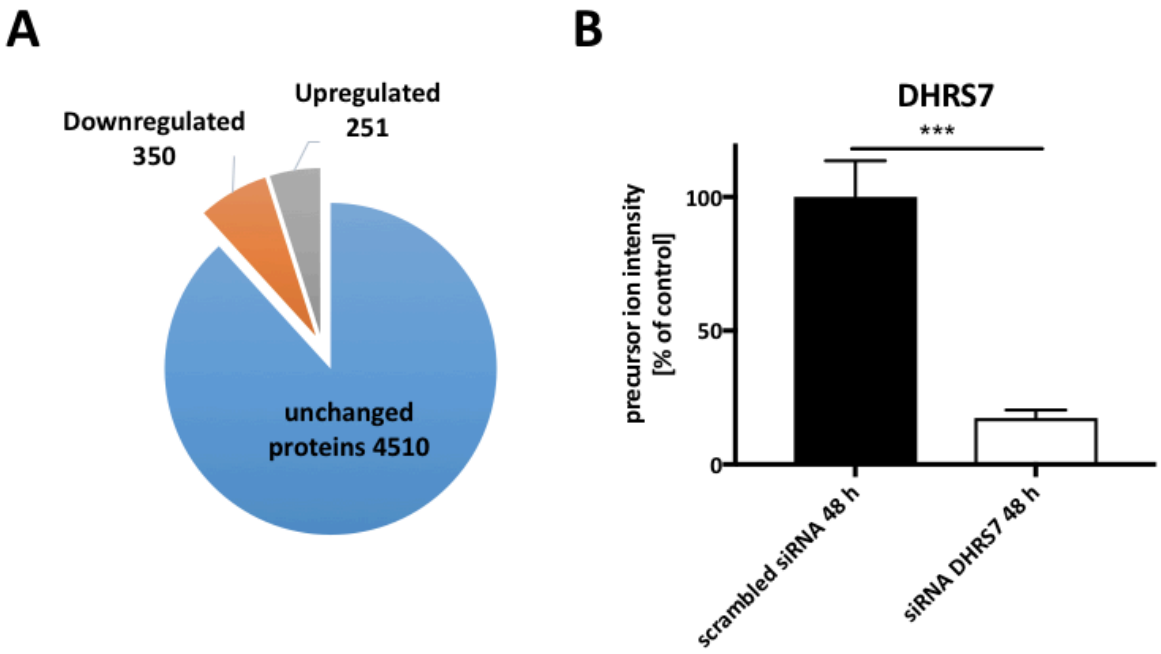

*Figure 30: A. Number of identified and qualitatively regulated proteins after DHRS7 siRNA mediated depletion after 48 h in LNCaP based on one peptide with Scaffold; B. Regulation of DHRS7 protein according to Scaffold under the DHRS7 knock-down time point 48 h. Data are depicted from three independent experiments measured in the six cation exchange fractions and are expressed as mean ± SD. ***=p<0.0005.*

Following single peptide filtering, the total number proteins identified corresponded to 5111, of which 350 were downregulated and 251 were upregulated (Figure 31A). DHRS7 (accession number Q9Y394) was identified by 10 exclusive peptides which accounted for 44% protein coverage (149 amino acids out of 339) (Figure 30A). The protein levels of DHRS7 was depleted ca.82.6 % in the DHRS7 knock-down condition compared to scrambled control (Figure 30B). Fourteen of the upregulated proteins were uniquely expressed in the siRNA DHRS7 condition (Supplemental Table 9), and 24 of the downregulated proteins were uniquely expressed in the siRNA scrambled control condition (Supplemental Table 10). Proteins identified with expression changes of greater than 1.5 fold for both the siRNA scrambled and siRNA DHRS7 conditions are shown in Supplemental Tables 11-12 (section 9.1.1.4).

Regulated proteins presented in Tables 9-12 are involved in several important cellular processes with regards to the phenotype observed in DHRS7 depleted LNCaP cells such as cell cycle, proliferation, migration and adhesion. For example, with respect to cell cycle and proliferation, Cyclin-T2, anaphase promoting complex 1 ANAPC1, CDK1 was downregulated with 0.5 fold. EGFR was only identified in the siRNA DHRS7 treated LNCaP cells. Additionally, the retinoblastoma associated protein RB1 was downregulated ca. 0.2 fold (Table 12). With respect to migration and adhesion, fibronectin, E-Cadherin, and catenin alpha 1 were downregulated ca. 0.3 fold, ca. 0.6 fold and ca. 0.6 fold, respectively. Desmocollin-2 and CD166 antigen also named ALCAM were upregulated ca. 9.0 fold and ca.2.4 fold, respectively. Interestingly, unique expression of Occludin was detected in the scrambled siRNA control condition. Unexpected, the androgen receptor was downregulated 0.6 fold (Table 12). Interestingly, among the regulated proteins with low annotated function and playing important roles in differential pathways, proteins involved in membrane lipid metabolic pathway such as monoacylglycerol lipase ABHD2 [227], the lysosomal spingomyelin phosphodiesterase SMPD1 [228, 229], and LPCAT1 [230] were highly regulated with an upregulation of 4.6 fold, 7.7 fold and downregulated of 0.2 fold, respectively.

The proteins in Tables 9-12 represent interesting candidates for follow up studies to further investigate their involvement in the observed proliferative phenotype. However, first confirmation of the altered expression of selected proteins must be confirmed by more traditional cell biology techniques such as immunoblotting. Additionally, the mass spectrometry analysis method for the identification and quantification of proteins can still be improved. This may be achieved by Increasing the number of peptides used to identify individual proteins. Furthermore, it needs to be considered that proteins uniquely detected in one condition (Tables 9 and 10) are often close to the limit of detection, thus may not contribute to the functional effects observed.

5.2.2.2 Untargeted Proteomics Analysis Following Time-Dependent DHRS7 Silencing

5.2.2.2.1 Samples Preparation

The method development and the first proteomic analysis of DHRS7 depleted LNCaP cells at the 48 h timepoint discussed in results section 5.2.2.1 allowed for sufficient global protein identification and quantification, which highlighted some potentially important alterations in protein expression. In the following work, the sensitivity of the assay was further improved using HPLC fractionation following the use of sensitive Orbitrap Lumos mass-spectrometer. Combined fractions were measured in triplicate. To allow for more accurate coverage to perform protein quantification, only proteins identified by at least three unique peptides were selected. Moreover, to better discriminate between the cause and consequence of the observed protein alterations, three time points, 24 h, 36 h and 48 h, following DHRS7

depletion, were selected. Additionally, at 0 h a non-treated sample was lysed and served as a technical control to exclude false negative or false positive protein detection. The sample preparation protocol flow diagram used to analyze the proteome of DHRS7 depleted LNCaP cells shown in Figure 31A. The results of the proteome analysis were later compared with the results of the other functional assays tested in order to identify proteins which may drive the LNCaP cells aggressive phenotype following DHRS7 depletion. Cells transfected with DHRS7 siRNA or scrambled control showed no morphological abnormalities before lysis at any of the time points tested (Figure 31B). DHRS7 immunoblot confirmed the time dependent DHRS7 protein depletion of LNCaP cells at 24 h, 36 h and 48 h (Figure 31C). Samples in ice cold urea lysis buffer were reduced, alkylated and protein filtrated to remove low molecular weight proteins and contaminants such as EDTA. Sample proteins were collected in fractions 2 and 3 where they are concentrated, evident by an increased OD280 value (Figure 31D) (absolute protein concentrations of each sample are shown in Figure 31E). Sample protein in fractions 2 and 3 were pooled, trypsin and Lys C digested, and de-salted (peptide concentrations of each sample are shown in Figure 31F) and 150 µg of sample peptides were fractionated by high performance liquid chromatography (HPLC) and pooled into 6 individual fractions. Peptide analysis was performed with the sensitive Orbitrap Lumos mass-spectrometer in triplicate.

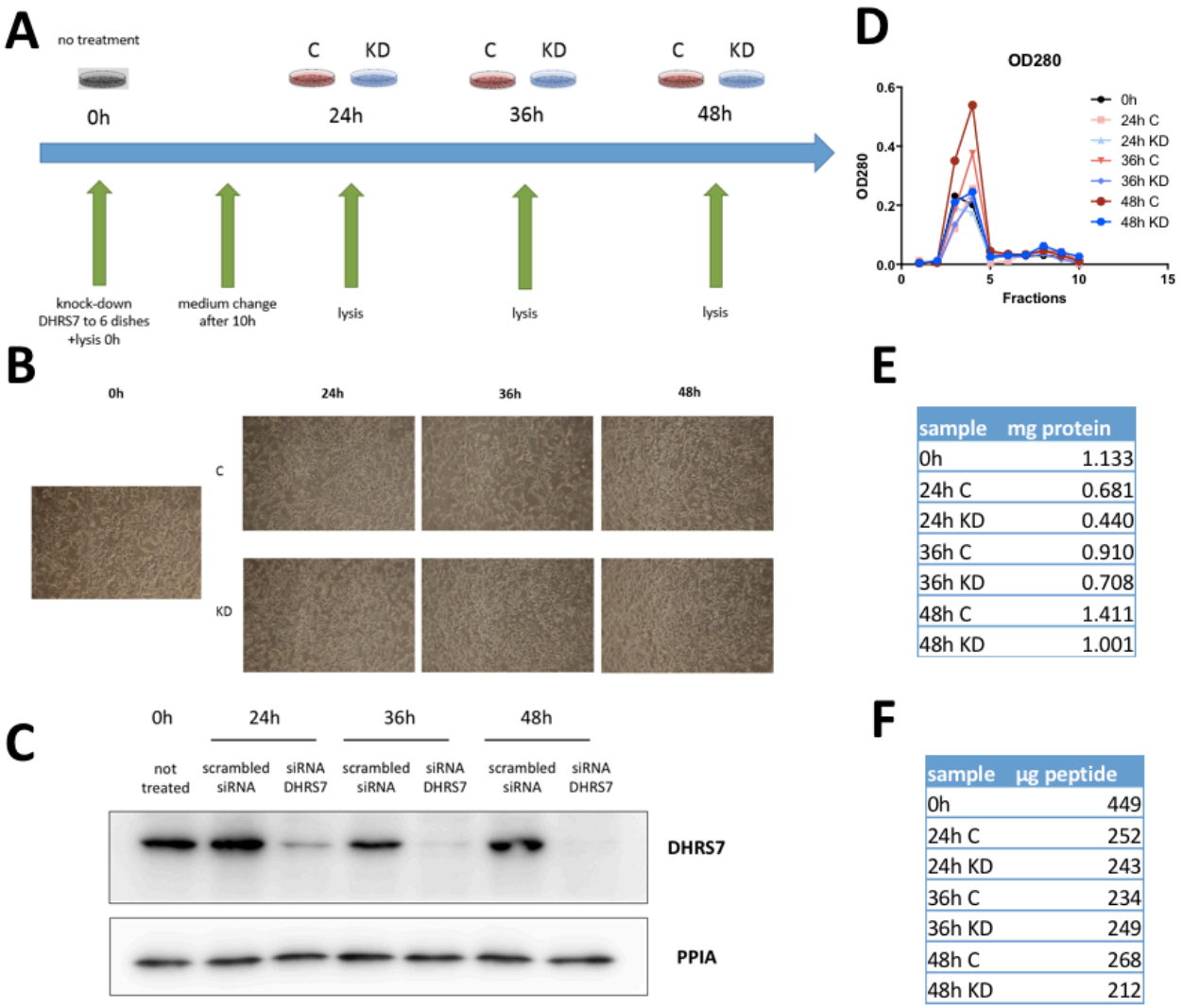

Figure 31: Design and samples preparation of DHRS7 silencing in LNCaP after 24 h, 36 h, and 48 h. A. Experimental design (C= scrambled siRNA, KD=DHRS7 siRNA); B. Representative pictures 10x magnification of LNCaP cells after different time points of knock-down previous lysis, C. Western blotting of 20 µg lysed samples for DHRS7 immunodetection, D. OD280 after protein filtration showing signal detection of protein specific for fractions 3 and 4, E. Protein amount of pulled fractions 3 and 4, F. Peptide quantification based on measured OD280 after digestion of 1050 µg for the no treatment sample "0h" and of 350 µg protein for the other samples. C= scrambled siRNA, KD=siRNA DHRS7.

According to the Figure 31B, cells looked optically good and were processed for lysis with ice-cold urea buffer. According to Figure 31C, DHRS7 was judged to be enough downregulated. After the protein filtration in which proteins were collected in fractions 2 and 3 (noticeable through increased OD280 in these two fractions as shown in Figure 31D, which amount is shown in Figure 31E), proteins were digested and desalted. From the measured amount of peptides (Figure 31F), 150 µg were used for HPLC fractionation and were further combined into six pools (pools of every sixth fraction), consequently subjected to the mass spectrometry and bioinformatics analysis.

5.2.2.2.2 Untargeted Characterization of LNCaP Phenotype

After protein identification with a 5% FDR, the results were filtered for identification based on three peptides. The relative quantification was performed using Scaffold. The quantified data are presented following statistical analysis using Perseus. The number of identified and regulated proteins for each timepoint (Figure 32A, cluster analysis highlights upregulated proteins in red and downregulated proteins in green), and the regulation of DHRS7 (accession number Q9Y394) is shown in Figure 32B.

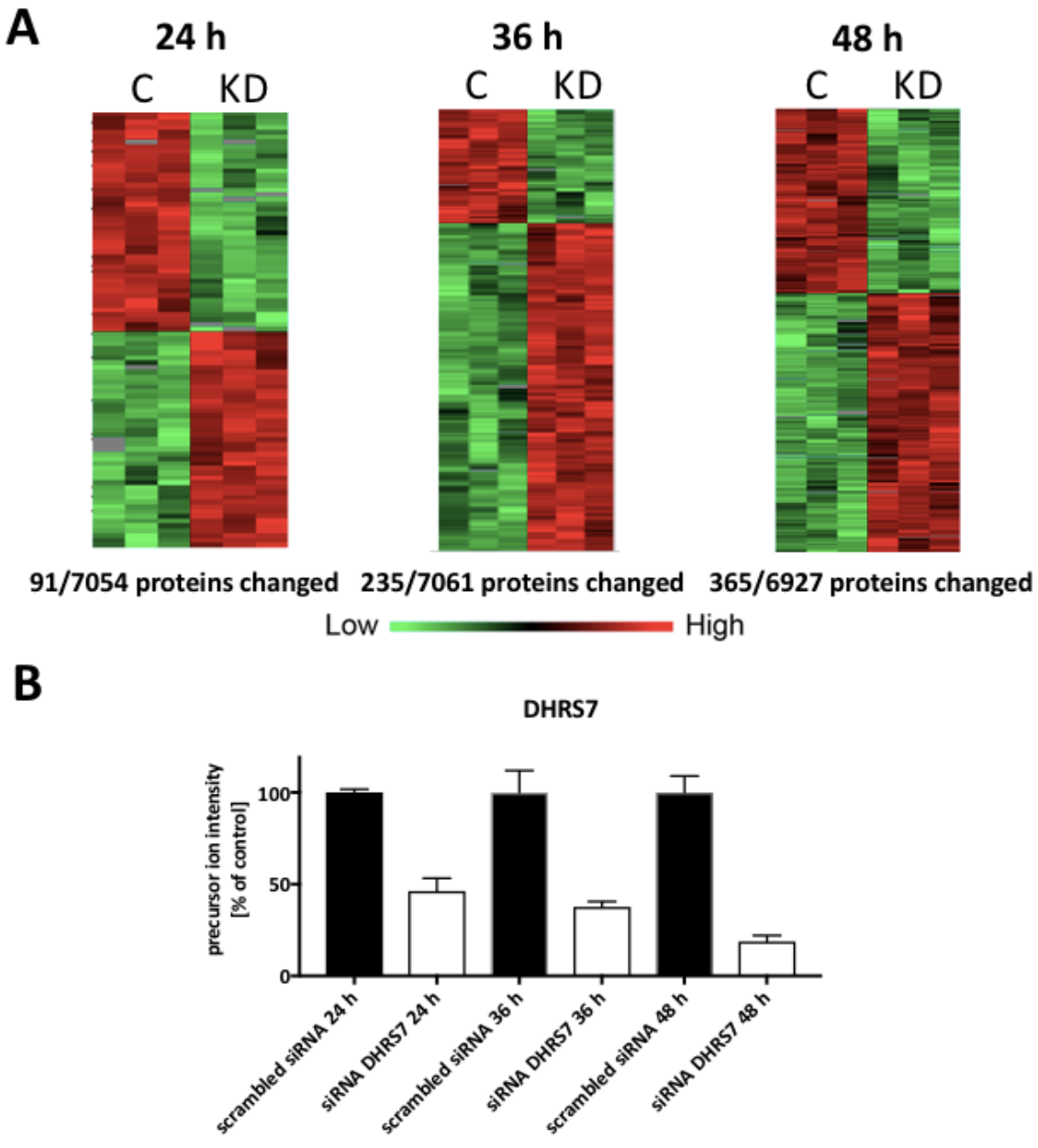

Figure 32: Untargeted proteomics analysis under three different time points 24h, 36h, and 48h as measured by Scaffold. A. Proteins changed in the three different time points 24h, 36h, and 48h (data are expressed as mean of three technical replicates of an independent experiment measured in six HPLC fractions. Green=downregulated, red=upregulated). B. downregulation of DHRS7 expressed as mean ± SD of precursor ion intensities values. C = scrambled siRNA, KD = siRNA DHRS7.

Clustering analysis showed the number of proteins with an altered expression increased with time (figure 32A) (ca. 1.3% for 24 h, ca. 3.33% for 36 h, and ca. 5.27% for 48 h) from a total of ca. 7000 ± 62 proteins identified. The substantial increase in the proteins identified from the whole cell lysate compared to the previous method performed in results section 5.2.2.1 reflects the higher sensitivity of the assay, even though stricter filtering rules were applied (proteins were only identified if 3 unique peptides were detected not just 1 unique peptide as in the previous method).

The expression levels of DHRS7 were depleted in a time dependent manner, ca. 54%, 63%, and 82%, for the time points 24 h, 26 h, and 48 h, respectively (figure 32B).

Proteins changed consistently over the 3 time points are presented in Table 3, under the heading "always changed". Proteins changed at the 24 h and 36 h time points are presented in Table 4 under the heading "early changed". Proteins changed at the 36 h and 48 h timepoint are presented in Table 5 under the heading "late changed". Additionally, proteins changed at the 24 h and 48 h timepoint were filtered for 0.666 fold (downregulation) and 1.5 fold (upregulation) change of scrambled siRNA versus siRNA DHRS7 condition and are presented in the supplemental Tables 13-14. Finally, uniquely expressed proteins identified following siRNA DHRS7 knock-down (labelled as "KD") or the siRNA scrambled control (labelled as "C") are depicted as average values and are presented with the additional "not treated" sample control (labelled as "NT") (Table 6).

Table 3: Proteins always changed in the three time points 24 h, 36 h, 48 h.

Proteins always changed (24 h, 36 h, 48 h)		
Common name	Short Name	Regulation
Leucine-rich repeat neuronal protein 1	LRRN1	upregulation
Paternally-expressed gene 3 protein	PEG3	upregulation
Endoribonuclease Dicer	DICER1	upregulation
Zinc finger CCHC domain-containing protein 3	ZCCHC3	upregulation
Anillin	ANLN	downregulation
Cadherin-1	CDH1	downregulation
Spondin-2	SPON2	downregulation
Serine/threonine-protein kinase Chk1	CHEK1	downregulation
Cytokine receptor-like factor 3	CRLF3	downregulation
Dehydrogenase/reductase SDR family member 7	DHRS7	downregulation
MAX gene-associated protein	MGA	downregulation
Molybdenum cofactor sulfurase	MOCOS	downregulation
Mortality factor 4-like protein 1	MORF4L1	downregulation
Serum response factor-binding protein 1	SRFBP1	downregulation
TATA element modulatory factor	TMF1	downregulation
Ubiquitin-conjugating enzyme E2 Q1	UBE2Q1	downregulation

Table 4: Proteins changed in the two time points 24 h and 36 h.

Early changed proteins (24 h - 36 h)		
Common name	Short Name	Regulation
Testis-expressed protein 2	TEX2	upregulation
C-Maf-inducing protein	CMIP	upregulation
Disintegrin and metalloproteinase domain-containing protein 10	ADAM10	downregulation
Occludin	OCLN	downregulation
Transcription initiation factor TFIID subunit 7	TAF7	downregulation
Tumor protein p63-regulated gene 1-like protein	TPRG1L	downregulation

Table 5: Proteins changed in the two time points 36 h and 48 h.

Late changed proteins (36 h - 48 h)		
Common name	Short Name	Regulation
Kelch repeat and BTB domain-containing protein 7	KBTBD7	upregulation
Trinucleotide repeat-containing gene 6C protein	TNRC6C	upregulation
Methionine aminopeptidase 2	METAP2	upregulation
Hornerin	HRNR	upregulation
Collagen alpha-1(VI) chain	COL6A1	upregulation
Keratin, type II cytoskeletal 1	KRT1	upregulation
CD166 antigen	ALCAM	upregulation
DNA replication licensing factor MCM2	MCM2	downregulation
Catenin beta-1	CTNNB1	downregulation
Fibronectin	FN1	downregulation
Signal transducer and activator of transcription 2	STAT2	downregulation
E3 ubiquitin-protein ligase UHRF1	UHRF1	downregulation
DNA polymerase delta subunit 2	POLD2	downregulation
Charged multivesicular body protein 7	CHMP7	downregulation
Putative oxidoreductase GLYR1	GLYR1	downregulation
DNA replication licensing factor MCM7	MCM7	downregulation
Pseudouridylate synthase 7 homolog	PUS7	downregulation
Inositol polyphosphate 5-phosphatase OCRL-1	OCRL	downregulation
TATA element modulatory factor	TMF1	downregulation
E3 ubiquitin-protein ligase CBL	CBL	downregulation
Hexokinase-2	HK2	downregulation
Replication factor C subunit 2	RFC2	downregulation
Proline-rich protein PRCC	PRCC	downregulation
Enhancer of mRNA-decapping protein 3	EDC3	downregulation
Lymphokine-activated killer T-cell-originated protein kinase	PBK	downregulation
Retinoblastoma-associated protein	RB1	downregulation
Ubiquitin-conjugating enzyme E2 T	UBE2T	downregulation
Chromosome-associated kinesin KIF4A	KIF4A	downregulation
UAP56-interacting factor	FYTTD1	downregulation
Uveal autoantigen with coiled-coil domains and ankyrin repeats	UACA	downregulation
Sperm-specific antigen 2	SSFA2	downregulation
Fibronectin type-III domain-containing protein 3A	FNDC3A	downregulation
E3 ubiquitin-protein ligase ZNF598	ZNF598	downregulation
Protein timeless homolog	TIMELESS	downregulation
DnaJ homolog subfamily C member 3	DNAJC3	downregulation

Allograft inflammatory factor 1-like	AIF1L	downregulation
Kinetochore protein NDC80 homolog	NDC80	downregulation
Mitotic checkpoint serine/threonine-protein kinase BUB1 beta	BUB1B	downregulation
Fanconi anemia group I protein	FANCI	downregulation
Kinesin-like protein KIF11	KIF11	downregulation
Exportin-4	XPO4	downregulation
Kinesin-like protein KIF14	KIF14	downregulation
Zinc finger CCCH-type antiviral protein 1-like	ZC3HAV1L	downregulation
Disks large-associated protein 5	DLGAP5	downregulation
DNA polymerase delta catalytic subunit	POLD1	downregulation
Targeting protein for Xklp2	TPX2	downregulation
UV-stimulated scaffold protein A	UVSSA	downregulation
TBC1 domain family member 5	TBC1D5	downregulation
Nuclear distribution protein nudE homolog 1	NDE1	downregulation
Adenosine deaminase	ADA	downregulation
Hyaluronan mediated motility receptor	HMMR	downregulation
MICAL-like protein 1	MICALL1	downregulation
Kinesin-like protein KIF22	KIF22	downregulation
Interferon regulatory factor 6	IRF6	downregulation
Kinesin-like protein KIF20A	KIF20A	downregulation
Tonsoku-like protein	TONSL	downregulation
Condensin-2 complex subunit D3	NCAPD3	downregulation
Thymidylate synthase	TYMS	downregulation
Protein regulator of cytokinesis 1	PRC1	downregulation
Protein KHNYN	KHNYN	downregulation
Uncharacterized protein KIAA1671	KIAA1671	downregulation
RalBP1-associated Eps domain-containing protein 2	REPS2	downregulation

Table 6: Uniquely expressed proteins in the siRNA DHRS7 (labelled as "KD") or the siRNA scrambled control (labelled as "C") conditions for the time points 24 h, 36 h, and 48 h. Numbers represent the mean of precursor ion intensities values.

Accession	Protein Name	Short Name	MW	average NT24h	average C24h	average KD24h	average NT36h	average C36h	average KD36h	average NT36h	average C36h	average KD36h
Q8IZV5	Retinol dehydrogenase 10	RDH10	38 kDa	0	0	84500000	0	0	77200000	9980000	0	81800000
Q96S53	Dual specificity testis-specific protein kinase 2	TESK2	64 kDa	0	0	41900000	19500000	0	57300000	0	0	56700000
Q8IUH5	Palmitoyltransferase ZDHHC17	ZDHHC17	73 kDa	5820000	39800000	49200000	0	0	41800000	0	0	62800000
O75460	Serine/threonine-protein kinase/endoribonuclease IRE1	IRE1	110 kDa	10800000	29900000	9770000	19900000	0	37800000	0	0	29800000
Q9Y3Q8	TSC22 domain family protein 2	TSC22D2	41 kDa	378000000	595000000	416000000	95100000	53100000	222000000	0	0	257000000
Q969E8	Pre-rRNA-processing protein TSR2 homolog	TSR2	21 kDa	345000000	232000000	137000000	304000000	96300000	132000000	0	0	363000000
Q9BXS6	Nucleolar and spindle-associated protein 1	NUSAP1	49 kDa	87500000	116000000	0	93500000	146000000	0	119000000	90900000	7860000
Q9HAW4	Claspin	CLSPN	151 kDa	55300000	62600000	0	50200000	128000000	0	31600000	37500000	0
Q06190	Serine/threonine-protein phosphatase 2A regulatory subunit B'' subunit alpha	PPP2R3A	130 kDa	12000000	48000000	0	19900000	50600000	0	26400000	33500000	0
P50219	Motor neuron and pancreas homeobox protein 1	MNX1	41 kDa	71500000	39400000	0	34100000	72200000	0	52900000	42000000	0
Q8TEY5	Cyclic AMP-responsive element-binding protein 3-like protein 4	CREB3L4	43 kDa	105000000	8180000	0	145000000	52600000	0	78500000	70100000	0
O75419	Cell division control protein 45 homolog	CDC45	66 kDa	117000000	16500000	45700000	107000000	100000000	0	104000000	52900000	0
Q7Z401	C-myc promoter-binding protein	DENND4A	209 kDa	775000000	44200000	26200000	27100000	81500000	0	40400000	51100000	0
Q9UIU6	Homeobox protein SIX4	SIX4	83 kDa	154000000	41900000	13400000	159000000	50200000	0	132000000	56300000	0
P20248	Cyclin-A2	CCNA2	49 kDa	157000000	234000000	63300000	104000000	145000000	0	125000000	125000000	0
Q9HCJ3	Ribonucleoprotein PTB-binding 2	RAVER2	74 kDa	97200000	94400000	18400000	16100000	19700000	0	73600000	59100000	0
Q7L2Z9	Centromere protein Q	CENPQ	31 kDa	25500000	33100000	21700000	39300000	50900000	0	41700000	57700000	0
Q9UBQ6	Exostosin-like 2	EXTL2	37 kDa	130000000	109000000	93200000	87800000	95400000	0	137000000	101000000	0
Q6IBW4	Condensin-2 complex subunit H2	NCAPH2	68 kDa	217000000	221000000	69800000	240000000	254000000	18700000	151000000	156000000	0
Q9NRZ9	Lymphoid-specific helicase	HELLS	97 kDa	290000000	142000000	22300000	374000000	366000000	30600000	298000000	231000000	0
Q9Y3D5	28S ribosomal protein S18c, mitochondrial	MRPS18C	16 kDa	242000000	81300000	325000000	209000000	220000000	193000000	155000000	161000000	0
P28749	Retinoblastoma-like protein 1	RBL1	121 kDa	69600000	65000000	12600000	81000000	70200000	8160000	50600000	72800000	0
Q5MNZ6	WD repeat domain phosphoinositide-interacting protein 3	WDR45B	38 kDa	113000000	77000000	83700000	455000000	227000000	203000000	274000000	203000000	0
Q5XKP0	MICOS complex subunit MIC13	MIC13	13 kDa	359000000	463000000	270000000	157000000	98700000	224000000	244000000	244000000	0
Q9NPB8	Glycerophosphocholine phosphodiesterase GPCPD1	GPCPD1	76 kDa	11300000	48400000	104000000	40300000	81600000	35600000	39200000	42300000	0
Q659A1	Little elongation complex subunit 2	ICE2	110 kDa	24400000	61000000	21100000	37000000	42900000	86400000	28800000	15600000	0

Some of the proteins highlighted in Tables 3-6 and 13 were selected for further analysis based on the change in their expression levels and of related proteins in the first proteomics analysis (results section 5.2.2.1).

5.2.2.2.2.1 Characterization of LNCaP Phenotype for Nuclear Receptors and SDR Expression

Untargeted proteomics has the advantage of allowing assessment of a huge number of proteins that can be used also for a qualitative phenotypic characterization. However, these data are not absolute values and proteins can be misdetected because of not enough technical sensitivity or suboptimal samples preparation. For this reason, it is useful to compare and correlate proteins identified by untargeted proteomics with other high-throughput expression analyses such as microarray. As highlighted in section 2.2 of the introduction, known SDRs associated to cancer are often involved in steroidal, retinoic acid, lipids and prostaglandins metabolism. Consequently, I first evaluated the expression of nuclear receptors according to [231] known to be involved in these pathways (table 7), the SDRs and the phenotypically related AKR family in the LNCaP cell line (table 8). This was tested by comparing the mean relative signal intensity obtained for the scrambled control siRNA treated LNCaP cells (24 h time point) of the microarray performed in [147] with the proteins identified in the untageted proteomics analysis of scrambled siRNA and siRNA DHRS7 in results section 5.2.2.2.2 Figure 32A (time point 24 h).

Table 7: Identification and relative quantification of nuclear receptor expression in LNCaP. These proteins were identified based on three different peptides of the 24 h siRNA treated samples and compared with microarray relative signal intensity values of the 24 h scrambled siRNA treated sample of published work [147].

Protein name	Accession nr	protein identified in proteomics	mean relative signal intensity microarray*
AR	P10275	**yes**	9.75
PPARδ	Q03181	ND	8.10
RXRα	P19793	**yes**	7.73
ROR1	Q01973	ND	7.46
RXRβ	P28702	**yes**	7.37
RARα	P10276	ND	6.86
PTGFR	P43088	ND	6.50
RORγ	P51449	ND	6.44
PPARα	Q07869	ND	6.01
PPARγ	P37231	ND	5.65
PTGDR2	Q9Y5Y4	ND	5.61
AHR	P35869	ND	5.49
PTGER1	P34995	ND	4.91
PTGER2	P35408	ND	4.46
ERβ	Q92731	ND	4.23
RORα	P35398	ND	3.95
ERα	P03372	ND	3.80
GR	P04150	ND	3.60
RORβ	Q92753	ND	3.55
RXRγ	P48443	**yes**	3.40
PR	P06401	ND	3.35

Table 8: Identification and relative quantification of SDRs and AKRs in LNCaP. Receptors expression in LNCaP were identified based on three different peptides of the 24 h siRNA treated samples and compared with microarray relative signal intensity values of the 24 h scrambled siRNA treated sample of published work [147].

Enzyme family	Protein name	Accession nr	protein identified in proteomics	mean relative signal intensity microarray*
SDR	**RDH10**	Q8IZV5	**Yes (only siRNA DHRS7)**	10.05
	HSD17β4	P51659	**yes**	10.00
	RDH11	Q8TC12	**yes**	9.97
	HSD17β10	Q99714	**yes**	9.32
	DHRS7B	Q6IAN0	**yes**	8.48
	HSD17β8	Q92506	**yes**	8.00
	HSDL1	Q3SXM5	**yes**	8.00
	HSDL2	Q6YN16	**yes**	7.90
	HSD11β2	P80365	**yes**	7.70
	DHRS11	Q6UWP2	**yes**	7.61
	HSD3β7	Q9H2F3	**yes**	7.60
	DHRS13	Q6UX07	**yes**	7.75
	DHRS7	Q9Y394	**yes**	7.59
	HSD17β1	P14061	ND	7.56
	HSD3β7	Q9H2F3	**yes**	7.67
	CBR1	P82279	**yes**	7.18
	CBR3	Q9BUF7	**yes**	7.03
	DHRS1	Q96LJ7	**yes**	6.89
	DHRS3	O75911	ND	6.82
	11β1L	Q7Z5J1	ND	6.54
	RDH13	Q8NBN7	**yes**	6.46
	17β11	Q8NBQ5	**yes**	6.44
	17β14	Q9BPX1	ND	5.49
	DHRS12	A0PJE2	ND	5.43
	RDH12	Q96NR8	ND	5.20
	RDH16	O75452	ND	5.13
	HSD17β6	O14756	ND	5.00
	RDH8	Q9NYR8	ND	4.71
	DHRS2	Q13268	**yes**	4.44
	DHRS7C	A6NNS2	ND	4.10
	HSD17β12	Q53GQ0	**yes**	3.80
	HSD11β1	P28845	ND	3.70
	HSD17β2	P37059	ND	3.63
	HSD17β3	P37058	ND	3.16
	HSD17β13	Q7Z5P4	ND	2.90
	DHRS4	Q9BTZ2	**yes**	2.50
	HSD17β7	P56937	**yes**	ND
	RDH14	Q9HBH5	**yes**	ND
	CBR4	Q8N4T8	**yes**	ND
AKR	**AKR1A1**	P14550	**yes**	9.3
	AKR7A2	O43488	**yes**	6.3
	AKR1B1	P15121	ND	4.8
	AKR7L	Q8NHP1	**yes**	4.3
	AKR7A3	O95154	ND	4.3
	AKR1C1	Q04828	ND	4.1
	AKR1β10	O60218	ND	4
	AKR1C2	P52895	**yes**	4
	AKR1β15	C9JRZ8	ND	3.7
	AKR1C3	P42330	**yes**	3.7

	AKR1E2'	Q96JD6	ND	3.2
	AKR1CL1	Q5T2L2	ND	2.9
	AKR1D1	P51857	ND	2.6
	AKR1C4	**P17516**	**yes**	2.2

As expected, the major nuclear receptor expressed in the LNCaP prostate cancer cell line is the AR, supported by both proteomic analysis and microarray (Table 7). However, most of the nuclear receptor detected by the microarray analysis were not identified by the untargeted proteomics approach, even those receptors with high mean relative signal intensity values in the microarray (e.g. PPARδ, or ROR1). On the other side, SDRs and AKRs expressing medium mean relative signal intensity values on the microarray (ca. 6.8) are generally identified by the proteomics technique (Table 5). GR, PR, ERα, and ERβ and steroidal metabolism relevant enzymes AKR1C1-AKR1C2 and AKR1C3 seems to be absent or expressed at low levels (in the proteomics analysis AKR1C2 and well as AKR1C3 was not detected in all the technical replicates) (Table 8). The human glioma and non-small-cell lung cancer associated RDH10 (see Table 1 of the introduction) was detected with highest microarray value but only in the siRNA DHRS7 condition (Table 6). RDH11 is also highly expressed suggesting potential for retinoic acid metabolism by the LNCaP cells. Other identified SDRs with high mean relative signal intensity values in the microarray are HSD17β4 and HSD17β10, known both to metabolize DHT [81, 232]. AKR1C2 showed low expression levels, however, has a Km for DHT of 1400 µM [206]. These observations are important to help answer my hypothesis set out in chapter 1, which was to evaluate if DHRS7 has the potential to metabolise DHT and effectively suppress AR transactivation and thus explain its possible tumor suppressive role in LNCaP cells. This aspect is evaluated within the next subchapter.

5.2.2.2.2.2 Characterization of Protein Changes related to Androgen Receptor Regulations

Experimental evidence in chapter 1 (section 4) revealed that DHT is metabolized by DHRS7 (observation also supported by the recent publication by Zemanová et al. [208]). Additionally, experiments performed in HEK 293 cells overexpressing DHRS7 revealed that DHRS7 might suppress AR nuclear translocation and downstream transcriptional regulation in the concentration range from 1 to 100 nM [191]. In this sub-chapter, the global proteome generated following DHRS7 siRNA depletion of LNCaP cells was used to identify if the expression levels of the AR and its downstream target proteins KLK3 and TMPRSS2 were significantly altered. The relationship between DHT, the AR and DHRS7 was then tested following DHRS7 siRNA depletion in the LNCaP cell line which endogenously express AR and DHRS7 (Figure 33).

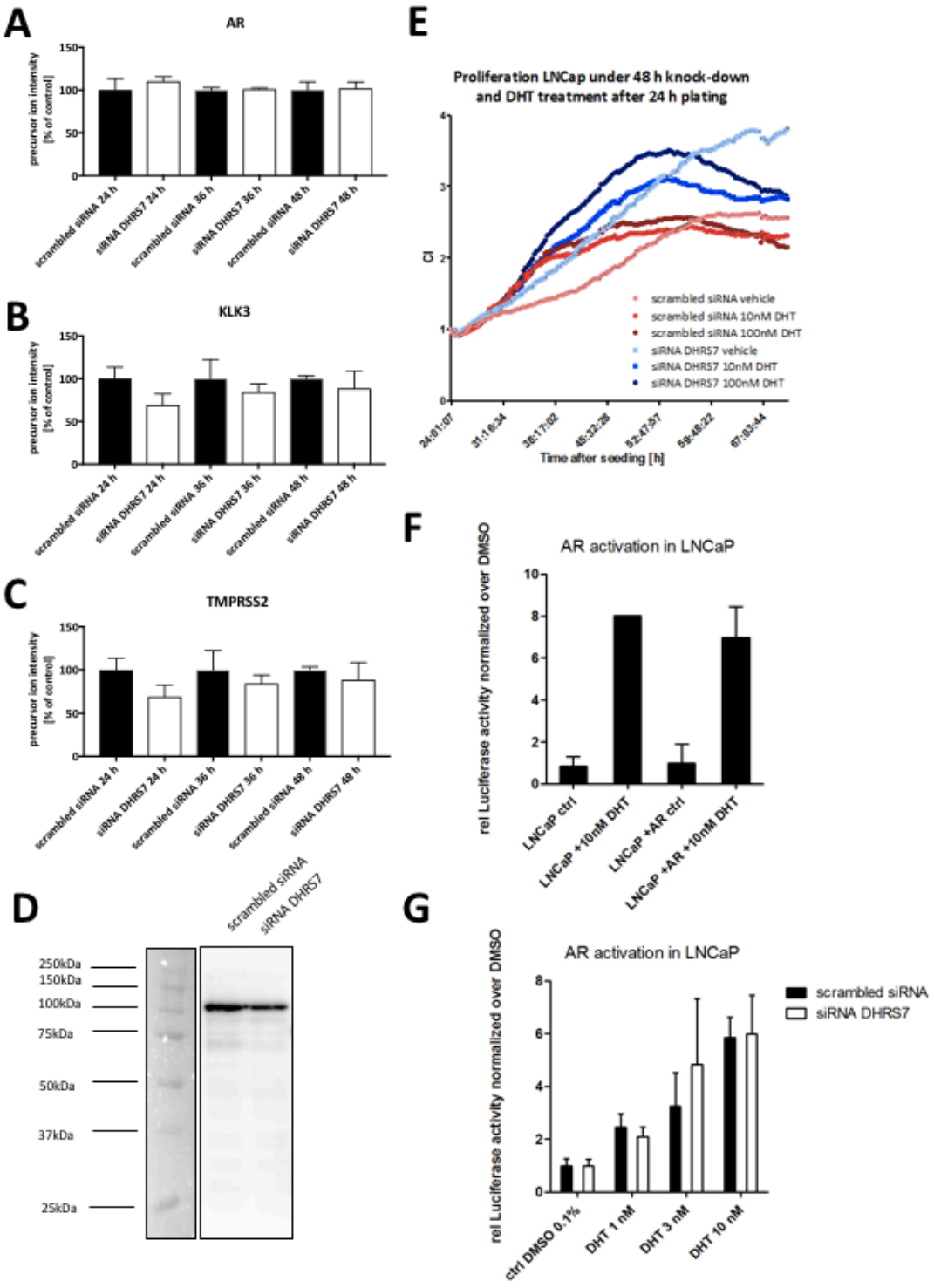

Figure 33: Functional characterization of endogenous AR signaling in LNCaP with and without siRNA mediated DHRS7 knock-down. A-C. AR, KLK3 and TMPRSS2 relative protein quantification measured with untargeted proteomics D. Quantification of AR in the 48 h scrambled and siRNA DHRS7 treated protein lysates; E. Time course of normalized Cell Index (CI) measurements measured trough xCELLigence after 24 h seeding of siRNA mediated DHRS7 knock-down of 48 h in LNCaP and 10 nM or 100 nM DHT treatment; F. Endogenous and overexpressed AR activation in LNCaP under 10 nM DHT (mean of duplicates ±SD); G. Endogenous and overexpressed AR activation in LNCaP with treatment of 1-3-10 nM DHT under DHRS7 downregulation (mean of triplicates ±SD).

The proteomics experiment performed in result section 5.2.2.1 for the fixed 48 h timepoint, showed a downregulation of the AR following DHRS7 depletion (Table 12, section 9.1.1.4 of the supplementary data). However, this was not observed in the proteomic analysis of the time-dependent DHRS7 knock-down (tables 3-6 and 13), of which the relative quantification of the AR protein is depicted in Figure 33A. However, downstream KLK3 and TMPRSS2 show a tendency for downregulation against the hypothesis of DHRS7 mediated increased protein amount as expected in the case of a relevant increased AR transactivation activity under DHRS7 depletion (Figures 33B-C). AR protein was quantified by western blotting and no differences in expression were observed between DHRS7 depleted LNCaP cells (48 h timepoint) and scrambled control (Figure 33D).

The effect of DHT (10 nM and 100 nM) on proliferation was tested by xCELLigence following siRNA DHRS7 depletion and siRNA scrambled control in LNCaP cells. SiRNA depletion of DHRS7 in LNCaP cells reproducibly show an increased proliferation compared to scrambled control (light pink and light blue line) (Figure 33E). Under both experimental conditions, DHT induces proliferation compared to control (Figure 33E). Specifically, DHT treatment of siRNA depleted DHRS7 LNCaP cells showed a concentration and time dependent increase in proliferation which peaked at ca. 52 after seeding (blue for 10 nM DHT, dark blue for 100 nM) (Figure 33E). DHT treatment of siRNA scrambled control LNCaP cells only showed a time dependent increase in proliferation which also peaked at ca. 52 after seeding (orange 10 nM DHT and dark red 100 nM DHT) (Figure 33E). Further confirming the activation of the AR by DHT, the AR downstream target genes KLK3 and TMPRSS2, as shown by Simon Stücheli in his master thesis, were increased (unpublished data). Thus, the addition of DHT increased the proliferation rate of LNCaP cells confirming its functional ability to mediated proliferation in this cell line. The final experiments were performed using a Concentration range between 1- 10 nM. The AR transactivation assay, previously tested in HEK293 cells overexpressing DHRS7 [191] was performed in LNCaP cells. First, in a control experiment endogenous AR was positively transactivated 8 fold with 10 nM DHT (Figure 33F). DHT mediated AR transactivation following siRNA DHRS7 depletion showed a dose-dependent increase in AR transactivation, however, no differences were observed between siRNA DHRS7 depleted LNCaP cells and the siRNA scrambled control (Figure 33G). The findings of these experiments were further supported by the thesis work of Simon Stücheli, which conclusively show that DHRS7 plays no role in the control of the AR in the LNCaP cells line, by performing immunoblots and mRNA quantification showing no changes in AR nuclear translocation or induction of AR downstream genes in DHRS7 depleted LNCaP cells treated with DHT compared to scrambled siRNA control (unpublished data).

5.2.2.2.2.3 Characterization of Protein Changes related to Proliferation, Adhesion and Migration

In the context of human prostate cancer progression and LNCaP proliferation, three main clinically relevant mechanisms have been described according to Bluemn et al. [31]: 1) AR mediated, 2) the AR independent, neuroendocrine dependent, and 3) the AR independent, neuroendocrine independent. In the previous results section, we excluded the AR mediated pathway as a mechanism by which the LNCaP cells increase proliferation following DHRS7 depletion.

Evidence to support the AR independent, neuroendocrine dependent pathway was provided by Bluemn et al. [31]. The study uncovered the following proteins relevant for proliferation, migration and invasion LNCaP that may be important for proliferation: PCSDK1, NKX2-1, CHGA, CHGB, SCG3, CHRNB2, ELAVL4, SYP, ENO2, and SCN3A. The global proteomic analysis data presented in this thesis was only able to detect ENO2, however its expression levels was not changed in the DHRS7 siRNA depleted LNCaP cells compared to scrambled siRNA controls (data not shown).

Evidence to support the AR and neuroendocrine independent pathway, was also provided by Bluemn et al. [31]. The study uncovered to following pathways relevant for proliferation, migration and invasion in LNCaP: mitogen-activated protein kinase (MAPK) and fibroblast growth factor (FGF) pathways. Proteins relevant for these pathways detected in the global proteomic analysis data presented in this thesis in all the tested conditions were EGFL7 (a protein promoting metastasis in hepatocellular carcinoma [233]) (Figure 34 A), FGFR1 oncogenic partner (Figure 34 B), EGFR (Figure 34 C-D), and GRB10 (direct substrate of the p42/44 MAPK [234] (Figure 34 E).

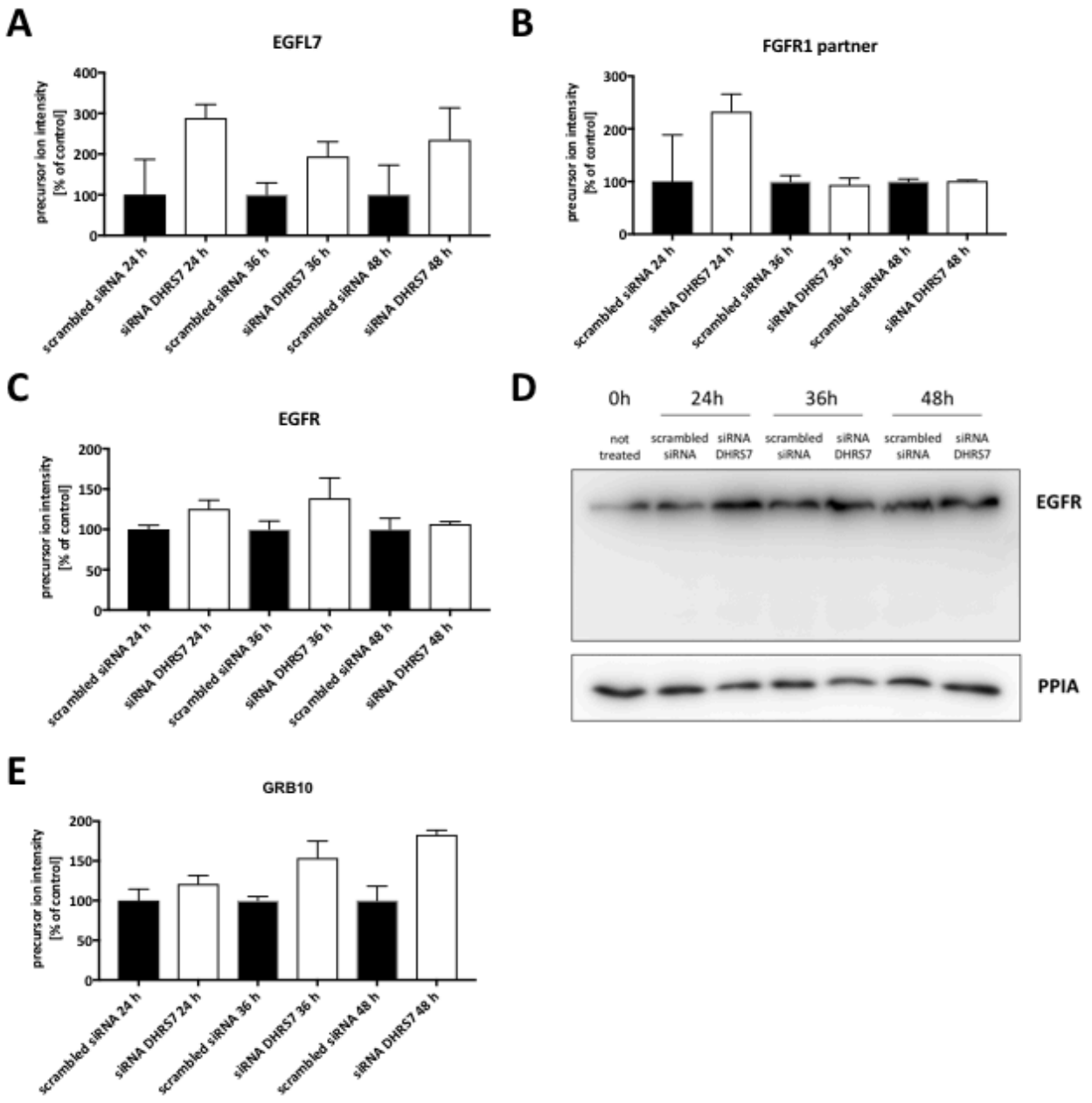

Figure 34: Relative protein quantification of EGFL7 (A), FGFR1 partner (B), EGFR (C) with relative western blotting (D), and of GRB10 (E) measured in scrambled siRNA control and siRNA DHRS7 treated LNCaP for 24 h, 36 h, and 48 h. Untargeted proteomic data are expressed as mean ± SD. D.

A trend was observed for the upregulation for EGFL7 in all the three time points in the DHRS7 siRNA depleted LNCaP cells compared to scrambled siRNA controls (Figure 34A). A trend was observed also for the upregulation FGF1 oncogenic partner at the 24 h timepoint only, and trend for upregulation for EGFR was also noted, however, this observation was not clearly reflected in immunoblot analysis (Figure 34C and D). Interestingly, in Figure 34 E, GRB10 was time-dependently upregulated reaching an upregulation

of 1.8 fold under 48 h DHRS7 knock-down, and this was consistent with results of the 2.2 fold upregulation of the 1st proteomics analysis under DHRS7 knock-down of 48 h (supplemental Table 11).

Among the most regulated proteins in the global proteomic analysis data were a series of cell cycle relevant proteins (tables 3-6 and 13). To better understand the dynamic of the proliferation changes and the potential role of the identified proteins, the cell cycle was evaluated more in detail by flow cytometry analysis and the cell cycle proteins identified in the proteome study at the 48 h timepoint were compared (Figure 35).

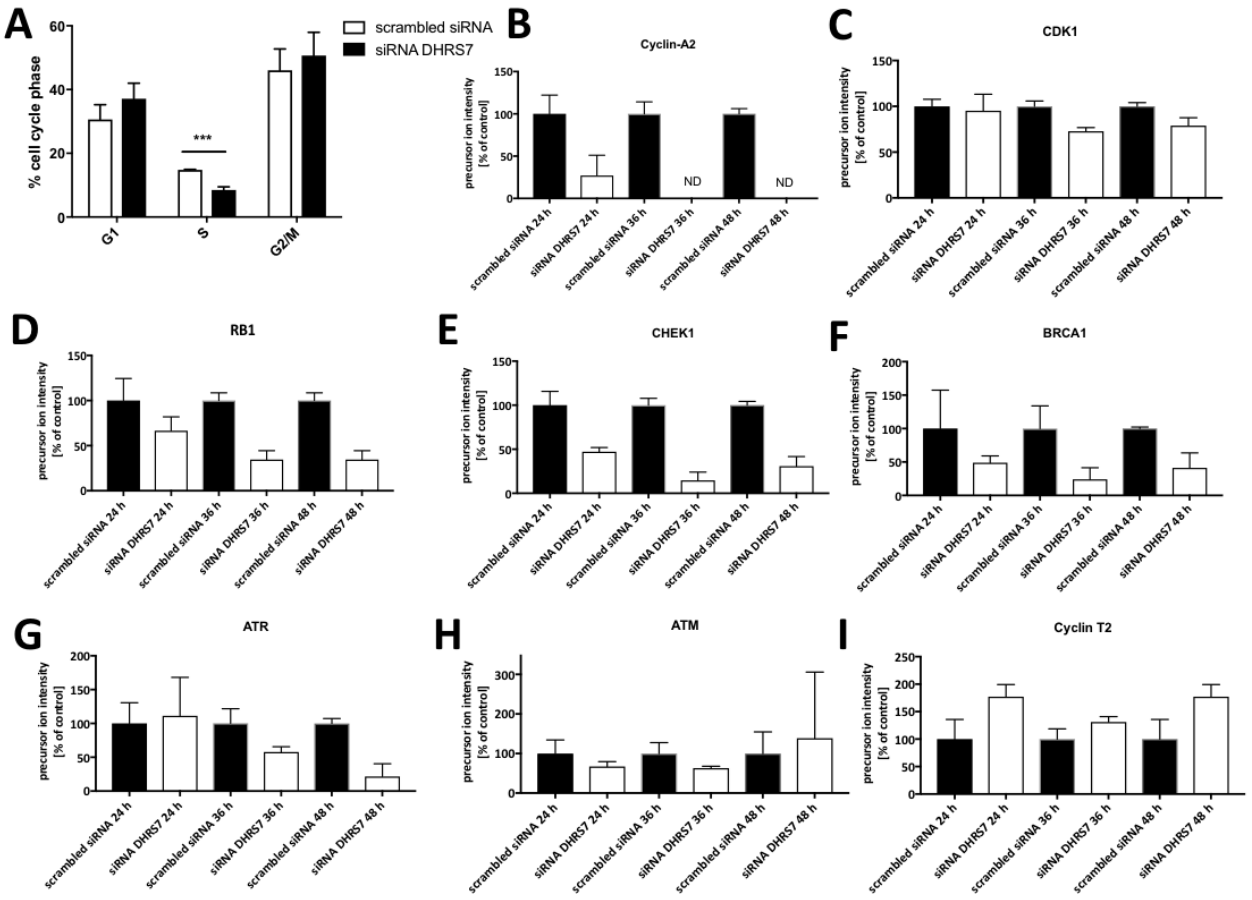

*Figure 35: Cell cycle analysis under DHRS7 depletion. Percentage of cells in cell cycle phases under 48 h DHRS7 knock-down (mean ±SD of three independent experiments) (A). Relative quantification of the proteins involved in cell cycle regulation Cyclin-A2 (B), CDK1 (C), RB1 (D), CHEK1 (E), BRCA1 (F), ATR (G), ATM (H), and Cyclin T2 (I) measured in scrambled siRNA control and siRNA DHRS7 treated LNCaP for 24 h, 36 h, and 48 h with untargeted proteomic. Results are expressed as mean ± SD. ***=p<0.0005.*

A 50% decrease in LNCaP cells in the S-phase of the cell cycle was detected following 48 h DHRS7 siRNA depletion compared to scrambled siRNA controls (Figure 35A). This was supported by the downregulation of the claspin protein, which was undetectable in the siRNA DHRS7 treated conditions (table 6), and also

downregulated at the mRNA level [147]. Claspin is a protein that is stabilized in S-phase but degraded in mitosis and is absent from cells in early G1 phase [235]. Consistent with this observation, the S-phase related protein Cyclin-A2 was downregulated following DHRS7 siRNA depletion at the 24 h timepoint, and undetectable at the 36 h and 48 h timepoint (Figure 35B). On the other side, CDK1, a protein that complexes with Cyclin-A2 and together are key regulators the S-phase [236], showed an ca. 20% decrease at 36 h and 48 h (Figure 35C). The tumor suppressor RB1, a protein downstream of Cyclin -A2 and involved in G1/S transition [237], however a time-dependent downregulation (Figure 35D). CHEK1 and the tumor suppressor BRCA1 were also downregulated (Figure 35E-F). These two proteins were also downregulated at the mRNA level, as showed by Seibert et al. [147]. The DNA damage sensing protein ATR and ATM [238] showed alternative regulatory patterns, as ATR showed a time-dependent downregulation (Figure 35G), whereas ATM did not change (Figure 35H). Finally, cyclin-T2, a protein that has been shown to interact with the C-terminal domain of RB1 [239], was upregulated at the 24 h and 48 h time points following DHRS7 siRNA depletion compared to scrambled siRNA controls (Figure 35I).

In the contest of adhesion and migration, phenotypical alterations can be observed through the cell adhesion molecules (CAMs); transmembrane receptors that facilitate adhesion between cell membranes or to the extracellular membranes (ECM). As result section 5.2.2.1 and Tables 3-6 and 13 highlighted, adhesion related proteins E-Cadherin (also called CDH1, a calcium dependent CAM that has a crucial role in cell-cell adhesion), fibronectin (glycoprotein of the extracellular matrix also used for adhesion assays in Figure 24), spondin-2 (a secreted cell adhesion extracellular protein that has been found to be over-expressed in prostate cancer [245]), catenin alpha 1 (forming together with CDH1 the cadherin–catenin complex [240]), CD166 antigen (a cell adhesion molecule that works in a calcium-independent manner [241]), desmocollin-2 (a transmembrane cadherin involved in the interaction of plaque proteins and intermediate filaments mediating cell-cell adhesion that may also contribute to epidermal cell positioning [242]), and occludin (a protein that is able to induce adhesion [243]) were reproducibly regulated under DHRS7 siRNA depletion. The relative quantification of these proteins, together with anillin (a protein that regulates the intracellular junctions in epithelial cells [244]), and the catenin alpha related catenin beta 1 [240], is depicted in Figure 36.

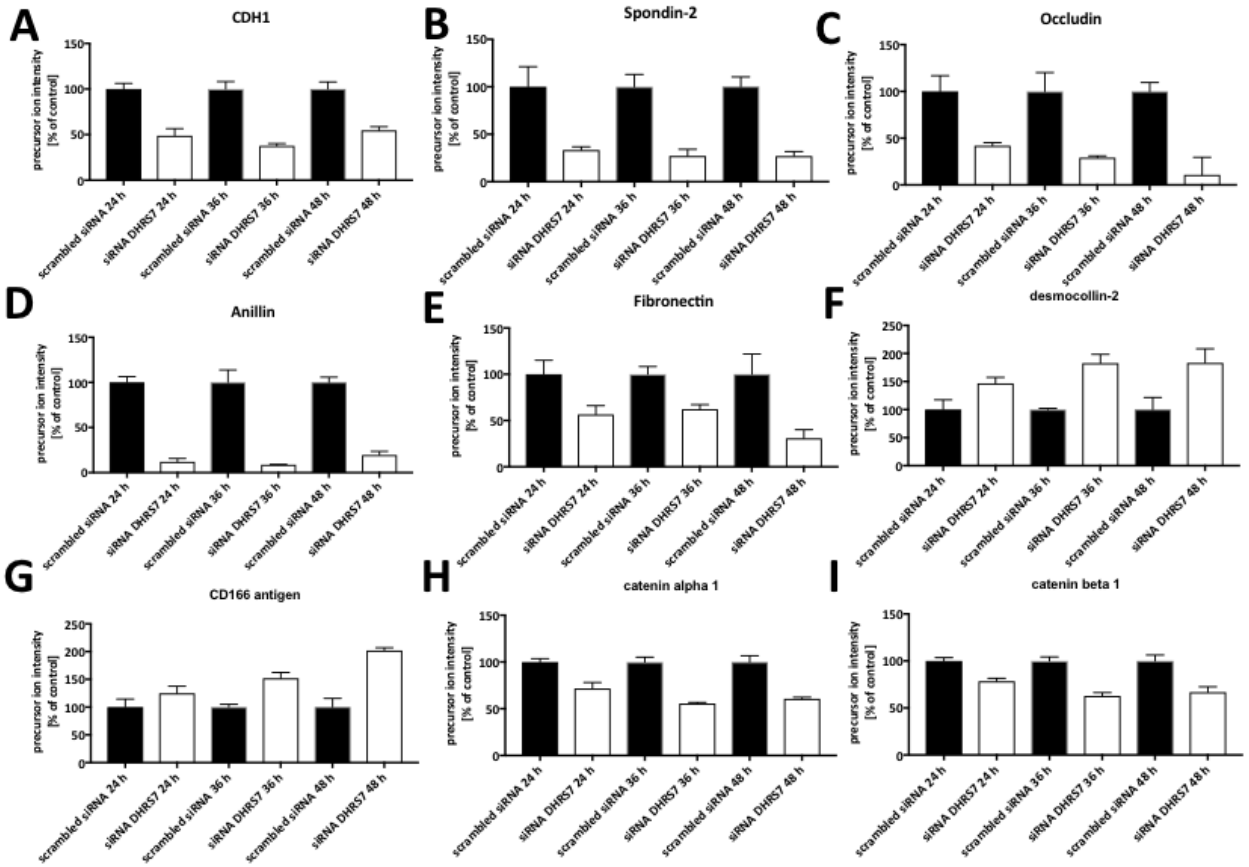

Figure 36: Relative quantification of the proteins involved in adhesion CDH1 (A), Spondin-2 (B), Occludin (C), Anillin (D), FIbronectin (E), desmocollin-2 (F), and CD166 antigen (G) catenin alpha 1 (H), catenin beta 1 (I), measured in scrambled siRNA control and siRNA DHRS7 treated LNCaP for 24 h, 36 h, and 48 h with untargeted proteomic expressed as mean ± SD.

CDH1, spondin-2, occludin, and anillin protein were all consistently downregulated at all the three time points tested (Figure 36A-D). Interestingly, occludin showed a time dependent downregulation (Figure 36D). Fibronectin was downregulated after 36h and 48h with a trend to be downregulated at the 24 h timepoint following DHRS7 siRNA depletion (Figure 36E). On the other side, desmocollin-2 is upregulated ca. 1.6 fold and CD166 antigen showed a time-dependent upregulation maximizing at ca. 2 fold increase (Figure 36F and G). Catenin alpha 1 and catenin beta 1 show similar patterns of downregulation (Figure 36H-I). All the trends in protein regulation described in the 2nd global proteomic analysis at three time points correlated with the observations made for the first proteomics experiment (results section 5.2.2.1).

CDH-1 was previously regulated at the mRNA level [147] as well as at the protein level (unpublished data in the master thesis of Simon Stücheli) following DHRS7 siRNA depletion in LNCaP cells and represents an interesting protein with a tumor suppressor role. To further study the regulation of CDH-1 following DHRS7

depletion, LNCaP cells were immunostained for CDH-1 and detected under a fluorescence microscope (Figure 37B).

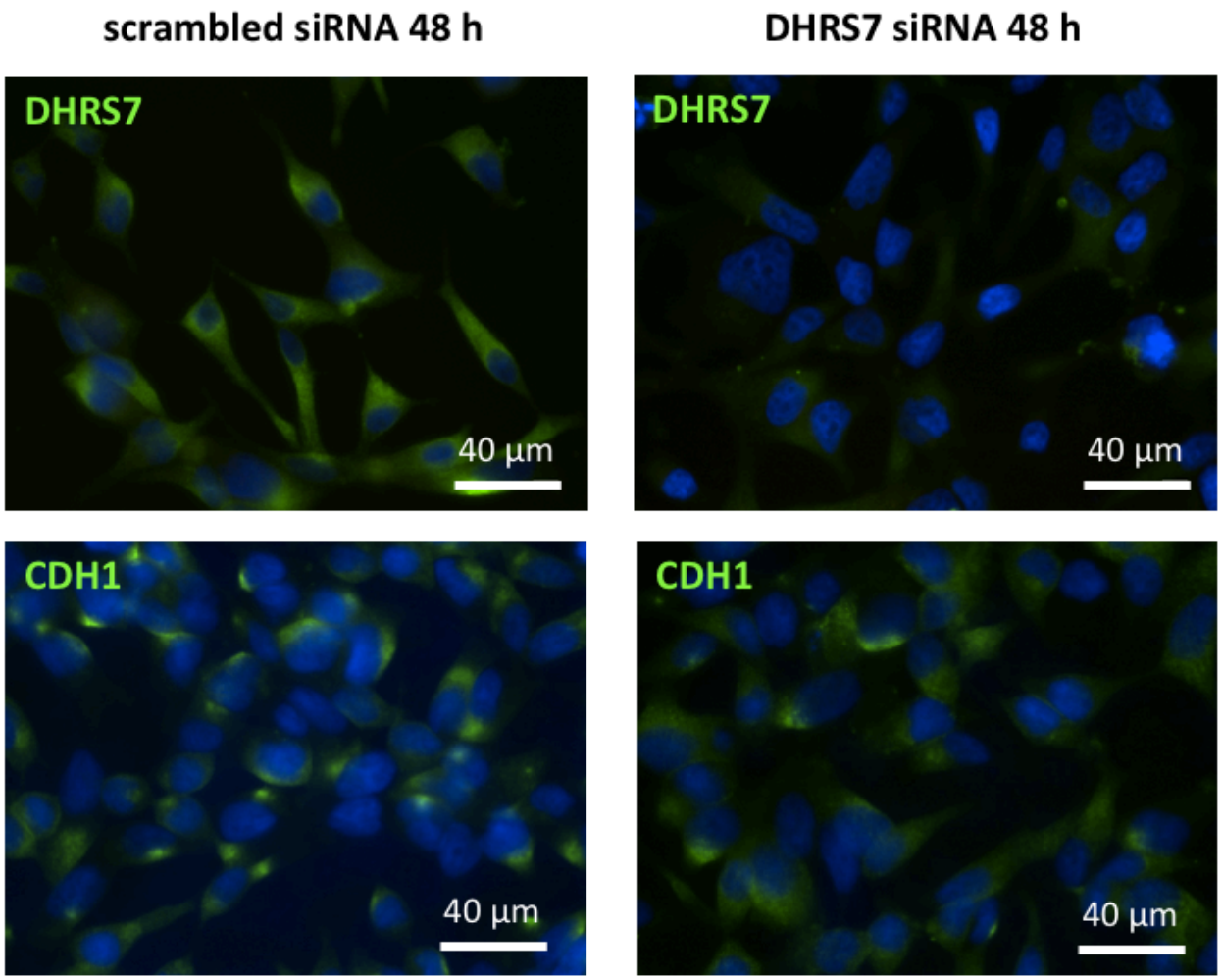

Figure 37: Immunofluorescence of DHRS7 (A-B) and CDH-1 (C-D) in LNCaP under siRNA scrambled and siRNA DHRS7 48 h treatment. Images were taken with 40x magnification.

Interestingly, LNCaP cells that were depleted for the endoplasmic reticulum localized DHRS7 (Figure 37A-B), presented a disperse CDH1 signal compared to control (Figure 37C-D).

5.2.2.2.2.4 Characterization of Protein Changes related to Membrane Lipid Pathways

As depicted in Figure 36, several regulated cell adhesion molecules were identified and were changed already after 24 h following DHRS7 siRNA depletion in LNCaP cells. These proteins are usually localized at the cellular phospholipid bilayer membrane and could be involved in the membrane fatty acid metabolism pathways, suggested in results section 5.2.2.1. The proteins involved in membrane lipid pathways SMPD1 and LPCAT1 (regulated in Table 11 and Table 12, respectively), and the proteins involved in the membrane lipid transport and metabolism TEX2 (Table 4), ABHD2 (a triacylglycerol lipase and ester hydrolase [245], Tables 13-14), and FAR1 (an SDR enzyme that controls ether glycerophopsholipid synthesis [246] also depicted in Figure 3 and regulated as shown in Table 14) were analyzed according to the relative quantification data from the untargeted LNCaP proteome under DHRS7 time-dependent depletion (Figure 39A-E).

Additionally, another protein potentially involved in lipid metabolism pathway or alternatively to the retinoic acid metabolism pathway, is RDH10, an SDR and a potential proto-oncogene which localizes in lipid droplets (see chapter 2.2 of the introduction). As RDH10 was only detected in the DHRS7 siRNA depleted LNCaP cells at all the time points tested and not in the scrambled siRNA controls (table 6 and 8), it was investigated for retinoic acid metabolism activation following DHRS7 depletion. This was done first through evaluating the protein amount of the nuclear receptors RXR alpha and beta that did not change (data not shown), as well as the downstream target proteins RAI1 and RARA were selected for protein analysis using the global proteome data and RNA quantification (Figure 39F-H).

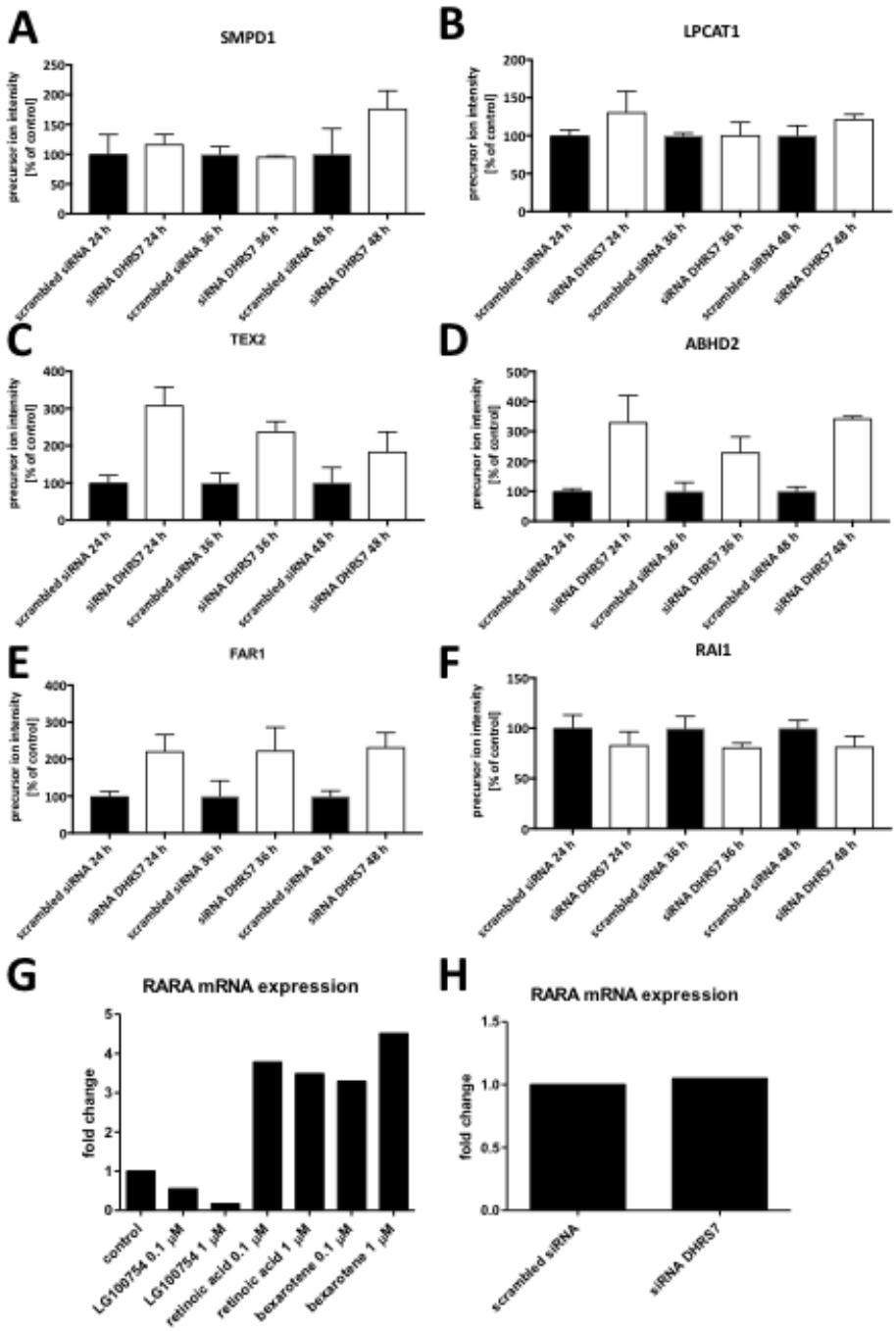

§

Figure 38: Relative quantification of proteins involved in membrane lipid metabolism measured in scrambled siRNA control and siRNA DHRS7 treated LNCaP for 24 h, 36 h, and 48 h with untargeted proteomic: SMPD1 (A), LPCAT1 (B), TEX2 (C), ABHD2 (D), and FAR1 (E). F. Relative quantification of RAI measured in scrambled siRNA control and siRNA DHRS7 treated LNCaP for 24 h, 36 h, and 48 h with untargeted proteomic; G. mRNA quantification of RARA after treatment with the RARA inhibitor LG100754 and the RARA inducers retinoic acid and bexarotene (mean of three replicate values); H. mRNA quantification of RARA after 48 h DHRS7 knock-down (mean of three replicate values).

SMPD1 and LPCAT1 protein expression did not change following DHRS7 siRNA depletion at any time point compared to scrambled siRNA control (Figure 39A-B). TEX2, ABHD2 and FAR1 protein expression levels were upregulated following DHRS7 siRNA depletion: TEX2 with 3 fold and slightly decreasing under the two following time points (Figure 39C)., and ABHD2 3.3, 1.8, and 3.45 fold, for 24 h, 36 h, and 48 h time points, respectively (Figure 39D). Finally, FAR1, was ca 2 folds upregulated under all the time points compared to scrambled siRNA control (Figure 39E).

Changes in the protein levels of RAI1 was observed (Figure 39F). RARA was undetectable in the global proteomic analysis. However, a control experiment using positive inducers of retinoic acid receptors, LG100754 and bexarotene, upregulated RARA mRNA levels in LNCaP cells (Figure 39G), however no changes were observed in RARA mRNA levels following DHRS7 siRNA depletion at the 48 h timepoint compared to scrambled siRNA control (Figure 39H), suggesting no relevant DHRS7 mediated retinoic acid metabolism observed downstream to the retinoic acid receptors.

5.2.3 Discussion

The untargeted analysis of the LNCaP proteome following siRNA depletion first for the timepoint 48 h with a decreased sensitivity, and afterwards with a more sensitive approach time-dependent DHRS7 downregulation, allowed to identify interesting groups of changed proteins to dissect mechanisms related to functional phenotypical changes related to knock-down of DHRS7. These groups of altered proteins are partly describing the phenotypical changes observed by Seibert el al. [147] for proliferation/cell cycle, adhesion, and migration pathways, and allowed the identification of new interesting players involved in membrane lipid metabolism pathway and/or with cancer associated roles. This suggested mechanisms for the establishment of the functional phenotype observed in the prostate cancer cell line LNCaP following DHRS7 depletion. Moreover, careful analysis of proteins involved in these mechanisms allowed to test hypotheses on a androgen-dependent effect of DHRS7 mediated regulation as discussed in chapter 1 (section 4).

With the conclusions made in chapter 1, DHT seemed to be a potential physiologically relevant substrate of DHRS7. Nevertheless, in the prostate cancer cell model LNCaP that endogenously express DHRS7, untargeted proteomics and endogenous AR transactivation experiments provided strong evidence against a physiological role of DHRS7 in DHT metabolism and the effects upon knockdown of this enzyme seem to be androgen-independent. This observation was also supported by the master thesis work of Simon Stücheli (unpublished data).

Alternative to an AR dependent mechanism driving proliferation upon DHRS7 downregulation, prostate cancer cell proliferation and aggressiveness can be driven by truly AR-independent mechanisms, as also outlined in the introduction in chapter 2.2. In this regard, Bluemn et al. [31] identified two main mechanisms studied with selected LNCaP androgen independent colonies: a neuroendocrine dependent and a neuroendocrine independent pathway. The identification of EGFR, EGFL7 and FGFR1 and the observation of the trend for upregulation of EGFL7 and the upregulation of GRB10 may suggest investigating further the AR and neuroendocrine independent pathway. However, the phosphorylation of the MAPK and FGF pathways involving these tyrosine kinase activity related proteins should be studied to help rule in/out AR and neuroendocrine driven proliferation in the LNCaP cells following DHRS7 depletion. In this regard, it must be in fact considered that important proteins to assess these mechanisms might be not quantified because of the sample preparation, as highlighted by the disconnect between the microarray and proteomic analysis with respect to the nuclear receptors and SDRs and AKRs enzymes. The method for sample preparation was in fact not being optimized to specifically detect membrane receptors

or nuclear proteins (e.g. the microsomal or cytoplasmic SDRs and AKRs enzymes were increasingly detected compared to the nuclear receptors).

As the modulation of proliferation depend on altered cell cycle control, cell cycle analysis and related proteins such as cyclins, CDKs, and cell-cycle modulators, were investigated and revealed a decrease in the S-phase under treatment with siRNA DHRS7 as detected by flow cytometry and the downregulation of Cyclin-A2 and Claspin. Interestingly, these proteins are both regulated by ubiquitination and proteosomal degradation processes, of which different proteins in these systems are downregulated (tables 3-6 and 13, 14). However, these proteins might also refer to the modulation of unfolded protein response degradation as a consequence of cellular stress [247]. The decrease in S phase accompanied by the increase in proliferation as observed by xCELLigence experiments suggested proliferating cells with a short S-phase. This could be influenced by cell growth control relevant proteins such as RB1, CHECK1, BRCA1 and spondin-2, that were detected ot be downregulated. The relationship of DHRS7 with S-phase modulation is also supported by an abstract indicating that the breast cancer cell line MCF-7 transfected with DHRS7 was shown to have an increased number of cells in the S-phase [153], and that LNCaP cells treated with miR-663, which reported an increased number of cells in S-phase cell cycle, showed an upregulation in DHRS7 protein [151]. Interestingly, Jiao et al. [151] describe these changes in relation to a transition of LNCaP androgen dependent phenotype towards a castration resistant prostate cancer phenotype, suggesting again association of DHRS7 with altered proliferation to be AR independent.

Proteins involved in adhesion and migration were consistently and mostly early downregulated, as the case of the tumor suppressor CDH1. The loss of epithelial surface markers such as CDH1 or fibronectin can be a hallmark of epithelial-mesenchymal transition [248], however this process is also characterized by the acquisition of mesenchymal markers such as vimentin and N-cadherin, that were not regulated or detected through the untargeted proteomics approach, respectively. Alternatively, the investigated adhesion and migration regulated proteins can also indicate an adaptation to changed metabolism residing in the cellular membrane. In this regard, the potential proto-oncogene proteins involved in membrane lipid transport and metabolism such as RDH10 and ABHD2 were upregulated. Interestingly, literature reported upregulation of DHRS7 following different lipids treatments [155, 158, 159], suggesting a potential role of DHRS7 in lipid metabolism.

Modulation of RDH10 and ABHD2 expression through DHRS7 may be dependent on different pathways and could be hypothesized according to the available literature. Indeed, RDH10 is an SDR involved in the transport of lipid droplets that seems to be upregulated by reduction of retinoic acid (product of all-trans

retinal) [249]. This could support the hypothesis from Stambergova et al. of all-trans-retinal as a substrate for DHRS7 [145] which under siRNA mediated DHRS7 downregulation could lead to increased all-trans-retinal which could upregulate RDH10 and thus lead to an increase in proliferation as observed in the glioma cell lines U87 and U251 [96]. However, the change in proliferation seems not to be mediated through retinoic acid relevant receptor activity. Alternatively, the upregulation of RDH10 might be a consequence of an increase in acyl ester biosynthesis with increased lipid droplet formation as investigated by Jiang et al. [95]. In regards to the monoacylglycerol lipase ABHD2, it is seems that the upregulation of ABHD2 could be due to androgens [250] or by acting with a genome-independent action, such as a membrane progesterone receptor [227]. Alternatively, this could be a compensatory mechanism after knockdown of DHRS7, possibly involving fatty acid metabolism. Interestingly, ABHD2 is able to couple heightened lipogenesis with lipolysis to produce fatty acid networks by mediating degradation of 1-arachidonoylglycerol (1AG) and 2-arachidonoylglycerol (2AG) from the cellular membrane to glycerol and arachidonic acid converting monoglycerides [227]. Arachidonic acid, an omega-6 fatty acid, is associated to increased proliferation in prostate cancer [251]. Moreover, Obinata et al reported ABHD2 to cause changes in proliferation and migration in the prostate cancer cell lines LNCaP and VCaP upon stable transfection, and that higher ABHD2 protein expression positively correlated with high Gleason score and pathological N stage as well as low prostate cancer-specific survival rates [250]. On the other side, ABHD2 was shown to be elevated in LNCaP versus androgen-independent human prostate cancer cell lines, where the siRNA mediated silencing of the functional homologous monoacylglycerol lipase MAGL was shown to increase prostate cancer aggressiveness and correlated to epithelial-to-mesenchymal transition [252].

To support these hypotheses, the expression of ABHD2 and RDH10 in DHRS7 knock-down samples is being evaluated through western blotting and will be followed by a quantitative targeted proteomics experiments targeting ABHD2 and RDH10 under DHRS7 siRNA mediated downregulation. Additionally, the effect of DHRS7 on these proteins can be investigated by ABHD2 and/or RDH10 knock-down or inhibition in LNCaP as well as in androgen independent prostate cancer cell lines with functional proliferation, migration and adhesion experiments. In addition, the role of these proteins associated with lipid metabolism could be investigated trough immunofluorescence experiments with intracellular neutral and polar lipid stainings (e.g. with Nile Red that allows to reveal lipid droplets and their composition [253], as was already shown in LNCaP by Sadowski et al. [254]).

6 General Discussion

The “deorphanization” of enzymes is an important step toward the uncovering of their physiological roles. The enzymes of the SDR superfamily are particularly difficult to deorphanize as they have a wide spectrum of substrates, they often lack structural information, share poor primary structure similarity, are often embedded in organelle membrane bilayers and do not have a common activity element that could be used as suitable high-throughput assay to assess potential substrates. In regard to the orphan enzyme DHRS7, the identification of its substrate would help to uncover its role in health and pathological conditions, as it has been shown to be a potential tumour suppressor in prostate cancer [147]. As the 3D protein structure resolution of DHRS7 has not been accomplished so far, and only few publications are available, and revealing conflicting results of potential substrates with suggestions of few candidates with low non-physiological affinity, further studies are needed in order to attempt to characterize the function of DHRS7. This thesis is aimed (1) to identify DHRS7’s substrates through a targeted “deorphanization” approach (chapter 1), and (2) to understand the potential physiological role of DHRS7 through DHRS7 knock-down and functional assays in cancer cell lines with high endogenous DHRS7 expression as well as with an untargeted proteomics approach (chapter 2). These approaches allowed to characterize *in vitro* DHRS7 activity by revealing 3α or 20β reduction on carbonyl moieties of steroidal structures, observe adhesion and migration changes in the breast cancer cell line MCF-7 under DHRS7 depletion, and suggesting interesting protein changes related to a proto-oncogene signature phenotype such as ABHD2 and/or RDH10 that could reveal a feedback mechanism established indirectly rather than by a direct DHRS7 substrate role. However, DHRS7 remains an “orphan” enzyme and hypotheses generated with the untargeted proteomics approach need to be further tested.

With a targeted deophanization approach performed in chapter 1, the substrates and products measured in DHRS7 overexpressing HEK 293 cells allowed to provide experimental proof of reduction of the endogenous metabolites DHT, cortisone, and potentially on 17αHOProg leading to products reduced on 3α or 20β carbonyl moieties. The discovery of weak substrates is important as it can allow the search for more relevant substrates, as well as for inhibitors. On the other side, this will allow to test activity following purification of the enzyme and test for activity enrichment per amount of protein. An inhibitor, if specific, could help in investigating the role of DHRS7 both *in vitro* and *in vivo* as the timing would be more acute than upon knock-down. However, this strategy represented a low throughput and time-consuming approach. The *in vitro* screening tool with cell lysate of stably expressing DHRS7 cell lines to screen for novel substrates that was developed based on the observed reactivity toward DHT, was used to find novel

candidate substrates and inhibitors while addressing the problem of limited resources. This represented a valuable screening tool, as SDRs don't have a common specific assay to monitor activity in unpurified conditions. Nevertheless, this approach was not successful in finding novel high affinity candidates. In regards to the deorphanization of SDRs using lysate activity assays, the literature reports a similarly negative outcome for the poorly described SDRs, hydroxysteroid dehydrogenase like 2 (HSDL2) and short-chain dehydrogenase/reductase-orphan (SDR-O) where activity was monitored through NADPH consumption [255].

Regarding the strategy used by Zemanová et al. [208] which used a combination of *in silico* homology and substrates docking models with *in vitro* assays for the deorphanization of DHRS7, albeit without success in defining physiologically relevant endogenous substrates, I believe that this approach was novel and interesting since this was the first attempt of this combination of techniques to deorphanize human SDRs. However, in my opinion, the use of a homology model of DHRS7 based on 11βHSD1 provided a weak platform in order to predict potential substrates mainly due to the low homology of 38% sequence identity between the two proteins [208]. Additionally, the two proteins showed different affinity for cortisone and produced different metabolites as showed by our study with activity in intact HEK 293 cells [191]. Moreover, we showed that the active site of the two enzymes faced different cellular compartements with DHRS7 facing the cytosol, and 11βHSD1 facing the inside of the endoplasmic reticulum [191]. Interestingly, this strategy of *in silico* and *in vitro* assays was successful to deorphanize two plant SDRs [256], however, the *in silico* model was based on high homology with these two orphan enzymes (amino acid identity of 79%). *In silico* homology studies could give important information on the pocket binding active site for hypotheses generation. Interestingly, in addition to Zemanová's study, Dr. Katharina Beck, a Post-Doc in our lab, observed an elongated cone-shaped pocket binding site that may allow access for binding of large lipophilic metabolites, other lipid mediators and different eicosanoids (unpublished data).

As highlighted in section 2.5 of the introduction, a high-throughput untargeted method is recommended as a "deorphanization" approach when limited information is available on the enzyme of interest [177-179]. This approach was adopted for hypotheses generation regarding DHRS7 relevant cancer associated mechanisms in the prostate cancer cell line LNCaP with DHRS7 siRNA mediated knock-down. LNCaP was shown to be the cell model with the strongest functional effects following DHRS7 depletion compared to the breast cancer cell line MCF-7 and the adrenal cancer cell line H295R. The proteomic data showed several changed proteins potentially involved in tumor biogenesis, the regulation of which may be directly controlled by a substrate of DHRS7 or indirectly regulated as a result of DHRS7 depletion. Alternatively,

some of the changed proteins may not directly be involved in tumor biogenesis but to yet unidentified pathways, also observed by other SDRs associated to human cancer (see section 2.3 of the introduction). Another high-throughput approach to evaluate lipid metabolism supporting changes observed as for RDH10, TEX2, FAR1 and ABHD2, could be lipidomics. Nevertheless, limitations to use a time-dependent silencing approach to detect changed proteins or lipids could also mask important DHRS7 relevant changes and thus stable overexpression or down-regulation could be considered and used as controls in such high-throughput experiments as performed successfully for 17βHSD1 by Aka et al. [70] with a stable expression and following analysis by proteomics approach.

On the other side, novel approaches to help deorphanization could be done by better understanding physiological impairments in an *in vivo* system, for example using knock-out or knock-in animals. The option of performing an inducible knock-out animal would have the advantage to eliminate embryonic death if the mutation could be lethal, provide a kinetic assessment on DHRS7 loss of function *in vivo* and provide support of siRNA mediated silencing observation made by proteomics with a human cell model. Alternatively, the option of having a tissue specific knock-out mouse would allow to study specific organ phenotypes decreasing systemic interferences, embryonic lethal effects and gathering organ specific observations [178]. Relevance of prostate and breast cancer related effects observed in this thesis could be investigated in prostate and breast tissues in these *in vivo* models.

In conclusion, DHRS7 remains an “ophan” SDR with an important role in prostate cancer but the investigations performed in this thesis releaved useful information for next steps towards the identification of a function of DHRS7. From one side the observations of *in vitro* reductive activity towards steroidal compounds according to steroidal molecular symmetry and specifically for DHT could allow to find functionally relevant substrates and inhibitors. On the other side, further characterization of regulated proteins following DHRS7 depletion in the endogenously DHRS7 expressing model LNCaP suggested an androgen receptor independent mechanism leading to increased cancer aggressiveness which could be driven by interesting upregulated proto-oncogenes, for which interactions with DHRS7 need to be further investigated.

7 Acknowledgements

I would like to thank Prof. Dr. Alex Odermatt for the supervision of my PhD thesis and for allowing me to perform this work in his laboratory. I thank Prof. Dr. Michael Arand for co-refereeing my PhD thesis and being part of my thesis committee. Both Prof. Alex Odermatt and Prof. Micheal Arand supported my continuous education in toxicology, for which I am very grateful. A special thank you goes to Prof. Paul Jenö and Suzanne Moes, who supported me for the proteomics work, performed the analysis with the mass spectrometer, helped with the analysis of the data and with useful discussions. I would like to express a huge thank you to Dr. Adam Lister for the scientific discussions, the friendship, and for the exceptional proofreading of my thesis. Further, I would like to express my gratitude to Simon Stücheli, who helped me with his master thesis work and now as a PhD student, working with passion for his experiments, and providing good quality data and critical useful discussions. I also want to gratefully thank Dr. Denise Kratschmar for analyzing a great number of LC-MS/MS samples improving technical sensitivity to her best, and the important support for the publication. I would like to thank Rafa, my sister Althea, my father and my mother as well as the rest of the family and my friends for their continuous support through all my endeavors. Without them this would have not been possible. Many thanks go to all the past and present members of the Molecular & Systems Toxicology group (Dr. Maria Tsachaki, Dr. Julia Birk, Dr. Katharina Beck, Dr. Thomas Hammond, Dr. Petra Stajhar, Dr. Julia Seibert, Michael Weingartner, Melanie Patt, Silvia Inderbinen, Philipp Marbet, Tobias di Marco, and Sharavan Kanagaratnam) for the suggestions, their support, and the good times we all had together. Finally, a special thank you goes to Dr. Ester Lovsin Barle, who inspired me to start pursuing a doctoral degree to continue my education in toxicology and for the further work ahead in this interesting field.

8 Literature

1. Ferlay, J., et al., *Cancer incidence and mortality worldwide: sources, methods and major patterns in GLOBOCAN 2012.* Int J Cancer, 2015. **136**(5): p. E359-86.
2. Sant, M., et al., *Cancer survival in Europe, 1999-2007: Doing better, feeling worse?* Eur J Cancer, 2015. **51**(15): p. 2101-2103.
3. Perez-Cornago, A., et al., *Prospective investigation of risk factors for prostate cancer in the UK Biobank cohort study.* Br J Cancer, 2017. **117**(10): p. 1562-1571.
4. Cuzick, J., et al., *Prevention and early detection of prostate cancer.* Lancet Oncol, 2014. **15**(11): p. e484-92.
5. Travis, R.C., et al., *A Meta-analysis of Individual Participant Data Reveals an Association between Circulating Levels of IGF-I and Prostate Cancer Risk.* Cancer Res, 2016. **76**(8): p. 2288-2300.
6. Lee, S.H. and M.M. Shen, *Cell types of origin for prostate cancer.* Curr Opin Cell Biol, 2015. **37**: p. 35-41.
7. Coffey, *The molecular biology, endocrinology and physiology of the prostate and seminal vesicles.* Campbell's Textbook of Urology. 1992, Philadelphia: Saunders. 221–266.
8. Packer, J.R. and N.J. Maitland, *The molecular and cellular origin of human prostate cancer.* Biochim Biophys Acta, 2016. **1863**(6 Pt A): p. 1238-60.
9. Kimura, N., et al., *Immunocytochemical localization of androgen receptor with polyclonal antibody in paraffin-embedded human tissues.* J Histochem Cytochem, 1993. **41**(5): p. 671-8.
10. Iwamura, M., et al., *Androgen receptor immunostaining and its tissue distribution in formalin-fixed, paraffin-embedded sections after microwave treatment.* J Histochem Cytochem, 1994. **42**(6): p. 783-8.
11. Verhagen, A.P., et al., *Differential expression of keratins in the basal and luminal compartments of rat prostatic epithelium during degeneration and regeneration.* Prostate, 1988. **13**(1): p. 25-38.
12. Stewart, R.J., et al., *Vascular endothelial growth factor expression and tumor angiogenesis are regulated by androgens in hormone responsive human prostate carcinoma: evidence for androgen dependent destabilization of vascular endothelial growth factor transcripts.* J Urol, 2001. **165**(2): p. 688-93.
13. Colombel, M., et al., *Androgens repress the expression of the angiogenesis inhibitor thrombospondin-1 in normal and neoplastic prostate.* Cancer Res, 2005. **65**(1): p. 300-8.
14. Feldman, B.J. and D. Feldman, *The development of androgen-independent prostate cancer.* Nat Rev Cancer, 2001. **1**(1): p. 34-45.
15. Taplin, M.E. and S.M. Ho, *Clinical review 134: The endocrinology of prostate cancer.* J Clin Endocrinol Metab, 2001. **86**(8): p. 3467-77.
16. Abraham, L.K.L.L.T., *Histology and Cell Biology: An Introduction to Pathology*. Third Edition ed. Sperm Transport and Maturation, ed. E. Saunders. 2012, Philadelphia. 627.
17. Rizner, T.L. and T.M. Penning, *Role of aldo-keto reductase family 1 (AKR1) enzymes in human steroid metabolism.* Steroids, 2014. **79**: p. 49-63.
18. Roy, A.K., et al., *Regulation of androgen action.* Vitam Horm, 1999. **55**: p. 309-52.

19. Levin, E.R. and S.R. Hammes, *Nuclear receptors outside the nucleus: extranuclear signalling by steroid receptors.* Nat Rev Mol Cell Biol, 2016. **17**(12): p. 783-797.

20. Losel, R. and M. Wehling, *Nongenomic actions of steroid hormones.* Nature reviews. Molecular cell biology, 2003. **4**(1): p. 46-56.

21. Gao, J., J.T. Arnold, and J.T. Isaacs, *Conversion from a paracrine to an autocrine mechanism of androgen-stimulated growth during malignant transformation of prostatic epithelial cells.* Cancer Res, 2001. **61**(13): p. 5038-44.

22. Labrie, F., *Combined blockade of testicular and locally made androgens in prostate cancer: a highly significant medical progress based upon intracrinology.* J Steroid Biochem Mol Biol, 2015. **145**: p. 144-56.

23. Mohler, J.L., et al., *Activation of the androgen receptor by intratumoral bioconversion of androstanediol to dihydrotestosterone in prostate cancer.* Cancer Res, 2011. **71**(4): p. 1486-96.

24. Gregory, C.W., et al., *A mechanism for androgen receptor-mediated prostate cancer recurrence after androgen deprivation therapy.* Cancer Res, 2001. **61**(11): p. 4315-9.

25. Gregory, C.W., et al., *Androgen receptor stabilization in recurrent prostate cancer is associated with hypersensitivity to low androgen.* Cancer Res, 2001. **61**(7): p. 2892-8.

26. Tilley, W.D., et al., *Mutations in the androgen receptor gene are associated with progression of human prostate cancer to androgen independence.* Clin Cancer Res, 1996. **2**(2): p. 277-85.

27. Otsuka, T., et al., *Androgen receptor W741C and T877A mutations in AIDL cells, an androgen-independent subline of prostate cancer LNCaP cells.* Tumour Biol, 2011. **32**(6): p. 1097-102.

28. Taplin, M.E., et al., *Androgen receptor mutations in androgen-independent prostate cancer: Cancer and Leukemia Group B Study 9663.* J Clin Oncol, 2003. **21**(14): p. 2673-8.

29. Culig, Z., et al., *Androgen receptor activation in prostatic tumor cell lines by insulin-like growth factor-I, keratinocyte growth factor and epidermal growth factor.* Eur Urol, 1995. **27 Suppl 2**: p. 45-7.

30. McGuire, W.L., G.C. Chamness, and S.A. Fuqua, *Estrogen receptor variants in clinical breast cancer.* Mol Endocrinol, 1991. **5**(11): p. 1571-7.

31. Bluemn, E.G., et al., *Androgen Receptor Pathway-Independent Prostate Cancer Is Sustained through FGF Signaling.* Cancer Cell, 2017. **32**(4): p. 474-489 e6.

32. van der Kwast, T.H., et al., *Androgen receptors in endocrine-therapy-resistant human prostate cancer.* Int J Cancer, 1991. **48**(2): p. 189-93.

33. McDonnell, T.J., et al., *Expression of the protooncogene bcl-2 in the prostate and its association with emergence of androgen-independent prostate cancer.* Cancer Res, 1992. **52**(24): p. 6940-4.

34. Chen, G., et al., *Up-regulation of Wnt-1 and beta-catenin production in patients with advanced metastatic prostate carcinoma: potential pathogenetic and prognostic implications.* Cancer, 2004. **101**(6): p. 1345-56.

35. Adamo, P. and M.R. Ladomery, *The oncogene ERG: a key factor in prostate cancer.* Oncogene, 2016. **35**(4): p. 403-14.

36. Baca, S.C., et al., *Punctuated evolution of prostate cancer genomes.* Cell, 2013. **153**(3): p. 666-77.

37. Bethel, C.R., et al., *Decreased NKX3.1 protein expression in focal prostatic atrophy, prostatic intraepithelial neoplasia, and adenocarcinoma: association with gleason score and chromosome 8p deletion.* Cancer Res, 2006. **66**(22): p. 10683-90.

38. Mazaris, E. and A. Tsiotras, *Molecular pathways in prostate cancer.* Nephrourol Mon, 2013. **5**(3): p. 792-800.

39. UK, C.R. *Prostate Cancer - Symptoms*. 15 Aug 2015.

40. Partin, A.W., et al., *The use of prostate specific antigen, clinical stage and Gleason score to predict pathological stage in men with localized prostate cancer.* J Urol, 1993. **150**(1): p. 110-4.

41. Epstein, J.I., et al., *The 2005 International Society of Urological Pathology (ISUP) Consensus Conference on Gleason Grading of Prostatic Carcinoma.* Am J Surg Pathol, 2005. **29**(9): p. 1228-42.

42. Litwin, M.S. and H.J. Tan, *The Diagnosis and Treatment of Prostate Cancer: A Review.* JAMA, 2017. **317**(24): p. 2532-2542.

43. Yue, S., et al., *Cholesteryl ester accumulation induced by PTEN loss and PI3K/AKT activation underlies human prostate cancer aggressiveness.* Cell Metab, 2014. **19**(3): p. 393-406.

44. de Bono, J.S., et al., *Abiraterone and increased survival in metastatic prostate cancer.* N Engl J Med, 2011. **364**(21): p. 1995-2005.

45. Saini, S., *PSA and beyond: alternative prostate cancer biomarkers.* Cell Oncol (Dordr), 2016. **39**(2): p. 97-106.

46. Oppermann, U., et al., *Short-chain dehydrogenases/reductases (SDR): the 2002 update.* Chem Biol Interact, 2003. **143-144**: p. 247-53.

47. Penning, T.M., et al., *Aldo-keto reductase (AKR) 1C3: role in prostate disease and the development of specific inhibitors.* Mol Cell Endocrinol, 2006. **248**(1-2): p. 182-91.

48. Penning, T.M., et al., *Human 3alpha-hydroxysteroid dehydrogenase isoforms (AKR1C1-AKR1C4) of the aldo-keto reductase superfamily: functional plasticity and tissue distribution reveals roles in the inactivation and formation of male and female sex hormones.* Biochem J, 2000. **351**(Pt 1): p. 67-77.

49. Bhatia, C., et al., *Towards a systematic analysis of human short-chain dehydrogenases/reductases (SDR): Ligand identification and structure-activity relationships.* Chem Biol Interact, 2015. **234**: p. 114-25.

50. Pilka, E.S., et al., *Structural basis for substrate specificity in human monomeric carbonyl reductases.* PLoS One, 2009. **4**(10): p. e7113.

51. Murakami, A., et al., *Decreased carbonyl reductase 1 expression promotes malignant behaviours by induction of epithelial mesenchymal transition and its clinical significance.* Cancer Lett, 2012. **323**(1): p. 69-76.

52. Osawa, Y., et al., *Decreased expression of carbonyl reductase 1 promotes ovarian cancer growth and proliferation.* Int J Oncol, 2015. **46**(3): p. 1252-8.

53. Guo, C., et al., *Induction of PGF2alpha synthesis by cortisol through GR dependent induction of CBR1 in human amnion fibroblasts.* Endocrinology, 2014. **155**(8): p. 3017-24.

54. Ziboh, V.A., J.T. Lord, and N.S. Penneys, *Alterations of prostaglandin E2-9-ketoreductase activity in proliferating skin.* J Lipid Res, 1977. **18**(1): p. 37-43.

55. Inazu, N., et al., *Carbonyl reductase from human testis: purification and comparison with carbonyl reductase from human brain and rat testis.* Biochim Biophys Acta, 1992. **1116**(1): p. 50-6.

56. Ke, J., et al., *Prostaglandin E2 (PGE2) promotes proliferation and invasion by enhancing SUMO-1 activity via EP4 receptor in endometrial cancer.* Tumour Biol, 2016. **37**(9): p. 12203-12211.

57. Wermuth, B., et al., *Carbonyl reductase provides the enzymatic basis of quinone detoxication in man.* Biochem Pharmacol, 1986. **35**(8): p. 1277-82.

58. Wermuth, B., *Purification and properties of an NADPH-dependent carbonyl reductase from human brain. Relationship to prostaglandin 9-ketoreductase and xenobiotic ketone reductase.* J Biol Chem, 1981. **256**(3): p. 1206-13.

59. Lopez de Cerain, A., et al., *Carbonyl reductase and NADPH cytochrome P450 reductase activities in human tumoral versus normal tissues.* Eur J Cancer, 1999. **35**(2): p. 320-4.

60. Hanamura, T., et al., *Human 3beta-hydroxysteroid dehydrogenase type 1 in human breast cancer: clinical significance and prognostic associations.* Cancer Med, 2016. **5**(7): p. 1405-15.

61. Hahn, A.W., S.K. Pal, and N. Agarwal, *HSD3B1-A Predictive Biomarker in Advanced Prostate Cancer.* JAMA Oncol, 2017.

62. Chang, B.L., et al., *Joint effect of HSD3B1 and HSD3B2 genes is associated with hereditary and sporadic prostate cancer susceptibility.* Cancer Res, 2002. **62**(6): p. 1784-9.

63. Ross, R.W., et al., *Inherited variation in the androgen pathway is associated with the efficacy of androgen-deprivation therapy in men with prostate cancer.* J Clin Oncol, 2008. **26**(6): p. 842-7.

64. Wu, G., et al., *Variant allele of HSD3B1 increases progression to castration-resistant prostate cancer.* Prostate, 2015. **75**(7): p. 777-782.

65. Simard, J., et al., *Molecular biology and genetics of the 3 beta-hydroxysteroid dehydrogenase/delta5-delta4 isomerase gene family.* J Endocrinol, 1996. **150 Suppl**: p. S189-207.

66. Payne, A.H., et al., *The multiple murine 3 beta-hydroxysteroid dehydrogenase isoforms: structure, function, and tissue- and developmentally specific expression.* Steroids, 1997. **62**(1): p. 169-75.

67. Suzuki, T., et al., *17Beta-hydroxysteroid dehydrogenase type 1 and type 2 in human breast carcinoma: a correlation to clinicopathological parameters.* British journal of cancer, 2000. **82**(3): p. 518-23.

68. Sasano, H., et al., *Aromatase and 17 beta-hydroxysteroid dehydrogenase type 1 in human breast carcinoma.* J Clin Endocrinol Metab, 1996. **81**(11): p. 4042-6.

69. Aka, J.A., et al., *17beta-hydroxysteroid dehydrogenase type 1 stimulates breast cancer by dihydrotestosterone inactivation in addition to estradiol production.* Mol Endocrinol, 2010. **24**(4): p. 832-45.

70. Aka, J.A., et al., *17beta-hydroxysteroid dehydrogenase type 1 modulates breast cancer protein profile and impacts cell migration.* Breast Cancer Res, 2012. **14**(3): p. R92.

71. Zhang, C.Y., et al., *Reductive 17beta-hydroxysteroid dehydrogenases which synthesize estradiol and inactivate dihydrotestosterone constitute major and concerted players in ER+ breast cancer cells.* J Steroid Biochem Mol Biol, 2015. **150**: p. 24-34.

72. Moeller, G. and J. Adamski, *Multifunctionality of human 17beta-hydroxysteroid dehydrogenases.* Mol Cell Endocrinol, 2006. **248**(1-2): p. 47-55.

73. Mindnich, R., G. Moller, and J. Adamski, *The role of 17 beta-hydroxysteroid dehydrogenases.* Mol Cell Endocrinol, 2004. **218**(1-2): p. 7-20.

74. Audet-Walsh, E., et al., *The impact of germline genetic variations in hydroxysteroid (17-beta) dehydrogenases on prostate cancer outcomes after prostatectomy.* Eur Urol, 2012. **62**(1): p. 88-96.

75. Zhongyi, S., et al., *Transgenic male mice expressing human hydroxysteroid dehydrogenase 2 indicate a role for the enzyme independent of its action on sex steroids.* Endocrinology, 2007. **148**(8): p. 3827-36.

76. Moeller, G. and J. Adamski, *Integrated view on 17beta-hydroxysteroid dehydrogenases.* Mol Cell Endocrinol, 2009. **301**(1-2): p. 7-19.

77. Markus, M., et al., *The organelles containing porcine 17 beta-estradiol dehydrogenase are peroxisomes.* Eur J Cell Biol, 1995. **68**(3): p. 263-7.

78. van Grunsven, E.G., et al., *Peroxisomal D-hydroxyacyl-CoA dehydrogenase deficiency: resolution of the enzyme defect and its molecular basis in bifunctional protein deficiency.* Proc Natl Acad Sci U S A, 1998. **95**(5): p. 2128-33.

79. Rasiah, K.K., et al., *HSD17B4 overexpression, an independent biomarker of poor patient outcome in prostate cancer.* Mol Cell Endocrinol, 2009. **301**(1-2): p. 89-96.

80. True, L., et al., *A molecular correlate to the Gleason grading system for prostate adenocarcinoma.* Proc Natl Acad Sci U S A, 2006. **103**(29): p. 10991-6.

81. Ko, H.K., et al., *Loss of an Androgen-Inactivating and Isoform-Specific HSD17B4 Splice Form Enables Emergence of Castration-Resistant Prostate Cancer.* Cell Rep, 2018. **22**(3): p. 809-819.

82. Baes, M., et al., *Inactivation of the peroxisomal multifunctional protein-2 in mice impedes the degradation of not only 2-methyl-branched fatty acids and bile acid intermediates but also of very long chain fatty acids.* J Biol Chem, 2000. **275**(21): p. 16329-36.

83. Huyghe, S., et al., *Peroxisomal multifunctional protein 2 is essential for lipid homeostasis in Sertoli cells and male fertility in mice.* Endocrinology, 2006. **147**(5): p. 2228-36.

84. Wang, X., et al., *Synergistic control of sex hormones by 17beta-HSD type 7: a novel target for estrogen-dependent breast cancer.* J Mol Cell Biol, 2015. **7**(6): p. 568-79.

85. Torn, S., et al., *Production, purification, and functional analysis of recombinant human and mouse 17beta-hydroxysteroid dehydrogenase type 7.* Biochem Biophys Res Commun, 2003. **305**(1): p. 37-45.

86. Szajnik, M., et al., *17beta Hydroxysteroid dehydrogenase type 12 (HSD17B12) is a marker of poor prognosis in ovarian carcinoma.* Gynecol Oncol, 2012. **127**(3): p. 587-94.

87. Nagasaki, S., et al., *17Beta-hydroxysteroid dehydrogenase type 12 in human breast carcinoma: a prognostic factor via potential regulation of fatty acid synthesis.* Cancer research, 2009. **69**(4): p. 1392-9.

88. Song, D., et al., *Expression of aromatase and 17beta-hydroxysteroid dehydrogenase types 1, 7 and 12 in breast cancer. An immunocytochemical study.* J Steroid Biochem Mol Biol, 2006. **101**(2-3): p. 136-44.

89. Jansson, A.K., et al., *17beta-hydroxysteroid dehydrogenase 14 affects estradiol levels in breast cancer cells and is a prognostic marker in estrogen receptor-positive breast cancer.* Cancer Res, 2006. **66**(23): p. 11471-7.

90. Luu-The, V., P. Tremblay, and F. Labrie, *Characterization of type 12 17beta-hydroxysteroid dehydrogenase, an isoform of type 3 17beta-hydroxysteroid dehydrogenase responsible for estradiol formation in women.* Mol Endocrinol, 2006. **20**(2): p. 437-43.

91. Day, J.M., et al., *17beta-hydroxysteroid dehydrogenase Type 1, and not Type 12, is a target for endocrine therapy of hormone-dependent breast cancer.* Int J Cancer, 2008. **122**(9): p. 1931-40.

92. Moon, Y.A. and J.D. Horton, *Identification of two mammalian reductases involved in the two-carbon fatty acyl elongation cascade.* J Biol Chem, 2003. **278**(9): p. 7335-43.

93. Muthusamy, S., et al., *Estrogen receptor beta and 17beta-hydroxysteroid dehydrogenase type 6, a growth regulatory pathway that is lost in prostate cancer.* Proceedings of the National Academy of Sciences of the United States of America, 2011. **108**(50): p. 20090-4.

94. Ishizaki, F., et al., *Androgen deprivation promotes intratumoral synthesis of dihydrotestosterone from androgen metabolites in prostate cancer.* Sci Rep, 2013. **3**: p. 1528.

95. Jiang, W. and J.L. Napoli, *The retinol dehydrogenase Rdh10 localizes to lipid droplets during acyl ester biosynthesis.* J Biol Chem, 2013. **288**(1): p. 589-97.

96. Guan, F., et al., *Retinol dehydrogenase-10 promotes development and progression of human glioma via the TWEAK-NF-kappaB axis.* Oncotarget, 2017. **8**(62): p. 105262-105275.

97. Bankovic, J., et al., *Identification of genes associated with non-small-cell lung cancer promotion and progression.* Lung Cancer, 2010. **67**(2): p. 151-9.

98. Wu, B.X., et al., *Cloning and characterization of a novel all-trans retinol short-chain dehydrogenase/reductase from the RPE.* Invest Ophthalmol Vis Sci, 2002. **43**(11): p. 3365-72.

99. Tang, X.H. and L.J. Gudas, *Retinoids, retinoic acid receptors, and cancer.* Annu Rev Pathol, 2011. **6**: p. 345-64.

100. Kuznetsova, E.S., et al., *[Abnormal expression of genes that regulate retinoid metabolism and signaling in non-small-cell lung cancer].* Mol Biol (Mosk), 2016. **50**(2): p. 255-65.

101. Kedishvili, N.Y., et al., *Evidence that the human gene for prostate short-chain dehydrogenase/reductase (PSDR1) encodes a novel retinal reductase (RalR1).* J Biol Chem, 2002. **277**(32): p. 28909-15.

102. Hu, L., et al., *Downregulation of DHRS9 expression in colorectal cancer tissues and its prognostic significance.* Tumour Biol, 2016. **37**(1): p. 837-45.

103. Chetyrkin, S.V., et al., *Characterization of a novel type of human microsomal 3alpha -hydroxysteroid dehydrogenase: unique tissue distribution and catalytic properties.* J Biol Chem, 2001. **276**(25): p. 22278-86.

104. Markova, N.G., et al., *Expression pattern and biochemical characteristics of a major epidermal retinol dehydrogenase.* Mol Genet Metab, 2003. **78**(2): p. 119-35.

105. Matsumoto, R., et al., *Aldo-keto reductase 1C1 induced by interleukin-1beta mediates the invasive potential and drug resistance of metastatic bladder cancer cells.* Sci Rep, 2016. **6**: p. 34625.

106. Tai, H.L., et al., *Overexpression of aldo-keto reductase 1C2 as a high-risk factor in bladder cancer.* Oncol Rep, 2007. **17**(2): p. 305-11.

107. Ji, Q., et al., *Selective loss of AKR1C1 and AKR1C2 in breast cancer and their potential effect on progesterone signaling.* Cancer Res, 2004. **64**(20): p. 7610-7.

108. Ji, Q., et al., *Selective reduction of AKR1C2 in prostate cancer and its role in DHT metabolism.* Prostate, 2003. **54**(4): p. 275-89.

109. Ji, Q., et al., *Impaired dihydrotestosterone catabolism in human prostate cancer: critical role of AKR1C2 as a pre-receptor regulator of androgen receptor signaling.* Cancer Res, 2007. **67**(3): p. 1361-9.

110. Penning, T.M., *The aldo-keto reductases (AKRs): Overview.* Chem Biol Interact, 2015. **234**: p. 236-46.

111. Fung, K.M., et al., *Increased expression of type 2 3alpha-hydroxysteroid dehydrogenase/type 5 17beta-hydroxysteroid dehydrogenase (AKR1C3) and its relationship with androgen receptor in prostate carcinoma.* Endocr Relat Cancer, 2006. **13**(1): p. 169-80.

112. Miller, V.L., et al., *Aldo-keto reductase family 1 member C3 (AKR1C3) is expressed in adenocarcinoma and squamous cell carcinoma but not small cell carcinoma.* Int J Clin Exp Pathol, 2012. **5**(4): p. 278-89.

113. Mantel, A., et al., *Aldo-keto reductase 1C3 is overexpressed in skin squamous cell carcinoma (SCC) and affects SCC growth via prostaglandin metabolism.* Exp Dermatol, 2014. **23**(8): p. 573-8.

114. Wu, C.H., et al., *Clinical implications of aldo-keto reductase family 1 member C3 and its relationship with lipocalin 2 in cancer of the uterine cervix.* Gynecol Oncol, 2014. **132**(2): p. 474-82.

115. Chang, N.W., et al., *High levels of arachidonic acid and peroxisome proliferator-activated receptor-alpha in breast cancer tissues are associated with promoting cancer cell proliferation.* The Journal of nutritional biochemistry, 2013. **24**(1): p. 274-81.

116. Tian, Y., et al., *AKR1C3 overexpression may serve as a promising biomarker for prostate cancer progression.* Diagn Pathol, 2014. **9**: p. 42.

117. Hagberg Thulin, M., et al., *Osteoblasts promote castration-resistant prostate cancer by altering intratumoral steroidogenesis.* Mol Cell Endocrinol, 2016. **422**: p. 182-191.

118. Downs, T.M., et al., *PTHrP stimulates prostate cancer cell growth and upregulates aldo-keto reductase 1C3.* Cancer Lett, 2011. **306**(1): p. 52-9.

119. Zhang, B., et al., *Human 3alpha-hydroxysteroid dehydrogenase type 3: structural clues of 5alpha-DHT reverse binding and enzyme down-regulation decreasing MCF7 cell growth.* Biochem J, 2016. **473**(8): p. 1037-46.

120. Suzuki-Yamamoto, T., et al., *cDNA cloning, expression and characterization of human prostaglandin F synthase.* FEBS Lett, 1999. **462**(3): p. 335-40.

121. Sharma, K.K., et al., *Deoxycorticosterone inactivation by AKR1C3 in human mineralocorticoid target tissues.* Mol Cell Endocrinol, 2006. **248**(1-2): p. 79-86.

122. Penning, T.M., *Aldo-Keto Reductase (AKR) 1C3 inhibitors: a patent review.* Expert Opin Ther Pat, 2017. **27**(12): p. 1329-1340.

123. Persson, B. and Y. Kallberg, *Classification and nomenclature of the superfamily of short-chain dehydrogenases/reductases (SDRs).* Chem Biol Interact, 2013. **202**(1-3): p. 111-5.

124. Bray, J.E., B.D. Marsden, and U. Oppermann, *The human short-chain dehydrogenase/reductase (SDR) superfamily: a bioinformatics summary.* Chemico-biological interactions, 2009. **178**(1-3): p. 99-109.

125. Kavanagh, K.L., et al., *Medium- and short-chain dehydrogenase/reductase gene and protein families : the SDR superfamily: functional and structural diversity within a family of metabolic and regulatory enzymes.* Cell Mol Life Sci, 2008. **65**(24): p. 3895-906.

126. Kallberg, Y., et al., *Short-chain dehydrogenase/reductase (SDR) relationships: a large family with eight clusters common to human, animal, and plant genomes.* Protein Sci, 2002. **11**(3): p. 636-41.

127. Wu, X., et al., *SDR-type human hydroxysteroid dehydrogenases involved in steroid hormone activation.* Mol Cell Endocrinol, 2007. **265-266**: p. 71-6.

128. Skarydova, L. and V. Wsol, *Human microsomal carbonyl reducing enzymes in the metabolism of xenobiotics: well-known and promising members of the SDR superfamily.* Drug Metab Rev, 2012. **44**(2): p. 173-91.

129. Oppermann, U.C., C. Filling, and H. Jornvall, *Forms and functions of human SDR enzymes.* Chem Biol Interact, 2001. **130-132**(1-3): p. 699-705.

130. Persson, B., et al., *The SDR (short-chain dehydrogenase/reductase and related enzymes) nomenclature initiative.* Chemico-biological interactions, 2009. **178**(1-3): p. 94-8.

131. Krozowski, Z., *The short-chain alcohol dehydrogenase superfamily: variations on a common theme.* J Steroid Biochem Mol Biol, 1994. **51**(3-4): p. 125-30.

132. Bennett, M.J., et al., *Structure of 3 alpha-hydroxysteroid/dihydrodiol dehydrogenase complexed with NADP+.* Biochemistry, 1996. **35**(33): p. 10702-11.

133. Jez, J.M., et al., *Comparative anatomy of the aldo-keto reductase superfamily.* Biochem J, 1997. **326 (Pt 3)**: p. 625-36.

134. Penning, T.M., *Human hydroxysteroid dehydrogenases and pre-receptor regulation: insights into inhibitor design and evaluation.* J Steroid Biochem Mol Biol, 2011. **125**(1-2): p. 46-56.

135. *IUPAC-IUB Joint Commission on Biochemical Nomenclature (JCBN). The nomenclature of steroids. Recommendations 1989.* European journal of biochemistry, 1989. **186**(3): p. 429-58.

136. Lathe, R. and Y. Kotelevtsev, *Steroid signaling: ligand-binding promiscuity, molecular symmetry, and the need for gating.* Steroids, 2014. **82**: p. 14-22.

137. Penning, T.M. and M.C. Byrns, *Steroid hormone transforming aldo-keto reductases and cancer.* Ann N Y Acad Sci, 2009. **1155**: p. 33-42.

138. Odermatt, A. and P. Klusonova, *11beta-Hydroxysteroid dehydrogenase 1: Regeneration of active glucocorticoids is only part of the story.* J Steroid Biochem Mol Biol, 2015. **151**: p. 85-92.

139. Labrie, F., et al., *The key role of 17 beta-hydroxysteroid dehydrogenases in sex steroid biology.* Steroids, 1997. **62**(1): p. 148-58.

140. Odermatt, A., P. Strajhar, and R.T. Engeli, *Disruption of steroidogenesis: Cell models for mechanistic investigations and as screening tools.* J Steroid Biochem Mol Biol, 2016. **158**: p. 9-21.

141. Miller, W.L. and R.J. Auchus, *The molecular biology, biochemistry, and physiology of human steroidogenesis and its disorders.* Endocr Rev, 2011. **32**(1): p. 81-151.

142. Krogh, A., et al., *Predicting transmembrane protein topology with a hidden Markov model: application to complete genomes.* J Mol Biol, 2001. **305**(3): p. 567-80.

143. Haeseleer, F. and K. Palczewski, *Short-chain dehydrogenases/reductases in retina.* Methods in enzymology, 2000. **316**: p. 372-83.

144. Fagerberg, L., et al., *Analysis of the human tissue-specific expression by genome-wide integration of transcriptomics and antibody-based proteomics.* Mol Cell Proteomics, 2014. **13**(2): p. 397-406.

145. Stambergova, H., et al., *Human DHRS7, promising enzyme in metabolism of steroids and retinoids?* The Journal of steroid biochemistry and molecular biology, 2016. **155**(Pt A): p. 112-9.

146. Stambergova, H., et al., *Biochemical properties of human dehydrogenase/reductase (SDR family) member 7.* Chem Biol Interact, 2014. **207**: p. 52-7.

147. Seibert, J.K., et al., *A role for the dehydrogenase DHRS7 (SDR34C1) in prostate cancer.* Cancer medicine, 2015.

148. Korfali, N., et al., *The nuclear envelope proteome differs notably between tissues.* Nucleus, 2012. **3**(6): p. 552-64.

149. Malik, P., et al., *Cell-specific and lamin-dependent targeting of novel transmembrane proteins in the nuclear envelope.* Cell Mol Life Sci, 2010. **67**(8): p. 1353-69.

150. Romanuik, T.L., et al., *LNCaP Atlas: gene expression associated with in vivo progression to castration-recurrent prostate cancer.* BMC medical genomics, 2010. **3**: p. 43.

151. Jiao, L., et al., *miR-663 induces castration-resistant prostate cancer transformation and predicts clinical recurrence.* J Cell Physiol, 2014. **229**(7): p. 834-44.

152. Zhu, M.L. and N. Kyprianou, *Role of androgens and the androgen receptor in epithelial-mesenchymal transition and invasion of prostate cancer cells.* FASEB J, 2010. **24**(3): p. 769-77.

153. Zhang Wei-Hong, Z.X.-C., Xing Shen-Yang, Li Ze-Zhong, Gong Peng-Tao, Li Jian-Hua, Yang Yu, Ni Jin-Song, *Effect of DHRS7 on cell cycle of human breast cancer MCF-7 cells and its expression in breast cancer tissue.* Journal of Jilin University (Medicine Edition), 2012.

154. Keildson, S., et al., *Expression of phosphofructokinase in skeletal muscle is influenced by genetic variation and associated with insulin sensitivity.* Diabetes, 2014. **63**(3): p. 1154-65.

155. Martinez, S.C., et al., *Inhibition of Foxo1 protects pancreatic islet beta-cells against fatty acid and endoplasmic reticulum stress-induced apoptosis.* Diabetes, 2008. **57**(4): p. 846-59.

156. Wang, W.B., et al., *Serial expression analysis of liver regeneration-related genes in rat regenerating liver.* Mol Biotechnol, 2009. **43**(3): p. 221-31.

157. Sadi, G., M.C. Baloglu, and M.B. Pektas, *Differential gene expression in liver tissues of streptozotocin-induced diabetic rats in response to resveratrol treatment.* PLoS One, 2015. **10**(4): p. e0124968.

158. Liao, B.M., et al., *Proteomic analysis of livers from fat-fed mice deficient in either PKCdelta or PKCepsilon identifies Htatip2 as a regulator of lipid metabolism.* Proteomics, 2014. **14**(21-22): p. 2578-87.

159. Pan, Z., et al., *Screening and identification of differentially expressed genes in goose hepatocytes exposed to free fatty acid.* J Cell Biochem, 2010. **111**(6): p. 1482-92.

160. Babelova, A., et al., *Next generation sequencing of sex-specific genes in the livers of obese ZSF1 rats.* Genomics, 2015. **106**(4): p. 204-13.

161. Cui, J.Y. and C.D. Klaassen, *RNA-Seq reveals common and unique PXR- and CAR-target gene signatures in the mouse liver transcriptome.* Biochim Biophys Acta, 2016. **1859**(9): p. 1198-217.

162. Timsit, Y.E. and M. Negishi, *CAR and PXR: the xenobiotic-sensing receptors.* Steroids, 2007. **72**(3): p. 231-46.

163. Albalat, R., et al., *Evolution of retinoid and steroid signaling: vertebrate diversification from an amphioxus perspective.* Genome Biol Evol, 2011. **3**: p. 985-1005.

164. Lodhi, I.J., et al., *Inhibiting adipose tissue lipogenesis reprograms thermogenesis and PPARgamma activation to decrease diet-induced obesity.* Cell Metab, 2012. **16**(2): p. 189-201.

165. Arai, S., et al., *Functional loss of DHRS7C induces intracellular Ca2+ overload and myotube enlargement in C2C12 cells via calpain activation.* Am J Physiol Cell Physiol, 2017. **312**(1): p. C29-C39.

166. Treves, S., et al., *SRP-35, a newly identified protein of the skeletal muscle sarcoplasmic reticulum, is a retinol dehydrogenase.* Biochem J, 2012. **441**(2): p. 731-41.

167. Ruiz, A., et al., *Over-expression of a retinol dehydrogenase (SRP35/DHRS7C) in skeletal muscle activates mTORC2, enhances glucose metabolism and muscle performance.* Sci Rep, 2018. **8**(1): p. 636.

168. Tomlinson, J.W., et al., *11beta-hydroxysteroid dehydrogenase type 1: a tissue-specific regulator of glucocorticoid response.* Endocr Rev, 2004. **25**(5): p. 831-66.

169. Atanasov, A.G., et al., *Hexose-6-phosphate dehydrogenase determines the reaction direction of 11beta-hydroxysteroid dehydrogenase type 1 as an oxoreductase.* FEBS letters, 2004. **571**(1-3): p. 129-33.

170. Odermatt, A., et al., *Why is 11beta-hydroxysteroid dehydrogenase type 1 facing the endoplasmic reticulum lumen? Physiological relevance of the membrane topology of 11beta-HSD1.* Mol Cell Endocrinol, 2006. **248**(1-2): p. 15-23.

171. Atanasov, A.G., et al., *Direct protein-protein interaction of 11beta-hydroxysteroid dehydrogenase type 1 and hexose-6-phosphate dehydrogenase in the endoplasmic reticulum lumen.* Biochimica et biophysica acta, 2008. **1783**(8): p. 1536-43.

172. Hosfield, D.J., et al., *Conformational flexibility in crystal structures of human 11beta-hydroxysteroid dehydrogenase type I provide insights into glucocorticoid interconversion and enzyme regulation.* J. Biol. Chem., 2005. **280**(6): p. 4639-4648.

173. Rantakari, P., et al., *Hydroxysteroid (17{beta}) dehydrogenase 12 is essential for mouse organogenesis and embryonic survival.* Endocrinology, 2010. **151**(4): p. 1893-901.

174. Moon, Y.A. and J.D. Horton, *Identification of two mammalian reductases involved in the two-carbon fatty acyl elongation cascade.* The Journal of biological chemistry, 2003. **278**(9): p. 7335-43.

175. Geissler, W.M., et al., *Male pseudohermaphroditism caused by mutations of testicular 17 beta-hydroxysteroid dehydrogenase 3.* Nat Genet, 1994. **7**(1): p. 34-9.

176. Luu-The, V., *Analysis and characteristics of multiple types of human 17beta-hydroxysteroid dehydrogenase.* J Steroid Biochem Mol Biol, 2001. **76**(1-5): p. 143-51.

177. Babcock, J.J. and M. Li, *Deorphanizing the human transmembrane genome: A landscape of uncharacterized membrane proteins.* Acta Pharmacol Sin, 2014. **35**(1): p. 11-23.

178. Guengerich, F.P., et al., *Approaches to deorphanization of human and microbial cytochrome P450 enzymes.* Biochim Biophys Acta, 2011. **1814**(1): p. 139-45.

179. Prosser, G.A., G. Larrouy-Maumus, and L.P. de Carvalho, *Metabolomic strategies for the identification of new enzyme functions and metabolic pathways.* EMBO Rep, 2014. **15**(6): p. 657-69.

180. Seddon, A.M., P. Curnow, and P.J. Booth, *Membrane proteins, lipids and detergents: not just a soap opera.* Biochim Biophys Acta, 2004. **1666**(1-2): p. 105-17.

181. Zhao, X.Y., et al., *Glucocorticoids can promote androgen-independent growth of prostate cancer cells through a mutated androgen receptor.* Nat Med, 2000. **6**(6): p. 703-6.

182. Li, M.T., et al., *Androgen and retinoic acid interaction in LNCaP cells, effects on cell proliferation and expression of retinoic acid receptors and epidermal growth factor receptor.* BMC Cancer, 2002. **2**: p. 16.

183. Gediya, L.K., et al., *Improved synthesis of histone deacetylase inhibitors (HDIs) (MS-275 and CI-994) and inhibitory effects of HDIs alone or in combination with RAMBAs or retinoids on growth of human LNCaP prostate cancer cells and tumor xenografts.* Bioorg Med Chem, 2008. **16**(6): p. 3352-60.

184. Esquenet, M., et al., *LNCaP prostatic adenocarcinoma cells derived from low and high passage numbers display divergent responses not only to androgens but also to retinoids.* J Steroid Biochem Mol Biol, 1997. **62**(5-6): p. 391-9.

185. de Launoit, Y., et al., *Characteristics of the biphasic action of androgens and of the potent antiproliferative effects of the new pure antiestrogen EM-139 on cell cycle kinetic parameters in LNCaP human prostatic cancer cells.* Cancer Res, 1991. **51**(19): p. 5165-70.

186. Wilding, G., M. Chen, and E.P. Gelmann, *Aberrant response in vitro of hormone-responsive prostate cancer cells to antiandrogens.* Prostate, 1989. **14**(2): p. 103-15.

187. Brinkmann, A.O., et al., *The human androgen receptor: domain structure, genomic organization and regulation of expression.* J Steroid Biochem, 1989. **34**(1-6): p. 307-10.

188. Schuurmans, A.L., et al., *Regulation of growth and epidermal growth factor receptor levels of LNCaP prostate tumor cells by different steroids.* Int J Cancer, 1988. **42**(6): p. 917-22.

189. Shan, J.D., et al., *Steroid-involved transcriptional regulation of human genes encoding prostatic acid phosphatase, prostate-specific antigen, and prostate-specific glandular kallikrein.* Endocrinology, 1997. **138**(9): p. 3764-70.

190. Sonnenschein, C., et al., *Negative controls of cell proliferation: human prostate cancer cells and androgens.* Cancer Res, 1989. **49**(13): p. 3474-81.

191. Araya, S., et al., *DHRS7 (SDR34C1) - A new player in the regulation of androgen receptor function by inactivation of 5alpha-dihydrotestosterone?* J Steroid Biochem Mol Biol, 2017.

192. Tsachaki, M., et al., *Determination of the topology of endoplasmic reticulum membrane proteins using redox-sensitive green-fluorescence protein fusions.* Biochimica et biophysica acta, 2015. **1853**(7): p. 1672-82.

193. Livak, K.J. and T.D. Schmittgen, *Analysis of relative gene expression data using real-time quantitative PCR and the 2(-Delta Delta C(T)) Method.* Methods, 2001. **25**(4): p. 402-8.

194. Rogoff, D., et al., *Contribution of hexose-6-phosphate dehydrogenase to NADPH content and redox environment in the endoplasmic reticulum.* Redox Rep, 2010. **15**(2): p. 64-70.

195. Schuster, D., et al., *The discovery of new 11beta-hydroxysteroid dehydrogenase type 1 inhibitors by common feature pharmacophore modeling and virtual screening.* J Med Chem, 2006. **49**(12): p. 3454-66.

196. Mohler, J.L., M.A. Titus, and E.M. Wilson, *Potential prostate cancer drug target: bioactivation of androstanediol by conversion to dihydrotestosterone.* Clin Cancer Res, 2011. **17**(18): p. 5844-9.

197. Biswas, M.G. and D.W. Russell, *Expression cloning and characterization of oxidative 17beta- and 3alpha-hydroxysteroid dehydrogenases from rat and human prostate.* J Biol Chem, 1997. **272**(25): p. 15959-66.

198. Bauman, D.R., et al., *Identification of the major oxidative 3alpha-hydroxysteroid dehydrogenase in human prostate that converts 5alpha-androstane-3alpha,17beta-diol to 5alpha-dihydrotestosterone: a potential therapeutic target for androgen-dependent disease.* Mol Endocrinol, 2006. **20**(2): p. 444-58.

199. Balk, S.P., *Increased expression of genes converting adrenal androgens to testosterone in castration-recurrent prostate cancer*, in *Androgen action in prostate cancer*, D.M. Tindall, J. L., Editor. 2009, Springer: New York. p. 123-139.

200. He, X.Y., et al., *Oxidative 3alpha-hydroxysteroid dehydrogenase activity of human type 10 17beta-hydroxysteroid dehydrogenase.* J Steroid Biochem Mol Biol, 2003. **87**(2-3): p. 191-8.

201. He, X.Y., et al., *Characterization and localization of human type10 17beta-hydroxysteroid dehydrogenase.* Eur J Biochem, 2001. **268**(18): p. 4899-907.

202. He, X.Y., et al., *Human brain short chain L-3-hydroxyacyl coenzyme A dehydrogenase is a single-domain multifunctional enzyme. Characterization of a novel 17beta-hydroxysteroid dehydrogenase.* The Journal of biological chemistry, 1999. **274**(21): p. 15014-9.

203. Pettersson, H., et al., *CYP7B1-mediated metabolism of 5alpha-androstane-3alpha,17beta-diol (3alpha-Adiol): a novel pathway for potential regulation of the cellular levels of androgens and neurosteroids.* Biochim Biophys Acta, 2009. **1791**(12): p. 1206-15.

204. Yantsevich, A.V., et al., *Human steroid and oxysterol 7alpha-hydroxylase CYP7B1: substrate specificity, azole binding and misfolding of clinically relevant mutants.* FEBS J, 2014. **281**(6): p. 1700-13.

205. Skarka, A., et al., *Purification and reconstitution of human membrane-bound DHRS7 (SDR34C1) from Sf9 cells.* Protein expression and purification, 2014. **95**: p. 44-9.

206. Nishizawa, M., et al., *Close kinship of human 20alpha-hydroxysteroid dehydrogenase gene with three aldo-keto reductase genes.* Genes Cells, 2000. **5**(2): p. 111-25.

207. Michaelis, L. and M.M. Menten, *The kinetics of invertin action. 1913.* FEBS Lett, 2013. **587**(17): p. 2712-20.

208. Zemanova, L., et al., *The identification of new substrates of human DHRS7 by molecular modeling and in vitro testing.* Int J Biol Macromol, 2017.

209. Domagk, G.F. and R. Chilla, *Glucose-6-phosphate dehydrogenase from Candida utilia.* Methods Enzymol, 1975. **41**: p. 205-8.

210. Grigoryev, D.N., et al., *Pregnenolone stimulates LNCaP prostate cancer cell growth via the mutated androgen receptor.* J Steroid Biochem Mol Biol, 2000. **75**(1): p. 1-10.

211. Lin, Y.C., et al., *Genome dynamics of the human embryonic kidney 293 lineage in response to cell biology manipulations.* Nat Commun, 2014. **5**: p. 4767.

212. Kalitin, N.N. and A.F. Karamysheva, *RARalpha mediates all-trans-retinoic acid-induced VEGF-C, VEGF-D, and VEGFR3 expression in lung cancer cells.* Cell Biol Int, 2016. **40**(4): p. 456-64.

213. Taherian, A., et al., *Differences in integrin expression and signaling within human breast cancer cells.* BMC Cancer, 2011. **11**: p. 293.

214. Salomon, A., et al., *Loss of beta-catenin in adrenocortical cancer cells causes growth inhibition and reversal of epithelial-to-mesenchymal transition.* Oncotarget, 2015. **6**(13): p. 11421-33.

215. OECD, *Guidance Document on Standardised Test Guidelines for Evaluating Chemicals for Endocrine Disruption - Series on Testing and Assessment No. 150, ENV/JM/MONO(2012)22.* Environment Directorate Joint Meeting of the Chemicals Committee and the Working Party on Chemicals, Pesticides and Biotechnology, 2012.

216. Strajhar, P., et al., *Steroid profiling in H295R cells to identify chemicals potentially disrupting the production of adrenal steroids.* Toxicology, 2017. **381**: p. 51-63.

217. Seibert, J.K., *Characterization of the 11ß-hydroxysteroid dehydrogenase 1-related short-chain dehydrogenase/reductase DHRS7*, in *Departement Pharmazeutische Wissenschaften, Molecular and Systems Toxicology*. 2015, Univeristy of Basel: http://edoc.unibas.ch/diss/DissB_11333. p. 96.

218. Hilscherova, K., et al., *Assessment of the effects of chemicals on the expression of ten steroidogenic genes in the H295R cell line using real-time PCR.* Toxicol Sci, 2004. **81**(1): p. 78-89.

219. Need, E.F., et al., *The unique transcriptional response produced by concurrent estrogen and progesterone treatment in breast cancer cells results in upregulation of growth factor pathways and switching from a Luminal A to a Basal-like subtype.* BMC Cancer, 2015. **15**: p. 791.

220. Cochrane, D.R., et al., *Role of the androgen receptor in breast cancer and preclinical analysis of enzalutamide.* Breast Cancer Res, 2014. **16**(1): p. R7.

221. ATCC. *ATCC: The Global Bioresource Center*.

222. Muller-Vieira, U., M. Angotti, and R.W. Hartmann, *The adrenocortical tumor cell line NCI-H295R as an in vitro screening system for the evaluation of CYP11B2 (aldosterone synthase) and CYP11B1 (steroid-11beta-hydroxylase) inhibitors.* J Steroid Biochem Mol Biol, 2005. **96**(3-4): p. 259-70.

223. Jain, M., et al., *KIAA0101 is overexpressed, and promotes growth and invasion in adrenal cancer.* PLoS One, 2011. **6**(11): p. e26866.

224. Kettenbach, A.N. and S.A. Gerber, *Rapid and reproducible single-stage phosphopeptide enrichment of complex peptide mixtures: application to general and phosphotyrosine-specific phosphoproteomics experiments.* Anal Chem, 2011. **83**(20): p. 7635-44.

225. Dephoure, N. and S.P. Gygi, *A solid phase extraction-based platform for rapid phosphoproteomic analysis.* Methods, 2011. **54**(4): p. 379-86.

226. Wisniewski, J.R., et al., *Universal sample preparation method for proteome analysis.* Nat Methods, 2009. **6**(5): p. 359-62.

227. Miller, M.R., et al., *Unconventional endocannabinoid signaling governs sperm activation via the sex hormone progesterone.* Science, 2016. **352**(6285): p. 555-9.

228. Acuna, M., et al., *Structural and functional analysis of the ASM p.Ala359Asp mutant that causes acid sphingomyelinase deficiency.* Biochem Biophys Res Commun, 2016. **479**(3): p. 496-501.

229. Brady, R.O., et al., *The metabolism of sphingomyelin. II. Evidence of an enzymatic deficiency in Niemann-Pick diseae.* Proc Natl Acad Sci U S A, 1966. **55**(2): p. 366-9.

230. Moessinger, C., et al., *Human lysophosphatidylcholine acyltransferases 1 and 2 are located in lipid droplets where they catalyze the formation of phosphatidylcholine.* J Biol Chem, 2011. **286**(24): p. 21330-9.

231. Germain, P., et al., *Overview of nomenclature of nuclear receptors.* Pharmacol Rev, 2006. **58**(4): p. 685-704.

232. Mostaghel, E.A., *Beyond T and DHT - novel steroid derivatives capable of wild type androgen receptor activation.* Int J Biol Sci, 2014. **10**(6): p. 602-13.

233. Wu, F., et al., *Novel role for epidermal growth factor-like domain 7 in metastasis of human hepatocellular carcinoma.* Hepatology, 2009. **50**(6): p. 1839-50.

234. Langlais, P., et al., *Phosphorylation of Grb10 by mitogen-activated protein kinase: identification of Ser150 and Ser476 of human Grb10zeta as major phosphorylation sites.* Biochemistry, 2005. **44**(24): p. 8890-7.

235. Bennett, L.N. and P.R. Clarke, *Regulation of Claspin degradation by the ubiquitin-proteosome pathway during the cell cycle and in response to ATR-dependent checkpoint activation.* FEBS Lett, 2006. **580**(17): p. 4176-81.

236. Katsuno, Y., et al., *Cyclin A-Cdk1 regulates the origin firing program in mammalian cells.* Proc Natl Acad Sci U S A, 2009. **106**(9): p. 3184-9.

237. Neganova, I. and M. Lako, *G1 to S phase cell cycle transition in somatic and embryonic stem cells.* J Anat, 2008. **213**(1): p. 30-44.

238. Marechal, A. and L. Zou, *DNA damage sensing by the ATM and ATR kinases.* Cold Spring Harb Perspect Biol, 2013. **5**(9).

239. Simone, C., et al., *Physical interaction between pRb and cdk9/cyclinT2 complex.* Oncogene, 2002. **21**(26): p. 4158-65.

240. Takeichi, M., *Multiple functions of alpha-catenin beyond cell adhesion regulation.* Curr Opin Cell Biol, 2018. **54**: p. 24-29.

241. van Kempen, L.C., et al., *Molecular basis for the homophilic activated leukocyte cell adhesion molecule (ALCAM)-ALCAM interaction.* J Biol Chem, 2001. **276**(28): p. 25783-90.

242. Nuber, U.A., et al., *The widespread human desmocollin Dsc2 and tissue-specific patterns of synthesis of various desmocollin subtypes.* Eur J Cell Biol, 1995. **66**(1): p. 69-74.

243. Suzuki, T., et al., *PKC eta regulates occludin phosphorylation and epithelial tight junction integrity.* Proc Natl Acad Sci U S A, 2009. **106**(1): p. 61-6.

244. Wang, D., et al., *F-actin binding protein, anillin, regulates integrity of intercellular junctions in human epithelial cells.* Cell Mol Life Sci, 2015. **72**(16): p. 3185-3200.

245. M, N.K., et al., *Molecular characterization of human ABHD2 as TAG lipase and ester hydrolase.* Biosci Rep, 2016. **36**(4).

246. Honsho, M., S. Asaoku, and Y. Fujiki, *Posttranslational regulation of fatty acyl-CoA reductase 1, Far1, controls ether glycerophospholipid synthesis.* J Biol Chem, 2010. **285**(12): p. 8537-42.

247. Shringarpure, R., et al., *Ubiquitin conjugation is not required for the degradation of oxidized proteins by proteasome.* J Biol Chem, 2003. **278**(1): p. 311-8.

248. Serrano-Gomez, S.J., M. Maziveyi, and S.K. Alahari, *Regulation of epithelial-mesenchymal transition through epigenetic and post-translational modifications.* Mol Cancer, 2016. **15**: p. 18.

249. Sandell, L.L., et al., *RDH10 oxidation of Vitamin A is a critical control step in synthesis of retinoic acid during mouse embryogenesis.* PLoS One, 2012. **7**(2): p. e30698.

250. Obinata, D., et al., *Abhydrolase domain containing 2, an androgen target gene, promotes prostate cancer cell proliferation and migration.* Eur J Cancer, 2016. **57**: p. 39-49.

251. Hughes-Fulford, M., et al., *Arachidonic acid activates phosphatidylinositol 3-kinase signaling and induces gene expression in prostate cancer.* Cancer Res, 2006. **66**(3): p. 1427-33.

252. Nomura, D.K., et al., *Monoacylglycerol lipase exerts dual control over endocannabinoid and fatty acid pathways to support prostate cancer.* Chem Biol, 2011. **18**(7): p. 846-56.

253. Daemen, S., et al., *Microscopy tools for the investigation of intracellular lipid storage and dynamics.* Mol Metab, 2016. **5**(3): p. 153-63.

254. Sadowski, M.C., et al., *The fatty acid synthase inhibitor triclosan: repurposing an anti-microbial agent for targeting prostate cancer.* Oncotarget, 2014. **5**(19): p. 9362-81.

255. Kowalik, D., et al., *In search for function of two human orphan SDR enzymes: hydroxysteroid dehydrogenase like 2 (HSDL2) and short-chain dehydrogenase/reductase-orphan (SDR-O).* J Steroid Biochem Mol Biol, 2009. **117**(4-5): p. 117-24.

256. Reinhardt, N., et al., *Substrate flexibility and reaction specificity of tropinone reductase-like short-chain dehydrogenases.* Bioorg Chem, 2014. **53**: p. 37-49.

9 Supplementary Data

9.1.1.1 *Supplementaries of the Publication "DHRS7 (SDR34C1) – a New player in the regulation of androgen receptor function by inactivation of 5α-dihydrotestosterone?*

Quantification of steroids in cell culture supernatants

1.1. Chemicals and reagents

Acetonitrile and formic acid of UHPLC-grade were purchased from Biosolve (Dieuze, France) or Sigma-Aldrich (St. Louis, MO, USA). Distilled water was obtained using a MilliQ water purification system (Millipore, Billerica, MA, USA). Cortisol-D_4 (≥ 98% isotopic purity) was purchased from Sigma-Aldrich. Cortisol, cortisone and 20β-dihydrocortisone (20βDHE) were purchased from Steraloids (Newport, RI, USA) and all other chemicals were obtained from Sigma-Aldrich of the highest grade available.

1.2. Instrumentation and analytical conditions

Evaporation: Samples were evaporated to dryness using a Genevac EZ-2 plus centrifugal vacuum evaporator (Genevac, Suffolk, UK).

Analytical instruments: Ultra-High performance liquid chromatography-tandem mass spectrometry (UHPLC-MS/MS) using an Agilent 1290 UHPLC instrument equipped with a binary solvent delivery system, an auto sampler (at 4°C), and a column oven, coupled to an Agilent 6490 triple quadrupole mass spectrometer equipped with a jet stream electrospray ionization interface (AJS-ESI) (Agilent Technologies, Basel, Switzerland) were used for steroids quantification.

Liquid chromatography: The chromatographic separation was performed on a Waters Acquity UPLC BEH C18, 1.7 µm, 2.1 × 150 mm column (Waters, Wexford, Ireland), at a column temperature of 40 ± 0.8°C. The mobile phase was water-acetonitrile-formic acid (70/30/0.1; v/v/v). Steroids were separated with a constant flow rate of 0.5 mL/min within 0-2.3 min, followed by 2 min column wash with 100% acetonitrile and subsequent column re-equilibration for 2 min with 30% acetonitrile. A methanol-water (75/25 v/v) mixture was used as needle and needle-seat flushing solvent for 10 s after sample injection. Samples were stored until analysis in the auto sampler (maintained at 4 ± 0.8°C). The injection volume was 2 µL per sample.

Mass spectrometry: Characteristic precursor ions and their corresponding product ions for multiple reaction monitoring (MRM) were defined by use of the compound optimizer software module included within the Mass Hunter Workstation software (Agilent Technologies, California, USA). Analytes were quantified using the corresponding mass transitions within individual time-segments: *Segment 1*: 20βDHE *m/z* 363.22→163 (28 V, Dwell 150 ms) and *m/z* 363.22→105 (44 V, Dwell 150 ms); *Segment 2*: Cortisone: *m/z* 361.2→163 (24 V, Dwell 100 ms) and *m/z* 361.2→121.1 (36 V, Dwell 50 ms); Cortisol: *m/z* 363.22→121.1 (28 V, Dwell 150 ms) and *m/z* 163.22→90.9 (60 V, Dwell 50 ms), Cortisol-D_4: *m/z* 367.2→121.2 (25 V, Dwell 75 ms). The AJS-ESI source conditions were set in the positive ion mode as following: Nitrogen gas temperature (290°C), gas flow (14 L/min), nebulizer (20 psi), sheath gas temperature (350°C), sheath gas flow (11 L/min), capillary voltage (4000 V), and nozzle voltage (1500 V) (Agilent Technologies, California, USA, B.08.00/Build 8.0.8023.0).

Data analysis: The MassHunter Workstation Acquisition Software Version B.08.00/Build 8.0.8023.0 and MassHunter Workstation Software Quantitative Analysis Version B.07.01 /Build 7.1.524.0, respectively (Agilent Technologies, California, USA) was used for data acquisition and subsequent data analysis.

Sample preparation: To each cell culture supernatant of sample or calibrator (400 µL) an internal standard solution containing cortisol-D_4 in acetonitrile (100 µL, 125 nM) was added. Proteins were precipitated by adding ice cold acetonitrile (1 mL) and samples were incubated in a thermoshaker by thoroughly shaking (20 min, 1300 rpm, 4°C). Samples were centrifuged (10 min, 16,000 × rcf, 4°C). Samples were evaporated to dryness and reconstituted in methanol (50 µL, 10 min, 1300 rpm, 4°C, thermoshaker).

Chromatographic performance: Ten-point calibration curves over the range of 0.98 to 250 nmol/L steroids were generated by a zero sample and nine calibrators in phenol red and serum free cell culture media. The coefficient of determination (R^2) was 0.99 and at least 75% of all calibrators had to be valid.

9.1.1.2 Sequences of primers used for qPCR

Gene	Forward primer	Reverse primer
DHRS7	GAGTTTGGTAGAATCGACTTTCTG	GAAAGAGGTACAGATATGATACCC
RARα	AAGCCCGAGTGCTCTGAGA	TTCGTAGTGTATTTGCCCAGC
AKR1C2	TGGAGCAATTCCCATCGACC	CCCTATGTCCTCCTTTACAGAC
PPIA	ATGGTCAACCCCACCGTGT	TCTGCTGTCTTTGGGACCTTGTC

9.1.1.3 LC/MS peaks

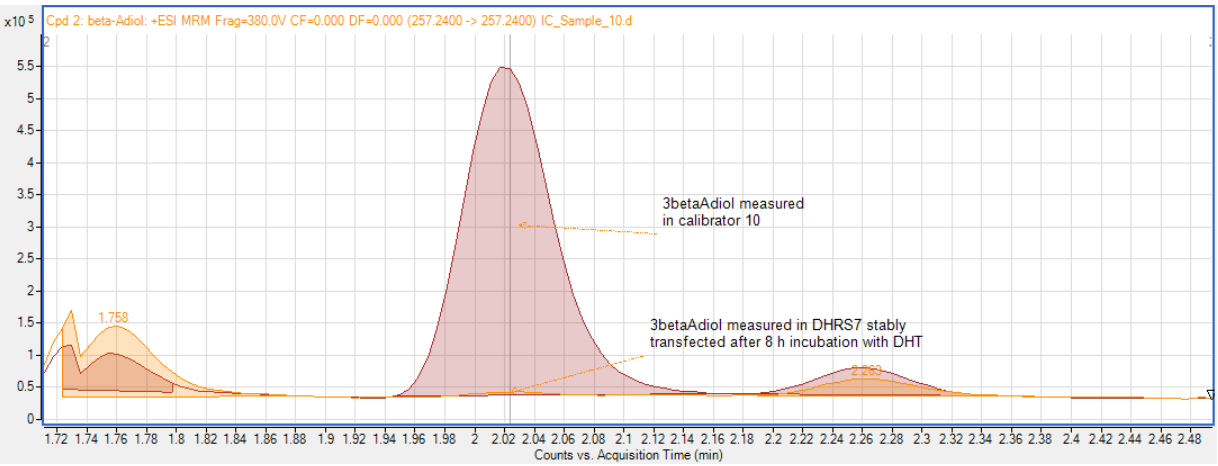

Figure 39: Absence of 3ßAdiol in HEK 293 after 24 h incubation with 200 nM 3αAdiol (in red peak of 3ßAdiol in calibrator with ca. 200nM, in orange compared to the supernatant from DHRS7 stably transfectedHEK 293 cells after 8 h incubation with DHT).

9.1.1.4 Regulated proteins after DHRS7 depletion 48 h

*Table 9: Proteins identified with one peptide uniquely present in the siRNA DHRS7 condition after 48 h timepoint with p-value >0.05. *depicted values correspond to the mean of ion precursor intensities with arbitrary unit.*

Proteins only detected in siRNA DHRS7 48 h	Accession Number	Molecular Weight	T-Test (p-value)	Mean scrambled siRNA*	Mean siRNA DHRS7*
Epidermal growth factor receptor	P00533	134 kDa	0.013	0	6134233.333
NADH dehydrogenase [ubiquinone] 1 alpha subcomplex subunit 11	Q86Y39	15 kDa	0.0029	0	5487366.667
Zinc transporter 1	Q9Y6M5	55 kDa	0.0031	0	9620266.667
Glycogen phosphorylase, liver form	P06737	97 kDa	0.0047	0	38062000
Pituitary tumor-transforming gene 1 protein-interacting protein	P53801	20 kDa	0.00022	0	3017866.667
DNA-directed RNA polymerase I subunit RPA43	Q3B726	37 kDa	0.0014	0	6281133.333
Putative tRNA (cytidine(32)/guanosine(34)-2'-O)-methyltransferase	Q9UET6	36 kDa	0.033	0	3461333.333
Neuroplastin	Q9Y639	44 kDa	0.032	0	5109600
Guanine nucleotide-binding protein subunit beta-like protein 1	Q9BYB4	36 kDa	0.003	0	4533733.333
Myotubularin-related protein 14	Q8NCE2	72 kDa	0.0091	0	3747233.333
Leucine-rich repeat neuronal protein 1	Q6UXK5	81 kDa	0.0027	0	1394400
Pleckstrin homology domain-containing family H member 3	Q7Z736	85 kDa	0.008	0	1471443.333
Selenoprotein M	Q8WWX9	16 kDa	0.0006	0	2260400
Dolichol-phosphate mannosyltransferase subunit 3	Q9P2X0	10 kDa	0.00017	0	3827900

*Table 10: Proteins identified with one peptide uniquely present in the siRNA scrambled control condition after 48 h timepoint with p-value >0.05. *depicted values correspond to the mean of ion precursor intensities with arbitrary unit.*

Proteins only deteted in scrambled siRNA control 48 h	Accession Number	Molecular Weight	T-Test (p-value)	Mean scrambled siRNA	Mean siRNA DHRS7
Mitotic checkpoint serine/threonine-protein kinase BUB1 beta	O60566	120 kDa	0.047	4463000	0
UAP56-interacting factor	Q96QD9	36 kDa	0.036	7686600	0
Chromosome transmission fidelity protein 8 homolog	P0CG13	13 kDa	0.0098	3595166.667	0
Serine/threonine-protein kinase TAO1	Q7L7X3	116 kDa	0.011	37481666.67	0
Ubiquitin-conjugating enzyme E2 Q1	Q7Z7E8	46 kDa	0.041	4524733.333	0
Neuroblastoma-amplified sequence	A2RRP1	269 kDa	0.011	1187736.667	0
Occludin	Q16625	59 kDa	0.0079	7191933.333	0
Serine/arginine-rich splicing factor 8	Q9BRL6	32 kDa	0.039	46151666.67	0
Neurobeachin-like protein 2	Q6ZNJ1	303 kDa	0.0078	5871733.333	0
Phosphatidylinositol 5-phosphate 4-kinase type-2 beta	P78356	47 kDa	0.0098	5000200	0
Striatin	O43815	86 kDa	0.046	6259166.667	0
Putative bifunctional UDP-N-acetylglucosamine transferase and deubiquitinase ALG13	Q9NP73	126 kDa	0.0066	5257200	0
UHRF1-binding protein 1	Q6BDS2	159 kDa	0.0043	2369066.667	0
Amyloid-like protein 2	Q06481	87 kDa	0.0041	5008266.667	0
Glutathione S-transferase A4	O15217	26 kDa	0.00086	1038156.667	0
Hyaluronan mediated motility receptor	O75330	84 kDa	0.0047	4065166.667	0
Kinesin-like protein KIF23	Q02241	110 kDa	0.018	1316083.333	0
N-acetyltransferase ESCO2	Q56NI9	68 kDa	0.02	84981	0
TLD domain-containing protein 1	Q6P9B6	51 kDa	0.0056	6137466.667	0
Nucleolar and spindle-associated protein 1	Q9BXS6	49 kDa	0.0013	869493.3333	0
Nicotinamide/nicotinic acid mononucleotide adenylyltransferase 1	Q9HAN9	32 kDa	0.00041	1082253.333	0
Centromere protein M	Q9NSP4	20 kDa	0.00088	687093.3333	0
Stromal membrane-associated protein 1	Q8IYB5	50 kDa	0.032	2196566.667	0

*Table 11: Proteins identified with one peptide upregulated in the siRNA DHRS7 condition after 48 h timepoint with p-value >0.05. *depicted values correspond to the mean of ion precursor intensities with arbitrary unit. MW=Molecular weight*

Upregulated Proteins	Accession Number	MW	T-Test (p-value):	Fold Change	Mean scrambled siRNA*	Mean siRNA DHRS7*
Cyclin-T2 - CCNT2 -	O60583	81 kDa	0.0005	380	10690.3333	4031333.33
FH1/FH2 domain-containing protein 1 - FHOD1 -	Q9Y613	127 kDa	0.043	24	313033.333	7473433.33
Anaphase-promoting complex subunit 1 - ANAPC1 -	Q9H1A4	217 kDa	0.019	24	120806.667	2861966.67
Small subunit processome component 20 homolog - UTP20 -	O75691	318 kDa	0.00051	19	1610613.33	30920333.3
Protein bicaudal D homolog 2 - BICD2 -	Q8TD16	94 kDa	0.049	13	322816.667	4084033.33
Protein phosphatase 1 regulatory subunit 21 - PPP1R21 -	Q6ZMI0	88 kDa	0.0032	9.7	830966.667	8041933.33
Transmembrane protein 238 - TMEM238 -	C9JI98	18 kDa	0.021	9.4	884370	8336033.33
Desmocollin-2 - DSC2 -	Q02487	100 kDa	0.04	9	4548700	40950000
Sphingomyelin phosphodiesterase - SMPD1	P17405	70 kDa	0.0093	7.7	628200	4842000
Solute carrier family 12 member 2 - SLC12A2 -	P55011	131 kDa	0.01	7.6	809666.667	6164033.33
Nucleolar protein 7 - NOL7 -	Q9UMY1	29 kDa	0.0039	7.2	520640	3723600
Zinc finger CCHC domain-containing protein 3 - ZCCHC3 -	Q9NUD5	44 kDa	0.0085	6.8	479500	3261500
Ceroid-lipofuscinosis neuronal protein 5 - CLN5 -	O75503	41 kDa	0.0069	6.7	1789266.67	12043333.3
Alpha-1-syntrophin - SNTA1 -	Q13424	54 kDa	0.018	6.2	743066.667	4602466.67
Gamma-aminobutyric acid receptor-associated protein - GABARAP -	O95166	14 kDa	0.00061	6.1	4634433.33	28303000
Choline transporter-like protein 2 - SLC44A2 -	Q8IWA5	80 kDa	0.024	5.6	1200266.67	6666633.33
Major vault protein - MVP	Q14764	99 kDa	0.013	5.3	3856533.33	20289333.3
Leucyl-cystinyl aminopeptidase - LNPEP -	Q9UIQ6	117 kDa	0.0049	5.2	1600333.33	8251066.67
Multidrug resistance-associated protein 1 - ABCC1 -	P33527	172 kDa	0.033	5.1	2026166.67	10372733.3
Gamma-aminobutyric acid receptor-associated protein-like 2 - GABARAPL2 -	P60520	14 kDa	0.042	5.1	1006500	5124866.67
Interleukin-1 receptor-associated kinase 1 - IRAK1 -	P51617	77 kDa	0.019	4.9	254493.333	1257600
MORC family CW-type zinc finger protein 3 - MORC3 -	Q14149	107 kDa	0.046	4.7	383086.667	1782930
Uridine diphosphate glucose pyrophosphatase - NUDT14 -	O95848	24 kDa	0.029	4.6	261366.667	1209333.33
Monoacylglycerol lipase ABHD2 - ABHD2 -	P08910	48 kDa	0.021	4.6	1278870	5829066.67
Coiled-coil domain-containing protein 86 - CCDC86 -	Q9H6F5	40 kDa	0.0047	4.5	5494233.33	24913333.3
Ganglioside-induced differentiation-associated protein 1 - GDAP1 -	Q8TB36	41 kDa	0.02	4.5	1288600	5780466.67
Golgi apparatus membrane protein TVP23 homolog B - TVP23B -	Q9NYZ1	24 kDa	0.037	4.2	2180133.33	9203566.67
Lysine-rich nucleolar protein 1 - KNOP1 -	Q1ED39	52 kDa	0.0077	4.2	4850166.67	20339333.3
F-box/LRR-repeat protein 8 - FBXL8 -	Q96CD0	41 kDa	0.038	4.2	447833.333	1860833.33
UPF0729 protein C18orf32 - C18orf32 - -	Q8TCD1	9 kDa	0.041	4.2	3027233.33	12574933.3
Neurochondrin - NCDN -	Q9UBB6	79 kDa	0.0054	3.7	6462800	24163000
Bystin - BYSL -	Q13895	50 kDa	0.011	3.3	4493500	14837000
Peroxisomal 2,4-dienoyl-CoA reductase - DECR2	Q9NUI1	31 kDa	0.012	3.2	2741933.33	8741433.33

WD repeat-containing protein 6 - WDR6 -	Q9NNW5	122 kDa	0.03	3.1	7835033.33	24640000
Uncharacterized protein KIAA1143 - KIAA1143 -	Q96AT1	17 kDa	0.033	3	7744633.33	23610666.7
Mannosyl-oligosaccharide glucosidase - MOGS	Q13724	92 kDa	0.00052	3	3354200	10130733.3
Endoribonuclease Dicer - DICER1 -	Q9UPY3	219 kDa	0.016	3	4363500	13085666.7
Acyl-coenzyme A thioesterase THEM4 - THEM4 -	Q5T1C6	27 kDa	0.022	3	3788566.67	11254400
Kinase D-interacting substrate of 220 kDa - KIDINS220 -	Q9ULH0	197 kDa	0.023	2.9	121733.333	354840
COBW domain-containing protein 3 - CBWD3 - -	Q5JTY5 (+3)	44 kDa	0.025	2.7	3865733.33	10616800
Nuclear receptor-binding protein - NRBP1 -	Q9UHY1	60 kDa	0.0037	2.7	16407966.7	44028333.3
Vacuolar protein sorting-associated protein 26B - VPS26B -	Q4G0F5	39 kDa	0.027	2.7	10441900	27934666.7
Ubiquitin carboxyl-terminal hydrolase 47 - USP47 -	Q96K76	157 kDa	0.00095	2.6	14854333.3	37907666.7
FUN14 domain-containing protein 2 - FUNDC2 -	Q9BWH2	21 kDa	0.037	2.5	10092740	25087666.7
Syntaxin-4 - STX4 -	Q12846	34 kDa	0.033	2.4	4848833.33	11820766.7
CD166 antigen - ALCAM -	Q13740	65 kDa	0.012	2.4	27607333.3	66789000
F-box only protein 22 - FBXO22 -	Q8NEZ5	45 kDa	0.014	2.4	7585300	17885666.7
Cell cycle control protein 50A - TMEM30A -	Q9NV96	41 kDa	0.0018	2.3	3180766.67	7402100
Grancalcin - GCA -	P28676	24 kDa	0.036	2.3	15142000	34778000
1-phosphatidylinositol 4,5-bisphosphate phosphodiesterase beta-4 - PLCB4 -	Q15147	134 kDa	0.0026	2.3	10687933.3	24248000
RNA-binding protein 24 - RBM24 -	Q9BX46 (+1)	25 kDa	0.0058	2.3	13974333.3	31665000
Leucine-rich repeat-containing protein 1 - LRRC1	Q9BTT6	59 kDa	0.021	2.3	571086.667	1291366.67
Septin-5 - SEPT5 -	Q99719	43 kDa	0.044	2.2	22010333.3	49362666.7
Growth factor receptor-bound protein 10 - GRB10 -	Q13322	67 kDa	0.015	2.2	34252666.7	76641000
Rab3 GTPase-activating protein non-catalytic subunit - RAB3GAP2 -	Q9H2M9	156 kDa	0.0023	2.2	23899000	53359333.3
Zinc finger FYVE domain-containing protein 16 - ZFYVE16 -	Q7Z3T8	169 kDa	0.031	2.2	3375433.33	7425233.33
Deubiquitinating protein VCIP135 - VCPIP1 -	Q96JH7	134 kDa	0.014	2.2	2244100	4874566.67
Golgin subfamily A member 7 - GOLGA7 -	Q7Z5G4	16 kDa	0.029	2.2	1003813.33	2171066.67
Tetratricopeptide repeat protein 27 - TTC27 -	Q6P3X3	97 kDa	0.0032	2.1	984946.667	2101166.67
Nuclear receptor 2C2-associated protein - NR2C2AP -	Q86WQ0	16 kDa	0.0098	2.1	18481333.3	38990000
All-trans-retinol 13,14-reductase - RETSAT -	Q6NUM9	67 kDa	0.013	2.1	9322400	19400000
Conserved oligomeric Golgi complex subunit 5 - COG5 -	Q9UP83	93 kDa	0.049	2	4568366.67	9364800
Pentatricopeptide repeat domain-containing protein 3, mitochondrial - PTCD3 -	Q96EY7	79 kDa	0.027	2	11595233.3	23385000
WD repeat-containing protein 44 - WDR44 -	Q5JSH3	101 kDa	0.047	2	9840366.67	19547666.7
Interferon-induced transmembrane protein 3 - IFITM3 -	Q01628	15 kDa	0.039	2	5308833.33	10472800
AN1-type zinc finger protein 5 - ZFAND5 -	O76080	23 kDa	0.029	1.9	2853733.33	5532633.33
N-alpha-acetyltransferase 35, NatC auxiliary subunit - NAA35 -	Q5VZE5	84 kDa	0.015	1.9	5037566.67	9718033.33
Phospholipase D3 - PLD3 -	Q8IV08	55 kDa	0.039	1.9	15086666.7	28448333.3
Epsin-1 - EPN1 -	Q9Y6I3	60 kDa	0.022	1.9	25987666.7	48619333.3
Small nuclear ribonucleoprotein Sm D1 - SNRPD1 -	P62314	13 kDa	0.047	1.9	309953333	577190000

Protein RRP5 homolog - PDCD11 -	Q14690	209 kDa	0.03	1.9	63249666.7	117323333
Methionine aminopeptidase 2 - METAP2 -	P50579	53 kDa	0.023	1.9	65720666.7	121586667
Electron transfer flavoprotein-ubiquinone oxidoreductase, mitochondrial - ETFDH -	Q16134	68 kDa	0.034	1.8	55942000	102983333
Lysosomal Pro-X carboxypeptidase - PRCP -	P42785	56 kDa	0.044	1.8	21343000	39264666.7
Ubiquitin conjugation factor E4 A - UBE4A -	Q14139	123 kDa	0.0013	1.8	31617000	57719333.3
Signal transducer and activator of transcription 3 - STAT3 -	P40763	88 kDa	0.005	1.8	127090000	228426667
Signal transducing adapter molecule 1 - STAM -	Q92783	59 kDa	0.00043	1.8	13477666.7	24119333.3
UBX domain-containing protein 6 - UBXN6 -	Q9BZV1	50 kDa	0.03	1.8	39616666.7	70780666.7
NADH dehydrogenase [ubiquinone] iron-sulfur protein 4, mitochondrial - NDUFS4 -	O43181	20 kDa	0.029	1.8	10694966.7	19078000
Sialate O-acetylesterase - SIAE -	Q9HAT2	58 kDa	0.035	1.8	7562600	13478000
Rho GTPase-activating protein 5 - ARHGAP5 -	Q13017	172 kDa	0.0038	1.8	5642466.67	9965666.67
Hydroxymethylglutaryl-CoA synthase, cytoplasmic - HMGCS1 -	Q01581	57 kDa	0.02	1.8	17903333.3	31588666.7
LanC-like protein 2 - LANCL2 -	Q9NS86	51 kDa	0.032	1.8	6997733.33	12338333.3
Glutathione S-transferase A1 - GSTA1 -	P08263	26 kDa	0.019	1.8	54535333.3	96112666.7
Carbonyl reductase family member 4 - CBR4 -	Q8N4T8	25 kDa	0.032	1.8	13520966.7	23691333.3
Desmoglein-2 - DSG2 -	Q14126	122 kDa	0.032	1.7	123671000	215800000
Myotubularin-related protein 12 - MTMR12 -	Q9C0I1	86 kDa	0.018	1.7	8086933.33	14059333.3
Type I inositol 1,4,5-trisphosphate 5-phosphatase - INPP5A -	Q14642	48 kDa	0.0014	1.7	1240433.33	2130233.33
28S ribosomal protein S34, mitochondrial - MRPS34 -	P82930	26 kDa	0.036	1.7	8370833.33	14339666.7
Prolyl endopeptidase - PREP -	P48147	81 kDa	0.00098	1.7	86911666.7	148503333
N-acylethanolamine-hydrolyzing acid amidase - NAAA -	Q02083	40 kDa	0.0085	1.7	4935133.33	8356933.33
Histidine triad nucleotide-binding protein 3 - HINT3 -	Q9NQE9	20 kDa	0.045	1.7	12915333.3	21741000
MAP kinase-activated protein kinase 2 - MAPKAPK2 -	P49137	46 kDa	0.02	1.7	11482466.7	19311333.3
5-oxoprolinase - OPLAH -	O14841	137 kDa	0.00071	1.7	28312333.3	47448000
Histone H3.1 - HIST1H3A -	P68431	15 kDa	0.017	1.7	131866667	218893333
ADP-ribosylation factor GTPase-activating protein 2 - ARFGAP2 -	Q8N6H7	57 kDa	0.033	1.7	19226333.3	31914000
Neogenin - NEO1 -	Q92859	160 kDa	0.0069	1.6	640800	1044063.33
FYVE and coiled-coil domain-containing protein 1 - FYCO1 -	Q9BQS8	167 kDa	0.018	1.6	17018666.7	27707333.3
Golgi SNAP receptor complex member 1 - GOSR1 -	O95249	29 kDa	0.01	1.6	23311333.3	37616000
Protein FAM160B1 - FAM160B1 -	Q5W0V3	87 kDa	0.042	1.6	26881666.7	43170333.3
Nardilysin - NRDC -	O43847	132 kDa	0.0024	1.6	40890333.3	65132000
V-type proton ATPase subunit d 1 - ATP6V0D1 -	P61421	40 kDa	0.049	1.6	89861000	142870000
Protein phosphatase 1 regulatory subunit 12A - PPP1R12A -	O14974	115 kDa	0.031	1.6	126200000	199633333
Periodic tryptophan protein 1 homolog - PWP1 -	Q13610	56 kDa	0.021	1.6	43414000	68633000
Caldesmon - CALD1 -	Q05682	93 kDa	0.0006	1.6	258150000	406343333
Epiplakin - EPPK1 -	P58107	556 kDa	0.0084	1.6	435493333	681030000
P98196	P98196-DECOY	?	0.0062	1.6	30954333.3	48210000

Serine/threonine-protein phosphatase 4 regulatory subunit 1 - PPP4R1 -	Q8TF05	107 kDa	0.049	1.6	3398333.33	5268433.33
Actin-related protein 2/3 complex subunit 5-like protein - ARPC5L -	Q9BPX5	17 kDa	0.008	1.5	87973000	136033333
Deoxyhypusine hydroxylase - DOHH -	Q9BU89	33 kDa	0.0029	1.5	5761033.33	8789366.67
Vacuolar protein sorting-associated protein 4B - VPS4B -	O75351	49 kDa	0.025	1.5	69679666.7	106297333
Lysophospholipase-like protein 1 - LYPLAL1 -	Q5VWZ2	26 kDa	0.0079	1.5	123190000	187803333
ADP-ribose pyrophosphatase, mitochondrial - NUDT9 -	Q9BW91	39 kDa	0.033	1.5	20666000	31305666.7
60S ribosomal protein L26 - RPL26 -	P61254	17 kDa	0.012	1.5	341073333	513093333

*Table 12: Proteins identified with one peptide that are downregulated in the siRNA DHRS7 condition after 48 h timepoint with p-value >0.05. *depicted values correspond to the mean of ion precursor intensities with arbitrary unit. MW=Molecular weight*

Downregulated Proteins	Accession Number	MW	T-Test (p-value):	Fold Change	Mean scrambled siRNA	Mean siRNA DHRS7
U4/U6 small nuclear ribonucleoprotein Prp31 - PRPF31 -	Q8WWY3	55 kDa	0.00088	0.7	60339666.7	40210666.7
Myeloid-derived growth factor - MYDGF -	Q969H8	19 kDa	0.0056	0.7	132110000	87550666.7
Dynein assembly factor 5, axonemal - DNAAF5 -	Q86Y56	94 kDa	0.026	0.7	21366666.7	14145000
Hematological and neurological expressed 1-like protein - HN1L -	Q9H910	20 kDa	0.0014	0.7	372240000	246303333
Peptidyl-prolyl cis-trans isomerase FKBP5 - FKBP5 -	Q13451	51 kDa	0.038	0.7	134650000	88972666.7
4F2 cell-surface antigen heavy chain - SLC3A2 -	P08195	68 kDa	0.021	0.7	41083666.7	27144666.7
Bifunctional lysine-specific demethylase and histidyl-hydroxylase MINA - MINA -	Q8IUF8	53 kDa	0.00029	0.7	22610000	14917333.3
Biotinidase - BTD -	P43251	61 kDa	0.012	0.7	3711966.67	2440166.67
Transcriptional repressor p66-beta - GATAD2B -	Q8WXI9	65 kDa	0.035	0.7	15452666.7	10053266.7
Structural maintenance of chromosomes protein 3 - SMC3 -	Q9UQE7	142 kDa	0.047	0.6	211476667	137026667
Protein SON - SON -	P18583	264 kDa	0.012	0.6	122663333	79457000
Hepatoma-derived growth factor-related protein 3 - HDGFRP3 -	Q9Y3E1	23 kDa	0.021	0.6	56415000	36471666.7
Guanosine-3',5'-bis(diphosphate) 3'-pyrophosphohydrolase MESH1 - HDDC3 -	Q8N4P3	20 kDa	0.022	0.6	25911666.7	16704666.7
Nuclear RNA export factor 1 - NXF1 -	Q9UBU9	70 kDa	0.036	0.6	55533666.7	35749333.3
E3 ubiquitin-protein ligase TRIM33 - TRIM33 -	Q9UPN9	123 kDa	0.044	0.6	14755333.3	9479233.33
Deoxycytidine kinase - DCK -	P27707	31 kDa	0.045	0.6	17360666.7	11096833.3
Polyadenylate-binding protein 2 - PABPN1 -	Q86U42	33 kDa	0.03	0.6	117093333	74747666.7
Calcium-transporting ATPase type 2C member 1 - ATP2C1 -	P98194	101 kDa	0.049	0.6	24508666.7	15629666.7
RNA-binding protein FUS - FUS -	P35637	53 kDa	0.043	0.6	252200000	159700000
Serine/threonine-protein kinase PAK 4 - PAK4 -	O96013	64 kDa	0.0018	0.6	179703333	113723333
DCC-interacting protein 13-beta - APPL2 -	Q8NEU8	74 kDa	0.016	0.6	13670333.3	8626933.33
ER membrane protein complex subunit 8 - EMC8 -	O43402	24 kDa	0.024	0.6	28409000	17850333.3
Guanine nucleotide-binding protein G(I)/G(S)/G(T) subunit beta-1 - GNB1 -	P62873	37 kDa	0.0025	0.6	182073333	113323333
Flap endonuclease 1 - FEN1 -	P39748	43 kDa	0.019	0.6	232373333	143696667

Mitochondrial amidoxime-reducing component 1 - MARC1 -	Q5VT66	38 kDa	0.037	0.6	79733333.3	49165666.7
Protein O-GlcNAcase - MGEA5 -	O60502	103 kDa	0.0073	0.6	90049333.3	55215666.7
Protein kinase C and casein kinase substrate in neurons protein 2 - PACSIN2 -	Q9UNF0	56 kDa	0.018	0.6	155186667	94659666.7
Replication factor C subunit 4 - RFC4 -	P35249	40 kDa	0.015	0.6	70807666.7	43170333.3
Extended synaptotagmin-1 - ESYT1 -	Q9BSJ8	123 kDa	0.0016	0.6	113763333	68581333.3
Guanine nucleotide-binding protein-like 3-like protein - GNL3L -	Q9NVN8	66 kDa	0.032	0.6	22311000	13450000
Serine/threonine-protein kinase PRP4 homolog - PRPF4B -	Q13523	117 kDa	0.00073	0.6	27613666.7	16646333.3
Pleiotropic regulator 1 - PLRG1 -	O43660	57 kDa	0.028	0.6	94285000	56549666.7
Protein FAM177A1 - FAM177A1 -	Q8N128	24 kDa	0.04	0.6	9473666.67	5556700
Protein diaphanous homolog 1 - DIAPH1 -	O60610	141 kDa	0.029	0.6	95480333.3	55918333.3
Cadherin-1 - CDH1 -	P12830	97 kDa	0.0063	0.6	114000333	66414666.7
N(G),N(G)-dimethylarginine dimethylaminohydrolase 1 - DDAH1 -	O94760	31 kDa	0.005	0.6	242170000	140800000
Deoxyuridine 5'-triphosphate nucleotidohydrolase, mitochondrial - DUT -	P33316	27 kDa	0.0019	0.6	225040000	130250000
Helicase-like transcription factor - HLTF -	Q14527	114 kDa	0.034	0.6	32126333.3	18461000
Androgen receptor - AR -	P10275	99 kDa	0.025	0.6	15104333.3	8644300
Dihydrofolate reductase - DHFR -	P00374	21 kDa	0.015	0.6	130416667	74368333.3
UDP-glucuronosyltransferase 2B17 - UGT2B17 -	O75795	61 kDa	0.0014	0.6	254520000	145053333
Src substrate cortactin - CTTN -	Q14247	62 kDa	0.0025	0.6	561090000	318900000
Ribonuclease H2 subunit B - RNASEH2B -	Q5TBB1	35 kDa	0.034	0.6	13147666.7	7453266.67
Cohesin subunit SA-2 - STAG2 -	Q8N3U4	141 kDa	0.031	0.6	62415333.3	35321000
Pre-mRNA-splicing factor 38B - PRPF38B -	Q5VTL8	64 kDa	0.032	0.6	17867666.7	10084366.7
Methyl-CpG-binding domain protein 3 - MBD3 -	O95983	33 kDa	0.023	0.6	19287333.3	10842366.7
Spermatogenesis-defective protein 39 homolog - VIPAS39 -	Q9H9C1	57 kDa	0.015	0.6	7495100	4193866.67
Mediator of DNA damage checkpoint protein 1 - MDC1 -	Q14676	227 kDa	0.023	0.6	51302333.3	28676666.7
Importin subunit alpha-1 - KPNA2 -	P52292	58 kDa	0.029	0.6	198726667	110908667
Catenin alpha-1 - CTNNA1 -	P35221	100 kDa	0.00015	0.6	1024306667	571203333
RNA-binding protein 47 - RBM47 -	A0AV96	64 kDa	0.028	0.5	74103666.7	40556000
Translocon-associated protein subunit alpha - SSR1	P43307	32 kDa	0.039	0.5	14410666.7	7840733.33
Serine/threonine-protein kinase MARK2 - MARK2 -	Q7KZI7	88 kDa	0.024	0.5	28894666.7	15622866.7
Acidic leucine-rich nuclear phosphoprotein 32 family member E - ANP32E -	Q9BTT0	31 kDa	0.0037	0.5	14957333.3	8031733.33
U2 snRNP-associated SURP motif-containing protein - U2SURP -	O15042	118 kDa	0.0045	0.5	92935000	49813666.7
Alpha-adducin - ADD1 -	P35611	81 kDa	0.024	0.5	27185000	14544900
DNA replication licensing factor MCM6 - MCM6 -	Q14566	93 kDa	0.0036	0.5	316050000	168463333
Heterogeneous nuclear ribonucleoprotein L-like - HNRNPLL -	Q8WVV9	60 kDa	0.032	0.5	50788333.3	26756333.3
Specifically androgen-regulated gene protein - SARG -	Q9BW04	64 kDa	0.022	0.5	280360000	147250000
Replication factor C subunit 2 - RFC2 -	P35250	39 kDa	0.0014	0.5	44585000	23255333.3
Sorting nexin-6 - SNX6 -	Q9UNH7	47 kDa	0.041	0.5	70926000	36871333.3
Leucine-rich repeat flightless-interacting protein 2 - LRRFIP2 -	Q9Y608	82 kDa	0.00031	0.5	27315000	14043333.3

BRI3-binding protein - BRI3BP -	Q8WY22	28 kDa	0.025	0.5	992646.667	503780
Epithelial splicing regulatory protein 1 - ESRP1 -	Q6NXG1	76 kDa	0.019	0.5	27299666.7	13854166.7
DNA replication licensing factor MCM5 - MCM5 -	P33992	82 kDa	0.00016	0.5	310466667	155763333
Prostatic acid phosphatase - ACPP -	P15309	45 kDa	0.01	0.5	50344666.7	25106333.3
Exosome component 10 - EXOSC10 -	Q01780	101 kDa	0.044	0.5	22266000	11036100
Protein flightless-1 homolog - FLII -	Q13045	145 kDa	0.0016	0.5	144420000	71350333.3
Protein NEDD1 - NEDD1 -	Q8NHV4	72 kDa	0.04	0.5	1455066.67	717840
Cyclin-dependent kinase 1 - CDK1 -	P06493	34 kDa	0.00088	0.5	251590000	123930000
Intron-binding protein aquarius - AQR -	O60306	171 kDa	0.03	0.5	37951333.3	18669333.3
Ubiquitin-associated protein 2 - UBAP2 -	Q5T6F2	117 kDa	0.019	0.5	22931000	11196600
Peptidylprolyl isomerase domain and WD repeat-containing protein 1 - PPWD1 -	Q96BP3	74 kDa	0.02	0.5	12883666.7	6264400
DNA topoisomerase 2-alpha - TOP2A -	P11388	174 kDa	0.018	0.5	76214000	36937333.3
Ubiquitin-conjugating enzyme E2 S - UBE2S -	Q16763	24 kDa	0.006	0.5	14214333.3	6843800
DNA polymerase alpha subunit B - POLA2 -	Q14181	66 kDa	0.013	0.5	9046766.67	4331266.67
Ladinin-1 - LAD1 -	O00515	57 kDa	0.0077	0.5	96205000	45984666.7
UPF0696 protein C11orf68 - C11orf68 -	Q9H3H3	27 kDa	0.035	0.5	11136266.7	5304866.67
DNA replication licensing factor MCM7 - MCM7 -	P33993	81 kDa	0.01	0.5	313270000	149110000
Cell division cycle protein 27 homolog - CDC27 -	P30260	92 kDa	0.012	0.5	9641500	4540400
DNA replication licensing factor MCM4 - MCM4 -	P33991	97 kDa	0.0027	0.5	320810000	150700000
Multiple myeloma tumor-associated protein 2 - MMTAG2 -	Q9BU76	29 kDa	0.035	0.5	4242100	1983000
Vacuolar protein sorting-associated protein 41 homolog - VPS41 -	P49754	99 kDa	0.048	0.5	6763766.67	3142200
FK506-binding protein 15 - FKBP15 -	Q5T1M5	134 kDa	0.011	0.5	12332000	5698400
cAMP-dependent protein kinase type I-alpha regulatory subunit - PRKAR1A -	P10644	43 kDa	0.0097	0.5	88999000	40927333.3
Transcription elongation factor A protein 1 - TCEA1	P23193	34 kDa	0.017	0.5	127013667	58220000
DnaJ homolog subfamily C member 9 - DNAJC9 -	Q8WXX5	30 kDa	0.049	0.5	32429666.7	14735433.3
SLC35A4 upstream open reading frame protein - SLC35A4 -	L0R6Q1	11 kDa	0.012	0.5	18572000	8383266.67
Atlastin-2 - ATL2 -	Q8NHH9	66 kDa	0.0079	0.5	14596000	6587466.67
AP2-associated protein kinase 1 - AAK1 -	Q2M2I8	104 kDa	0.0014	0.5	47178666.7	21255333.3
Cysteine-rich with EGF-like domain protein 2 - CRELD2 -	Q6UXH1	38 kDa	0.022	0.4	23810333.3	10658266.7
SWI/SNF complex subunit SMARCC1 - SMARCC1 -	Q92922	123 kDa	0.0036	0.4	121870000	53397333.3
Malectin - MLEC -	Q14165	32 kDa	0.0081	0.4	83075666.7	35951000
DNA replication licensing factor MCM3 - MCM3 -	P25205	91 kDa	0.0024	0.4	359126667	155023333
Glycylpeptide N-tetradecanoyltransferase 1 - NMT1	P30419	57 kDa	0.047	0.4	8332066.67	3570966.67
T-box transcription factor TBX3 - TBX3 -	O15119	79 kDa	0.045	0.4	12850366.7	5489833.33
Exosome complex component RRP45 - EXOSC9 -	Q06265	49 kDa	0.019	0.4	16237333.3	6861400
RING1 and YY1-binding protein - RYBP -	Q8N488	25 kDa	0.046	0.4	2545533.33	1072473.33
Nucleoside diphosphate-linked moiety X motif 19 - NUDT19 -	A8MXV4	42 kDa	0.0041	0.4	63818333.3	26728000
Adhesion G-protein coupled receptor G6 - ADGRG6	Q86SQ4	137 kDa	0.00079	0.4	24761333.3	10247433.3
Thymidine kinase, cytosolic - TK1 -	P04183	25 kDa	0.021	0.4	30389666.7	12562166.7
Serine/threonine-protein kinase VRK1 - VRK1 -	Q99986	45 kDa	0.0055	0.4	36439333.3	14997066.7
Condensin complex subunit 1 - NCAPD2 -	Q15021	157 kDa	0.016	0.4	36208333.3	14867333.3
Putative oxidoreductase GLYR1 - GLYR1 -	Q49A26	61 kDa	0.0017	0.4	38934333.3	15930666.7
Structural maintenance of chromosomes protein 2 - SMC2 -	O95347	136 kDa	0.0046	0.4	44526000	18206333.3

Bleomycin hydrolase - BLMH -	Q13867	53 kDa	0.016	0.4	140853333	57379333.3
Putative RNA-binding protein 15 - RBM15 -	Q96T37	107 kDa	0.00057	0.4	11558333.3	4675333.33
Protein FAM83H - FAM83H -	Q6ZRV2	127 kDa	0.038	0.4	7462933.33	2994433.33
Condensin complex subunit 2 - NCAPH -	Q15003	83 kDa	0.0041	0.4	17202333.3	6873833.33
DNA replication complex GINS protein PSF2 - GINS2	Q9Y248	21 kDa	0.046	0.4	3631400	1433533.33
Rho GTPase-activating protein 1 - ARHGAP1 -	Q07960	50 kDa	0.0045	0.4	43910000	17300666.7
Lysine-specific demethylase 3B - KDM3B -	Q7LBC6	192 kDa	0.046	0.4	6426433.33	2494966.67
Target of EGR1 protein 1 - TOE1 -	Q96GM8	57 kDa	0.035	0.4	1726333.33	664213.333
Trinucleotide repeat-containing gene 6B protein - TNRC6B -	Q9UPQ9	194 kDa	0.024	0.4	11080100	4240933.33
Zinc finger protein 24 - ZNF24 -	P17028	42 kDa	0.018	0.4	18022000	6877000
Leucine-rich repeat flightless-interacting protein 1 - LRRFIP1 -	Q32MZ4	89 kDa	0.00028	0.4	293090000	111086667
Adenosine deaminase - ADA -	P00813	41 kDa	0.011	0.4	24764000	9244433.33
Splicing factor 45 - RBM17 -	Q96I25	45 kDa	0.00017	0.4	70570666.7	25946666.7
Ubiquitin thioesterase OTU1 - YOD1 -	Q5VVQ6	38 kDa	0.0017	0.4	6262400	2297133.33
Crooked neck-like protein 1 - CRNKL1 -	Q9BZJ0	100 kDa	0.02	0.4	6093133.33	2218666.67
Short coiled-coil protein - SCOC -	Q9UIL1	18 kDa	0.0037	0.4	45145000	16360666.7
Cleavage and polyadenylation specificity factor subunit 1 - CPSF1 -	Q10570	161 kDa	0.042	0.4	11132033.3	3929133.33
DNA replication licensing factor MCM2 - MCM2 -	P49736	102 kDa	0.0047	0.3	250166667	87104000
Peroxisomal trans-2-enoyl-CoA reductase - PECR -	Q9BY49	33 kDa	0.041	0.3	5610166.67	1940200
Myelin basic protein - MBP -	P02686	33 kDa	0.019	0.3	13263666.7	4525833.33
DnaJ homolog subfamily C member 3 - DNAJC3 -	Q13217	58 kDa	0.026	0.3	18292000	6123166.67
Choline-phosphate cytidylyltransferase A - PCYT1A -	P49585	42 kDa	0.019	0.3	41143333.3	13565933.3
Zinc finger MYM-type protein 2 - ZMYM2 -	Q9UBW7	155 kDa	0.0065	0.3	5117400	1679133.33
Fibronectin - FN1 -	P02751	263 kDa	0.023	0.3	31833333.3	10212300
Actin-related protein 2/3 complex subunit 5 - ARPC5 -	O15511	16 kDa	0.00069	0.3	63042666.7	20153666.7
U3 small nucleolar ribonucleoprotein protein IMP4 - IMP4 -	Q96G21	34 kDa	0.049	0.3	8674400	2729700
Replication factor C subunit 1 - RFC1 -	P35251	128 kDa	0.021	0.3	10986400	3446226.67
DNA polymerase delta subunit 3 - POLD3 -	Q15054	51 kDa	0.0029	0.3	4851666.67	1509863.33
RAC-alpha serine/threonine-protein kinase - AKT1 -	P31749	56 kDa	0.0014	0.3	22954333.3	7135933.33
Transcription initiation factor TFIID subunit 7 - TAF7	Q15545	40 kDa	0.041	0.3	10568766.7	3276000
Ribonucleoside-diphosphate reductase subunit M2 - RRM2 -	P31350	45 kDa	0.0084	0.3	78819000	24406000
Guanine nucleotide-binding protein G(I)/G(S)/G(O) subunit gamma-12 - GNG12 -	Q9UBI6	8 kDa	0.025	0.3	7529666.67	2280966.67
Anterior gradient protein 2 homolog - AGR2 -	O95994	20 kDa	0.014	0.3	25477000	7714833.33
Protein virilizer homolog - KIAA1429 -	Q69YN4	202 kDa	0.012	0.3	2722833.33	818333.333
E3 ubiquitin-protein ligase ZNF598 - ZNF598 -	Q86UK7	99 kDa	0.017	0.3	21456666.7	6362233.33
Ubiquitin conjugation factor E4 B - UBE4B -	O95155	146 kDa	0.004	0.3	8614833.33	2550126.67
Cyclin-dependent kinases regulatory subunit 2 - CKS2 -	P33552	10 kDa	0.0033	0.3	61038333.3	17919000
Calpain-2 catalytic subunit - APN2 - SV=6	P17655	80 kDa	0.035	0.3	8358566.67	2394166.67
Ubiquitin-conjugating enzyme E2 T - UBE2T -	Q9NPD8	23 kDa	0.0056	0.3	21736000	6128533.33
WD repeat and HMG-box DNA-binding protein 1 - WDHD1 -	O75717	126 kDa	0.0071	0.3	23886666.7	6722830
TRPM8 channel-associated factor 1 - TCAF1 -	Q9Y4C2	102 kDa	0.043	0.3	6704733.33	1880310

Phosphatidylinositol 4,5-bisphosphate 3-kinase catalytic subunit delta isoform - PIK3CD -	O00329	119 kDa	0.04	0.3	7713800	2153146.67
Proline-rich protein PRCC - PRCC -	Q92733	52 kDa	0.00086	0.3	28373333.3	7676400
Complex I assembly factor TMEM126B, mitochondrial - TMEM126B -	Q8IUX1	26 kDa	< 0.00010	0.3	5279766.67	1425500
Histone PARylation factor 1 - HPF1 -	Q9NWY4	39 kDa	0.018	0.3	13968000	3764266.67
Kinesin-like protein KIF2C - KIF2C -	Q99661	81 kDa	0.038	0.3	2893066.67	765963.333
Ribosomal RNA processing protein 1 homolog B - RRP1B -	Q14684	84 kDa	0.002	0.3	10580000	2754833.33
Polyhomeotic-like protein 3 - PHC3 -	Q8NDX5	106 kDa	0.017	0.3	3763466.67	971473.333
Calcium/calmodulin-dependent protein kinase type 1 - CAMK1 -	Q14012	41 kDa	0.032	0.3	19511000	5030866.67
GA-binding protein alpha chain - GABPA -	Q06546	51 kDa	0.016	0.3	6824333.33	1751523.33
Tetratricopeptide repeat protein 19, mitochondrial - TTC19 -	Q6DKK2	42 kDa	0.018	0.3	15246666.7	3825033.33
Charged multivesicular body protein 1b - CHMP1B -	Q7LBR1	22 kDa	0.01	0.3	15579000	3905733.33
Sperm-specific antigen 2 - SSFA2 -	P28290	138 kDa	0.0066	0.2	28975333.3	7065933.33
General transcription factor 3C polypeptide 5 - GTF3C5 -	Q9Y5Q8	60 kDa	0.039	0.2	10761300	2516400
Lysophosphatidylcholine acyltransferase 1 - LPCAT1	Q8NF37	59 kDa	0.0056	0.2	4242533.33	989863.333
RalA-binding protein 1 - RALBP1 -	Q15311	76 kDa	0.019	0.2	8058700	1864100
Mitogen-activated protein kinase kinase kinase 7 - MAP3K7 -	O43318	67 kDa	0.03	0.2	1491933.33	339866.667
PHD finger protein 23 - PHF23 -	Q9BUL5	44 kDa	0.049	0.2	391750	88630
Chromosome transmission fidelity protein 18 homolog - CHTF18 -	Q8WVB6	107 kDa	0.039	0.2	3861366.67	855066.667
Integrator complex subunit 7 - INTS7 -	Q9NVH2	107 kDa	0.0076	0.2	5386066.67	1172533.33
Upstream-binding protein 1 - UBP1 -	Q9NZI7	60 kDa	< 0.00010	0.2	11561666.7	2471600
Golgin subfamily A member 1 - GOLGA1 -	Q92805	88 kDa	0.0077	0.2	15690000	3257673.33
Protein FAM3C - FAM3C -	Q92520	25 kDa	0.045	0.2	21694666.7	4447766.67
Multiple C2 and transmembrane domain-containing protein 2 - MCTP2 -	Q6DN12	100 kDa	0.045	0.2	1471100	300896.667
Spondin-2 - SPON2 -	Q9BUD6	36 kDa	0.0058	0.2	39396666.7	8029333.33
Protein FAM91A1 - FAM91A1 -	Q658Y4	94 kDa	0.023	0.2	15332000	3086156.67
Exosome complex component RRP43 - EXOSC8 -	Q96B26	30 kDa	0.049	0.2	20437666.7	4095466.67
Retinoblastoma-associated protein - RB1 -	P06400	106 kDa	0.004	0.2	9034666.67	1773333.33
Glutathione S-transferase theta-2 - GSTT2 -	P0CG29 (+1)	28 kDa	0.021	0.2	5644866.67	1107800
MKL/myocardin-like protein 2 - MKL2 -	Q9ULH7	118 kDa	0.0055	0.2	22776000	4356666.67
Chromatin assembly factor 1 subunit A - CHAF1A -	Q13111	107 kDa	0.023	0.2	12338733.3	2239566.67
Dehydrogenase/reductase SDR family member 7 - DHRS7 -	Q9Y394	38 kDa	0.00047	0.2	305790000	53371333.3
Gamma-tubulin complex component 3 - TUBGCP3 -	Q96CW5	104 kDa	0.024	0.2	1928700	320726.667
Serine/threonine-protein kinase PLK1 - PLK1 -	P53350	68 kDa	0.012	0.2	3583100	565766.667
Charged multivesicular body protein 7 - CHMP7 -	Q8WUX9	51 kDa	0.016	0.2	4817166.67	756566.667
Leucine-rich repeat-containing protein 57 - LRRC57 -	Q8N9N7	27 kDa	0.031	0.2	3175300	495700
Inactive ubiquitin carboxyl-terminal hydrolase 54 - USP54 -	Q70EL1	187 kDa	0.00054	0.2	16648333.3	2539433.33
Serine/threonine-protein phosphatase 6 regulatory subunit 1 - PPP6R1 -	Q9UPN7	97 kDa	0.048	0.2	6080766.67	920233.333

Enoyl-[acyl-carrier-protein] reductase, mitochondrial - MECR -	Q9BV79	40 kDa	0.034	0.1	25541000	3791000
A-kinase anchor protein 9 - AKAP9 -	Q99996	454 kDa	0.033	0.1	9843800	1444354.67
DNA polymerase delta catalytic subunit - POLD1 -	P28340	124 kDa	0.00072	0.1	11175366.7	1554533.33
Ribonuclease H2 subunit A - RNASEH2A -	O75792	33 kDa	0.033	0.1	4257966.67	564733.333
Thymidylate synthase - TYMS -	P04818	36 kDa	0.0094	0.1	9390800	1227833.33
Rhophilin-2 - RHPN2 -	Q8IUC4	77 kDa	0.036	0.1	1127416.67	144290
Testin - TES -	Q9UGI8	48 kDa	0.0036	0.1	49970333.3	6151400
MICAL-like protein 1 - MICALL1 -	Q8N3F8	93 kDa	0.0014	0.1	3130633.33	379370
CTD small phosphatase-like protein 2 - CTDSPL2 -	Q05D32	53 kDa	0.029	0.1	1544466.67	182783.333
Telomere-associated protein RIF1 - RIF1 -	Q5UIP0	274 kDa	0.0049	0.1	3102100	342863.333
Lymphokine-activated killer T-cell-originated protein kinase - PBK -	Q96KB5	36 kDa	0.0004	0.1	82287333.3	8991266.67
Replication factor C subunit 3 - RFC3 -	P40938	41 kDa	0.014	0.1	14326333.3	1508123.33
Huntingtin-interacting protein 1 - HIP1 -	O00291	116 kDa	0.018	0.09	4580833.33	410300
Anaphase-promoting complex subunit 7 - ANAPC7 -	Q9UJX3	67 kDa	0.014	0.09	14540466.7	1274900
Kinetochore protein Spc24 - SPC24 -	Q8NBT2	22 kDa	0.011	0.08	38930666.7	3185366.67
Zinc finger protein 281 - ZNF281 -	Q9Y2X9	97 kDa	0.0031	0.07	123798.333	8795
InaD-like protein - PATJ -	Q8NI35	196 kDa	0.0066	0.07	10458233.3	742066.667
E3 ubiquitin-protein ligase DTX3L - DTX3L -	Q8TDB6	84 kDa	0.037	0.07	9415500	649233.333
Protein NipSnap homolog 3A - NIPSNAP3A -	Q9UFN0	28 kDa	0.025	0.07	8498333.33	582533.333
Pseudouridylate synthase 7 homolog - PUS7 -	Q96PZ0	75 kDa	0.0024	0.07	30642333.3	2085766.67
ATPase family AAA domain-containing protein 2 - ATAD2 -	Q6PL18	159 kDa	0.00056	0.06	15407000	990733.333
Polycomb protein EED - EED -	O75530	50 kDa	0.032	0.06	8449333.33	506600
Charged multivesicular body protein 4a - CHMP4A -	Q9BY43	25 kDa	0.024	0.05	6981633.33	361400
Interferon regulatory factor 6 - IRF6 -	O14896	53 kDa	0.021	0.05	20022333.3	905266.667
Targeting protein for Xklp2 - TPX2 -	Q9ULW0	86 kDa	0.0046	0.04	8129233.33	345533.333
DNA ligase 1 - LIG1 -	P18858	102 kDa	0.012	0.04	2640300	111516.667
Zinc finger CCCH-type antiviral protein 1-like - ZC3HAV1L -	Q96H79	33 kDa	0.0014	0.03	5629566.67	141623.333
Ubiquitin-conjugating enzyme E2 R2 - UBE2R2 -	Q712K3	27 kDa	0.0021	0.02	14198666.7	284083.333
Kinetochore protein NDC80 homolog - NDC80 -	O14777	74 kDa	0.012	0.02	7338566.67	132932.333

9.1.1.5 Regulated proteins after DHRS7 depletion Following Time-dependent DHRS7 Silencing

Table 13: Proteins identified with three peptides regulated after 24 h timepoint for a time-dependent DHRS7 downregulation with a fold change of ≥ 1.5 fold (upregulation), or ≤ 0.666 (downregulation) and p-value >0.05.

Proteins changed after 24 h		
Common name	**Regulation**	**Fold change**
Chondroitin sulfate synthase 2 - CHPF -	upregulated	9.49
Sorbin and SH3 domain-containing protein 1 - SORBS1 -	upregulated	6.16
Motile sperm domain-containing protein 2 - MOSPD2 -	upregulated	5.03
Probable RNA-binding protein 23 - RBM23 -	upregulated	4.74
Putative Polycomb group protein ASXL1 - ASXL1 -	upregulated	4.14
CON__ENSEMBL:ENSBTAP00000007350	upregulated	3.72
Store-operated calcium entry-associated regulatory factor - SARAF -	upregulated	3.39
Monoacylglycerol lipase ABHD2 - ABHD2 -	upregulated	3.31
Leucine-rich repeat neuronal protein 1 - LRRN1 -	upregulated	3.20
Testis-expressed protein 2 - TEX2 -	upregulated	3.09
Paternally-expressed gene 3 protein - PEG3 -	upregulated	3.08
Golgi apparatus membrane protein TVP23 homolog B - TVP23B -	upregulated	3.01
Zinc finger CCHC domain-containing protein 3 - ZCCHC3 -	upregulated	3.00
Adenomatous polyposis coli protein - APC -	upregulated	2.80
CON__P15497	upregulated	2.80
CON__Q2TBQ1	upregulated	2.76
CON__Q3SZ57	upregulated	2.70
Methylosome subunit pICln - CLNS1A -	upregulated	2.61
SLIT and NTRK-like protein 3 - SLITRK3 -	upregulated	2.58
Coiled-coil domain-containing protein 93 - CCDC93 -	upregulated	2.54
CON__Q3SZH5	upregulated	2.40
Glutathione S-transferase A2 - GSTA2 - SV=4	upregulated	2.38
Endoribonuclease Dicer - DICER1 -	upregulated	2.24
Very-long-chain (3R)-3-hydroxyacyl-CoA dehydratase 3 - HACD3 -	upregulated	2.24
Forkhead box protein J2 - FOXJ2 -	upregulated	2.21
CON__Q95121	upregulated	2.14
CON__ENSEMBL:ENSBTAP00000016046	upregulated	2.14
Prolyl endopeptidase-like - PREPL -	upregulated	2.11
ATPase family AAA domain-containing protein 1 - ATAD1 -	upregulated	2.11
Protein FAM177A1 - FAM177A1 -	upregulated	2.10
Cytochrome c oxidase subunit 5B, mitochondrial - COX5B -	upregulated	2.01
Rho GTPase-activating protein 19 - ARHGAP19 -	upregulated	1.99
Sortilin - SORT1 -	upregulated	1.98
Glutamyl-tRNA(Gln) amidotransferase subunit A, mitochondrial - QRSL1 -	upregulated	1.97
Choline dehydrogenase, mitochondrial - CHDH -	upregulated	1.97
Protein YIPF3 - YIPF3 -	upregulated	1.96
NADH dehydrogenase [ubiquinone] 1 beta subcomplex subunit 10 - NDUFB10 -	upregulated	1.93
Xyloside xylosyltransferase 1 - XXYLT1 -	upregulated	1.91
CON__Q3ZBS7	upregulated	1.80
C-Maf-inducing protein - CMIP -	upregulated	1.74
Mortality factor 4-like protein 2 - MORF4L2 -	upregulated	1.68
FAST kinase domain-containing protein 5, mitochondrial - FASTKD5 -	upregulated	1.66
N-alpha-acetyltransferase 30 - NAA30 -	upregulated	1.66
CON__ENSEMBL:ENSBTAP00000024146	upregulated	1.65
Caldesmon - CALD1 -	upregulated	1.63

Polymerase delta-interacting protein 2 - POLDIP2 -	upregulated	1.57
WD repeat-containing protein 82 - WDR82 -	downregulated	0.62
Disintegrin and metalloproteinase domain-containing protein 10 - ADAM10 -	downregulated	0.57
Mitofusin-2 - MFN2 -	downregulated	0.57
Nuclear factor NF-kappa-B p100 subunit - NFKB2 - SV=4	downregulated	0.57
InaD-like protein - PATJ -	downregulated	0.56
Transcription initiation factor TFIID subunit 7 - TAF7 -	downregulated	0.56
Nucleolar complex protein 3 homolog - NOC3L -	downregulated	0.54
Probable helicase senataxin - SETX - SV=4	downregulated	0.51
AF4/FMR2 family member 4 - AFF4 -	downregulated	0.50
Protein 4.1 - EPB41 - SV=4	downregulated	0.50
RalA-binding protein 1 - RALBP1 -	downregulated	0.50
Rhophilin-2 - RHPN2 -	downregulated	0.50
Histone H1x - H1FX -	downregulated	0.49
Peroxisomal NADH pyrophosphatase NUDT12 - NUDT12 -	downregulated	0.49
Cadherin-1 - CDH1 -	downregulated	0.49
Cytokine receptor-like factor 3 - CRLF3 -	downregulated	0.48
Serine/threonine-protein kinase Chk1 - CHEK1 -	downregulated	0.47
Solute carrier family 2, facilitated glucose transporter member 1 - SLC2A1 -	downregulated	0.47
Dehydrogenase/reductase SDR family member 7 - DHRS7 -	downregulated	0.46
Keratin, type I cytoskeletal 9 - KRT9 -	downregulated	0.46
TATA element modulatory factor - TMF1 -	downregulated	0.45
Occludin - OCLN -	downregulated	0.42
Ceramide synthase 4 - CERS4 -	downregulated	0.36
UPF0415 protein C7orf25 - C7orf25 -	downregulated	0.36
MAP kinase-activating death domain protein - MADD -	downregulated	0.35
Molybdenum cofactor sulfurase - MOCOS -	downregulated	0.35
Little elongation complex subunit 2 - ICE2 -	downregulated	0.35
DCC-interacting protein 13-beta - APPL2 -	downregulated	0.34
Spondin-2 - SPON2 -	downregulated	0.33
Mortality factor 4-like protein 1 - MORF4L1 -	downregulated	0.33
Ubiquitin-conjugating enzyme E2 Q1 - UBE2Q1 -	downregulated	0.33
Probable JmjC domain-containing histone demethylation protein 2C - JMJD1C -	downregulated	0.32
Condensin-2 complex subunit H2 - NCAPH2 -	downregulated	0.32
FAS-associated death domain protein - FADD -	downregulated	0.31
Metallothionein-1X - MT1X -	downregulated	0.30
Tripartite motif-containing protein 5 - TRIM5 -	downregulated	0.28
Zinc finger protein 460 - ZNF460 -	downregulated	0.27
Serum response factor-binding protein 1 - SRFBP1 -	downregulated	0.23
MAX gene-associated protein - MGA -	downregulated	0.21
Mediator of RNA polymerase II transcription subunit 23 - MED23 -	downregulated	0.20
Sentrin-specific protease 8 - SENP8 -	downregulated	0.19
Small G protein signaling modulator 3 - SGSM3 -	downregulated	0.18
Tumor protein p63-regulated gene 1-like protein - TPRG1L -	downregulated	0.14
Anillin - ANLN -	downregulated	0.12

Table 14: Proteins identified with three peptides regulated after 48 h timepoint for a time-dependent DHRS7 downregulation with a fold change of ≥ 1.5 fold (upregulation), or ≤ 0.666 (downregulation) and p-value >0.05.

Common name	Regulation	Fold change
Transmembrane protein 168 - TMEM168 -	upregulated	7.69
Keratin, type I cytoskeletal 9 - KRT9 -	upregulated	6.25
WD and tetratricopeptide repeats protein 1 - WDTC1 -	upregulated	5.56
Bone morphogenetic protein receptor type-2 - BMPR2 -	upregulated	5.00
Transmembrane channel-like protein 4 - TMC4 -	upregulated	4.76
Palmitoyltransferase ZDHHC5 - ZDHHC5 -	upregulated	4.76
Phosphotriesterase-related protein - PTER -	upregulated	4.17
Kinase D-interacting substrate of 220 kDa - KIDINS220 -	upregulated	4.17
Alpha- and gamma-adaptin-binding protein p34 - AAGAB -	upregulated	4.00
3-ketodihydrosphingosine reductase - KDSR -	upregulated	3.85
Nesprin-1 - SYNE1 -	upregulated	3.85
Golgi pH regulator A - GPR89A -	upregulated	3.70
Monoacylglycerol lipase ABHD2 - ABHD2 -	upregulated	3.45
Zinc transporter 1 - SLC30A1 -	upregulated	3.23
Sialidase-1 - NEU1 -	upregulated	3.03
Acyl-CoA synthetase family member 2, mitochondrial - ACSF2 -	upregulated	3.03
Translation initiation factor IF-2, mitochondrial - MTIF2 -	upregulated	2.94
40S ribosomal protein S14 - RPS14 -	upregulated	2.78
Rab GTPase-activating protein 1-like, isoform 10 - RABGAP1L -	upregulated	2.70
Integrin beta-5 - ITGB5 -	upregulated	2.70
Squalene monooxygenase - SQLE -	upregulated	2.63
5'-nucleotidase domain-containing protein 3 - NT5DC3 -	upregulated	2.63
UPF0538 protein C2orf76 - C2orf76 -	upregulated	2.63
Zinc finger and SCAN domain-containing protein 18 - ZSCAN18 -	upregulated	2.63
Sodium bicarbonate cotransporter 3 - SLC4A7 -	upregulated	2.63
Choline dehydrogenase, mitochondrial - CHDH -	upregulated	2.56
Pleckstrin homology domain-containing family H member 3 - PLEKHH3 -	upregulated	2.56
Probable Xaa-Pro aminopeptidase 3 - XPNPEP3 -	upregulated	2.44
Golgi integral membrane protein 4 - GOLIM4 -	upregulated	2.44
Aprataxin - APTX -	upregulated	2.44
Testis-specific Y-encoded-like protein 1 - TSPYL1 -	upregulated	2.38
Methylcrotonoyl-CoA carboxylase subunit alpha, mitochondrial - MCCC1 -	upregulated	2.38
Fatty acyl-CoA reductase 1 - FAR1 -	upregulated	2.33
RNA-binding E3 ubiquitin-protein ligase MEX3C - MEX3C -	upregulated	2.27
Probable ATP-dependent RNA helicase DDX49 - DDX49 -	upregulated	2.27
Peroxisomal carnitine O-octanoyltransferase - CROT -	upregulated	2.22
Succinate-semialdehyde dehydrogenase, mitochondrial - ALDH5A1 -	upregulated	2.22
Mitochondrial peptide methionine sulfoxide reductase - MSRA -	upregulated	2.17
Probable ATP-dependent RNA helicase DDX28 - DDX28 -	upregulated	2.17
Probable proline--tRNA ligase, mitochondrial - PARS2 -	upregulated	2.17
Acid sphingomyelinase-like phosphodiesterase 3a - SMPDL3A -	upregulated	2.17
Methyl-CpG-binding protein 2 - MECP2 -	upregulated	2.17
N-acetylgalactosamine-6-sulfatase - GALNS -	upregulated	2.13
Cilia- and flagella-associated protein 20 - CFAP20 -	upregulated	2.13
D-2-hydroxyglutarate dehydrogenase, mitochondrial - D2HGDH -	upregulated	2.13
Ral GTPase-activating protein subunit alpha-2 - RALGAPA2 -	upregulated	2.04

Charged multivesicular body protein 2b - CHMP2B -	upregulated	2.00
Peptide deformylase, mitochondrial - PDF -	upregulated	2.00
Methylmalonyl-CoA mutase, mitochondrial - MUT -	upregulated	2.00
Ectonucleotide pyrophosphatase/phosphodiesterase family member 5 - ENPP5 -	upregulated	2.00
BAG family molecular chaperone regulator 1 - BAG1 -	upregulated	1.96
Peroxisomal membrane protein PEX14 - PEX14 -	upregulated	1.96
Zinc fingers and homeoboxes protein 1 - ZHX1 -	upregulated	1.92
Round spermatid basic protein 1 - RSBN1 -	upregulated	1.92
Protein prenyltransferase alpha subunit repeat-containing protein 1 - PTAR1 -	upregulated	1.92
Transcription termination factor 4, mitochondrial - MTERF4 -	upregulated	1.89
Autophagy protein 5 - ATG5 -	upregulated	1.89
Delta-aminolevulinic acid dehydratase - ALAD -	upregulated	1.89
Endoplasmic reticulum resident protein 44 - ERP44 -	upregulated	1.85
Neurochondrin - NCDN -	upregulated	1.85
ATP-binding cassette sub-family B member 7, mitochondrial - ABCB7 -	upregulated	1.85
28S ribosomal protein S31, mitochondrial - MRPS31 -	upregulated	1.85
Nitric oxide-associated protein 1 - NOA1 -	upregulated	1.85
Malonyl-CoA-acyl carrier protein transacylase, mitochondrial - MCAT -	upregulated	1.82
Growth factor receptor-bound protein 10 - GRB10 -	upregulated	1.82
Probable D-lactate dehydrogenase, mitochondrial - LDHD -	upregulated	1.82
Junction-mediating and -regulatory protein - JMY -	upregulated	1.82
Atypical kinase COQ8B, mitochondrial - COQ8B -	upregulated	1.82
Autophagy-related protein 2 homolog B - ATG2B -	upregulated	1.79
RISC-loading complex subunit TARBP2 - TARBP2 -	upregulated	1.79
Vesicle transport protein SEC20 - BNIP1 -	upregulated	1.79
NAD-dependent protein deacetylase sirtuin-2 - SIRT2 -	upregulated	1.75
Engulfment and cell motility protein 2 - ELMO2 -	upregulated	1.75
Phosphatidylinositol 3-kinase catalytic subunit type 3 - PIK3C3 -	upregulated	1.75
39S ribosomal protein L9, mitochondrial - MRPL9 -	upregulated	1.75
28S ribosomal protein S26, mitochondrial - MRPS26 -	upregulated	1.75
Suppressor of tumorigenicity 14 protein - ST14 -	upregulated	1.75
Phosphatidylinositol 4,5-bisphosphate 3-kinase catalytic subunit beta isoform - PIK3CB -	upregulated	1.75
L-2-hydroxyglutarate dehydrogenase, mitochondrial - L2HGDH -	upregulated	1.72
Type I inositol 1,4,5-trisphosphate 5-phosphatase - INPP5A -	upregulated	1.72
Tyrosine--tRNA ligase, mitochondrial - YARS2 -	upregulated	1.72
Glutamyl-tRNA(Gln) amidotransferase subunit B, mitochondrial - GATB -	upregulated	1.72
Elongation factor G, mitochondrial - GFM1 -	upregulated	1.72
Protein FAM45A - FAM45A -	upregulated	1.69
2-(3-amino-3-carboxypropyl)histidine synthase subunit 2 - DPH2 -	upregulated	1.69
Ribosome production factor 2 homolog - RPF2 -	upregulated	1.69
[F-actin]-monooxygenase MICAL1 - MICAL1 -	upregulated	1.69
NADH-cytochrome b5 reductase 1 - CYB5R1 -	upregulated	1.67
cAMP-dependent protein kinase type II-beta regulatory subunit - PRKAR2B -	upregulated	1.67
Acyl-CoA dehydrogenase family member 10 - ACAD10 -	upregulated	1.67
SPRY domain-containing protein 4 - SPRYD4 -	upregulated	1.67
Thyroid adenoma-associated protein - THADA -	upregulated	1.67
Aldehyde dehydrogenase, mitochondrial - ALDH2 -	upregulated	1.64
Zinc finger protein 217 - ZNF217 -	upregulated	1.64
Presequence protease, mitochondrial - PITRM1 -	upregulated	1.64

Homeobox protein Nkx-3.1 - NKX3-1 -	upregulated	1.64
Serine/threonine-protein phosphatase 6 regulatory subunit 2 - PPP6R2 -	upregulated	1.64
28S ribosomal protein S11, mitochondrial - MRPS11 -	upregulated	1.61
Citrate synthase, mitochondrial - CS -	upregulated	1.59
Integrin beta-1 - ITGB1 -	upregulated	1.59
Synaptojanin-2-binding protein - SYNJ2BP -	upregulated	1.59
Sesquipedalian-1 - FAM109A -	upregulated	1.56
Dipeptidyl peptidase 9 - DPP9 -	upregulated	1.56
ADP-ribosylation factor-related protein 1 - ARFRP1 -	upregulated	1.56
Protein CREG1 - CREG1 -	upregulated	1.56
Calcium/calmodulin-dependent protein kinase type II subunit delta - CAMK2D -	upregulated	1.56
Transcription intermediary factor 1-alpha - TRIM24 -	upregulated	1.54
Transcription factor Sp3 - SP3 -	upregulated	1.54
Calcium-binding protein 39 - CAB39 -	upregulated	1.54
Peptidyl-tRNA hydrolase ICT1, mitochondrial - MRPL58 -	upregulated	1.54
Protein fem-1 homolog B - FEM1B -	upregulated	1.54
Hydroxymethylglutaryl-CoA synthase, cytoplasmic - HMGCS1 -	upregulated	1.52
Mitochondrial proton/calcium exchanger protein - LETM1 -	upregulated	1.52
Signal transducer and activator of transcription 3 - STAT3 -	upregulated	1.52
Microsomal glutathione S-transferase 3 - MGST3 -	upregulated	1.52
Polypeptide N-acetylgalactosaminyltransferase 2 - GALNT2 -	upregulated	1.52
Unconventional myosin-XVIIIa - MYO18A -	upregulated	1.52
NAD-dependent malic enzyme, mitochondrial - ME2 -	upregulated	1.49
DNA replication licensing factor MCM6 - MCM6 -	downregulated	0.67
GTP-binding protein 1 - GTPBP1 -	downregulated	0.66
DNA topoisomerase 3-beta-1 - TOP3B -	downregulated	0.66
Protein S100-A13 - S100A13 -	downregulated	0.66
DnaJ homolog subfamily C member 9 - DNAJC9 -	downregulated	0.66
Thymocyte nuclear protein 1 - THYN1 -	downregulated	0.66
Kinetochore-associated protein 1 - KNTC1 -	downregulated	0.66
Sperm-associated antigen 5 - SPAG5 -	downregulated	0.65
Oxygen-dependent coproporphyrinogen-III oxidase, mitochondrial - CPOX -	downregulated	0.65
Gamma-soluble NSF attachment protein - NAPG -	downregulated	0.65
WD repeat and HMG-box DNA-binding protein 1 - WDHD1 -	downregulated	0.65
L-lactate dehydrogenase A chain - LDHA -	downregulated	0.65
Cyclin-dependent kinases regulatory subunit 1 - CKS1B -	downregulated	0.65
Tumor protein D53 - TPD52L1 -	downregulated	0.64
Sorting nexin-17 - SNX17 -	downregulated	0.64
Transcription initiation factor TFIID subunit 6 - TAF6 -	downregulated	0.63
Guanine nucleotide exchange factor MSS4 - RABIF -	downregulated	0.63
Ribosomal oxygenase 2 - RIOX2 -	downregulated	0.63
Exosome complex component RRP41 - EXOSC4 -	downregulated	0.62
DCC-interacting protein 13-beta - APPL2 -	downregulated	0.62
Protein zwilch homolog - ZWILCH -	downregulated	0.62
Crooked neck-like protein 1 - CRNKL1 -	downregulated	0.62
Src substrate cortactin - CTTN -	downregulated	0.61
Nucleoside diphosphate-linked moiety X motif 19 - NUDT19 -	downregulated	0.61
Zinc finger protein 638 - ZNF638 -	downregulated	0.61
5'-3' exoribonuclease 1 - XRN1 -	downregulated	0.61
InaD-like protein - PATJ -	downregulated	0.61

Testin - TES -	downregulated	0.60
Uncharacterized protein C1orf112 - C1orf112 -	downregulated	0.60
Gem-associated protein 6 - GEMIN6 -	downregulated	0.59
Forkhead box protein J2 - FOXJ2 -	downregulated	0.59
5'-AMP-activated protein kinase subunit gamma-1 - PRKAG1 -	downregulated	0.59
Monoacylglycerol lipase ABHD12 - ABHD12 -	downregulated	0.59
Kinesin-like protein KIF15 - KIF15 -	downregulated	0.58
Nucleolar pre-ribosomal-associated protein 1 - URB1 -	downregulated	0.58
Deoxyuridine 5'-triphosphate nucleotidohydrolase, mitochondrial - DUT -	downregulated	0.58
Activating transcription factor 7-interacting protein 1 - ATF7IP -	downregulated	0.58
CUE domain-containing protein 2 - CUEDC2 -	downregulated	0.57
DNA excision repair protein ERCC-6-like - ERCC6L -	downregulated	0.57
DNA replication complex GINS protein PSF3 - GINS3 -	downregulated	0.56
BTB/POZ domain-containing protein KCTD3 - KCTD3 -	downregulated	0.56
Lariat debranching enzyme - DBR1 -	downregulated	0.56
Replication factor C subunit 4 - RFC4 -	downregulated	0.56
Choline-phosphate cytidylyltransferase A - PCYT1A -	downregulated	0.56
MAP/microtubule affinity-regulating kinase 3 - MARK3 -	downregulated	0.56
Zinc finger protein 318 - ZNF318 -	downregulated	0.56
Cholinesterase - BCHE -	downregulated	0.56
RWD domain-containing protein 2A - RWDD2A -	downregulated	0.56
Solute carrier family 2, facilitated glucose transporter member 1 - SLC2A1 -	downregulated	0.55
Thymidine kinase, cytosolic - TK1 -	downregulated	0.55
Ankyrin repeat and zinc finger domain-containing protein 1 - ANKZF1 -	downregulated	0.55
SWI/SNF-related matrix-associated actin-dependent regulator of chromatin subfamily E member 1-related - HMG20B -	downregulated	0.55
Condensin complex subunit 2 - NCAPH -	downregulated	0.54
DNA (cytosine-5)-methyltransferase 1 - DNMT1 -	downregulated	0.53
E3 ubiquitin-protein ligase RING1 - RING1 -	downregulated	0.53
CDK5 regulatory subunit-associated protein 2 - CDK5RAP2 -	downregulated	0.53
Protein 4.1 - EPB41 -	downregulated	0.53
Non-canonical poly(A) RNA polymerase PAPD5 - PAPD5 -	downregulated	0.53
M-phase phosphoprotein 6 - MPHOSPH6 -	downregulated	0.52
CTD small phosphatase-like protein 2 - CTDSPL2 -	downregulated	0.52
CLIP-associating protein 1 - CLASP1 -	downregulated	0.52
Adhesion G-protein coupled receptor G6 - ADGRG6 -	downregulated	0.52
Protein phosphatase 1H - PPM1H -	downregulated	0.51
Histone-lysine N-methyltransferase NSD2 - NSD2 -	downregulated	0.51
WD repeat-containing protein 92 - WDR92 -	downregulated	0.51
DNA-binding protein SMUBP-2 - IGHMBP2 -	downregulated	0.51
SWI/SNF-related matrix-associated actin-dependent regulator of chromatin subfamily D member 1 - SMARCD1 -	downregulated	0.51
Protein HGH1 homolog - HGH1 -	downregulated	0.50
ATP-dependent RNA helicase DDX55 - DDX55 -	downregulated	0.49
Peroxisomal NADH pyrophosphatase NUDT12 - NUDT12 -	downregulated	0.49
Ankyrin repeat domain-containing protein 13A - ANKRD13A -	downregulated	0.48
Mitotic checkpoint serine/threonine-protein kinase BUB1 - BUB1 -	downregulated	0.48
RalA-binding protein 1 - RALBP1 -	downregulated	0.47
HAUS augmin-like complex subunit 4 - HAUS4 -	downregulated	0.47
Transcription initiation factor TFIID subunit 10 - TAF10 -	downregulated	0.47

Telomere-associated protein RIF1 - RIF1 -	downregulated	0.47
High affinity cationic amino acid transporter 1 - SLC7A1 -	downregulated	0.46
POU domain, class 2, transcription factor 1 - POU2F1 -	downregulated	0.46
DNA primase large subunit - PRIM2 -	downregulated	0.46
Zinc finger protein 460 - ZNF460 -	downregulated	0.44
Phosphatidylserine decarboxylase proenzyme, mitochondrial - PISD -	downregulated	0.44
Adaptin ear-binding coat-associated protein 2 - NECAP2 -	downregulated	0.43
Sister chromatid cohesion protein DCC1 - DSCC1 -	downregulated	0.43
Werner syndrome ATP-dependent helicase - WRN -	downregulated	0.43
3-keto-steroid reductase - HSD17B7 -	downregulated	0.42
Heterogeneous nuclear ribonucleoprotein L-like - HNRNPLL -	downregulated	0.42
Endonuclease III-like protein 1 - NTHL1 -	downregulated	0.42
Ubiquitin-conjugating enzyme E2 R2 - UBE2R2 -	downregulated	0.41
Small G protein signaling modulator 3 - SGSM3 -	downregulated	0.40
Putative E3 ubiquitin-protein ligase UBR7 - UBR7 -	downregulated	0.40
Aurora kinase B - AURKB -	downregulated	0.38
DNA polymerase alpha catalytic subunit - POLA1 -	downregulated	0.38
DENN domain-containing protein 4C - DENND4C -	downregulated	0.37
Calmin - CLMN -	downregulated	0.35
Chromosome transmission fidelity protein 18 homolog - CHTF18 -	downregulated	0.33
Tubulin-specific chaperone cofactor E-like protein - TBCEL -	downregulated	0.32
Telomere length regulation protein TEL2 homolog - TELO2 -	downregulated	0.32
Leucine-rich repeat-containing protein 57 - LRRC57 -	downregulated	0.32
Fanconi anemia group D2 protein - FANCD2 -	downregulated	0.31
Ras GTPase-activating-like protein IQGAP3 - IQGAP3 -	downregulated	0.31
Nuclear factor NF-kappa-B p100 subunit - NFKB2 -	downregulated	0.31
Tetratricopeptide repeat protein 39C - TTC39C -	downregulated	0.30
Spindle and kinetochore-associated protein 2 - SKA2 -	downregulated	0.30
Serine/threonine/tyrosine-interacting protein - STYX -	downregulated	0.28
Transport and Golgi organization protein 6 homolog - TANGO6 -	downregulated	0.28
Myomegalin - PDE4DIP -	downregulated	0.27
DNA polymerase delta subunit 3 - POLD3 -	downregulated	0.26
Putative D-tyrosyl-tRNA(Tyr) deacylase 2 - DTD2 -	downregulated	0.25
B-cell CLL/lymphoma 7 protein family member A - BCL7A -	downregulated	0.24
DNA dC->dU-editing enzyme APOBEC-3B - APOBEC3B -	downregulated	0.24
Ribonuclease P protein subunit p25-like protein - RPP25L -	downregulated	0.23
Serine/threonine-protein kinase MARK1 - MARK1 -	downregulated	0.22
Anterior gradient protein 2 homolog - AGR2 -	downregulated	0.22
Ras-responsive element-binding protein 1 - RREB1 -	downregulated	0.22
Serine/threonine-protein kinase ATR - ATR -	downregulated	0.22
WAS/WASL-interacting protein family member 2 - WIPF2 -	downregulated	0.21
Protein Spindly - SPDL1 -	downregulated	0.18
Autophagy-related protein 13 - ATG13 -	downregulated	0.15
Nucleolar and spindle-associated protein 1 - NUSAP1 -	downregulated	0.09